Synthesis and Application of Conjugated Materials containing 1,1'-Binaphthalene

Haojie Dai

Supervisor – Professor Martin Heeney

Submitted in partial fulfilment of the requirements for the degree of Doctor of Philosophy in Chemistry

Imperial College London

February 2020

If

By Rudyard Kipling

If you can keep your head when all about you
Are losing theirs and blaming it on you,
If you can trust yourself when all men doubt you,
But make allowance for their doubting too;
If you can wait and not be tired by waiting,
Or being lied about, don't deal in lies,
Or being hated, don't give way to hating,
And yet don't look too good, nor talk too wise:

If you can dream—and not make dreams your master;
If you can think—and not make thoughts your aim;
If you can meet with Triumph and Disaster
And treat those two impostors just the same;
If you can bear to hear the truth you've spoken
Twisted by knaves to make a trap for fools,
Or watch the things you gave your life to, broken,
And stoop and build 'em up with worn-out tools:

If you can make one heap of all your winnings
And risk it on one turn of pitch-and-toss,
And lose, and start again at your beginnings

And never breathe a word about your loss;

If you can force your heart and nerve and sinew

To serve your turn long after they are gone,

And so hold on when there is nothing in you

Except the Will which says to them: ‘Hold on!’

If you can talk with crowds and keep your virtue,

Or walk with Kings—nor lose the common touch,

If neither foes nor loving friends can hurt you,

If all men count with you, but none too much;

If you can fill the unforgiving minute

With sixty seconds’ worth of distance run,

Yours is the Earth and everything that’s in it,

And—which is more—you’ll be a Man, my son!

Declaration

This thesis describes work carried out in the Depart of Chemistry, Imperial College London, between October 2015 and October 2018, under the supervision of Professor Martin Heeney. The content of this thesis is the author's original work, unless stated otherwise.

Haojie Dai

Contributions

This work would not have been possible without the help of following people, to whom I send my whole-hearted gratitude.

The organic solar cell devices discussed in Chapter 2 and 3 were prepared and tested by Dr. Munazza Shahid at Imperial College London. The circular dichroism measurement in the end of Chapter 2 was conducted by Dr. Jessica Wade at Imperial College London.

Copyright

The copyright of this thesis rests with the author and is made available under a Creative Commons Attribution Non-Commercial No Derivatives licence. Researchers are free to copy, distribute or transmit the thesis on the condition that they attribute it, that they do not use it for commercial purposes and that they do not alter, transform or build upon it. For any reuse or redistribution, researchers must make clear to others the licence terms of this work.

Acknowledgements

My most profound and sincere appreciation and gratitude go to Prof. Martin Heeney for his unremitting and complimentary counsel.

I would like to thank Dr Lisa Haigh for her invaluable help with MS and LCMS; Peter Haycock for NMRs; Dr Karl Thorley and Adam Marsh for computational DFT help; Dr Jessica Wade for her help with optical circular dichroism measurement; Dr Mark Little and James Ponder Jr for being the most useful post docs; last but not least, Thomas Hodsden for being friendly, buying me chemicals without fuss or hesitation, and overall being very helpful.

To all the former and present Iain McCulloch and Martin Heeney's group members who were not mentioned above, thank you all for being good company over the course of my PhD.

I would also like to acknowledge the support of my family along with special thanks to Dr. Mark Daniels and Catherine Perry, without whom this thesis would be a fumbled, desperate waste and not the grievous manifestation of rarefied esoterica it became.

Abstract

Soluble processable organic semiconductors offer several advantages over their traditional inorganic counterparts. They can be processed by a variety of large-area techniques, are lightweight, robust and flexible. Furthermore, their properties can be readily tuned by modifications to the chemical structure of the semiconductor. This influences both the fundamental optoelectronic properties, such as band gap and energy levels, as well as the physical properties such as molecular aggregation and thin-film morphology.

This work is focussed upon the potential of 1,1'-binaphthyl (BN) derivatives as building blocks in the development of new materials for organic photovoltaics (OPV) applications. Due to steric interaction between the protons in the 8,8' position, BN is inherently twisted with a torsional angle of about 90°. Incorporation of BN into organic semiconducting materials was therefore expected to lead to non-planar materials with suppressed crystallisation in the solid state. This strategy was explored for novel acceptor materials for organic solar cells, in which large scale crystallisation can lead to detrimental device performance and stability. Two classes of BN cored semiconductors were synthesised, containing either diketopyrrolopyrrole or rhodanine end-groups with varying alkyl sidechains. Their optoelectronic performance is reported, along with preliminary device data.

Functionalised BN derivatives also exhibit atropisomerism, and their incorporation into organic semiconducting polymers and small molecules was also explored as an approach to afford chirally active, electronically functional materials.

Table of Contents

Declaration iii

Contributions iv

Copyright v

Acknowledgements vi

Abstract vii

Abbreviations xi

1. Introduction ..... - 1 -

1.1 Organic semiconductors: An Overview ..... - 1 -

1.1.1 Definition of organic semiconductors ..... - 1 -

1.1.2 Semiconductivity in organic materials ..... - 1 -

1.1.3 The fundamental electronic difference between inorganic and organic semiconductors ..... - 2 -

1.1.4 Two different classes of organic semiconductor materials ..... - 3 -

1.1.5 General synthetic approaches for organic semiconductors ..... - 6 -

1.2 Organic photovoltaics (OPVs) ..... - 8 -

1.2.1 Basic Operating principle ..... - 8 -

1.2.2 Basic device architecture ..... - 10 -

1.2.3 Characterisation of device performance ..... - 11 -

1.2.4 Molecular design ..... - 13 -

1.3 Organic light-emitting diodes (OLEDs) ..... - 15 -

1.3.1 Jablonski diagram ..... - 15 -

1.3.2 Basic device architecture ..... - 16 -

1.3.3 Chiral emissive OLEDs ..... - 17 -

2. The Synthesis of Diketopyrrolopyrrole Flanked 1,1'-Binaphthyl Materials . - 19 -

2.1 Overview ..... - 19 -

2.2 Binaphthyl and DPP(EH) series ..... - 22 -
2.2.1 Synthesis ..... - 22 -
2.2.2 Optoelectronic & Thermal Properties ..... - 36 -
2.3 Enantio-enriched binaphthyl and DPP(BH) based molecule ..... - 47 -
2.3.1 Synthesis ..... - 48 -
2.3.2 Opto-electric properties ..... - 60 -
3. Binaphthyl Rhodanine Based Small Molecule Acceptors ..... - 62 -
3.1 Overview ..... - 62 -
3.2 Syntheses ..... - 64 -
3.2.1 5,5'-([1,1'-Binaphthalene]-2,2'-diyl)bis(thiophene-2-carbaldehyde) (3.1) .... - 64 -
3.2.2 3-(2-Ethylhexyl)-2-thioxothiazolidin-4-one (3.2) ..... - 65 -
3.2.3 3-Butyl-2-thioxothiazolidin-4-one (3.4) ..... - 66 -
3.2.4 (5Z,5'E)-5,5'-(([1,1'-Binaphthalene]-2,2'-diylbis(thiophene-5,2-diyl))bis(methaneylylidene))bis(3-(2-ethylhexyl)-2-thioxothiazolidin-4-one) (3.6) ... - 67 -
3.2.5 (5Z,5'E)-5,5'-(([1,1'-Binaphthalene]-2,2'-diylbis(thiophene-5,2-diyl))bis(methaneylylidene))bis(3-ethyl-2-thioxothiazolidin-4-one) (3.5) & (5Z,5'E)-5,5'-(([1,1'-binaphthalene]-2,2'-diylbis(thiophene-5,2-diyl))bis(methaneylylidene))bis(3-butyl-2-thioxothiazolidin-4-one) (3.7) ..... - 68 -
3.3 Opto-electric, thermal properties & computational simulation ..... - 71 -
3.3.1 DFT ..... - 71 -
3.3.2 Cyclic Voltammetry (CV) ..... - 72 -
3.3.3 Ultraviolet-visible Spectroscopy (UV-Vis) ..... - 73 -
3.3.4 TGA & DSC ..... - 74 -
3.3.5 OPV device performance ..... - 75 -
4. Binaphthyl Based Polymers ..... - 78 -
4.1 Overview ..... - 78 -
4.2 Synthesis ..... - 78 -
4.3 Optical properties & Computational simulation ..... - 80 -

4.3.1 Ultraviolet-visible (UV-Vis) & Fluorescence Spectroscopy ..... - 80 -
4.3.2 DFT ..... - 82 -
4.4 Conclusions ..... - 85 -
5. Conclusions ..... - 86 -
Chapter 2: Binaphthyl DPP Based Materials ..... - 86 -
Chapter 3: Binaphthyl Rhodanine Based Small Molecule Acceptors ..... - 87 -
Chapter 4: Binaphthyl Based Polymers ..... - 87 -
6. Experimental ..... - 89 -
6.1 Chapter 2 ..... - 90 -
6.2 Chapter 3 ..... - 120 -
6.3 Chapter 4 ..... - 126 -
7. References ..... - 128 -
8. Appendix ..... - 140 -
8.1 Chapter 2 ..... - 140 -
8.2 Chapter 3 ..... - 181 -
8.3 Chapter 4 ..... - 195 -

Abbreviations

^{o}	Degrees
δ	Chemical shift
λ	Wavelength
BDT	Benzo[1,2-b:4,5-b']dithiophene
BHJ	Bulk heterojunction
BT	2,1,3-Benzothiadiazole
CF	Chloroform
DCM	Dichloromethane
CV	Cyclic voltammetry
DFT	Density functional theory
DMF	*N,N*-Dimethylformamide
DSC	Differential scanning calorimetry
E_g	Bandgap
CPL	Circularly polarised light
OLED	Organic light emitting diode
OPV	Organic photovoltaic
$PC_{61}BM$	[6,6]-Phenyl-C_{61}-butyric acid methyl ester
$PC_{71}BM$	[6,6]-Phenyl-C_{71}-butyric acid methyl ester
PCE	Power conversion efficiency
PL	Photoluminescence
THF	Tetrahydrofuran
UV-Vis	Ultraviolet-visible
V_{oc}	Open circuit voltage
EI	Electron ionisation

ESI	Electrospray ionisation
eV	Electron volt
FF	Fill factor
GPC	Gel permeation chromatography
HTL	Hole transport layer
ITO	Indium tin oxide
J_{sc}	Short circuit current
LUMO	Lowest unoccupied molecular orbital
$\overline{M_n}$	Number average molecular weight
$\overline{M_w}$	Weight average molecular weight
MALDI	Matrix-assisted laser desorption/ionisation
MS	Mass spectrometry
m/z	Mass to charge ratio
NBS	*N*-Bromosuccinimide
nm	Nanometre
NMR	Nuclear magnetic resonance
OFET	Organic field-effect transistor
n-BuLi	*n*-Butyllithium
P3HT	Poly(3-hexylthiophene)
R.T.	Room temperature
PEDOT:PSS	Poly(3,4-ethylenedioxy)thiophene/poly(styrene sulfonate)
T_g	Glass transition temperature
TLC	Thin layer chromatography
λ_{max}	Absorption maximum
HOMO	Highest occupied molecular orbital
HRMS	High resolution mass spectrometry

LDA	Lithium diisopropylamide
DMSO	Dimethyl sulfoxide

1. Introduction

1.1 Organic semiconductors: An Overview

1.1.1 Definition of organic semiconductors

Organic semiconductors are materials made of mainly C and H, including a few heteroatoms such as O, S, N etc. They find application in many devices such as solar cells, field-effect-transistors (FETs) and light-emitting diodes (LEDs). Therefore, they are a class of material that combines the electronic properties of semiconductors with the mechanical and chemical benefits of organic material (e.g. polymers). The chemical and mechanical benefits usually refer to solubility (thus enabling solution processing techniques such as printing) and their light weight and flexible nature. The fundamental properties of organic semiconductors can be tuned via chemical synthesis.

1.1.2 Semiconductivity in organic materials

A carbon atom has one 2s orbital and three 2p orbitals. The s and p orbitals can hybridise to produce three different hybridisations: sp^3, sp^2 and sp hybridisation (Figure 1-1). For sp^2 and sp hybridisation, one 2p orbital and two 2p orbitals remain unhybridised respectively.

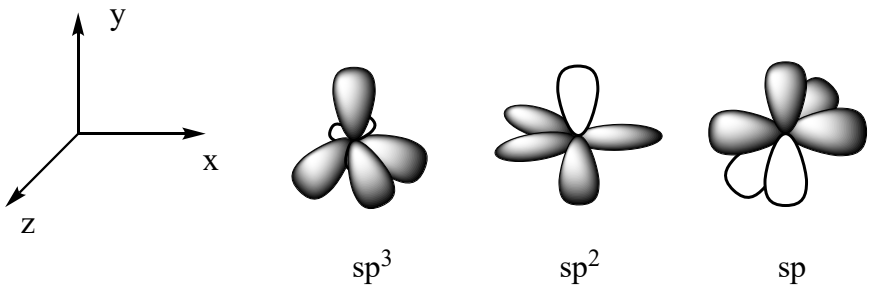


Figure 1-1: sp^3, sp^2 and sp hybridisation of carbon 2s and 2p orbitals.

In Figure 1-2, ethane, ethene and ethyne are used as examples to demonstrate the orbital hybridisation mentioned above. The σ bond between two carbon atoms is formed via overlapping of two hybridised orbitals, sp^3-sp^3 (for ethane), sp^2-sp^2 (for ethene) and sp-sp (for ethyne). Within an σ bond, electrons are shared between two atoms and are localised in space.

However, for ethene and ethyne, in addition to σ bonds, there are also π bonds forming due to overlapping of unhybridised p orbitals. The electrons in π bonds are delocalised.

An organic semiconductor is mainly made of sp^2 hybridised carbon atoms with π orbitals overlapping each other typically across the entire molecular backbone. Its structure appears as alternating single and double bonds (also known as conjugation). This allows electrons to delocalise across entire molecular backbone. Upon injection of charge, current can thus move along the molecular backbone and hop between molecules.

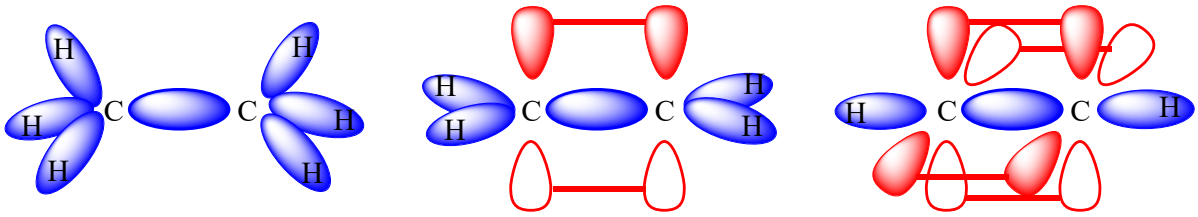


Figure 1-2: Molecular orbital diagrams of an sp^3 hybridised ethane molecule (left), an sp^2 hybridised ethene molecule (middle) and an sp hybridised ethyne molecule (right).

1.1.3 The fundamental electronic difference between inorganic and organic semiconductors

Traditional inorganic semiconductors have a low band gap, for example: 1.1 eV for Si, 0.67 eV for Ge. At room temperature, free charge carriers can be generated by thermal excitation from the valence band to the conduction band. The concentration of charge carriers generated is given by

$$N = N_{eff} e^{-E_g/2kT} \quad (1)$$

where N_{eff} is the effective density of valence or conduction band states, E_g is band gap, k is Boltzmann constant, and T is temperature. The intrinsic conductivities of inorganic semiconductors range from 10^{-8} to 10^{-2} Ω^{-1} cm^{-1} with the dielectric constant as large as $\varepsilon_r = 11$. Such a large dielectric constant screens coulomb interaction between electrons and holes

(known as dielectric screening). Therefore, light absorption at room temperature creates free electrons and holes.

On the other hand, the typical dielectric constant for organic semiconductors is about $\varepsilon_r = 3.5$. Therefore, photoexcitation does not create free holes and electrons, but bound electron-hole pairs, with a coulomb binding energy of about 0.5 - 1.0 eV. These are called excitons. The fact that organic semiconductors cannot generate free electrons and holes means that their conductivities arise from extrinsic approaches, such as charge injection at electrodes and/or chemical doping.

1.1.4 Two different classes of organic semiconductor materials

1.1.4.1 Small molecules

Organic semiconducting small molecules are typically crystalline materials with a high degree of order in the solid state. Depending on their processing, they can be utilized as single crystals or polycrystalline thin films, or amorphous glasses. For example, molecular beam deposition of pentacene to a -196 °C substrate results in amorphous pentacene thin film, whereas deposition at room temperature gives a highly ordered crystalline thin film with very few grain boundaries.[1]

Organic semiconductors that form crystals have a point lattice and basis. The basis is composed of molecules rather than atoms, which are commonly observed for inorganic crystals. Examples include naphthalene, tetracene, pentacene etc. Within the crystal, molecules are held together by van der Waals forces. Due to the high degree of order, molecular crystals typically have relatively high charge carrier mobility with values for single crystals up to 40 $cm^2\ V^{-1}\ s^{-1}$ reported for rubrene[2] (a derivative of tetracene). The integration of such single crystals into practical devices is challenging, however. For that reason, the deposition of molecular semiconductors like pentacene into thin films has been intensely investigated. Such films can be formed via a variety of high vacuum deposition techniques. The charge carrier mobility and transistor performance are very sensitive to the deposition process (substrate temperature, deposition rate etc.) since such films are polycrystalline and the grain boundaries between crystallites are the rate limiting step for charge transport. In addition, it is worth mentioning that soluble small molecules can form polycrystalline films as well.

1.1.4.2 Polymers

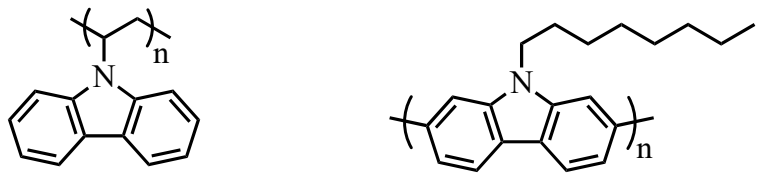
A polymer is a macromolecule composed of many repeating units. Usually the number of repeating units needs to be greater than 100 for a molecule to be considered as a polymer.[3] Anywhere up to 20 repeating units is called an oligomer, between 20 and 100 repeating units maybe called either a long oligomer or a short polymer depending on what the author would like to emphasize. Polymers can be amorphous or semicrystalline in nature.

1.1.4.2.1 Polymer structures and nomenclature

The arrangement of repeating units in the polymer backbone can vary to form different structures. For example, the simplest polymer consisting of a repeat sequence of the same monomer (here termed A) would be a homopolymer. If two different co-monomers are used (here termed A and B) then several different arrangements are possible; …ABABABABAB… is known as alternating copolymer; …AAAAABBBBB… is called a diblock copolymer; …ABBAABABBBAAB… is a statistical (or random) copolymer.

Nowadays, most organic semiconducting polymers fall into the category of main chain polymers, where electronically active units form the backbone of the polymer chain. However, if the electronically active parts are in the side chain and the backbone is electronically inert, they are referred as side chain polymers (Figure 1-3).

(i) (ii)



Side chain homopolymer Main chain homopolymer

Figure 1-3: Examples of (i) a side chain polymer poly(vinylcarbazole); (ii) a main chain polymer P(2,7-carbazole).

1.1.4.2.2 Polymer distribution

When a batch of polymer is synthesized, it will contain a distribution of polymers with different chain sizes. Therefore, finding a meaningful method to characterize the size distribution

becomes vitally important. Here we introduce weight average molecular weight ($\overline{M_w}$) and number average molecular weight ($\overline{M_n}$), which are commonly used in this field.

In mathematics, the average value $\overline{x}$ for any given quantity with a distribution of values x_i is given by:

$$\overline{x} = \sum_i x_i p_i \tag{2}$$

where p_i is the probability of x_i occurring. Therefore, for polymers if the probability for molecules with molar mass M_i occurring is proportional to its number fraction, then probability becomes

$$p_i = {N_i}/{\sum_j N_j} \tag{3}$$

where N_i is the number of molecules with molar mass M_i. Substituting p_i in equation (2) with equation (3) and replacing x_i with M_i, this yields number average molecular weight ($\overline{M_n}$).

$$\overline{M_n} = \sum_i \left(\frac{N_i}{\sum_j N_j}\right) M_i = \frac{\sum_i N_i M_i}{\sum_j N_j} \tag{4}$$

Similarly, if the probability for molecules with molar mass M_i occurring is proportional to its weight fraction.

$$p_i = \frac{N_i M_i}{\sum_j N_j M_j} \tag{5}$$

Substituting p_i in equation (2) with equation (5) and replacing x_i with M_i, one obtains the weight average molecular weight ($\overline{M_w}$).

$$\overline{M_w} = \sum_i \left(\frac{N_i M_i}{\sum_j N_j M_j}\right) M_i = \frac{\sum_i N_i M_i^2}{\sum_j N_j M_j} \tag{6}$$

The polydispersity index PDI (or Đ), which measures the spread of distribution, can be obtained by dividing weight average molecular weight ($\overline{M_w}$) by the number average molecular weight ($\overline{M_n}$).

$$PDI = {\overline{M_w}}/{\overline{M_n}} \tag{7}$$

Another quantity one maybe particularly interested in is the degree of polymerization (DP); it measures the average number of repeating units a polymer chain has. The degree of polymerization can be obtained by dividing (number) average molecular weight by the molar mass of the single repeating unit.

The distribution of polymers is typically measured via size exclusion chromatography (SEC), also called gel permeation chromatography (GPC). It is a technique that separates polymers purely based on their hydrodynamic radius in solution. An SEC instrument is composed of a pump to push the solvent (e.g. chlorobenzene) through the system, an injection port for sample injection, a column for holding a stationary phase and several detectors as well as software control.

The polymer sample is first dissolved in solvent. When dissolved, the polymers swell and typically fold upon themselves to form spherical structures. The higher molecular weight polymer molecules will form bigger spheres or more formally the polymer will have a larger hydrodynamic radius. The dissolved sample is then injected into the system to pass a column pre-packed with porous polymer beads (e.g. cross-linked polystyrene) with various pore sizes.

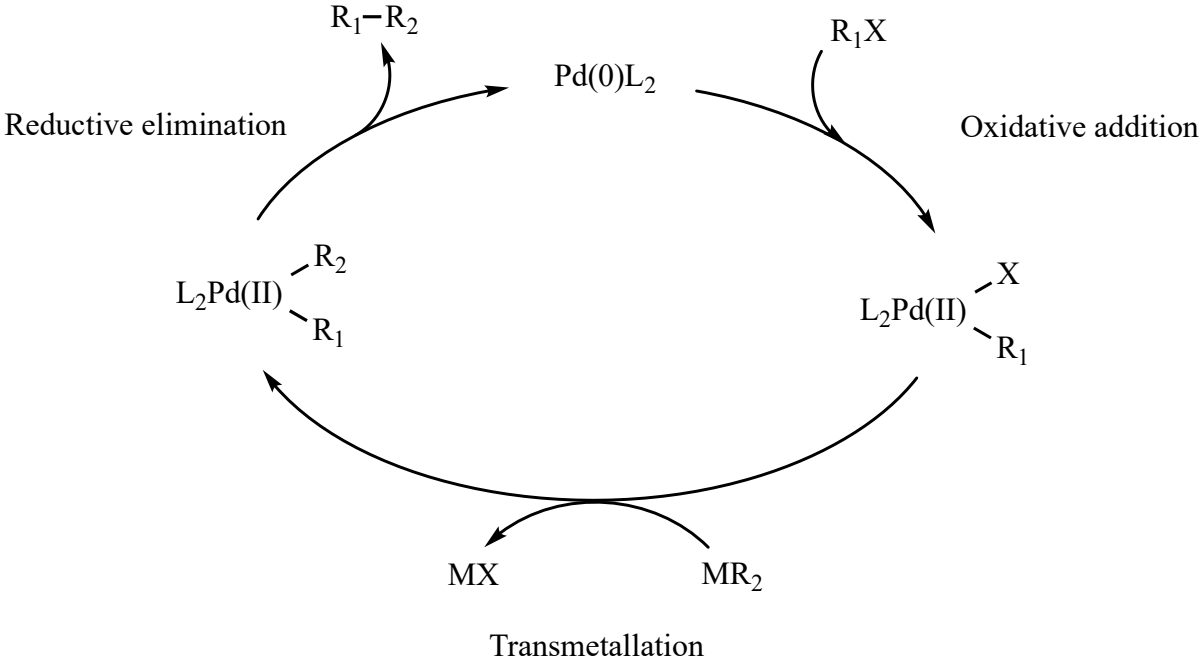
Polymers that are larger than the pore size get carried straight past by the mobile phase. Smaller polymers that can fit into the pore and will therefore have a more tortuous route through the column, taking a longer time to exit the column compared to the large ones. Upon leaving the column, the polymeric material is detected (by a variety of techniques) to produce a chromatogram, which shows the amount of material leaving the column at any one time with higher molecular weight polymer emerging first. The molecular weight is then determined by referencing to a calibration curve made with narrow polydispersity polymers of known molecular weight.

Some conjugated polymers can be problematic for SEC analysis because of their tendency to aggregate in solution. This gives a larger hydrodynamic radius and therefore can result in an over-estimation of molecular weight.

1.1.5 General synthetic approaches for organic semiconductors

Transition metal, particularly palladium, catalyzed cross-coupling is the most commonly encountered approach for the syntheses of organic semiconductors. Such reactions are important for forming carbon-carbon bonds between sp^2 hybridized systems and are thus very

important for organic semiconductors which are fully conjugated materials. Scheme 1-1 depicts the general catalytic cycle for a palladium catalyzed cross-coupling reaction. The first step is an oxidative addition where the palladium catalyst is inserted into an aryl-halide or aryl-pseudohalide bond ($R_1 – X$, where X represents halides and/or triflate and R_1 is a sp^2 hybridized aromatic or vinylene carbon). During this process the oxidation state of the palladium changes from zero to +2. Here we ignore the geometry of the resulting Pd(II) complex, but often the oxidative insertion affords a trans complex, which rapidly isomerizes to the cis complex shown. The cis complex can also be directly formed via the use of a bidentate ligand. Following oxidative addition, a transmetallation step occurs where X is replaced by an aromatic or a vinyl group R_2. The final step is reductive elimination where palladium (II) gets reduced back to palladium (0) with R_1, R_2 being eliminated from the cycle and forming a bond between each other, $R_1 – R_2$.



Scheme 1-1: General catalytic cycle for palladium catalysed cross-couplings.

For the transmetallation step, M denotes boronic acid and its derivatives (Suzuki); ZnCl and its derivatives (Negishi); $SnMe_3$ or $SnBu_3$ (Stille). Stille and Suzuki cross-coupling reactions are most commonly used for the syntheses of organic semiconductors.[4] For Stille cross-coupling, it runs under neutral conditions and can tolerate a large number of functional groups rendering it the favorable choice. However, organotin is highly toxic, thus it is only feasible to conduct

reactions at laboratory scale. Suzuki cross-coupling reactions on the other hand are regarded as generally non-toxic, but they occur under basic conditions, which can be intolerable for some functional groups. An added complication is that the reaction often occurs in biphasic conditions, with an aqueous base and a phase transfer catalyst. Furthermore, Suzuki cross-coupling typically requires more optimization than the Stille due to the additional factors and for small-scale reactions Stille is often preferred.

1.2 Organic photovoltaics (OPVs)

1.2.1 Basic Operating principle

Organic solar cells operate differently from their inorganic counterparts. Because of the low dielectric constant, electron-hole pairs (known as excitons) generated due to photoexcitation are coulombically bound. Therefore, to generate free electrons and holes, a blend of two different semiconductors is usually required. These are called the donor, for the electron rich semiconductor and acceptor for the electron deficient semiconductor. The LUMO-LUMO (or HOMO-HOMO) offset between donor and acceptor should be sufficiently large to break the exciton binding energy. The magnitude of this energy is a much debated value, but an oft-quoted figure is ~ 0.3 eV.[5]

Figure 1-4 depicts the energy level diagram of a simple binary system, in which photoexcitation of the donor material generates a coulomb bound electron-hole pair (exciton) (Figure 1-4 i). The exciton then diffuses towards donor-acceptor interface where it dissociates into free charge carriers via a charge transfer (CT) state (Figure 1-4 ii). Similarly, the acceptor material can also absorb photons and generate excitons and having the holes transferred to the donor if the difference between HOMO energies of donor and acceptor is sufficiently large. The dissociated free charge carriers can then drift/diffuse towards their respective electrodes to be collected (Figure 1-4 iii).

However, there are various loss mechanisms which can limit the charge collection. For example, the charges generated at the interface can recombine back to the ground state. This is referred as geminate recombination. Charges can also recombine with other free charge carriers known as non-geminate recombination / bimolecular recombination. Both loss mechanisms can greatly lower organic solar cell devices' efficiencies.

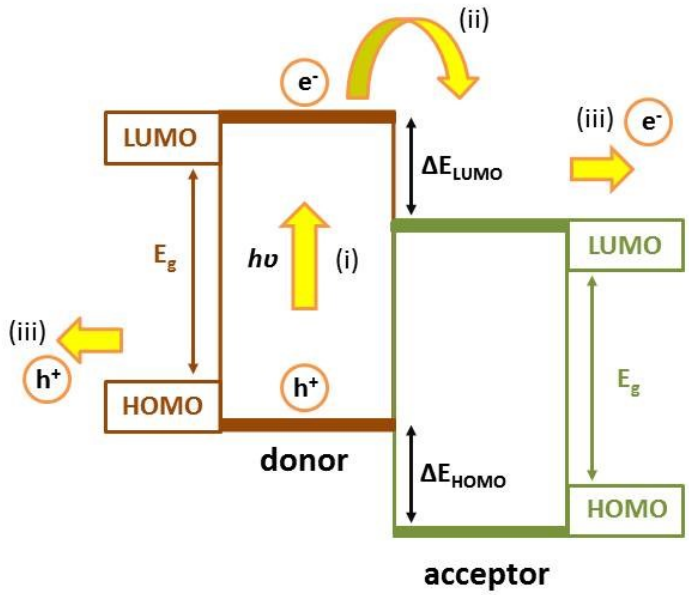


Figure 1-4: Energy level diagram for a simple binary donor-acceptor heterojunction system: i): photo-excitation of the donor material to generate an exciton; ii) charge dissociation and transfer at the donor-acceptor interface; iii) diffusion / drift of free charge carriers towards respective electrodes.

During an exciton's short lifespan, it typically diffuses up to ~ 10 nm[6] (for solution processed materials, vacuum deposited materials tend to have longer exciton diffusion length) before recombination. Since free charge carriers can only be generated at donor-acceptor interface, if the exciton does not reach the interface it results in a loss in efficiency. The short diffusion length poses a great challenge in active layer morphology engineering. To tackle this issue, scientists have come up with the idea of the bulk heterojunction. Figure 1-5 (a) shows the ideal bulk heterojunction morphology[7] where donor and acceptor interpenetrate each other like inter-digitated fingers with a domain size close to twice the exciton diffusion length, thus allowing optimal free charge generation and current flow. However, practically it is very difficult to achieve such defined active layer morphology on the required length scale. More typically both the donor and acceptor material are cast from a common solvent and a random mixture of domains is produced, something like Figure 1-5 (b). Control of the deposition conditions, as well as post-processing steps like annealing are necessary to produce the required phase

segregation on the 10-20 nm length scale. Typically, the cartoon of Figure 1-5 (b) is an oversimplification, and as well as donor and acceptor domains, mixed domains of both materials are also formed.

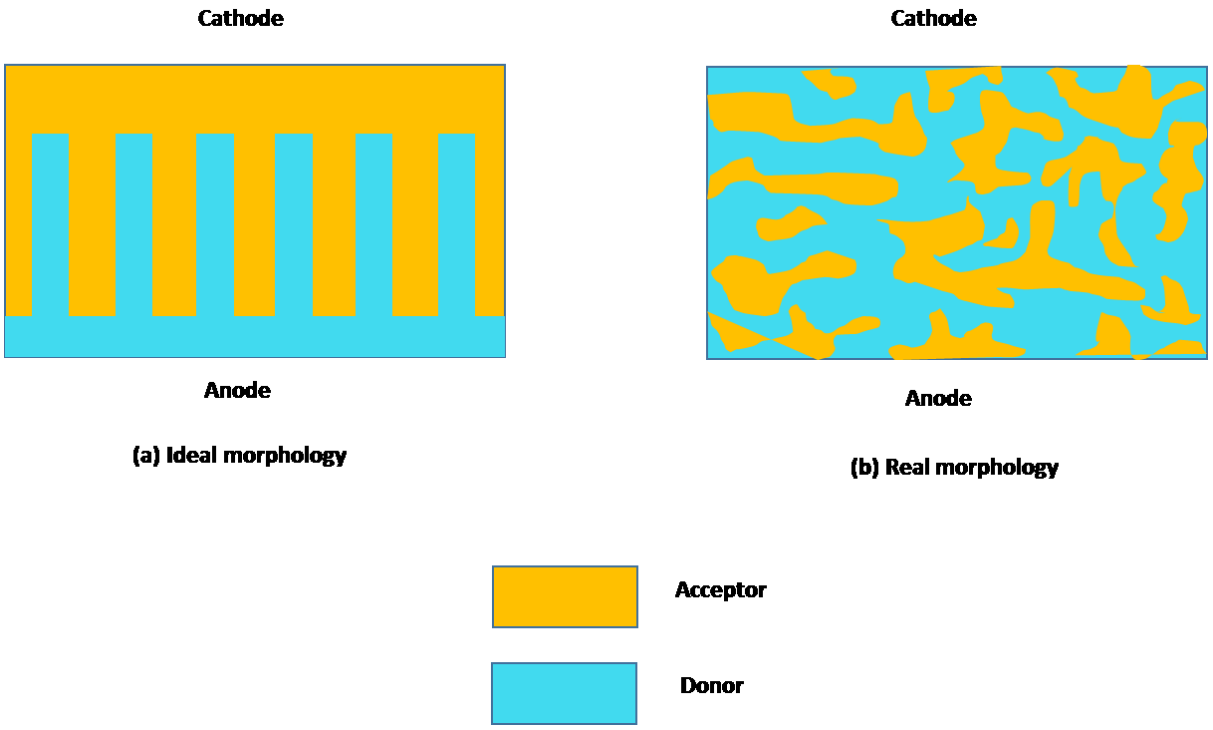


Figure 1-5: (a): ideal bulk heterojunction morphology; (b): actual morphology one usually gets for solution processed fabrication.

1.2.2 Basic device architecture

For a conventional binary bulk heterojunction solar cell, the active layer is typically sandwiched between two electrodes, a cathode and an anode. The cathode is usually made of a low work function metal such as aluminium and the anode is usually a high work function indium tin oxide. An electron transport layer is often sandwiched between the cathode and the active layer, it blocks holes from travelling thus reduces non-geminate recombination. Similarly in between the anode and the active layer, a hole transport layer often poly(3,4-ethylenedioxythiophene):poly(styrene sulfonic acid) (PEDOT: PSS) is used to block electrons (Figure 1-6 left). However, this conventional architecture has drawbacks. At first, aluminium is susceptible to oxidation. Furthermore, PEDOT: PSS is acidic, it can potentially react with the active layer and etch ITO. All these are detrimental to device performance. To tackle these issues, the inverted device architecture was introduced (Figure 1-6 right). It uses relatively air

stable metals such as Ag as anode and replaces acidic PEDOT: PSS with MoO_3. An n-type semiconductor such as ZnO/ TiO_x is typically used to facilitate electron collection.

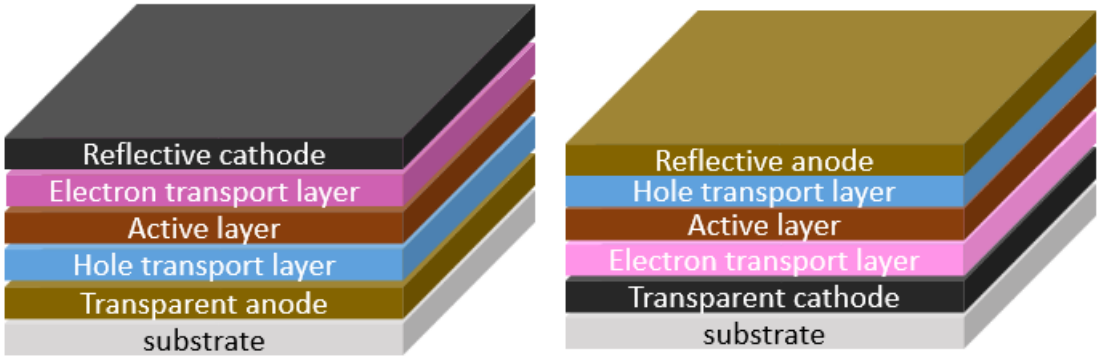


Figure 1-6: Conventional non-inverted device architecture (left) and inverted (right).

1.2.3 Characterisation of device performance

When an organic solar cell device is made, it is typically tested under standard illumination condition of AM 1.5G, 100 mW cm^{-2} and a current-voltage (*J-V*) curve is therefore generated (e.g. Figure 1-7).

On the *J-V* curve, there are open-circuit voltage (V_{oc}), short-circuit current (J_{sc}) and fill factor (FF). These are the key parameters used for determining solar cell efficiency.

Broadly speaking the short-circuit current (J_{sc}) is related to the number of photons an organic semiconductor can absorb, the greater the absorption, the greater the current. Therefore, materials with a low band gap are favoured since they will absorb more of the solar spectrum.

On the other hand, open-circuit voltage (V_{oc}) is related to the difference between the HOMO of the donor and the LUMO of the acceptor (Figure 1-8 B). There is always a compromise between J_{sc} and V_{oc} as lowering band gap to generate more current will also cause a drop in V_{oc}. In addition, one also needs to consider the LUMO-LUMO offset between donor and acceptor since it needs to be greater than the exciton bind energy to generate free charge carriers.

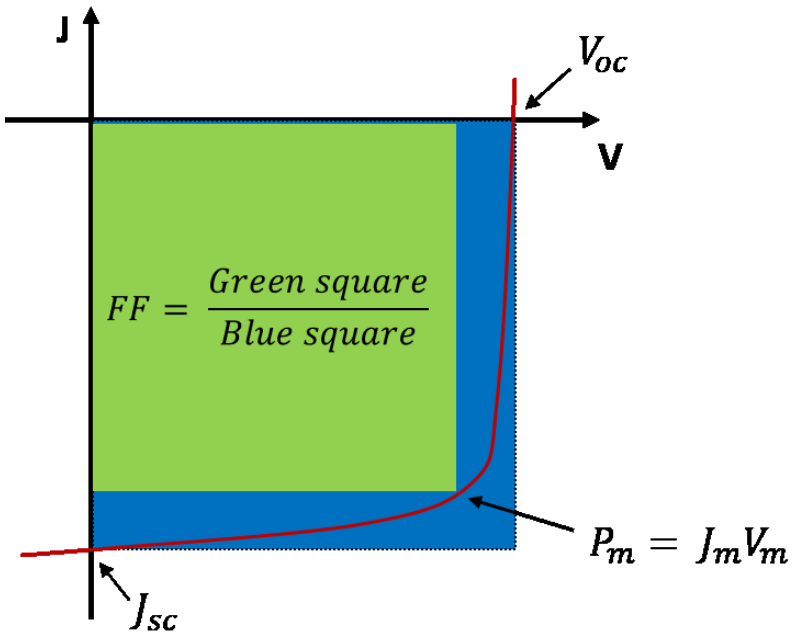


Figure 1-7: Current-voltage (*J-V*) curve of an illuminated solar cell.

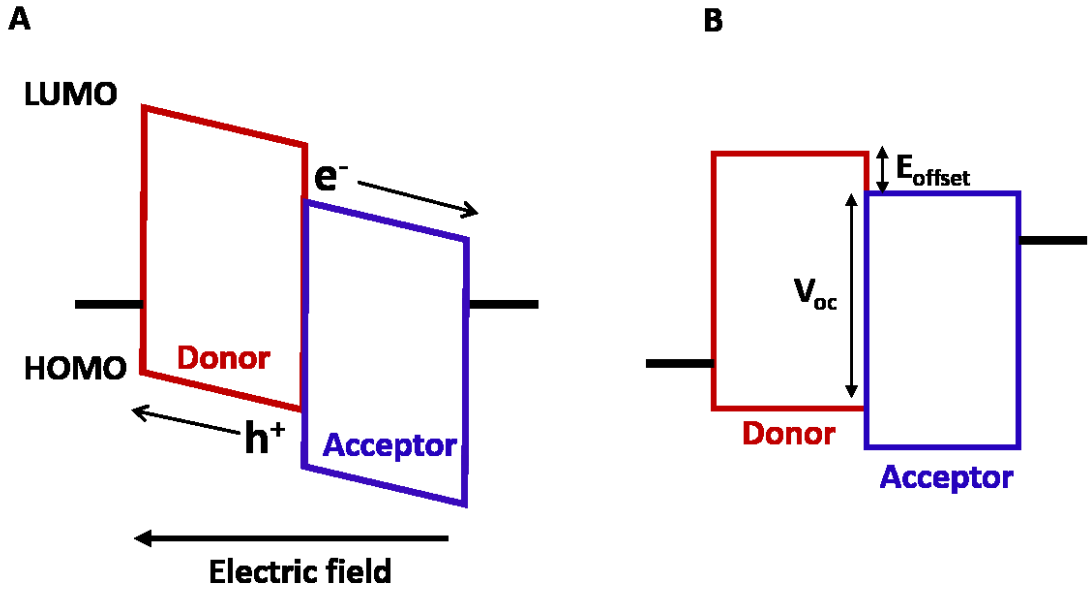


Figure 1-8: Energy level diagrams of a binary organic solar cell when A) the electrodes are short-circuited producing maximum photocurrent (J_{sc}) and B) when there is open circuit with no current but maximum voltage (V_{oc}).

Fill factor (FF) measures the squareness of *J-V* curve. It is the ratio between maximum power output (P_m) of a device and the theoretical potential maximum output of the device and it is given by:

$$FF = \frac{P_m}{J_{sc}V_{oc}} = \frac{J_m P_m}{J_{sc}V_{oc}} \tag{8}$$

If a device had fill factor of 1, it would have achieved open-circuit voltage without losing any current. This is not practically possible. Another parameter is power conversion efficiency (PCE), which is commonly used for comparing different devices' performances. The power conversion efficiency of a device is defined as the ratio between maximum power output of the device (P_m) and the input power of incident light (P_{in}; 100 mW cm^{-2} for standard condition):

$$PCE = \frac{P_m}{P_{in}} = \frac{J_m V_m}{P_{in}} = \frac{FF \cdot J_{sc} V_{oc}}{P_{in}} \quad (9)$$

1.2.4 Molecular design

At the outset of this PhD, donor materials had been studied extensively and people's interest towards organic solar cells had shifted to the development of alternative non-fullerene small molecule acceptors. Acceptor materials based on fullerene derivatives such as $PC_{61}BM$ (Figure 1-9) all have common drawbacks.[8] Firstly, fullerene acceptors have poor absorption in the visible and near IR region. Secondly, it is very difficult to chemically modify fullerene. At last, fullerene acceptors tend to phase segregate and form large domains that are detrimental to device performance. Therefore, seeking alternative non-fullerene acceptors that can tackle these issues became a hot topic.

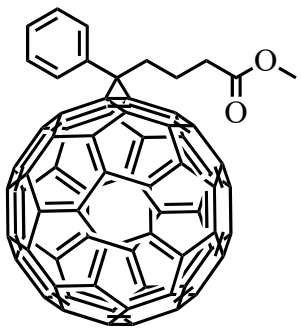


Figure 1-9: Chemical structure of $PC_{61}BM$.

We have chosen to synthesize non-fullerene small molecule acceptors based on the 1, 1'-binaphthalene core. Due to steric interaction between the protons in the 8, 8'- position, 1, 1'-

binaphthalene is inherently twisted with a torsional angle of about 90° (Figure 1-10). Therefore, it might be beneficial to active layer morphology as it may be able to prevent formation of large domains when blending with donor material. Furthermore, with suitable substituents in the 2 and 2' position, since binaphthalene is axially chiral we can potentially study the effect of relative ratio of each enantiomer on the morphology and device efficiency, which is an area that has not been well investigated.

The chirality of binaphthalene arises from atropisomerism, which is caused by hindered rotation about a single bond. The steric strain barrier to rotation is high enough to allow for isolation of individual conformer.

As for 1, 1'-binaphthalene, the rotation along the axial 1, 1'-bond is constrained. The corresponding two conformers were found to rotate plane polarized light in opposite directions. Therefore, two enantiomers are possible (R- and S-, Figure 1-11).

In chapter 2 and 3, the syntheses of different binaphthalene based acceptor series will be discussed along with the corresponding devices' performance.

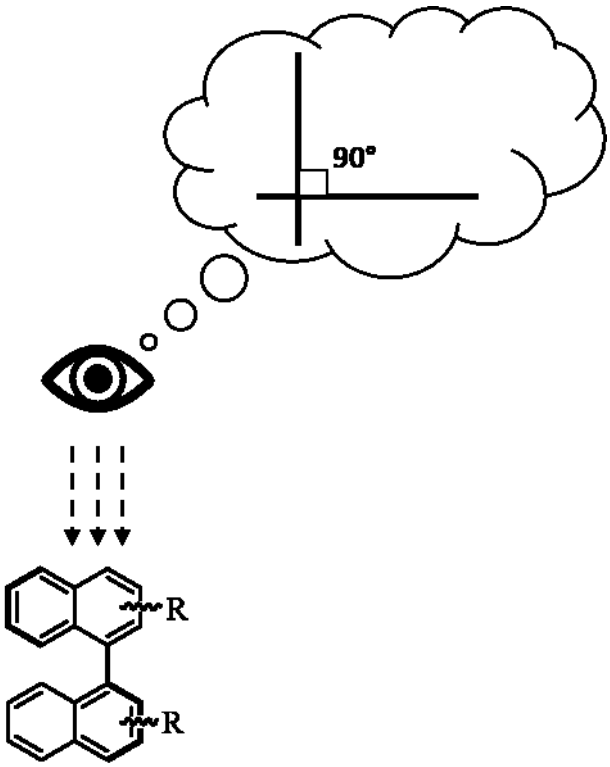
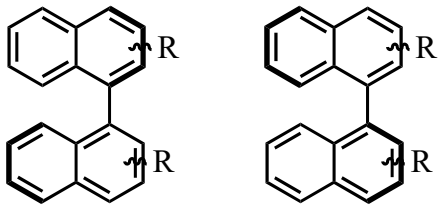


Figure 1-10: Viewing 1, 1'-binaphthalene from above shows it has approximately 90° torsional angle.



R-enantiomer S-enantiomer

Figure 1-11: Two axially chiral enantiomers of 1, 1'-binaphthyl.

1.3 Organic light-emitting diodes (OLEDs)

Fundamentally, organic light-emitting diodes work exactly opposite of how organic solar cells work. In organic solar cells, electrical current is generated after light absorption whereas for OLEDs, electrons and holes are injected into the material and recombine to give out light. More detailed explanations are given in the following sections.

1.3.1 Jablonski diagram

Figure 1-12 depicts three different electronic configurations in the ground and excited state. S_0 refers to singlet ground state where electrons are paired with each other with one spin up and one spin down. Promoting one electron to a higher energy level while maintaining the same spin state as before generates singlet excited state S_1. However, if the electron spin is reversed after excitation, it is known as a triplet excited state T_1.

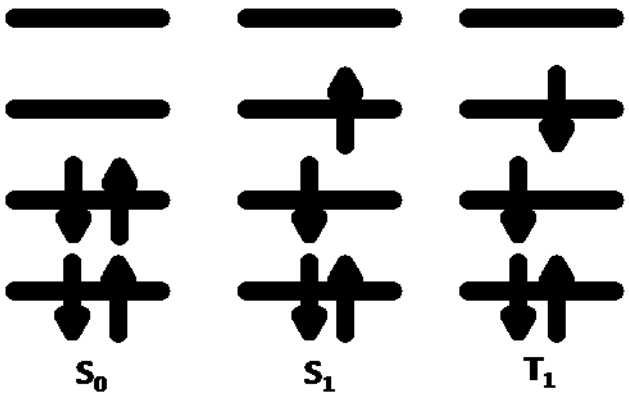


Figure 1-12: Electronic configuration in ground and excited states.

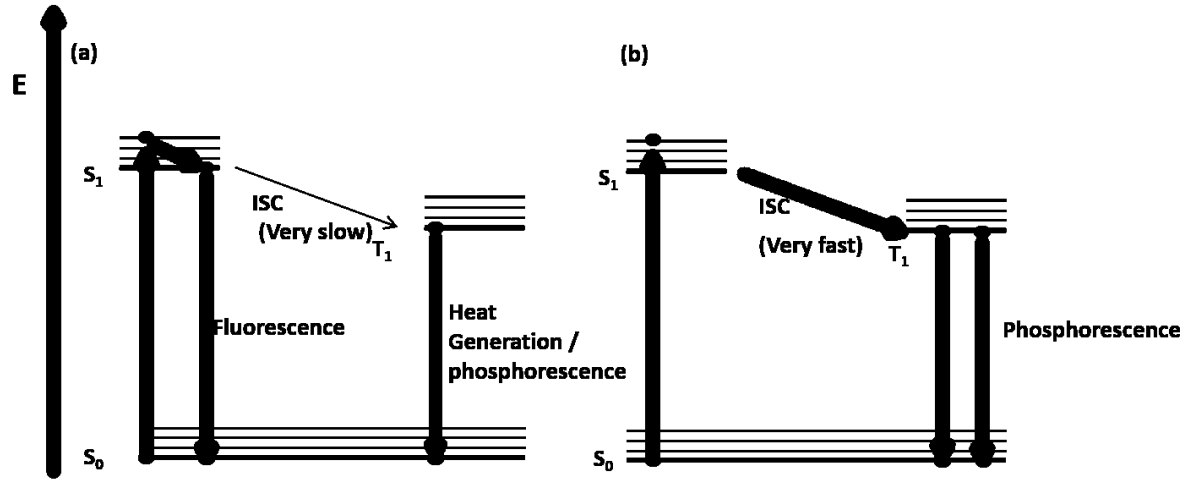


Figure 1-13: partial Jablonski diagram; a) fluorescent emission (singlet) and b) phosphorescent emission (triplet).

Fluorescence occurs when an electron decays back to the ground state S_0 from the singlet state S_1 with emission of a photon. Similarly, phosphorescence refers to photon emission from triplet to ground state (Figure 1-13). Phosphorescence has a much longer lifetime than fluorescence because transfer from T_1 to S_0 requires spin flip, which takes place over a long period of time, due to the Pauli exclusion principle. (Pauli exclusion principle states that any two fermions of the same type cannot occupy the same quantum state simultaneously).

T_1 is lower in energy compared to S_1, therefore phosphorescence emits light with a longer wavelength. Energy transfer from singlet to triplet (S_1 to T_1) state is known as inter-system crossing (ISC) and it is normally prohibited. However, such a rule can be broken if the phosphorescent emitting material has a heavy metal center, such as platinum or iridium, due to spin-orbit coupling.

1.3.2 Basic device architecture

Figure 1-14 depicts an example of OLED device architecture where on a glass substrate the emission layer is sandwiched between two electrodes. It is called emission layer because it is where electrons and holes are expected to recombine to emit photons.

Normally, other layers such as hole injection layer, electron transport layer are also incorporated using material suitable for each function to maximize device efficiency.

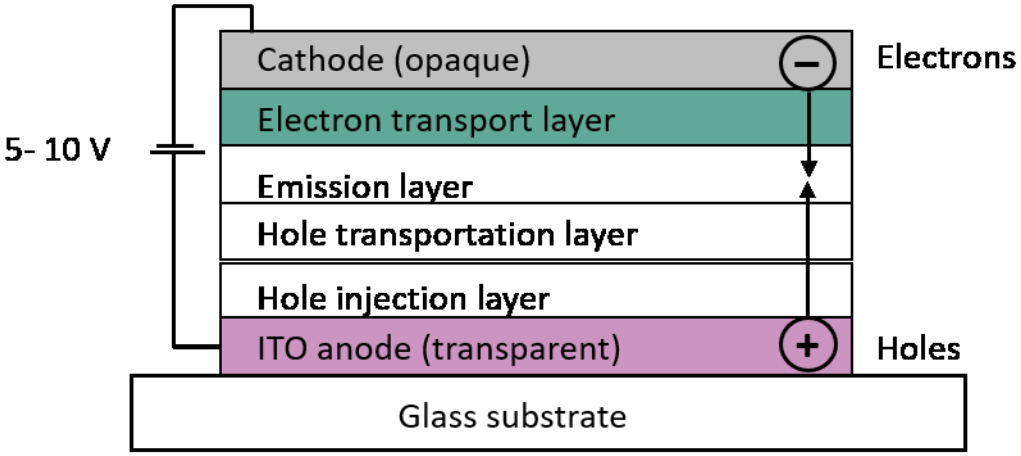


Figure 1-14: Basic device architecture of an OLED device.

1.3.3 Chiral emissive OLEDs

Photons are uncharged, massless and have spin number of 1. Each photon has two circular polarization states, left and right-circular polarization.[9–11]

In the right-circular polarization state, photons propagate as clockwise helices. Photons in the left-circular polarization state, they propagate as anti-clockwise helices.[9–11] The clockwise/ anti-clockwise helical propagation mode has chiral character. Therefore, it offers a beam of light chirality. This forms the basis of chiral optics.[12–16]

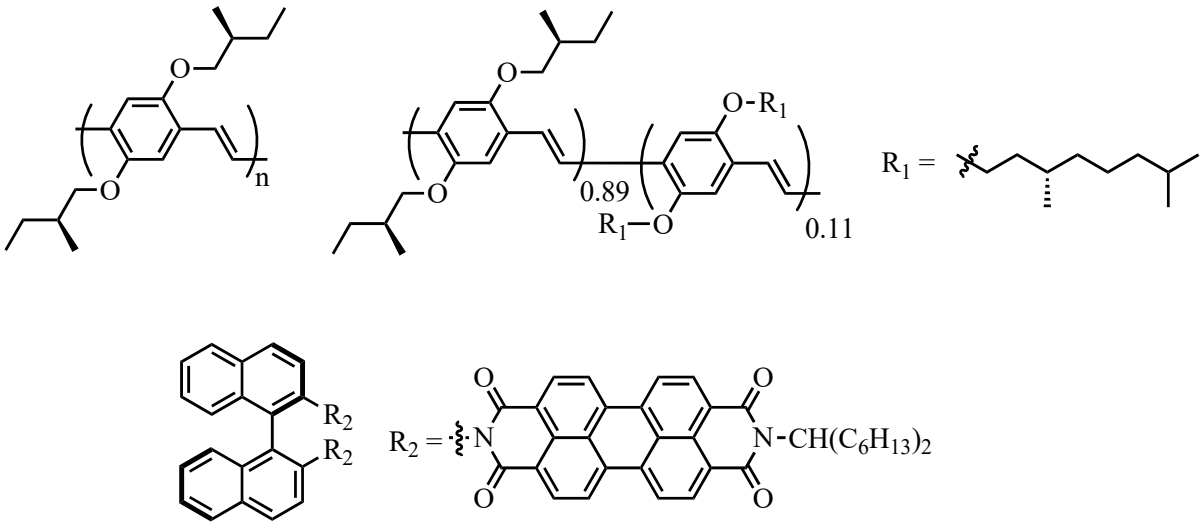


Figure 1-15: Examples of organic CPL emitters.

The emission of right- or left-circularly polarized light by any chiral non-racemic luminescent systems is known as circularly polarized luminescence (CPL).[12–16]

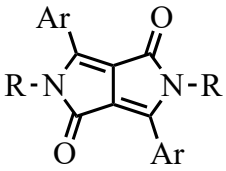
Figure 1-15 depicts a few examples of organic CPL emitters.[17,18] One common feature among all of them is that they all contain either chiral side chain or chiral chromophores in their structures.

Circularly polarized luminescence (CPL) has attracted great attention and interest due to its potential applications in many different aspects. For example, in three-dimensional displays[19] where circularly polarized light gives better resolution; in spintronic based devices for communication of spin information;[20] in bio-responsive imaging[21] and in the development of more efficient LCDs[19] and OLEDs.[22]

As for our project, since binaphthyl is chiral, we thought it would be interesting to synthesize a few chiral emissive binaphthyl based polymers for organic light-emitting diode (OLED) application. This is further discussed in Chapter 4.

2. The Synthesis of Diketopyrrolopyrrole Flanked 1,1'-Binaphthyl Materials

2.1 Overview



R = H, alkyl, aryl, acyl
Ar = aryl or heteroaryl

Figure 2-1: General structure of DPPs.

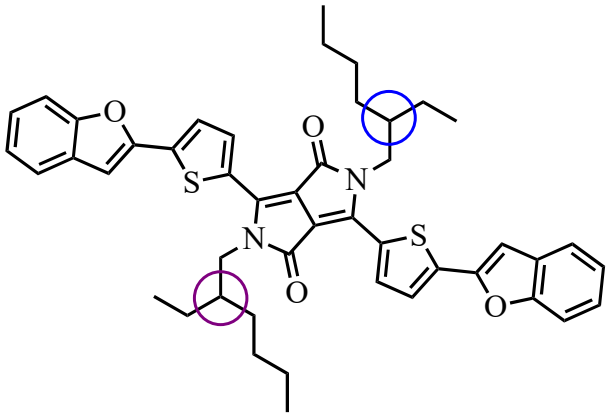


Figure 2-2: Chemical structure of DPP(TBFu)$_2$ with two chiral carbons circled.

Diketopyrrolopyrroles (DPPs) are a group of organic pigments discovered in the early 70s.[23] They are commonly employed as pigments in paints, varnish and are used in high quality printing[24–28] due to their intense colour, excellent stability, low solubility and simple synthesis. They can be made soluble via N-functionalization, after which they show strong fluorescence with near unity quantum yield.[29–31] Depending on the nature of the sidechain, DPP can also

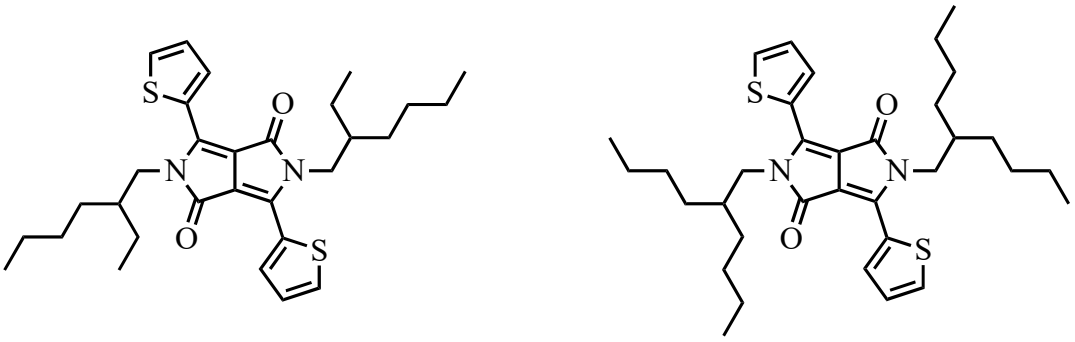
show a strong tendency to aggregate in the solid state with close intermolecular contacts and high charge carrier mobility. Because of these characteristics, DPP derivatives have been studied extensively in organic semiconducting applications, such as organic light emitting diodes (OLEDs), organic solar cells and organic field effect transistors (OFETs).[32–37]

As mentioned in order to make soluble and processable DPP derivatives, they must be functionalized with flexible sidechains. Typical sidechains include linear or branched alkyl sidechains, and the nature of the sidechain has an important influence on the assembly of the DPP in the solid state. Very large or bulky sidechains tend to suppress the aggregation of the DPP cores, whereas smaller or more linear sidechains can help to promote self-assembly. Many reported DPP derivatives utilize branched 2-ethylhexyl groups as the solubilizing sidechain. Although the solubilizing power is high, the 2-ethylhexyl group contains a chiral centre and the attachment of two such groups to the DPP core therefore potentially creates a mixture of different enantiomers. Surprisingly few studies have investigated this aspect, especially since different enantiomers might show different packing in the solid state.[38,39]

Initially Nguyen and co-workers[38] were able to separate the different enantiomers of a DPP containing p-type semiconductor. Three different isomers of compound DPP(TBFu)$_2$ (Figure 2-2) functionalised with two 2-ethylhexyl groups (R,R; S,S and meso (S,R and R,S)) were separated and their performance in thin-film transistors investigated. Interestingly the R,R- and S,S-enantiomers showed very similar crystal structures, thin-film morphologies and FET properties, while the mesomer exhibited different characteristics. According to their single-crystal structures, the meso isomer had a coplanar backbone favouring intermolecular $\pi - \pi$ stacking with a shorter $\pi - \pi$ distance. In contrast the chiral compounds (R,R - and S,S - isomers) exhibit twisted conjugated backbone with inferior intermolecular stacking and reduced FET performance. A later study by Castellano[39] synthesized similar DPP derivatives using enantiomerically enriched alkylating agents, allowing the preparation of single enantiomers. Such materials exhibited very similar optoelectronic properties in solution, but significantly different packing in the solid state.

Such studies clearly highlight that the presence of chiral centres can have an important role on the solid state properties of conjugated materials. In our approach, our target material also contained a binaphthyl core. Such a core has axial chirality due to the restricted rotation around the 1,1'-binaphthyl bond. Our initial target material utilized DPP functionalised with 2-ethylhexyl groups, but due to the presence of three potential chiral centres in this molecule, a

second target was designed using a symmetrical branched alkyl sidechain on the DPP (Figure 2-3). This affords a material with a single chiral centre, which should be simpler to prepare and/or separate.



DPP(EH) DPP(BH)

Figure 2-3: Chemical structures of DPP(EH) and DPP(BH).

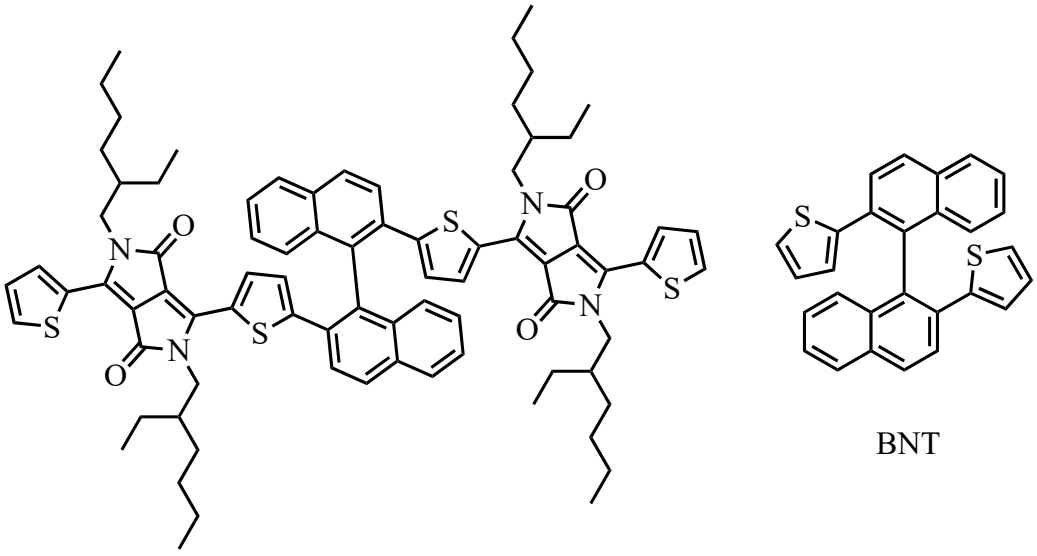
The binaphthyl core was chosen due to the twisted, cruciform shape it bestows on the target material. Materials with a twisted 3D geometry have been used to reduce intermolecular interactions and in solar cell blends have been shown to suppress the formation of large domains.[40–43] Such large domains are detrimental to solar cell performance, since they reduce interfacial area and therefore exciton harvesting.[44,45] Although such twisting can suppress large domains, it may have detrimental effects on intermolecular π-π stacking and thus charge transport ability of the acceptors in the blends.[46] In addition, the presence of the chiral centre is interesting for the possible emission (or detection)[47–49] of circularly polarised light, which has found applications in many different areas such as quantum computing,[50] asymmetric synthesis[51,52] and display technology.[19,22]

In this chapter, two different DPPs were synthesized (Figure 2-3) with different solubilizing sidechains. These were combined with a binaphthyl core for potential applications in OPVs and OLEDs. Section 2.2 focuses on the development of racemic binaphthyl-DPP(EH) series. Section 2.3 focuses on the development of enantioenriched binaphthyl and DPP(BH) based molecule.

2.2 Binaphthyl and DPP(EH) series

2.2.1 Synthesis

The first target molecule was BNDPP(EH) (Figure 2-4), in which two thiophene flanked DPP cores were attached to 2,2'-positions of a 1,1'-binaphthyl core. An obvious retrosynthetic strategy to such a material would be the addition of a suitably functionalized thienylDPP derivative to a dibromo binaphthyl derivative via some type of cross-coupling. Therefore, our initial work focused on the optimization of the cross-coupling reaction. Rather than using valuable DPP derivatives, the initial screening used simple thiophene to make the thienyl substituted binaphthyl BNT.



BNDPP(EH)

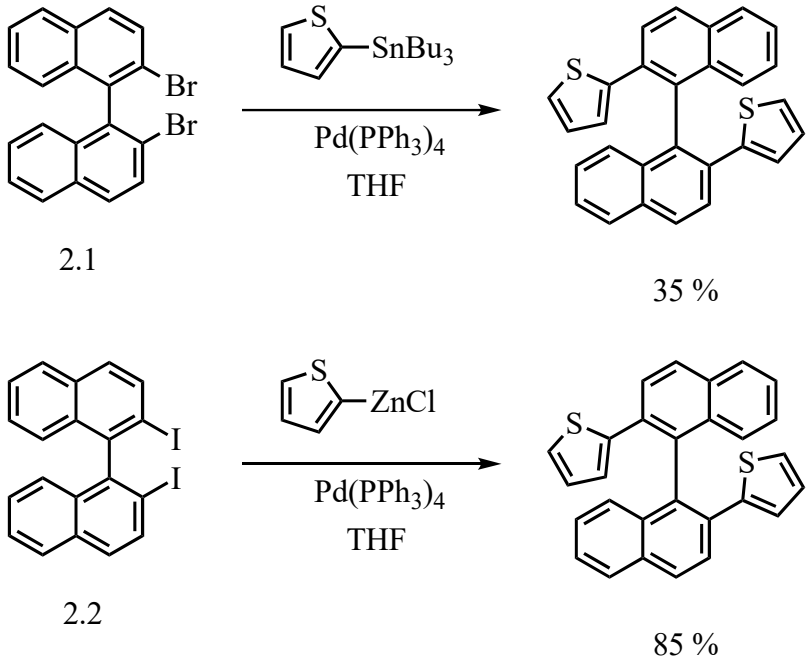
BNT

Figure 2-4: Chemical structures of BNDPP(EH) and BNT.

2.2.1.1 2,2'-Di(thiophen-2-yl)-1,1'-binaphthalene (BNT)

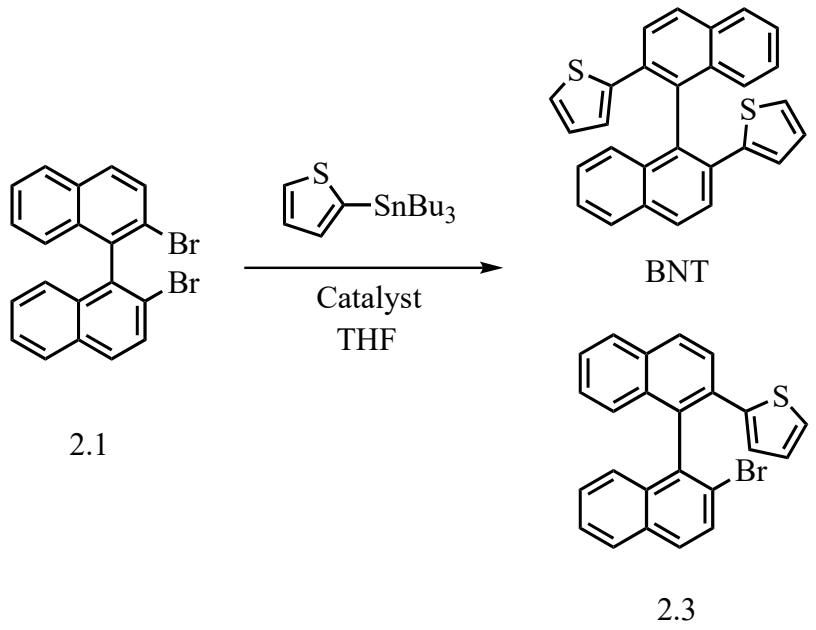
Following a thorough literature search, two methods[53,54] were found particularly interesting with regard to the synthesis of BNT, which was a known compound. The first approach[53] used toxic organo-tin based starting materials (Stille) with only 35 % yield, whereas the second approach[54] was the Negishi cross coupling utilizing the much safer thienyl-2-zinc chloride. This was reported to proceed in near quantitative yield (85 % for thermal reflux) (Scheme 2-1). Despite the better yield of the Negishi coupling, because the synthesis of BNT was used as

reference for the synthesis of BNDPP(EH) we still favoured the Stille route initially. This was because organozinc halides are normally prepared *in situ* and cannot be purified prior to use, whereas trialkyl tin derivatives are typically stable and can therefore usually be purified. Given we planned to use a thienyl flanked DPP as the organometallic partner, the potential to separate and purify a mono-substituted organotin reagent appeared advantageous. Therefore, given that the reported Stille was published more than fifteen years ago, and that more robust and functional new catalysts had been introduced since then, it would be sensible to re-optimize the reaction with different catalysts to try to improve the yield.



Scheme 2-1: Synthesis of BNT via Stille and Negishi approach with reported literature yields.

$Pd(dba)_2$ and PEPPSI-IPr were initially chosen for the reaction of commercially available 2-(tributylstannyl)thiophene with racemic 2,2'-dibromo-1,1'-binaphthyl. In particular the latter catalyst has reasonable air stableness with excellent reported reactivity.[55,56] However, after extended reaction in THF both catalysts only gave small amount of mono-substituted side product 2.3 (Scheme 2-2 and Table 2-1) with majority still being unreacted starting material. The steric bulkiness of the ligands and the butyl groups of the organo-tin compound maybe the reason for the slow reaction. It is also worth mentioning that the reported reaction using $Pd(PPh_3)_4$ was also repeated prior to trying with different catalysts. However, only 15 % isolated yield was obtained vs 35 % from the literature.



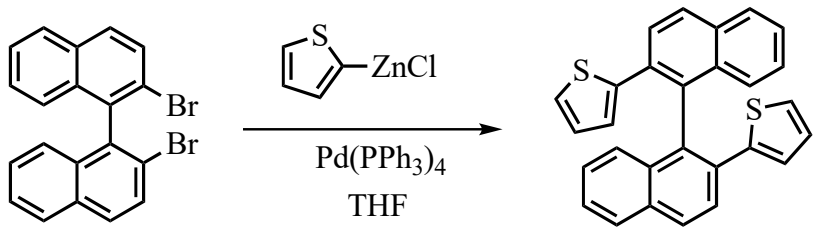
Scheme 2-2: Optimization of synthesis of BNT via Stille cross coupling with different catalysts.

Table 2-1: Results for the optimization of synthesis of BNT with different catalysts.

Catalyst	Ligand	Solvent	Additives	Yield / %
PEPPSI-IPr	---	Toluene	---	---
PEPPSI-IPr	---	Toluene	DMF; CuI	---
$Pd(dba)_2$	$P(Cy)_3$	Toluene	---	---

The reaction with $Pd(dba)_2$ was refluxed overnight whereas PEPPSI-IPr reactions were conducted at room temperature.

Given the slow reaction via attempted Stille cross coupling, the alternative Negishi cross coupling was attempted (Scheme 2-3 and Table 2-2). Initially the optimal catalyst loading of $Pd(PPh_3)_4$ was investigated, since in this project 2,2'-dibromo-1,1'-binaphthalene was used instead of 2,2'-diiodo-1,1'-binaphthalene (which the literature used). Three parallel reactions were run consecutively, each with 6 eq. of thienyl-2-zinc chloride, and with the only difference being the catalyst loading starting from 10 mol%. Hexadecane was also used as internal standard and the reactions were monitored by GC. GCMS analysis showed quantitative conversion in all cases suggesting 5 mol% $Pd(PPh_3)_4$ should be enough for the purpose (Table 2-2).



2.1 BNT

Scheme 2-3: Optimization of synthesis of BNT via Negishi cross coupling.

Table 2-2: Different catalyst loading attempted for the synthesis of BNT via Negishi cross coupling.

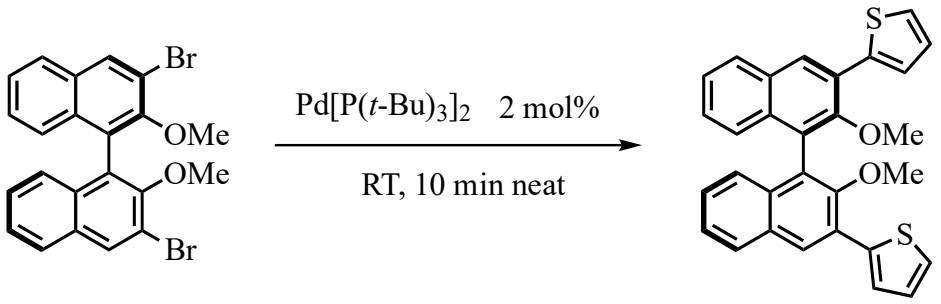
$Pd(PPh_3)_4$ / mol%	GCMS yield [a]
5	Quantitative
7.5	Quantitative
10	Quantitative

[a] Measured against hexadecane as internal standard. All the parallel reactions were conducted with 100 mg of 2,2'-dibromo-1,1'-binaphthalene and 6 eq. of 2-thienylzinc chloride under reflux of THF for two days.

Having established the optimal 5 mol% catalyst loading, the amount of the 2-thienylzinc chloride was subsequently investigated. Four parallel reactions were investigated with 3, 4, 5 and 6 equivalents of thienyl-2-zinc chloride. Only the reaction with 6 equivalents showed a full conversion to the desired product, and those with lower loadings all contained some of the mono-substituted side product 2.3. Based on those results, the optimal reaction conditions were established and extended to a much larger scale using 1 g and 5 g of starting material. Both reactions achieved near quantitative yield of BNT.

Just as the optimization for the synthesis of BNT was completed, an interesting piece of literature was published, in which Feringa et al[57] synthesized (R)-2,2'-(2,2'-dimethoxy-[1,1'-binaphthalene]-3,3'-diyl)dithiophene (2.5) by direct coupling between 2-thienyllithium and (R)-3,3'-dibromo-2,2'-dimethoxy-1,1'-binaphthalene (2.4) in neat condition (i.e. no solvent) with 81 % yield (Scheme 2-4).

This synthetic method was intriguing and could avoid the use of expensive thienyl-2-zinc chloride. Therefore, this method was also investigated for the preparation of BNT.



2.4 2.5

Scheme 2-4: Synthesis of 2.5 by direct coupling between 2-thienyllithium and 2.4 without solvent.

Table 2-3: Synthesis of BNT via direct coupling between 2.1 and 2-thienyl lithium.

Catalyst	Catalyst loading / mol%	Reaction time	BNT	Mono-coupled product 2.3	Starting material
$Pd(PPh_3)_4$	5	3 days	n/a	✓	✓
$Pd(PPh_3)_4$	10	Overnight	n/a	✓	✓
$Pd(PPh_3)_4$	15	Overnight	n/a	✓	✓
PEPPSI-IPr	5	Overnight	n/a	✓	✓
PEPPSI-IPr	10	Overnight	n/a	✓	✓
$Pd(dppf)Cl_2$	5	Overnight	n/a		✓
$Pd(t\text{-}Bu_3P)_2$	2	Overnight	n/a		✓
$Pd(t\text{-}Bu_3P)_2$	5	Overnight	n/a		✓
$Pd(t\text{-}Bu_3P)_2$	10	Overnight	n/a		✓

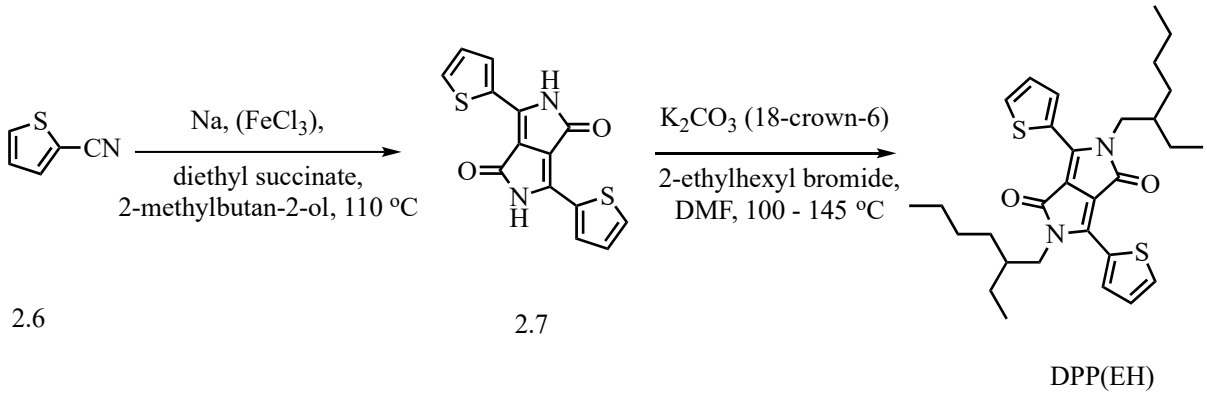
All the reactions were carried out at room temperature in neat condition.

Four different catalysts, $Pd(PPh_3)_4$, PEPPSI-IPr, $Pd(dppf)Cl_2$ and $Pd(t\text{-}Bu_3P)_2$ were tested for the direct coupling between 2.1 and 2-thienyl lithium. $Pd(PPh_3)_4$ (entry 1, 2, 3, Table 2-3) and PEPPSI-IPr (entry 4, 5, Table 2-3) showed some sort of reactivity as their corresponding TLCs showed the mono-coupled product 2.3. However, none of the desired product was observed, and varying the corresponding catalyst loadings did not alter the outcome. Whereas for other catalysts including $Pd(t\text{-}Bu_3P)_2$, only starting material was observed after reaction. This was surprising since $Pd(t\text{-}Bu_3P)_2$ was the catalyst that worked so well in the published study.[57]

Possibly because three tert-butyl groups are sterically too bulky for oxidative addition to happen at the 2,2'-positions of the binaphthyl.

To conclude, the synthesis of BNT was successfully optimized via Negishi approach. With 5 mol% $Pd(PPh_3)_4$, 6 equivalents of 2-thienylzinc chloride and 2 days of reflux in THF, quantitative yields of BNT can be obtained.

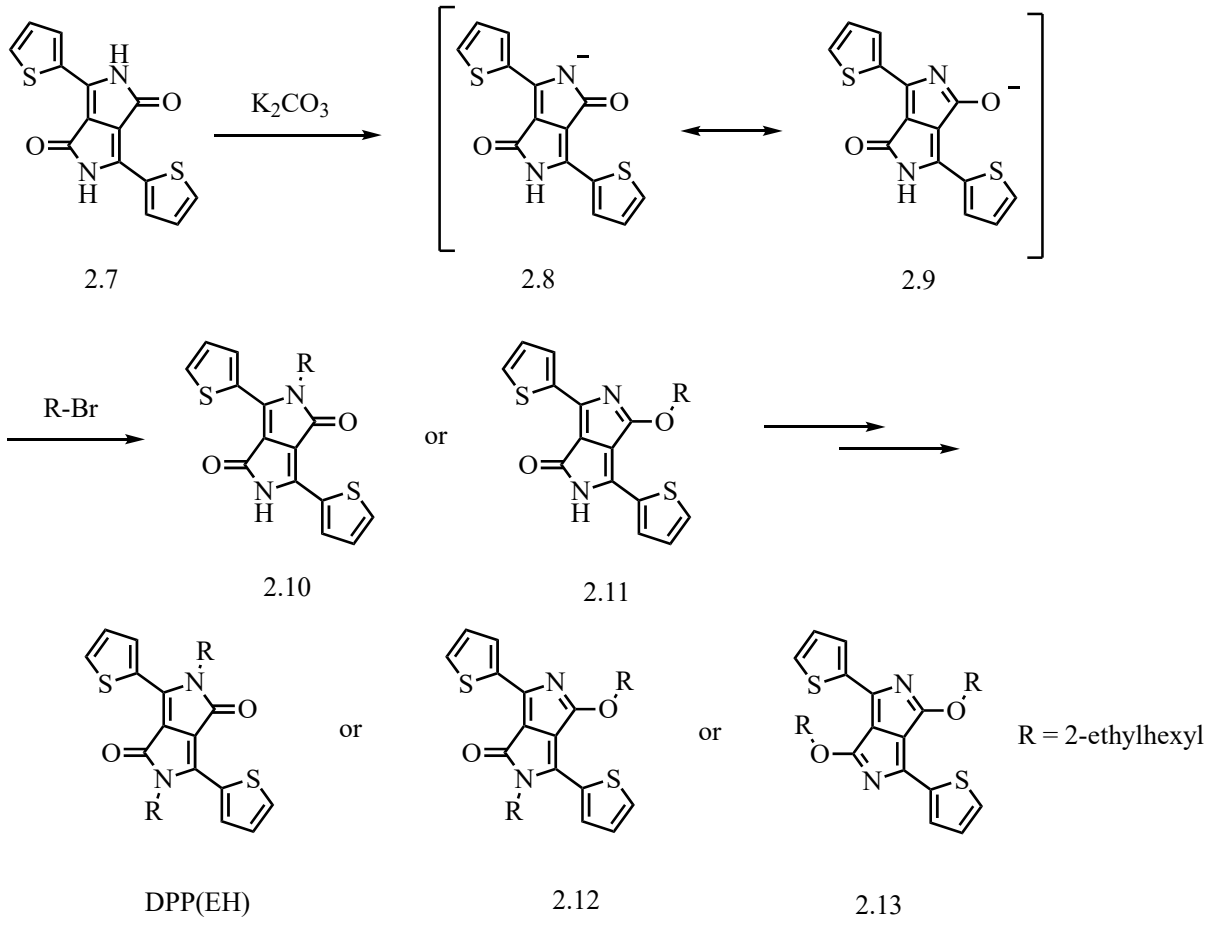
2.2.1.2 2,5-Bis(2-ethylhexyl)-3,6-di(thiophen-2-yl)-2,5-dihydropyrrolo[3,4-c]pyrrole-1,4-dione {DPP(EH)}



Scheme 2-5: Synthetic route towards DPP(EH) from thiophene-2-carbonitrile.

DPP(EH) was synthesized via a two-step synthesis (Scheme 2-5) starting from 2-cyanothiophene. For the synthesis of 2.7, when dissolving sodium in 2-methylbutan-2-ol, some literature[58–60] added a trace amount of $FeCl_3$, whilst some[61,62] did not. Both reactions with/without $FeCl_3$ were investigated and the addition of $FeCl_3$ was favoured since it significantly reduced sodium dissolution time. This is possibly because sodium is very reactive and it instantly interacts with moist in the air to form a sodium hydroxide layer when taken out of storage container, whereas addition of $FeCl_3$ helps with dissolution by interacting with the protective layer and exposing the underneath reactive elemental sodium. It is worth mentioning that reactions with/without $FeCl_3$ gave similar yield. The crude DPP (2.7) was very poorly soluble in common solvents due to a lack of solubilizing group. The literature[58,59,61,62] advised purification by washing the crude compound with lots of hot methanol until a colourless filtrate was observed. However, based on our practical experience we found that it was impossible to

obtain colourless filtrate, and the crude product was used once the majority of the coloured by-products were removed.



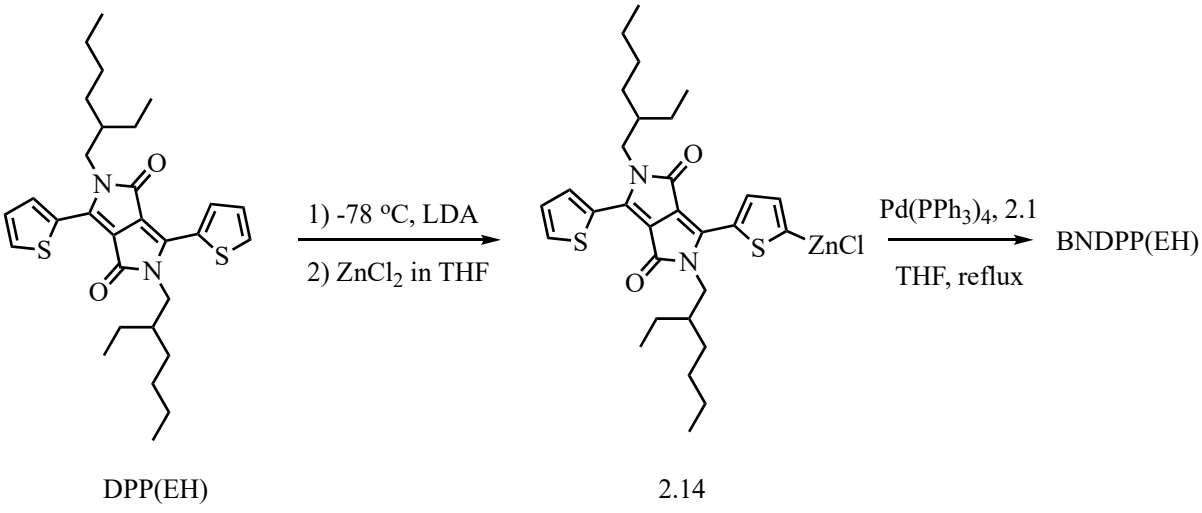
Scheme 2-6: Proposed mechanism for the synthesis of DPP(EH).

As for the synthesis of DPP(EH), the weak base potassium carbonate was used to deprotonate the crude DPP (2.7) (Scheme 2-6). The nucleophilic amide anion then attacks the 2-ethylhexyl bromide, possibly via S_N2, to produce the product. Some literature[62,63] also added a trace amount of 18-crown-6 during the reaction, to encapsulate the potassium ion to enhance the basicity of carbonate and nucleophilicity of the amide. As for this project, both syntheses with/without 18-crown-6 were tested and no significant difference on the final yield was observed.

Scheme 2-6 shows the proposed mechanism for the formation of DPP(EH), along with two possible side products 2.12 and 2.13, which are formed due to the resonance between intermediates 2.8 and 2.9.

For the reaction quench and work-up, two different approaches were tried. Method 1[61] involved quenching the crude with ice/water solution before extraction with DCM, then the combined organic phases were washed with plenty of water to remove residual DMF followed by drying with brine and Na_2SO_4. Method 2[63] involved pouring the cooled crude mixture into a large amount of distilled water, followed by stirring for 1 h and vacuum filtration. The solid was washed with water and methanol to remove residual DMF and water before drying under vacuum. After having tried out both methods, which offered similar yield, method 2 was strongly favoured as extracting DMF with water in method 1 proving to be laborious and difficult, especially on a large scale. In both cases the resulting crude products were purified by column chromatography. The desired product eluted second, with some of 2.12 and 2.13 observed at lower and higher Rf values in agreement with the literature.[64,65] The desired product was isolated with an average 30 % yield.

2.2.1.3 6,6'-([1,1'-Binaphthalene]-2,2'-diylbis(thiophene-5,2-diyl))bis(2,5-bis(2-ethylhexyl)-3-(thiophen-2-yl)-2,5-dihydropyrrolo[3,4-c]pyrrole-1,4-dione) {BNDPP(EH)}



Scheme 2-7: Synthesis of BNDPP(EH) via Negishi cross coupling.

The first attempt for the synthesis of BNDPP(EH) was conducted based on the already optimized reaction condition for the synthesis of BNT. Thus 2.14 (Scheme 2-7) was made *in*

situ by lithiating DPP(EH) with one equivalent of LDA at low temperature, followed by the addition of $ZnCl_2$ solution. To the resulting solution, $Pd(PPh_3)_4$ and 2.1 were subsequently added and the resulting mixture was refluxed for 2 days (although it was noted that no change in the TLC was observed after overnight reflux). The subsequent work-up and purification by column chromatography gave the desired product with only 5 % isolated yield (entry 1, Table 2-4). It is worth mentioning that substantial amounts of homo-coupled DPP(EH) (72 mg vs 17 mg of the desired product) were also isolated along with the major side product, which was mono-coupled product with one unreacted bromine, DPP(EH) and 2.1. The low yield was disappointing, but could be explained by several reasons:

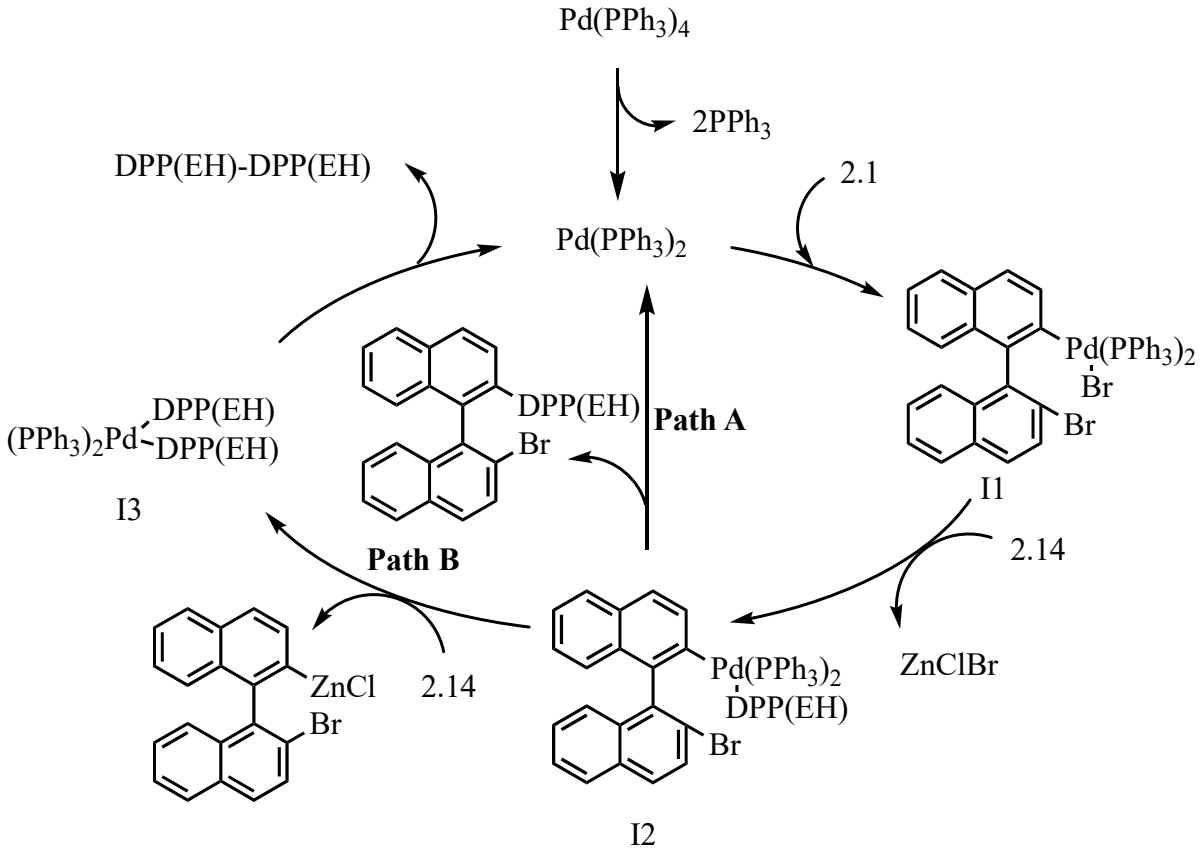
1. Both LDA and the resulting organozinc reagents are susceptible to hydrolysis by water. They were synthesized *in situ* and it was difficult to monitor their successful formation.
2. If organozinc formation proceeded without problem, sterically it was very demanding to incorporate two DPP(EH) units at the 2,2'-positions of binaphthyl.
3. Since there is significant amount of homo coupled DPP(EH), it suggests a competing path (Path B) was happening along the desired path (Path A), where I2 could potentially undergo ligand exchange with 2.14 to form I3, followed by reductive elimination to produce homo coupled DPP(EH) (Scheme 2-8).[66]

To try to tackle problem 3, 2.14 was lowered to 3 equivalents while maintaining the same catalyst loading (entry 2, Table 2-4). This was hoped to reduce the presence of excess organozinc chloride. However, the result was like previous with just 4 % isolated yield for the desired product. This also suggested that the formation of 2.14 was less likely to be the cause for the low yield (i.e. problem 1 on the list). Further optimization with increased catalyst loading yielded no improvement in the final yield (entry 3).

Table 2-4: First set of optimizations for the synthesis of BNDPP(EH).

2.14 / eq.	$Pd(PPh_3)_4$ / mol%	Time	Yield / %
6	5	2 days	5
3	5	Overnight	4
3	7.5	Overnight	4

All the reactions were refluxed in THF under inert atmosphere with 100 mg of 2,2'-dibromo-1,1'binaphthyl.

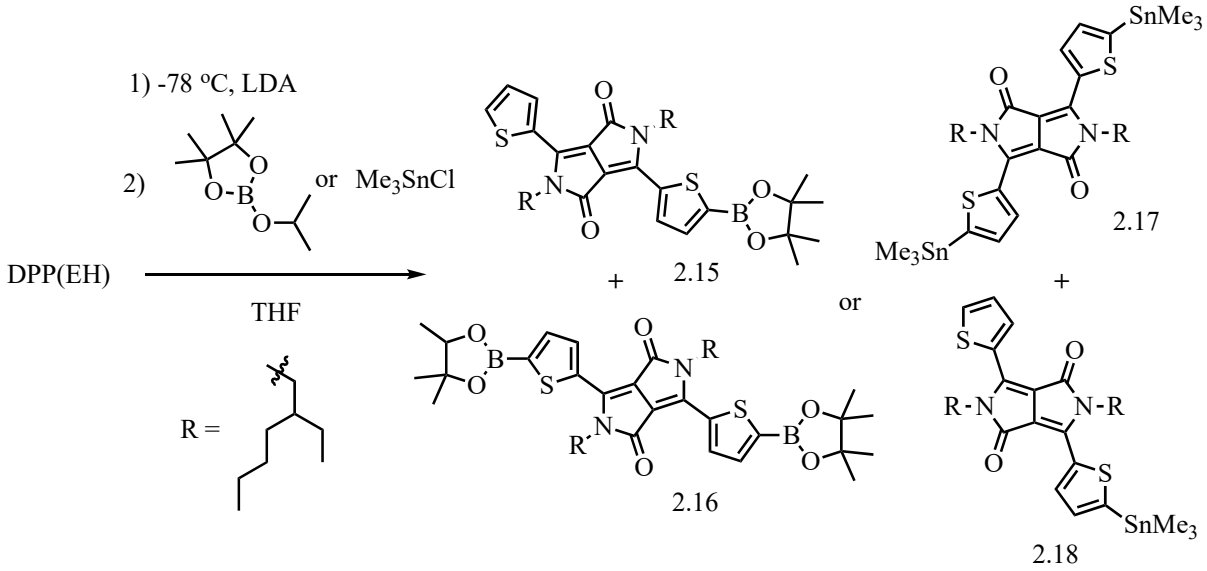


Scheme 2-8: Formation of mono-coupled product with one unreacted bromine and homo-coupled DPP(EH).

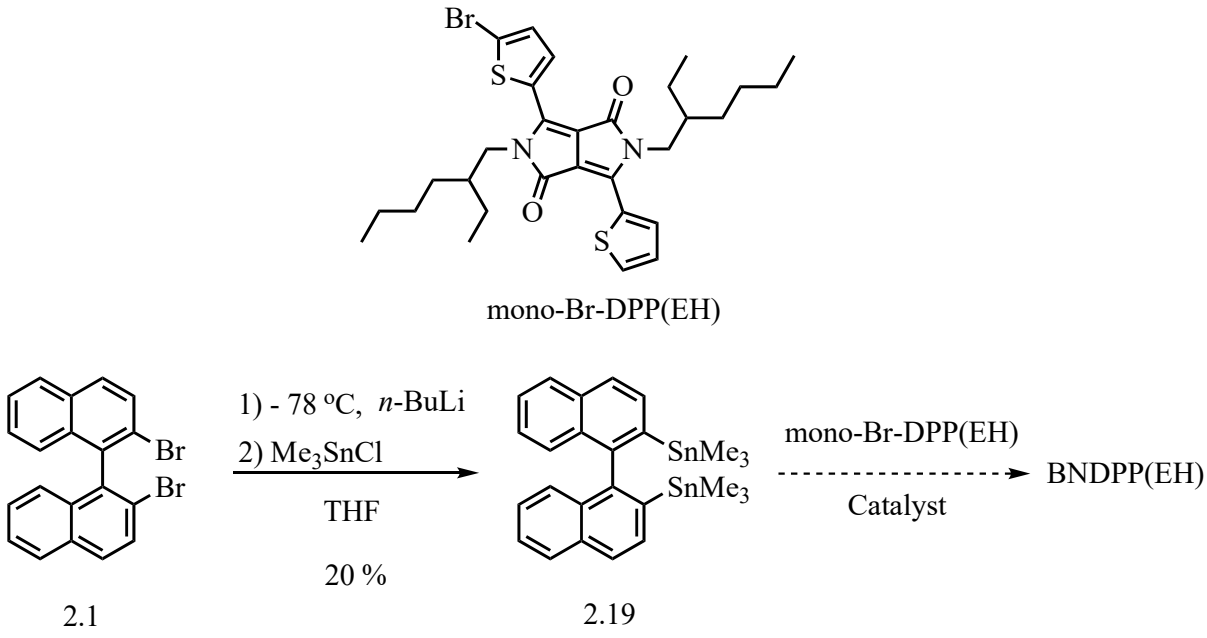
In case the problem was due to low yields of the formation of 2.14 the syntheses of 2.15 and 2.18 was attempted (Scheme 2-9). Both the boronic ester and trimethyl tin derivatives should be air-stable and therefore could potentially be purified by chromatographic methods. Interestingly treatment with one equivalent of LDA under identical conditions to the formation of the organozinc reagent, followed by the addition of either trimethyltin chloride or 2-isopropoxy-4,4,5,5-tetramethyl-1,3,2-dioxaborolane afforded a mixture of mono and disubstituted products, together with some unreacted starting material. This suggested that a similar mixture of organozinc reagents were also formed, which could also reduce yield. In the case of the boronic ester and organotin compounds, our attempts to separate the desired mono-coupled product by silica gel column chromatography were unsuccessful, as it was found that the C-B and C-Sn bonds cleaved on the column. At that time, there was no preparative GPC available in the group.

Due to these difficulties, it was decided to investigate the alternative cross-coupling in which the organometallic derivative was included on the binaphthyl component. Thus 2.19 was synthesized with 20 % yield (Scheme 2-10) by treatment of 2,2'-dibromo-1,1'-binaphthyl with

four equivalents of *n*-BuLi followed by trapping with trimethyltin chloride. After work-up, it was found that 2.19 was reasonably stable on silica and it could be isolated via flash chromatography. However, the synthesis was not continued as the overall yield was low and the high toxicity of trimethyl tin was a concern. At this stage, it was decided to investigate a second target compound.

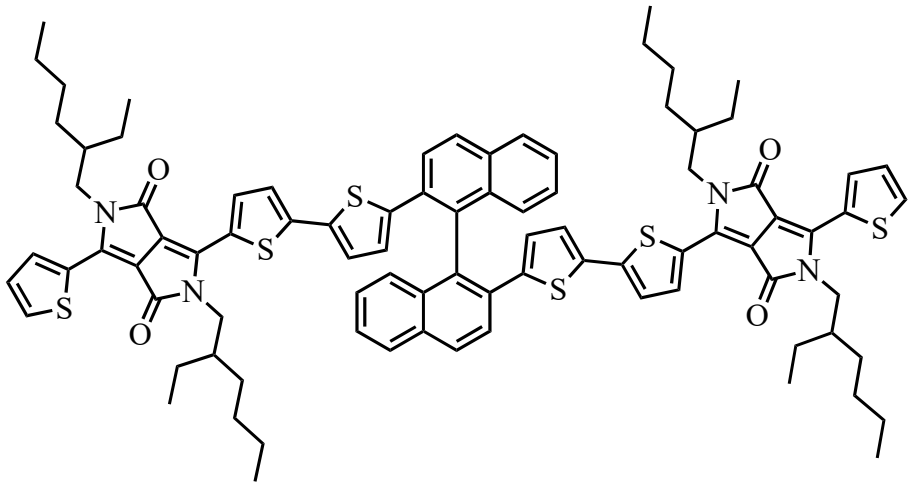


Scheme 2-9: Attempted mono-functionalization of DPP(EH) with trimethyl tin chloride and 2-isopropoxy-4,4,5,5-tetramethyl-1,3,2-dioxaborolane.



Scheme 2-10: Attempted synthesis of BNDPP(EH) via Stille cross coupling, the synthesis was stopped after the synthesis of 2.19.

2.2.1.4 6,6'-([1,1'-Binaphthalene]-2,2'-diylbis([2,2'-bithiophene]-5',5-diyl))bis(2,5-bis(2-ethylhexyl)-3-(thiophen-2-yl)-2,5-dihydropyrrolo[3,4-c]pyrrole-1,4-dione) {BNTDPP(EH)}



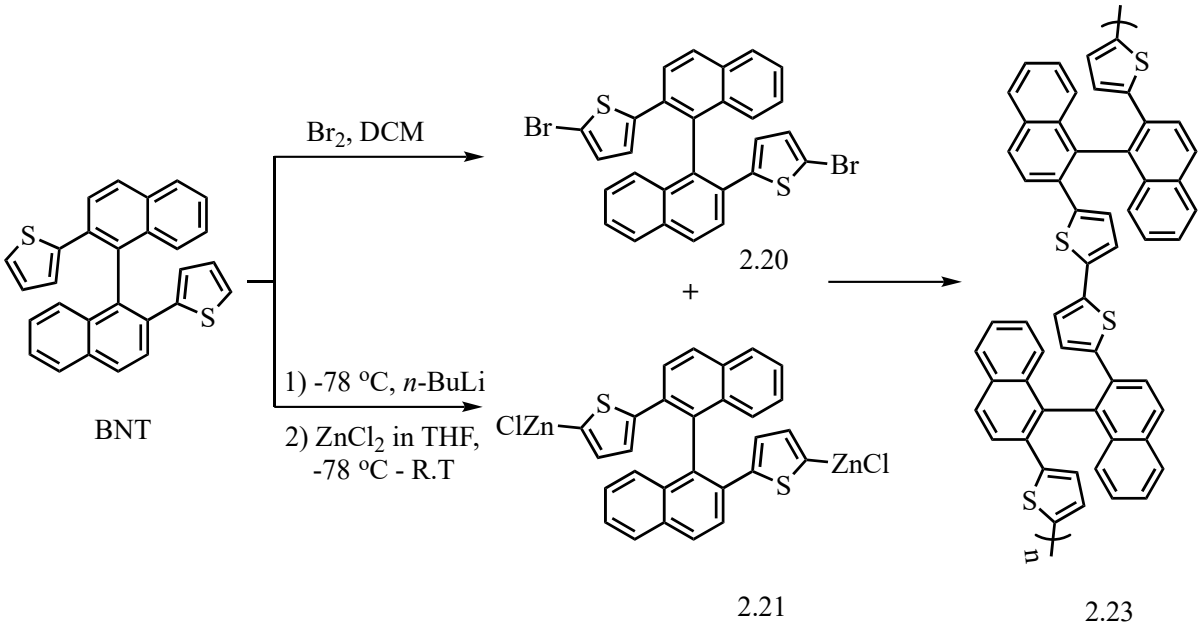
BNTDPP(EH)

Figure 2-5: Chemical structure of BNTDPP(EH).

At this point it was apparent that direct cross-coupling of 2,2'-dibromo-1,1'-binaphthyl with any DPP derivative was problematic, but we had established a successful protocol to the preparation of the thienyl functionalized binaphthyl compound BNT. This appeared to be a good candidate for further functionalization, since the thienyl group should be easy to functionalize in the alpha position. Subsequent cross-coupling with DPP was envisaged to be less problematic, since the steric environment at this position should be less crowded. Therefore, a new target material with an additional thiophene spacer, BNTDPP(EH) (Figure 2-5) was focused upon.

In terms of synthetic strategy, Li et al. published a paper where binaphthyl based conjugated polymer 2.23 was synthesized via Negishi polymerization (Scheme 2-11).[53] His synthesis of organozinc reagent 2.21 was therefore adopted for the synthesis of BNTDPP(EH). Such an approach required the mono-bromination of DPP(EH). This was successfully achieved in 44 % yield by the treatment of DPP(EH) with one equivalent of NBS. The resulting crude compound

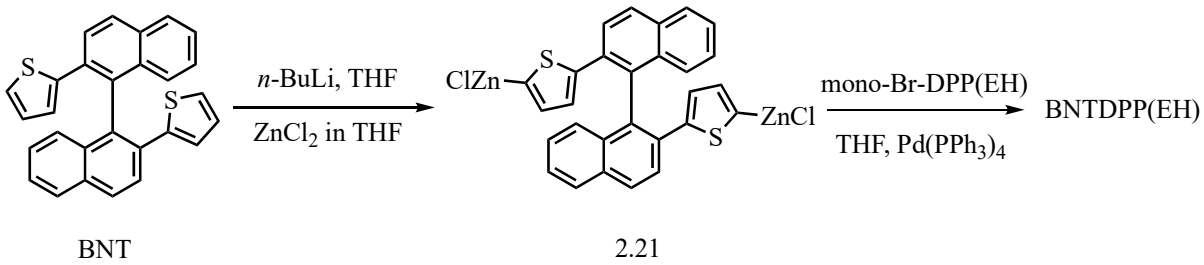
was a mixture of mono- and dibromo-DPP(EH), with some unreacted starting material and was purified by column chromatography using hexane and DCM as eluent.



Scheme 2-11: Synthesis of binaphthalene based conjugated polymer 2.23 via Negishi polymerisation.

The synthetic route for the synthesis of BNTDPP(EH) is shown in Scheme 2-12, and Table 2-5 illustrates the optimizations conducted. The first optimization (entry 1, Table 2-5) followed the exact same literature[53] method for the synthesis of 2.21, with 5 mol% $Pd(PPh_3)_4$ and 6 equivalents of mono-Br-DPP(EH) as coupling partner. After work-up and purification by column chromatography an encouraging yield of 14 % was found. Increasing the catalyst loading up to 15 mol% did not improve yield (entry 2 and 3). Because 2.21 was synthesized *in situ* and its formation could not be monitored quantitatively, the amount of *n*-BuLi and $ZnCl_2$ were increased substantially to ensure 2.21 was not the limiting factor (entry 4). However, the resulting yield (19 %) remained more or less the same.

As an alternative, the reaction with reversed polarity was also investigated (Scheme 2-13). Thus, BNT was readily brominated in the alpha positions by treatment with bromine. Reaction of the resulting 2.20 with six equivalents of the organozinc derivative of DPP (2.14) with 5 mol% $Pd(PPh_3)_4$ afforded 15 % yield, which was similar to the previous approach. It appears that incorporation of the spacing thiophene unit has helped relieve steric hindrance to a certain extent around the binaphthyl core since the yield improved (vs. 5 % for BNDPP(EH)).



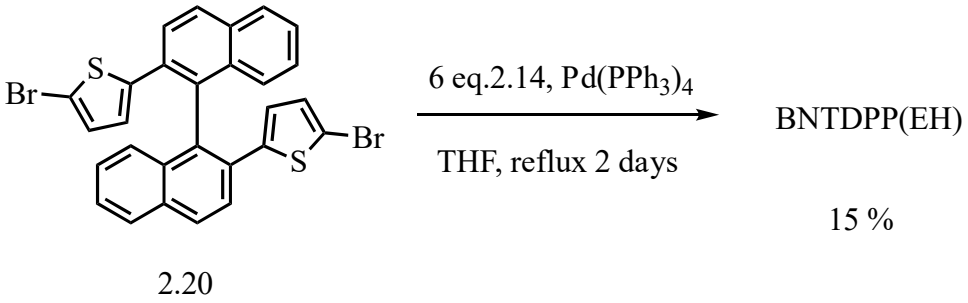
BNT 2.21

Scheme 2-12: Proposed synthetic route for the synthesis of BNTDPP(EH) via Negishi cross coupling.

Table 2-5: Optimization of synthesis of BNTDPP(EH) via Negishi cross coupling.

n-BuLi / eq.	$ZnCl_2$ in THF / eq.	$Pd(PPh_3)_4$ / mol%	Yield / %
3	4	5	14
3	4	10	15
3	4	15	12
6	8	15	19

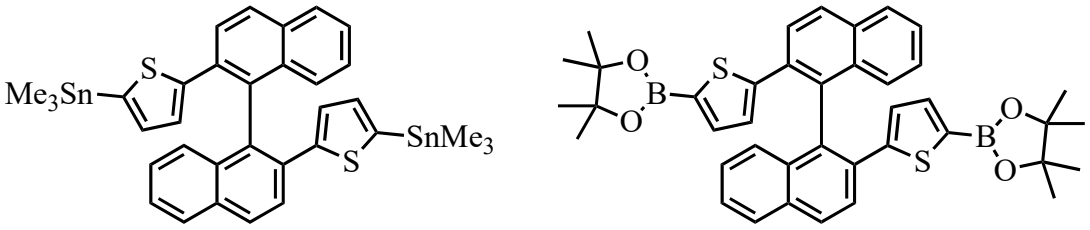
All the reactions were conducted with 6 eq. of mono-Br-DPP(EH) under reflux for 2 days with isolated yield.



2.20

Scheme 2-13: Reversing polarity between 2.21 and mono-Br-DPP(EH) for the synthesis of BNTDPP(EH).

Aside from the Negishi approach, the syntheses of 2.24 and 2.25 (Figure 2-6) were also attempted via the dilithiation and quenching with trimethyltin chloride and 2-isopropoxy-4,4,5,5-tetramethyl-1,3,2-dioxaborolane respectively. Although the crude products appeared to be predominately the desired products, attempts to purify them by column chromatography also failed for the same reason as that for 2.15 and 2.18, cleavage of the organometallic group.



2.24 2.25

Figure 2-6: Bi-functionalization of BNT with trimethyl tin (2.24) and boronic ester (2.25).

On that note and to conclude, BNTDPP(EH) was successfully synthesized via Negishi cross coupling with slightly better yield (around 15 %) than BNDPP(EH) (5 %).

2.2.2 Optoelectronic & Thermal Properties

2.2.2.1 Ultraviolet-visible Spectroscopy (UV-Vis) & Cyclic Voltammetry (CV)

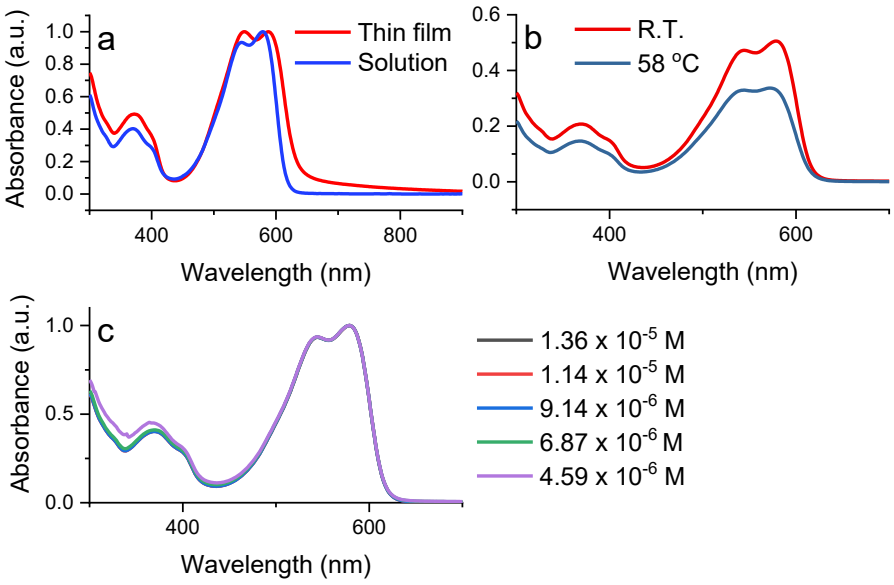


Figure 2-7: UV-Vis of BNDPP(EH): a) normalized thin film and solution ($CHCl_3$) UV-Vis at R.T.; b) solution ($CHCl_3$) UV-Vis at R.T and 58 °C of the same concentration; c) normalized solution ($CHCl_3$) UV-Vis at R.T. with various concentrations.

The UV-Vis absorption spectra of BNDPP(EH) (Figure 2-7) show a doublet type peak around 570 nm, similar to that for many DPP-containing molecules. The two longer wavelength peaks (ca 540, 580 nm) are ascribed to vibronic transitions, commonly referred as 0 – 0 (ca. 580 nm) and 0 – 1 (ca. 540 nm) transitions, with different relative ratios depending on the type of aggregate (for example *H* or *J* type aggregates). When the relative intensity of 0 – 0 over 0 – 1 is greater than 1, *J* type aggregation is favored, whereas a less than unity ratio indicates *H* aggregation is favoured.[67] As for BNDPP(EH), the relative ratio of the vibronic peaks are greater than 1, indicating *J* type aggregation is favored. However, upon film formation, the relative ratio became close to unity. This is tentatively attributed to the coexistence of both *J* and *H* type aggregates (Figure 2-7 a). Furthermore, the thin film absorption is slightly red-shifted (9 nm) (Table 2-6), suggestive of increased intermolecular contacts and ordering. Varying concentration does not change the relative ratio of the two vibronic peaks (Figure 2-7 c), indicative of predominant *J* aggregates in all solution concentration. Additional evidence of BNDPP(EH) *J* aggregates in solution came from temperature controlled UV-Vis spectroscopy study where upon increasing the temperature of the same solution, the relative intensity of the two vibronic peaks changes significantly, with the 580 nm peak becoming less pronounced (Figure 2-7 b), whereas if *H* type aggregate was favoured, it would have the similar relative ratio throughout despite changing in temperature.[68]

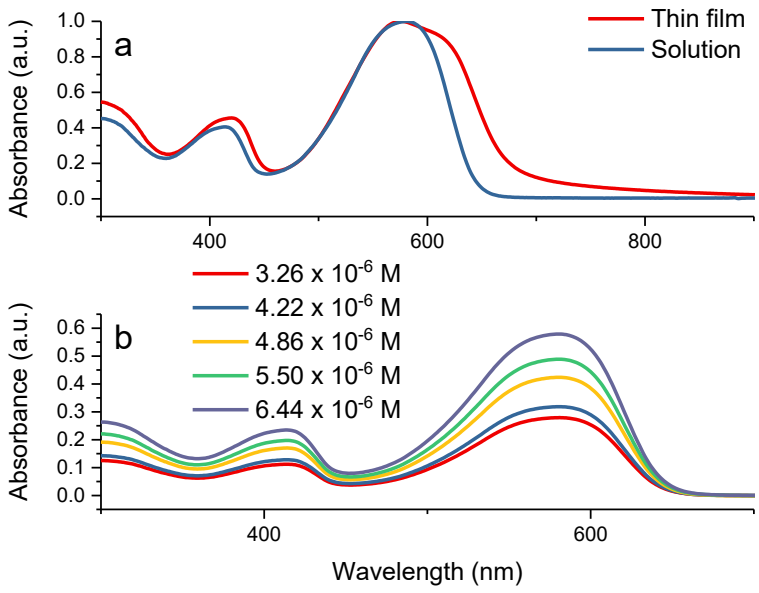


Figure 2-8: UV-Vis absorption spectra of BNTDPP(EH): a) normalized absorption of thin film vs solution ($CHCl_3$); b) various concentrations in $CHCl_3$ at R.T.

Like that of BNDPP(EH), the thin film UV-Vis absorption spectrum of BNTDPP(EH) is also red-shifted compared to its solution spectrum (Figure 2-8 a).

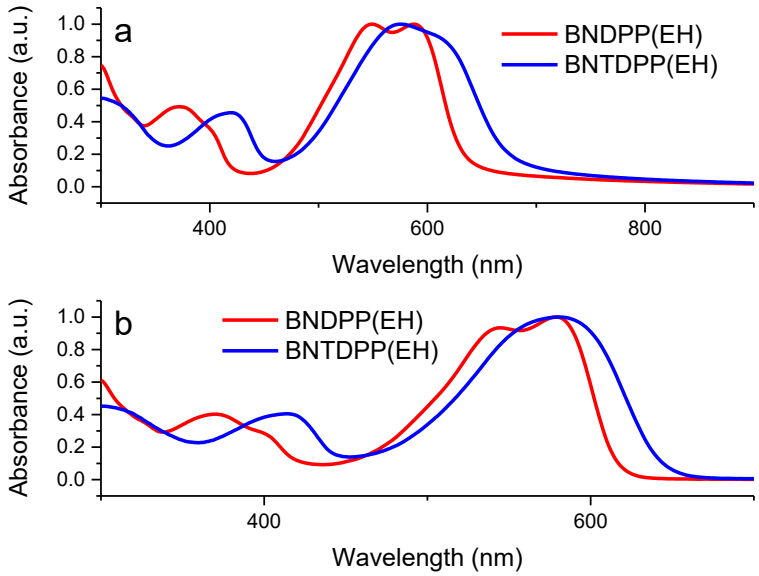


Figure 2-9: Normalized UV-Vis of BNDPP(EH) and BNTDPP(EH): a) thin film; b) solution ($CHCl_3$).

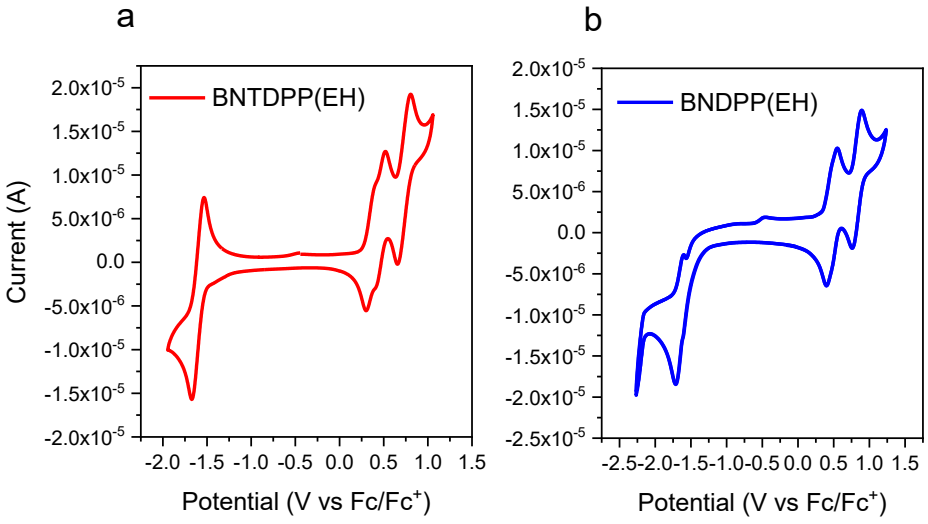


Figure 2-10: Cyclic voltammograms of a) BNTDPP(EH) and b) BNDPP(EH) in DCM solutions. Measurements were taken in DCM/[n-Bu_4N]PF_6 solutions (0.1 M) at a scan rate of 0.1 V s^{-1}.

Figure 2-9 draws the comparison between the UV-Vis absorptions of BNDPP(EH) and BNTDPP(EH) in solution and thin film. For both thin film and solution, the absorption onset and maxima of BNTDPP(EH) are slightly red-shifted compared to BNDPP(EH). This is a result of increased effective conjugation length due to incorporation of an additional thiophene unit.

The solution CV measurements of BNDPP(EH) and BNTDPP(EH) suggested BNTDPP(EH) has a narrower energy gap with higher HOMO and lower LUMO compared to BNDPP(EH) (Figure 2-10 and Table 2-6). They are in good agreement with UV-Vis measurements above. Both compounds were found to be somewhat soluble in acetonitrile, therefore, their corresponding thin film CV measurements could not successfully be obtained.

For BNTDPP(EH), both the oxidation and reduction peaks appear to be reversible. Whereas for BNDPP(EH), although both oxidation peaks are reversible, the reduction peak is not.

Table 2-6: Frontier energy levels and UV-Vis data of BNDPP(EH) and BNTDPP(EH).

	E_{HOMO} / eV	E_{LUMO} / eV	$E_{HOMO-LUMO}$ / eV	E_{abs} / eV	$\lambda_{max(solution)}$ / nm	$\lambda_{max(thin\ film)}$ / nm	$\varepsilon_{solution}$ / $10^4\ M^{-1}\ cm^{-1}$
BNDPP(EH)	-5.27	-3.08*	2.19	2.02	579	588	7.60
BNTDPP(EH)	-5.14	-3.19	1.95	1.91	579	579	8.86

The energies of HOMOs and LUMOs were measured by solution CV referencing against Fc/Fc^+ redox couple (4.8 eV): $E_{HOMO/LUMO}$ = - ($E_{1/2}^{ox/red}$ + 4.8) eV; * The cathodic peak potential of corresponding CV was used instead. E_{abs} are energy gaps calculated from the onset absorption of solution UV-Vis measurements of the acceptors.

2.2.2.2 DFT Study

In this section, all the computational simulations were performed using DFT with B3LYP, 6-31G(d,p) basis set. In order to simplify the calculations, all the alkyl side chains were substituted with methyl groups. For BNDPP(EH) and BNTDPP(EH), there are many possible geometries, finding the corresponding geometry with lowest ground state energy is complex and challenging, even with all the alkyl chains replaced with methyl groups. Therefore, to further simplify the tasks involved, the lowest energy ground state for DPP flanked with thiophene end groups was determined first before combining with 1,1'-binaphthyl core for

BNDPP. As for BNTDPP, since there is an additional bridging thiophene unit, the geometry of that unit was arbitrarily chosen and from that the ground state geometry was then simulated.

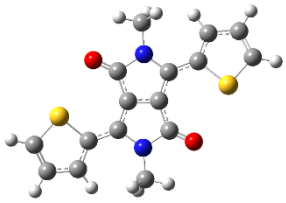
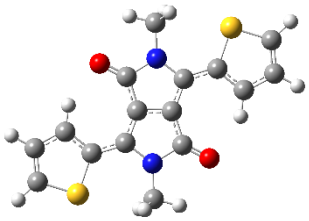
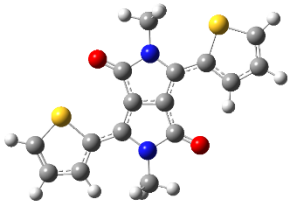
		
Thiophenes pointing at the carbonyl group	Thiophenes pointing away from carbonyl group	One thiophene pointing away and one facing carbonyl group
-1673.2624	-1673.2699	-1673.2662

Figure 2-11: Different ground state geometries of DPP with their corresponding energies in Hartree.

There are three possible geometries available for DPP flanked with thiophene units, with each thiophene (imaging the thiophene unit as an arrow with S atom being the tip of the arrow) either facing towards the carbonyl group (Figure 2-11, left) or away (Figure 2-11, middle) or mixed (one towards, one away, Figure 2-11, right). Their corresponding DFT simulations suggested that the conformer with thiophene units pointing away from the carbonyl group has the lowest ground state energy, in agreement with literature results.[69] Therefore, this geometry was chosen to combine with the 1,1'-binaphthyl core for BNDPP. It is also worth mentioning that the most stable conformer (Figure 2-11, middle) was deduced based on the strongest intramolecular hydrogen bonds stabilizing the planar shape of the molecule on its own in its gaseous state. However, the one with thiophenes pointing towards carbonyls are favoured when intermolecular interactions are considered. [69,70]

As a result, BNDPP also has three geometries available (Figure 2-12) (strictly speaking, since 1,1'-binaphthyl core is chiral, there are more than three possible geometries available, but in this case, the enantiomers should have the same energetics and we are only looking at S –).

Looking at the pointing directions of the bridging thiophene units, the BNDPP with left bridging thiophene pointing inwards and right bridging thiophene pointing outwards has the

lowest ground state energy (Figure 2-12 middle), although the difference in energy when compared to other two geometries is minor.

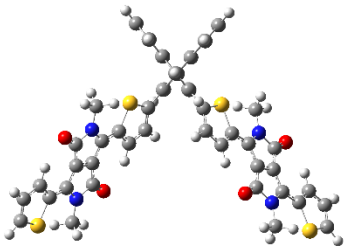
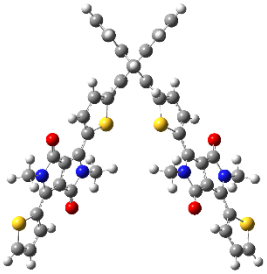
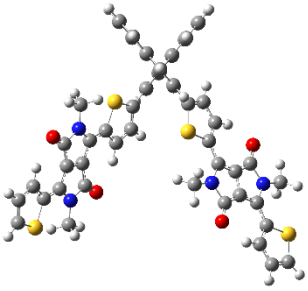
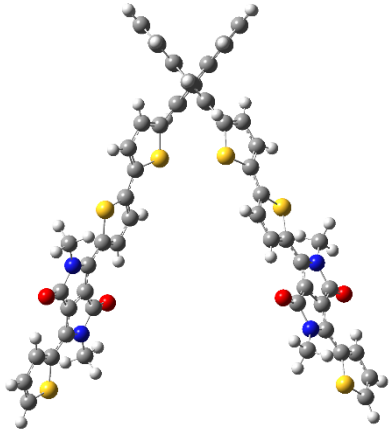
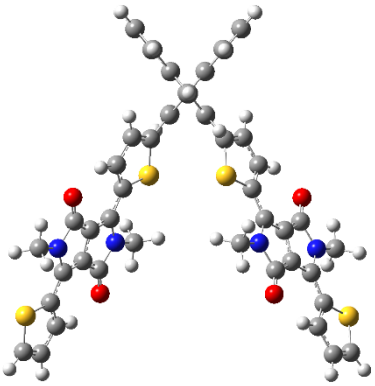
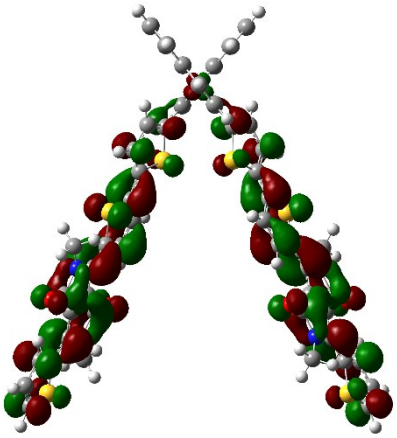
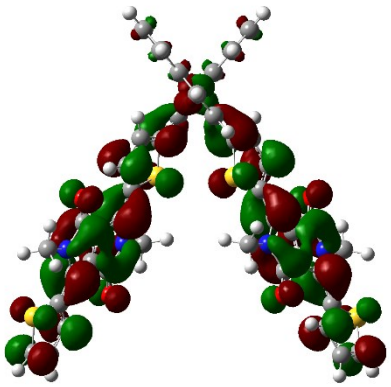
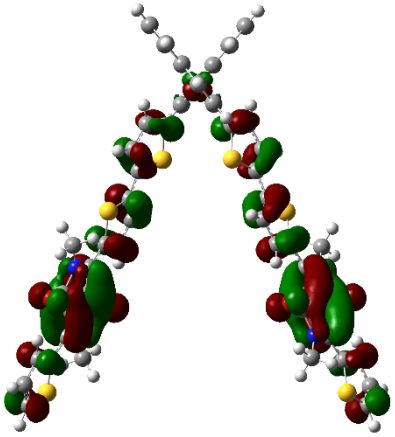
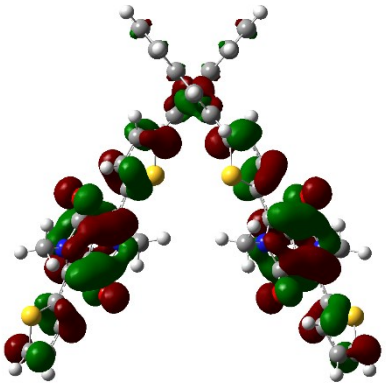
		
Left bridging thiophene pointing outwards, right bridging thiophene pointing inwards	Left bridging thiophene pointing inwards, right bridging thiophene pointing outwards	Both bridging thiophenes pointing outwards
-4114.7540	-4114.7551	-4114.7546

Figure 2-12: Different ground state geometries of BNDPP with their corresponding energies in Hartree.

Now moving to BNTDPP, as mentioned earlier, the geometry of the additional bridging thiophene units were arbitrarily chosen, and the resulting geometry after optimization was assumed to be the lowest ground state geometry of BNTDPP (Table 2-7 left).

A comparison of the dihedral angles of the binaphthyl cores was then drawn between the lowest energy ground state geometries of BNDPP and BNTDPP. As expected, the BNTDPP has a smaller dihedral angle (71.32 ° vs 77.71 ° for BNDPP) on the binaphthyl core suggesting it is more flexible, as a result of incorporation of one additional bridging thiophene elevating steric clash to a certain extent. Furthermore, BNTDPP has a narrower HOMO-LUMO energy gap with a higher lying HOMO.

Table 2-7: Comparison between DFT results of BNTDPP (left) and BNDPP (right).

	
BNTDPP	BNDPP
-5218.3930	-4114.7551
D = 77.32 °	D = 77.71 °
	
LUMO – 2.57 eV	LUMO – 2.51 eV
	
HOMO – 4.76 eV	HOMO – 4.82 eV
E_g = 2.19 eV	E_g = 2.31 eV

- 5218.3930 and - 4114.7551 were ground state energies in the units of Hartree. D is the dihedral angle of the corresponding binaphthyl core.

2.2.2.3 TGA and DSC

BNTDPP(EH) exhibited sufficient thermal stability to be incorporated into OPV devices, showing 5% weight loss (T5d) at a temperature as high as 397 °C in thermogravimetric analysis (TGA, Figure 2-13).

Initial differential scanning calorimetry (DSC) results (black, red and blue lines) indicate that the material melts at around 250 °C (the measured melting point is 242.3 – 243.2 °C) on the first heating cycle, but without an obvious crystallization on cooling. The 2nd and 3rd heating cycles exhibited a small peak at 250 °C. The lack of a crystallisation peak on cooling is likely due to slow crystallization. Therefore, a new cycle (green line) was repeated with holding of temperature at 120 °C for 3 hours (the peak circled in purple was due to holding temperature at 120 °C for 3 hours) to allow sufficient time for crystallization. However, the resulting melting peak at 250 °C still appeared much smaller vs the 1st cycle. This suggests that the material crystallizes very slowly, likely due to the nature of twisted binaphthyl backbone.

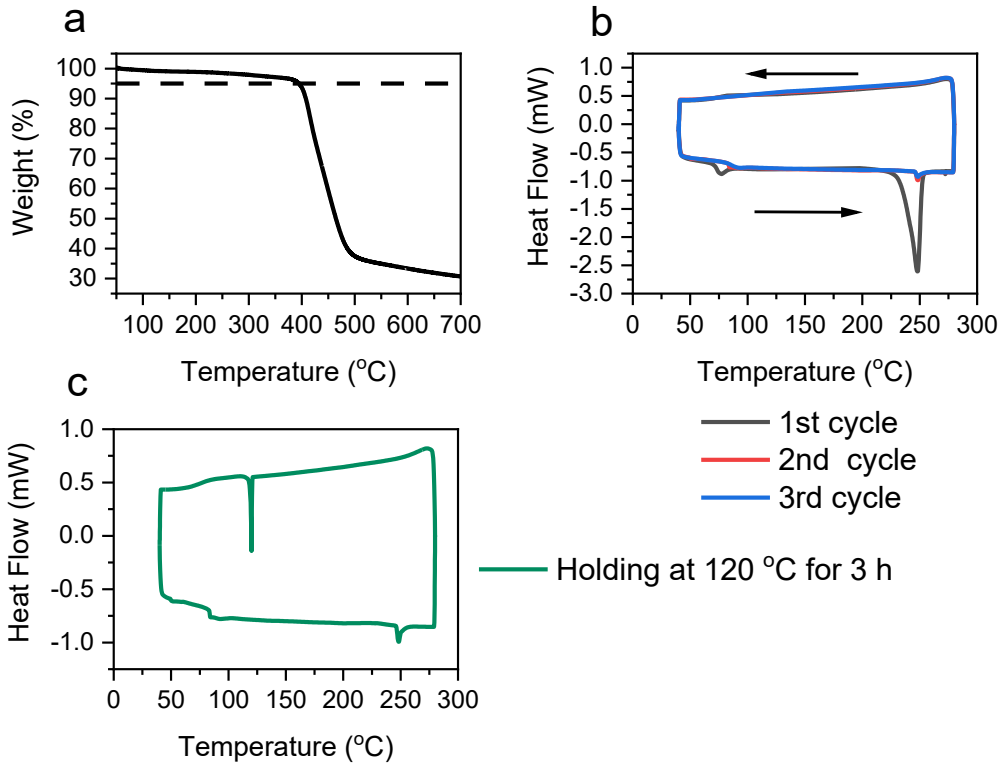


Figure 2-13: DSC (top right and bottom left, with rate of 10 °C min^{-1}) and TGA (top left) of BNTDPP(EH).

2.2.2.4 Device performance

Due to low yield and limited amount of material for BNDPP(EH), organic solar cell device performance tests were only conducted for BNTDPP(EH).

The HOMO and LUMO energies of BNTDPP(EH) from CV suggested it is a better donor candidate than an acceptor as its energetics hardly match well with other available donors (Figure 2-14 and Figure 2-15). Therefore, it was used as a donor material to blend with acceptor 3.6 and $PC_{71}BM$ (Figure 2-16 and Figure 2-17).

The results of device testing were disappointing as first few trials all showed no output current upon illumination, for blends with both PCBM and 3.6. The reasons for the lack of performance are unclear, and due to the limited amount of material further investigation was limited. However, because the binaphthyl core is chiral and its enantioenriched/enantiomerically pure isomer might be useful for detecting/modifying circularly polarized light in OLED application, our next focus was on the synthesis of enantioenriched binaphthyl DPP based compound.

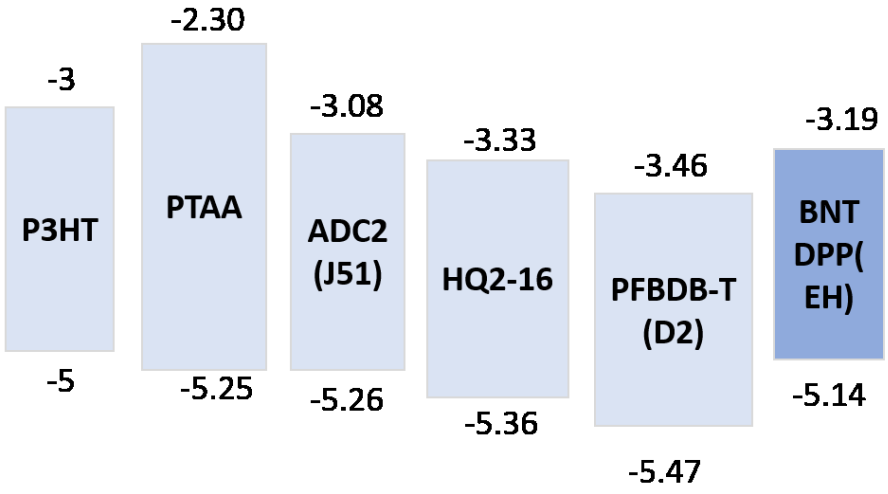


Figure 2-14: HOMO and LUMO energies of other donor materials vs BNTDPP(EH).

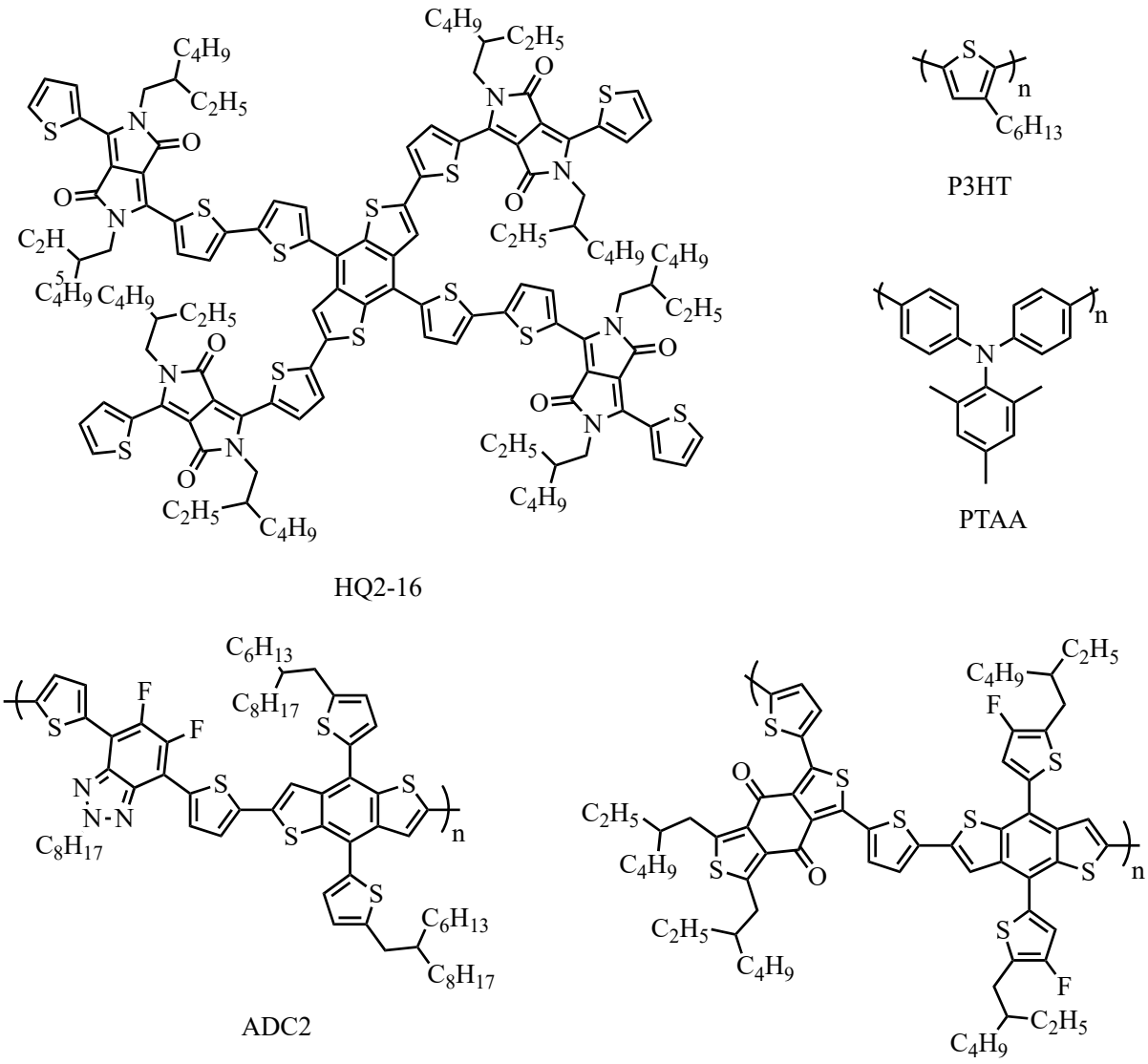


Figure 2-15: Chemical structures of the donors in Figure 2-14.

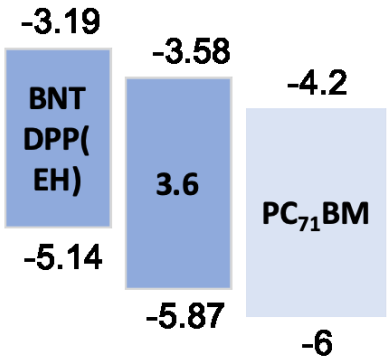
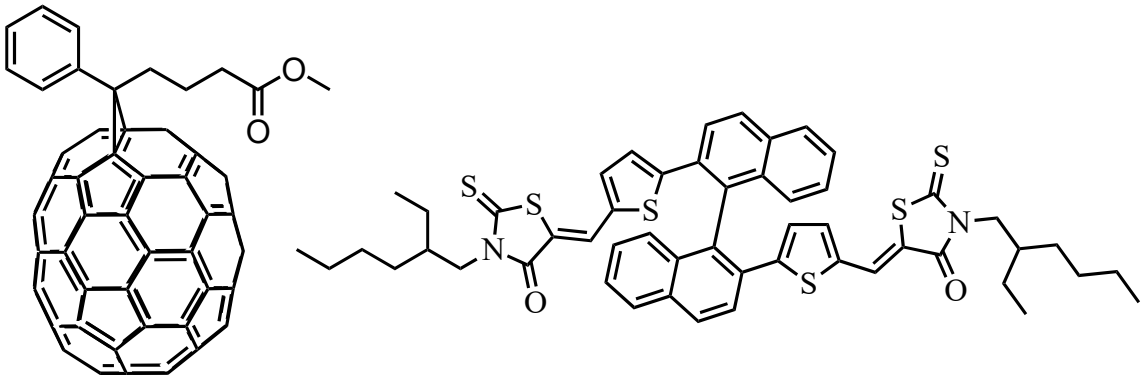


Figure 2-16: HOMO and LUMO energy levels of acceptor 3.6 and $PC_{71}BM$ with respect to BNTDPP(EH).



$PC_{71}BM$

3.6

Figure 2-17: Chemical structures of acceptor 3.6 and $PC_{71}BM$.

2.3 Enantio-enriched binaphthyl and DPP(BH) based molecule

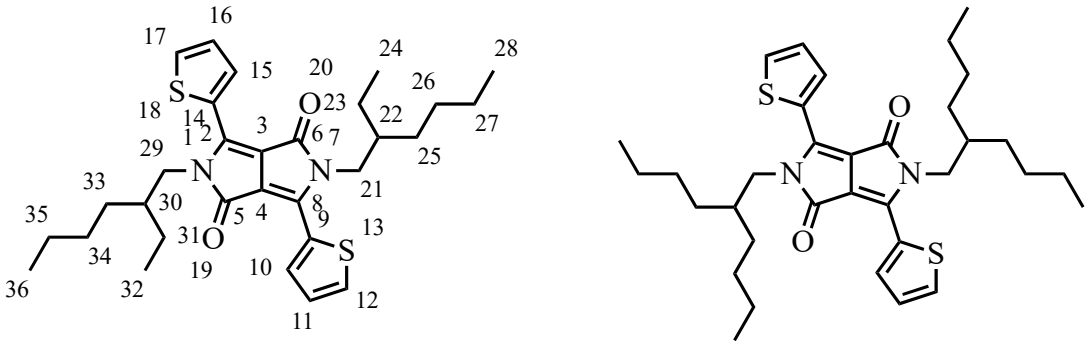


Figure 2-18: DPP(EH) with atom numeration and DPP(BH).

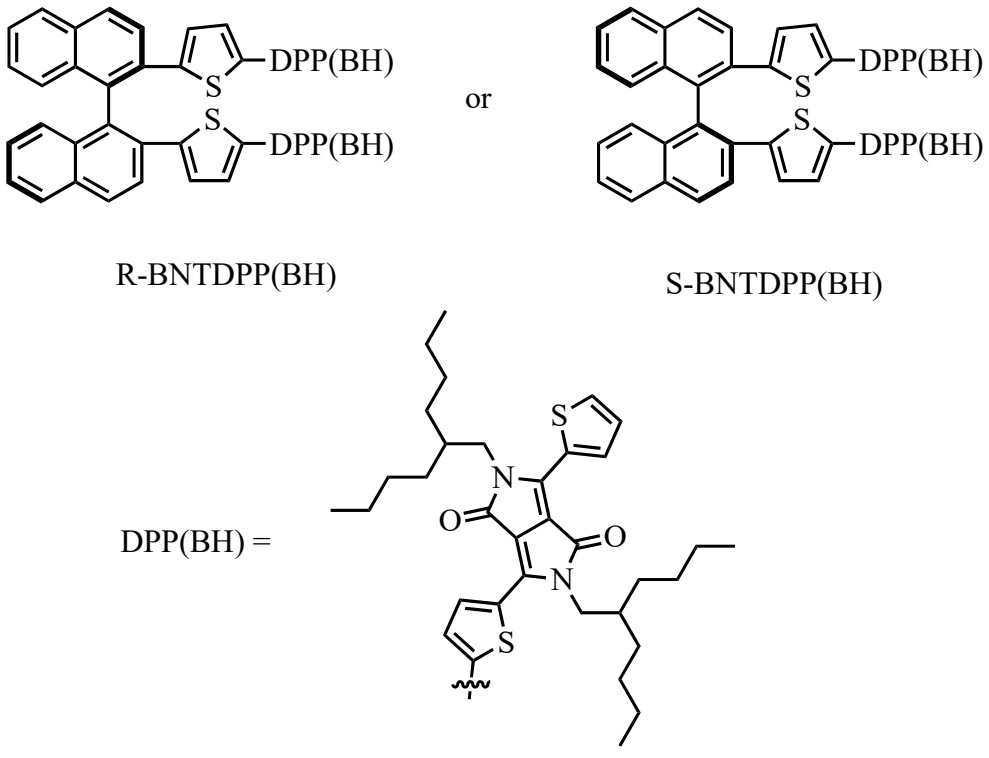


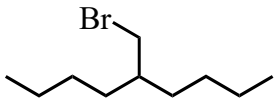
Figure 2-19: Chemical structures of R-BNTDPP(BH) and S-BNTDPP(BH).

Figure 2-18 shows the structure of DPP(EH) with atom numeration; as discussed it has two chiral centers, carbon 22 and 30 (the ones that are two carbons away from nitrogen). This will

create complexity when cross-coupling it with 1,1'-binaphthyl core as it will produce several diastereomers. To tackle this problem and simplify the matter, an additional two carbons were added to each alkyl chain to make it achiral - DPP(BH). The following session will discuss the synthesis and characterization of enantioenriched BNTDPP(BH) (Figure 2-19).

2.3.1 Synthesis

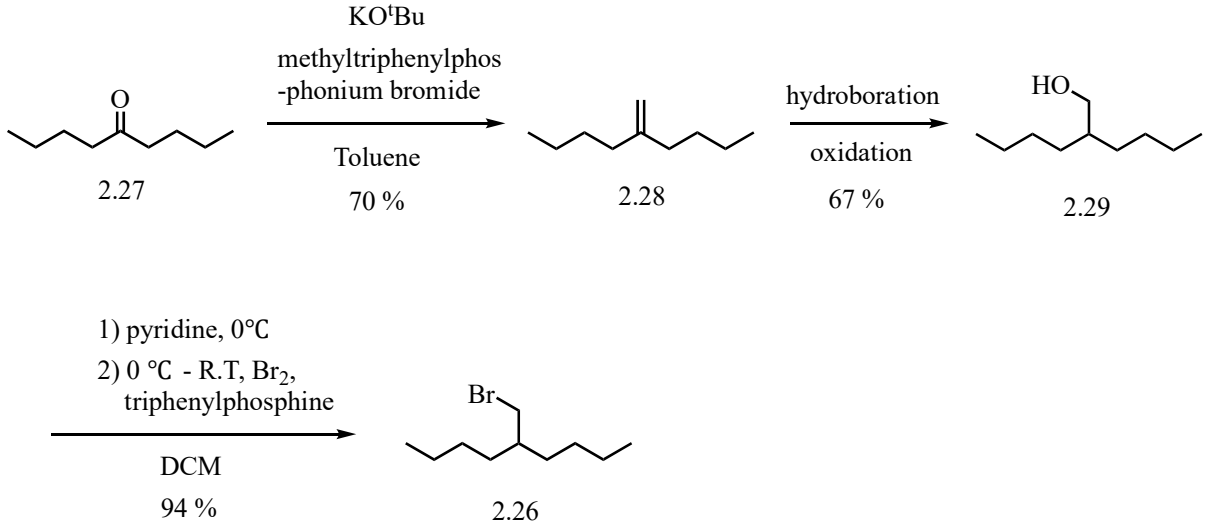
2.3.1.1 2,5-Bis(2-butylhexyl)-3,6-di(thiophen-2-yl)-2,5-dihydropyrrolo[3,4-c]pyrrole-1,4-dione {DPP(BH)}



2.26

Figure 2-20: Chemical structure of 5-(bromomethyl)nonane.

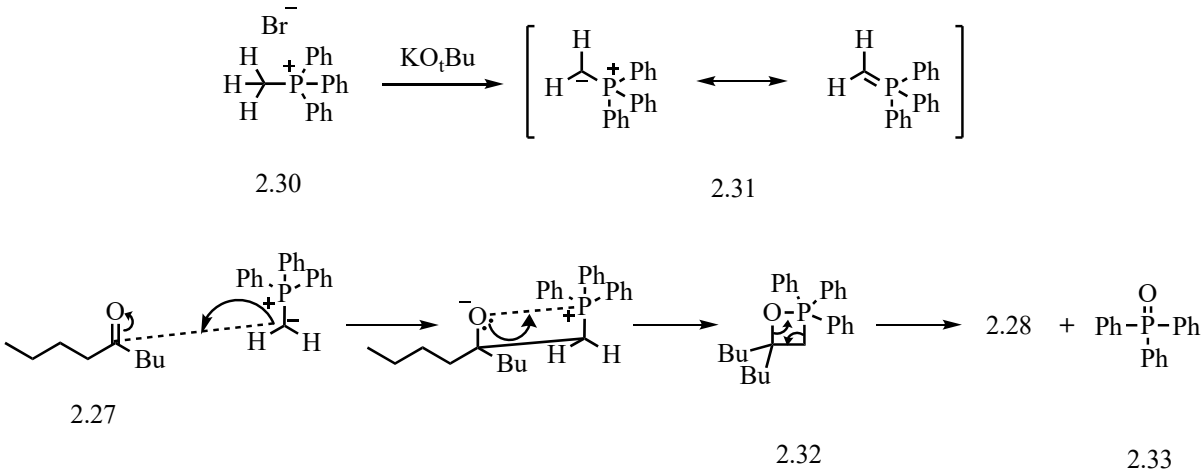
The synthesis of DPP(BH) follows the exact same method as that for DPP(EH) except that the alkylating agent, 5-(bromomethyl)nonane 2.26 (Figure 2-20), was not commercially available and needed to be synthesized first.



Scheme 2-14: Proposed synthetic route for the synthesis of 2.26.

Scheme 2-14 shows the synthetic route towards the synthesis of 2.26, which is a known synthesis, starting from commercially available 2.27.[71]

2.3.1.1.1 5-Methylenenonane (2.28)[71]



Scheme 2-15: Mechanism for the synthesis of 5-methylenenonane 2.28.

The first step of synthesis towards 2.26 involves converting 2.27 into the symmetrical alkene 2.28. This proceeded via Wittig olefination (Scheme 2-15) where methyltriphenylphosphonium bromide 2.30 was first converted to reactive ylide 2.31 by potassium tert-butoxide, this then undergoes stepwise interaction with 5-nonanone 2.27 to form a four-membered cyclic intermediate 2.32. 2.32 then ring opens to produce the desired 2.28 and triphenylphosphine oxide 2.33. The driving force for last step is the formation of a very stable triphenylphosphine oxide.

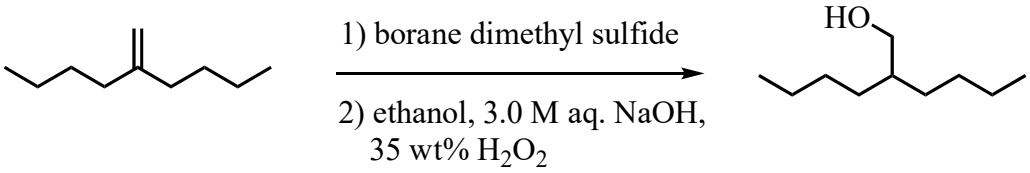
The synthesis of 2.28 was complicated by the fact that 2.28 and toluene have very similar boiling points, and therefore initial attempts to remove the toluene under reduced pressure resulted in significant loss of product. To circumvent this, silica was added to the reaction mixture after work-up before the solvent was removed under reduced pressure. The majority of 2.28 adhered to the silica and could be subsequently purified by filtering through a pad of silica using hexane as eluent.

Methyltriphenylphosphonium bromide 2.30 was poorly soluble in toluene. It formed a cloudy suspension when dissolving in toluene. In the literature[71] procedure, it suggested ~ 21 mL of

toluene per gram of 2.30. However, I found that a more concentrated solution of 15 mL of toluene per gram of 2.30 worked well without a drop in yield. This helped with scale-up significantly as it allowed for 20 g of 2.27 to be reacted in one batch (with the use of 2.5 L round bottom flask) compared to only 10 g for the original conditions.

Aside from using toluene as solvent, THF was also investigated. Even though 2.30 was highly soluble in THF allowing a more concentrated solution to be used, for the same given amount of reaction time, the yield obtained was much lower than that for toluene (22 % vs. 70 %). The lower yield probably relates to the reduced rate of reaction at the lower temperature of refluxing THF versus refluxing toluene.

2.3.1.1.2 2-Butylhexan-1-ol (2.29)



2.28 2.29

67 % (lit. 69 %)

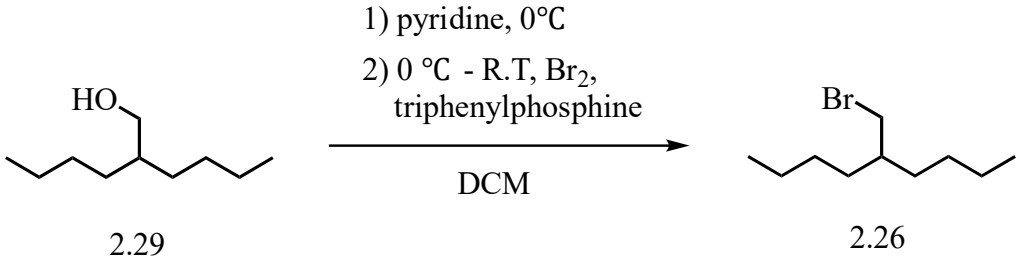
Scheme 2-16: Synthesis of 2.29 via Nolte et al. method.[71]

Nolte et al.[71] synthesized 2.29 with 69 % yield (Scheme 2-16). An initial small-scale test reaction gave 67 % yield. However, upon attempting to scale up, a noticeable issue was immediately spotted, the literature approach used a very large excess of aqueous NaOH and hydrogen peroxide (87.5 mL of 3.0 M aq. NaOH and 87.5 mL of 35 wt% H_2O_2 per gram of 2.28). It was difficult to scale up the synthesis by following the exact literature procedure and further optimization was required.

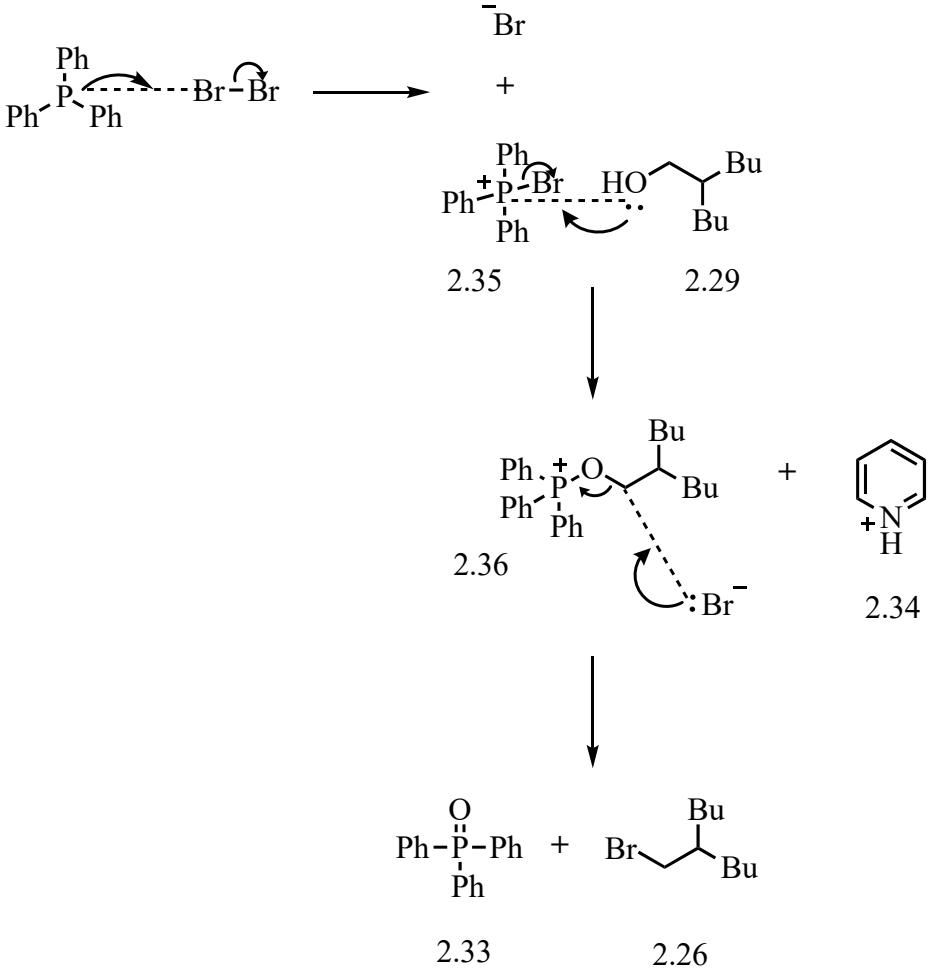
Following the exact same method but with much less 3.0 M aq. NaOH and 35 wt% H_2O_2, 17.5 mL each (still in great molar excess) per gram of 2.28. The result was somewhat surprising as the yield was dropped to 29 %. Borane dimethyl sulfide was then swapped with more reactive

borane-THF complex, which is sterically much less bulky, and the yield was increased to 67 %. Subsequent scale up syntheses gave an average yield about 70 %.

2.3.1.1.3 5-(Bromomethyl)nonane (2.26)[72]



Scheme 2-17: Converting alcohol 2.29 into alkyl halide 2.26.



Scheme 2-18: Proposed mechanism for the synthesis of 2.26.

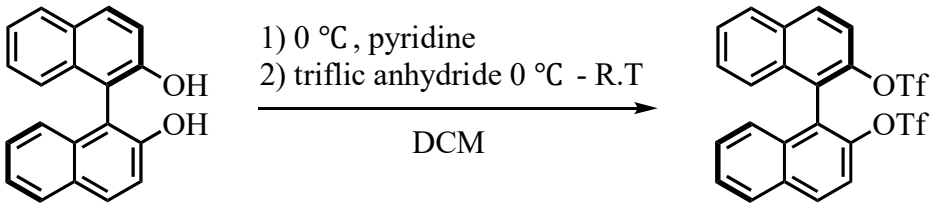
The conversion of the alcohol to the bromide was achieved by a modified Appel reaction. A solution of 2.29 in pyridine was added to a preformed solution of triphenylphosphine dibromide, which was formed by adding liquid bromine to triphenylphosphine in DCM at low temperature.

Scheme 2-18 depicts the proposed reaction mechanism for the synthesis of 2.26. Triphenylphosphine interacts with bromine to produce cationic 2.35, the oxygen of 2.29 then donates a lone pair to the phosphonium ion with elimination of bromide, the bromide anion then attacks the carbon atom of the C-O bond via S_N2 to produce the desired product 2.26 and triphenylphosphine oxide 2.33.

As for the project, an initial test reaction used commercially available triphenylphosphine dibromide and it offered 40 % yield. Substituting the commercial one with freshly synthesized triphenylphosphine dibromide improved the yield to 86 %.

The subsequent synthesis of DPP(BH) was conducted following the exact same procedure as that for DPP(EH) with 30 % yield.

2.3.1.2 Enantioenriched BNT

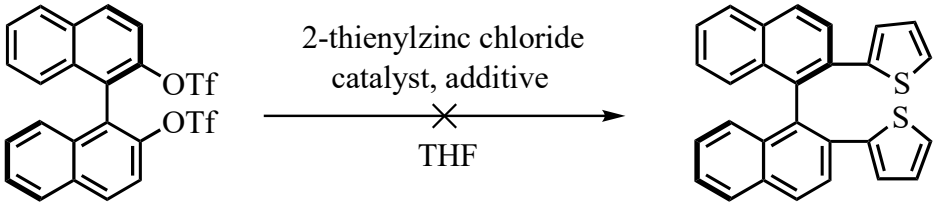


2.37 94 % 2.38

Scheme 2-19: Synthesis of (*R*)-(-)-1,1'-bi-2-naphthol bis(trifluoromethanesulfonate).

Having established a route to the DPP with symmetrical side chains, our attention turned to the binaphthyl derivative. Single enantiomers of 2,2'-diiodo-1,1'-binaphthalene and 2,2'-dibromo-1,1'-binaphthalene were commercially available on request, but they were prohibitively expensive. However the alcohol functionalised analogue, *R*)-(+)-1,1'-bi(2-naphthol) (2.37, Scheme 2-19), was commercially available and inexpensive (100 g for £ 38.00, Fluorochem)[73]. Although an alcohol is not a suitable partner for a cross-coupling reaction, it is readily convertible to a triflate, which is well-established as a good leaving group for Pd catalysed

cross-coupling reactions. The synthesis of the bis(triflate) 2.38 was readily achieved by treatment of the R enantiomer with triflic anhydride in pyridine, affording a high yield of 94%. The optical rotation was in good agreement with the literature ($[\alpha]^{25}_D$ = -155.4 (*c* = 1.01, chloroform) vs. lit.[74] $[\alpha]^{20}_D$ = -147.7 (*c* = 1.01, chloroform)) suggesting no loss of optical activity during the reaction.



2.38 R-BNT

Scheme 2-20: Unsuccessful Negishi cross coupling between 2.38 and 2-thienylzinc chloride.

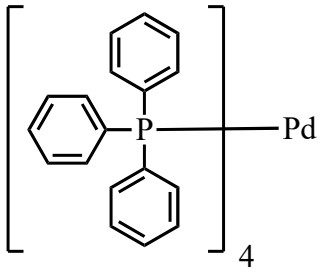
Table 2-8: Optimization of Negishi cross coupling between 2.38 and 2-thienylzinc chloride.

Catalyst	Catalyst loading / mol%	Additives	Yield / %
$Pd(PPh_3)_4$	5	--	--
$Pd(PPh_3)_4$	5	LiOAc	--
PEPPSI-IPr	5	--	--
$Pd(amphos)Cl_2$	5	--	--

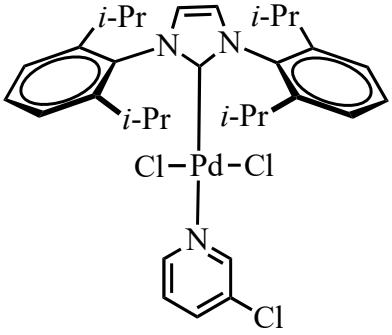
All the reactions were conducted with 6 eq. of 2-thienylzinc chloride in an oven-dried 20 mL microwave vial under following reaction conditions: 30 s pre-stirring; 90 ºC 1 min, 120 ºC 30 min.

With the triflate in hand, we substituted it for the dibromide in our established Negishi cross-coupling with 2-thienylzinc chloride (Scheme 2-20). However, disappointingly only starting material was observed at the end of reaction (entry 1, Table 2-8). Additives are sometimes used to promote the reaction with triflate. Based on the use of LiOAc in a Stille reaction, this was attempted in the current example but had no effect (entry 2). Alternative catalysts (entry 3 and 4) all came back with the same negative results. The additional steric bulkiness of the triflate group may be supressing oxidative addition in this reaction, although we note that the triflate starting group has been successfully used in the synthesis of (*S*)-2,2'-dibutyl-1,1'-binaphthalene (Figure 2-22) via Kumada cross-coupling.[75]

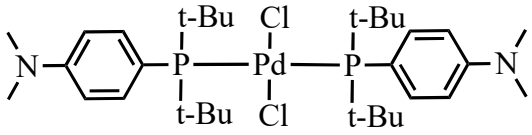
As an alternative, we considered the conversion of the triflate to the diamino compound 2.39 and then to the di-iodo (or dibromo) 2.40 by the Sandmeyer reaction. This should be amenable to the Negishi cross coupling following our established procedure (Scheme 2-21).



$Pd(PPh_3)_4$



PEPPSI-IPr



$Pd(amphos)Cl_2$

Figure 2-21: Chemical structures of the catalysts used in Table 2-8.

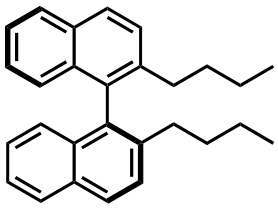
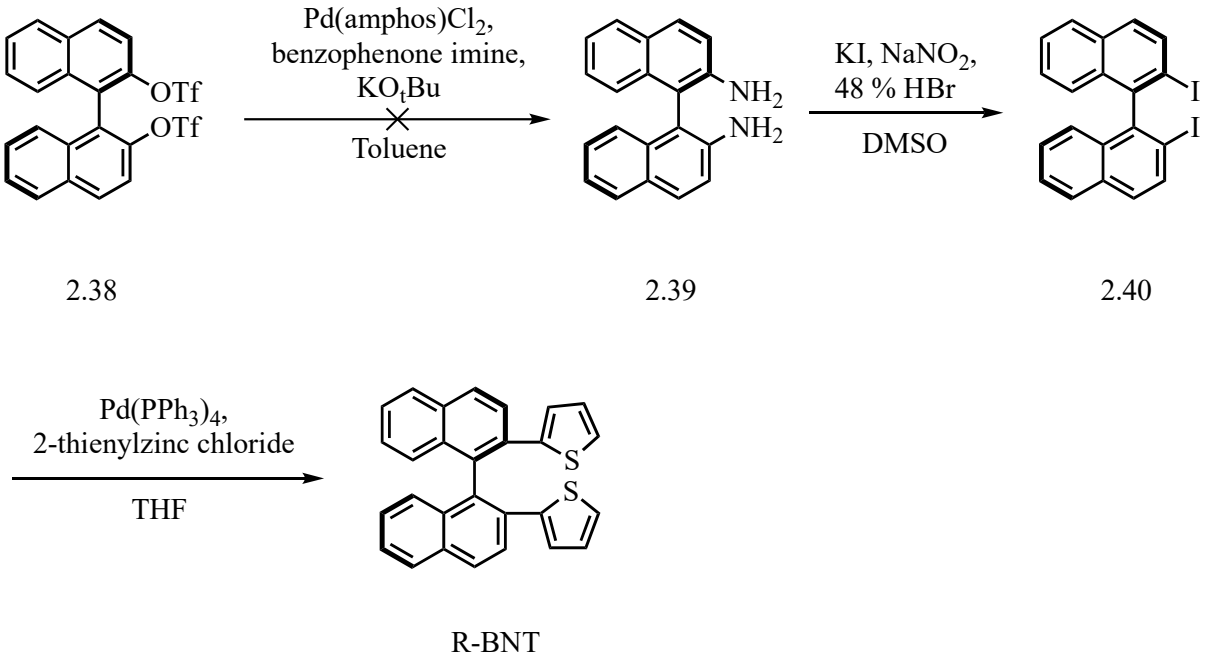
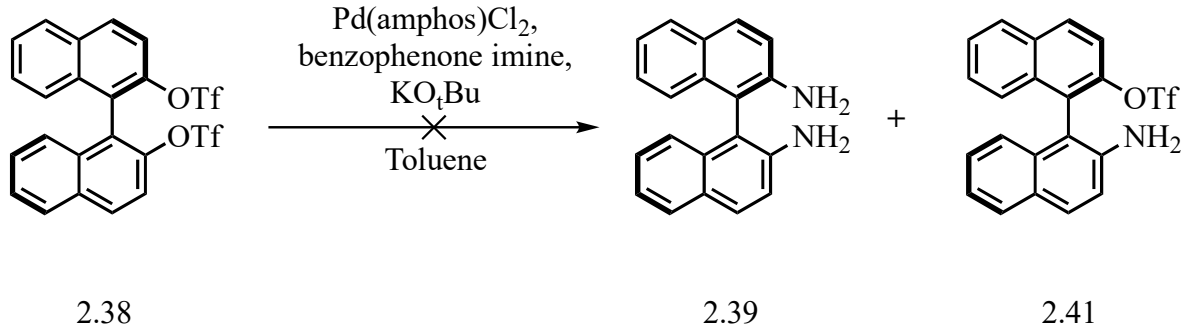


Figure 2-22: Chemical structure of (*S*)-2,2'-dibutyl-1,1'-binaphthalene.



Scheme 2-21: Alternative approach for the synthesis of R-BNT.

2.3.1.2.1 (*R*)-(+)-1,1′-binaphthyl-2,2′-diamine (2.39)



Scheme 2-22: Synthesis of 2.39 using Siva et al. method.[76]

The initial attempted synthesis of 2.39 (Scheme 2-22) was based on the publication of Siva et al. using a Pd catalyzed Buchwald coupling.[76] However, the desired product could not be synthesized, even though numerous attempts were made. Table 2-9 shows various parallel reactions conducted in attempt to synthesize 2.39. All reactions were tested against a genuine sample of 2.39 (purchased at small scale). All the reactions contained starting material and a second product, which was initially assumed to be the mono-substituted side product 2.41.

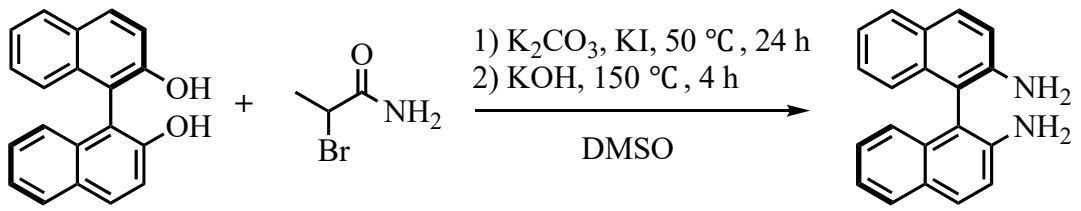
However, characterization confirmed it was actually [1,1'-binaphthalene]-2,2'-diol (a chemical structure of its R-configuration is 2.37 as shown in Scheme 2-19), which presumably resulted from hydrolysis of the triflate during aqueous work-up. The reason behind the lack of reaction was unclear.

Table 2-9: Unsuccessful optimizations of the synthesis of 2.39.

Pd(amphos)Cl_2 / mol%	Benzophenone imine / eq.	KO_tBu / eq.	Yield / %
a tiny spoon amount	2.3	2	--
5	2.3	2	--
5	3.5	3	--
10	3.5	3	--
10	6	6	--

All the reactions were conducted in toluene at 95 ºC; reaction time for entry 1 is up to 2 days; reaction time for the rest is overnight. Reaction work-up used 1.5 N HCl for neutralization followed by addition of aq. NaOH for basification, before extracting with ethyl acetate, washing with brine and drying with sodium sulfate.

Zhang et al.[77] published a patent in which 2.39 was synthesized directly from 2.37 (Scheme 2-23). Although the underlying mechanism is unknown, our attempts to repeat the reaction met with reasonable success and 2.39 was isolated with 22 % yield in an initial attempt (lit. 88 %). However, the corresponding optical rotation measurement suggested that a certain extent of epimerization occurred during reaction ($[\alpha]^{25}_D$ = + 76.3 (*c* = 0.5, chloroform) vs. lit.[78] $[\alpha]^{20}_D$ = + 244 (*c* = 0.5, chloroform)) possibly due to heating at high temperature (150 °C), thus rendering this synthetic approach unfavourable.



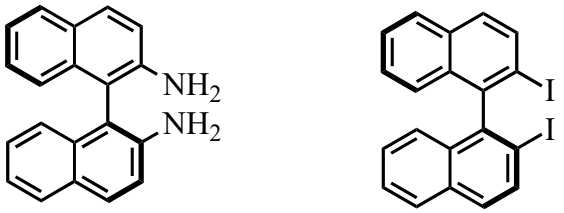
2.37 2.39

22 % (lit. 88 %)

Scheme 2-23: Synthesis of 2.39 via Zhang et al. method.[77]

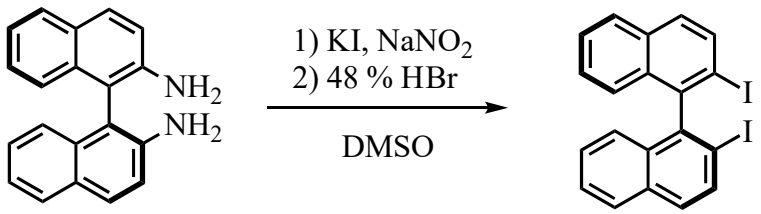
2.3.1.2.2 (*S*)-2,2'-diiodo-1,1'-binaphthalene (2.43)

At this point during the investigation of Zhang et al.'s method, a lower cost commercial supply of (*S*)-(-)-1,1′-binaphthyl-2,2′-diamine (2.42) was found. Therefore, attention focused on the conversion to the di-iodo compound 2.43.



2.42 2.43

Figure 2-23: Chemical structures of (*S*)-(-)-1,1′-binaphthyl-2,2′-diamine (2.42) and (*S*)-1,1'-binaphthalene-2,2'-diiodo.



2.42 2.43

250 mg
1.5 g

16 %
45 % (lit. 53 %)

Scheme 2-24: Synthesis of (*S*)-1,1'-binaphthalene-2,2'-diiodo (2.43) following Yamamoto's method.

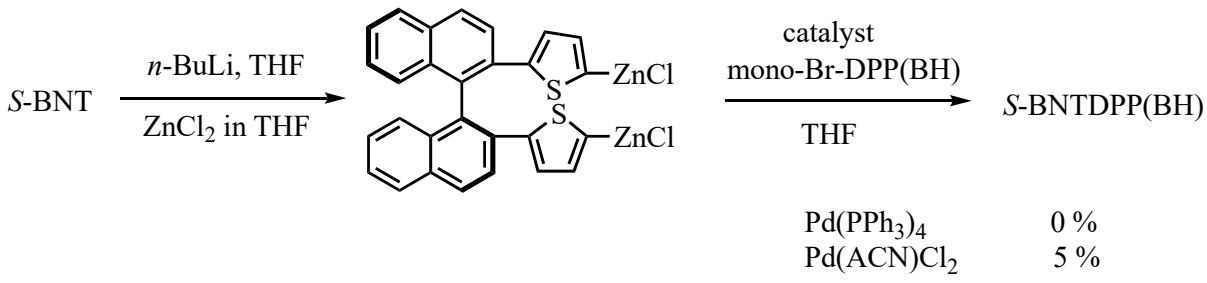
The traditional method[78–81] for converting (*S*)-(-)-1,1′-binaphthyl-2,2′-diamine (2.42) to (*S*)-1,1'-binaphthalene-2,2'-diiodo (2.43) involves low temperature, multi-step addition of reagents, a large amount of concentrated acid with excess foam formation (which is not safe), and is often time consuming. However, Yamamoto et al.[82] proposed a much safer and time-saving method (Scheme 2-24) in which the whole reaction was conducted at room temperature with a small amount of concentrated HBr without excess foam formation, and a reaction time of just 1h. The only drawback was that the method is only applicable to two specific amounts: 250 mg

and 1.5 g scale, with larger quantities reporting to afford an inferior yield.[82] As for this project, both scales were attempted with 16 % and 45 % yield for 250 mg and 1.5 g of 2.42 (Scheme 2-24) respectively.

2.3.1.2.3 *S*-2,2'-di(thiophen-2-yl)-1,1'-binaphthalene (*S*-BNT)

The synthesis of S-BNT followed the exact same method as that for the racemic one, except the reaction time was much shorter, with just one-hour reflux in THF compared to 2 days for 2.1, without compromising in yield (96 %). Corresponding optical rotation measurement gave $[\alpha]^{25}_{D}$ = + 17.0 (*c* = 1.0, chloroform) (lit.[54] $[\alpha]^{21}_{D}$ = -15.7 (*c* = 1.0, chloroform) for its *R* – enantiomer) suggesting no epimerization occurred despite heating.

2.3.1.3 S-6,6'-([1,1'-binaphthalene]-2,2'-diylbis([2,2'-bithiophene]-5',5-diyl))bis(2,5-bis(2-butylhexyl)-3-(thiophen-2-yl)-2,5-dihydropyrrolo[3,4-c]pyrrole-1,4-dione) {S-BNTDPP(BH)}



Scheme 2-25: Synthetic route of *S*-BNTDPP(BH).

The exact same method used for the synthesis of BNTDPP(EH) was adopted for the synthesis of *S*-BNTDPP(BH) (Scheme 2-25). However, the result was somewhat disappointing as there was no desired product at the end of reaction. It is possible that adding additional two carbons on DPP(EH) has further increased the steric clash for oxidative addition, therefore ultimately preventing the formation of *S*-BNTDPP(BH). Therefore, $Pd(PPh_3)_4$ was swapped with sterically less bulky $Pd(ACN)Cl_2$. Gratifyingly the reaction worked, albeit in low yield (5 % isolated yield, ~ 15 mg of product for 100 mg of *S*-BNT). Due to time constraint, further

optimization was not conducted. Corresponding optical rotation measurement offered $[\alpha]^{25}_{D}$ of approximately -18000. Such a number clearly indicates a problem with the measurement, in this case possibly because the molecule absorbs at the sodium D line (589 nm), which in turn interferes with the optical rotation measurement. Unfortunately, a polarimeter with a different light source was not available.

2.3.1.3.1 Analytical HPLC analysis

A racemic version of BNTDPP(BH) was synthesized for method development. Unfortunately, numerous attempts from both the HPLC-MS technician and myself gave no satisfactory result. Figure 2-24 shows the best separation achieved with DCM, where a doublet type peak appeared around 25 min time corresponding to the two enantiomers.

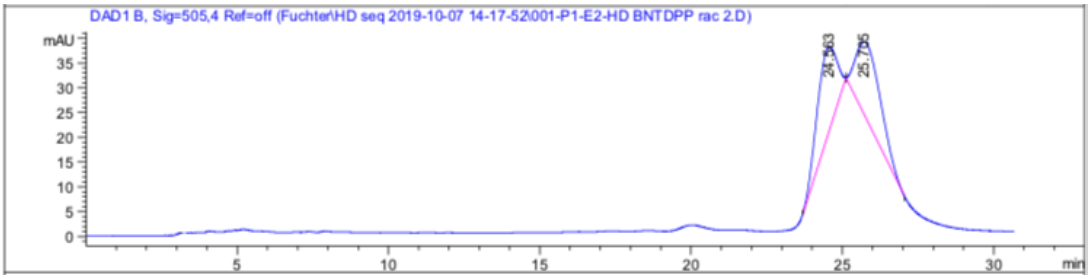


Figure 2-24: Best separation achieved on analytical HPLC with DCM.

2.3.2 Opto-electric properties

2.3.2.1 Ultraviolet-visible Spectroscopy (UV-Vis)

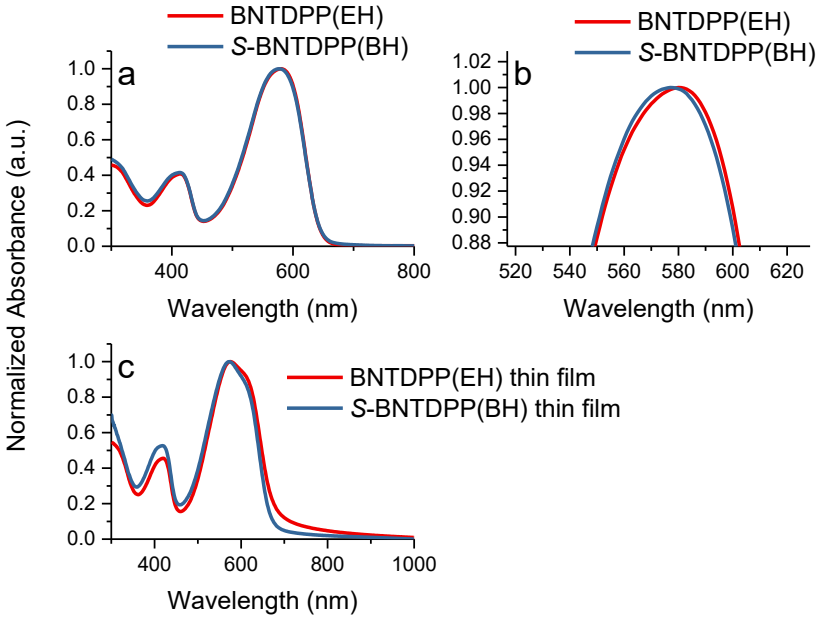


Figure 2-25: Comparison of solution and thin film UV-Vis of BNTDPP(EH) and enantioenriched *S*-BNTDPP(BH): a) solution UV-Vis of the materials; b) zoom in of a; c) thin film UV-Vis of the materials.

Both thin film and solution UV-Vis of enantioenriched S-BNTDPP(BH) appear slightly blue shifted compared to that of BNTDPP(EH) (Figure 2-25 and Table 2-10). This is possibly because the longer alkyl chain of butylhexyl disrupts aggregation more significantly than ethylhexyl.

Table 2-10: Comparison of UV-Vis results of BNTDPP(EH) and *S*-BNTDPP(BH).

	$\lambda_{max\ (solution)}$ / nm	$\lambda_{max\ (thin\ film)}$ / nm	$\varepsilon_{solution}$ / 10^4 M^{-1} cm^{-1}
BNTDPP(EH)	579	579	8.86
S-BNTDPP(BH)	577	573	9.34

2.3.2.2 Circular dichroism

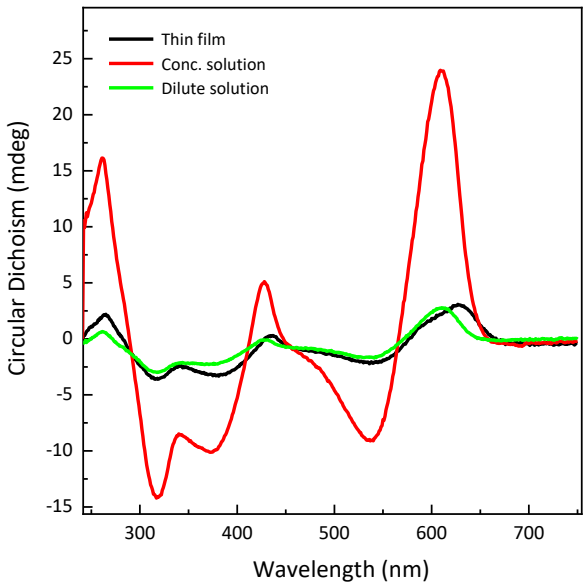


Figure 2-26: Circular dichroism spectra of *S*-BNTDPP(BH): thin film was casted at 10 mg/mL concentration, so is the concentration of the conc. solution CD measurement; dilute solution CD was measured by diluting the conc. solution for approximately 8 fold.

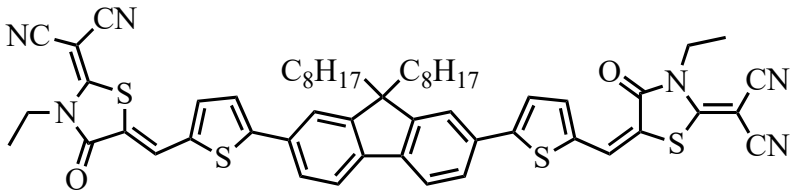
Solution circular dichoism showed a positive absorption maximum at 609 nm (Figure 2-26 red line), and a negative absorption maximum at 317 nm. There was no change in the absorption wavelength observed when diluting concentration. However, as for thin film, its absorptions are slightly red-shifted vs solution.

Due to time constraint, further analyses were not conducted.

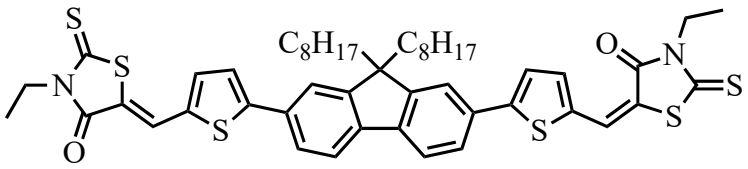
3. Binaphthyl Rhodanine Based Small Molecule Acceptors

3.1 Overview

Rhodanine derivatives have been commonly incorporated in dye chemistry for the fabrication of strong push-pull chromophores.[83–85] At the onset of this PhD, there had been several high performance small molecule donors published containing rhodanine groups.[86–89] However, very few acceptor materials had contained rhodanine units.[90] End-capping of a conjugated core with the rhodanine group affords electron withdrawing character to the periphery of the molecule due to the ketone and thioketone groups.[91] Furthermore, rhodanine allows for tunability of solubility via alteration of the imide alkyl chain.



Flu-CNRH



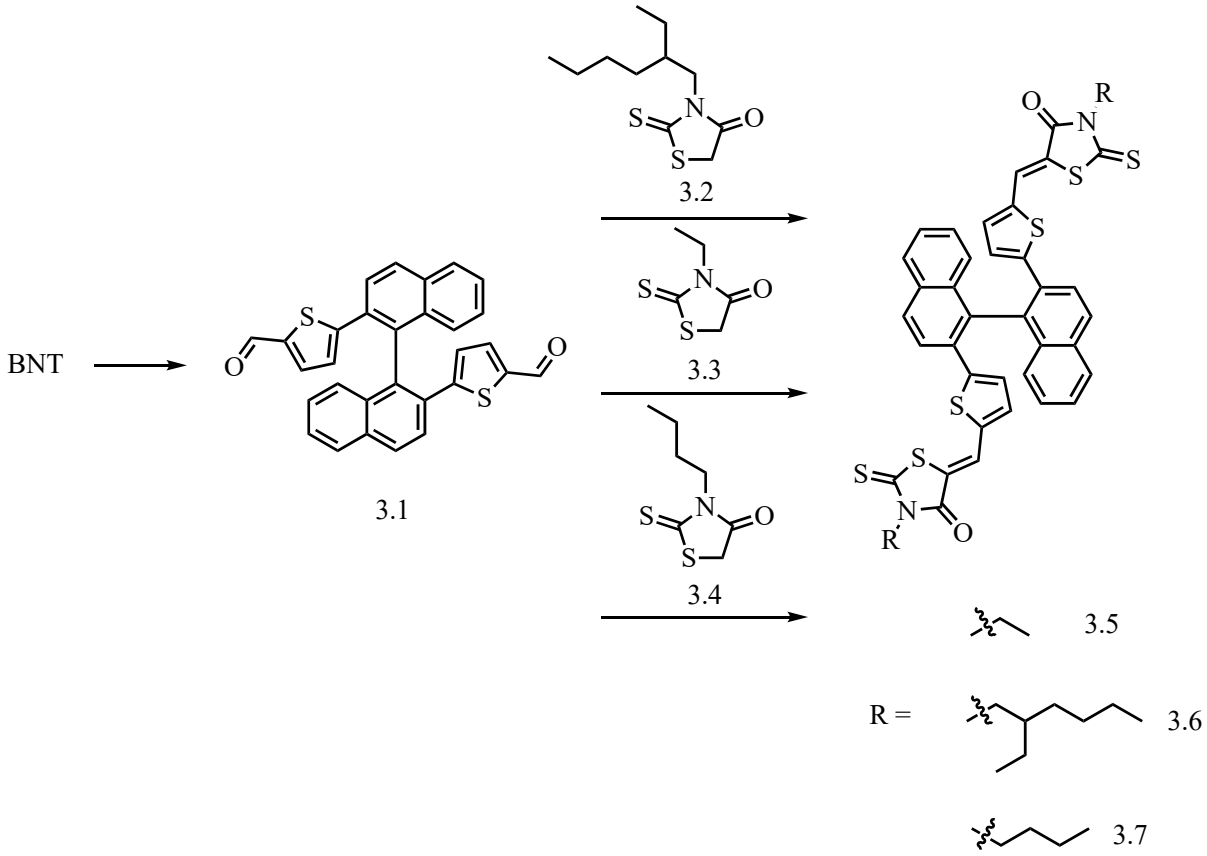
Flu-RH

Figure 3-1: Chemical structure of Flu-CNRH and Flu-RH.

Conventional tuning of rhodanine involves modification on the alkyl chain attached to the nitrogen and/or on the thioketone. Modification of the thioketone typically involves the conversion to a dicyanomethylene group, which is even more electron withdrawing than the thioketone and therefore can further lower the HOMO and LUMO of acceptor molecules. An example of such a system is shown on Figure 3-1, where Flu-CNRH has lower lying HOMO and LUMO than its non-modified counterpart Flu-RH. This in turn enables Flu-CNRH to

match the energetics of various low band gap donor materials with which Flu-RH was not compatible.[92]

The optimization of solubility and film morphology can be achieved via side-chain engineering in terms of length and bulkiness. For example, ITBTR-C6 end-capped with linear hexyl substituted rhodanine groups showed optimal film morphology with highest power conversion efficiency of 8.26 % among ITBTRs with various linear chain lengths (i.e. C2, C4, C6 and C8).[93]



Scheme 3-1: Synthetic routes towards binaphthyl and rhodanine based acceptors.

As for this chapter, three rhodanine derivatives (3.2, 3.3, 3.4, Scheme 3-1) with various alkyl chains attached to nitrogen were end-capped to BNT to produce a new acceptor series (3.5, 3.6, 3.7, Scheme 3-1). The electron withdrawing nature of rhodanine derivatives combined with the electron rich nature of BNT is thought to reduce band gap via the push-pull effect. This in turn will enable absorption of solar spectrum to a wider range, which is beneficial to device performance. The effect of the side chain length and bulkiness on the film morphology and solar cell efficiency was the focus of interest.

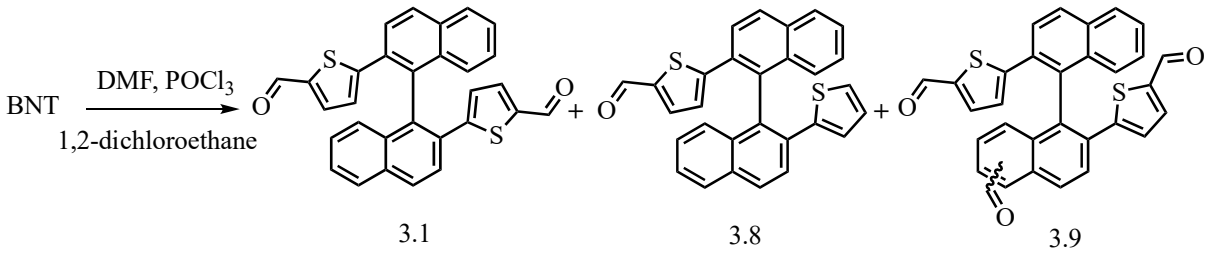
The following is divided into two sections. Section 3.2 will focus on the synthetic details of the target compounds. Section 3.3 will discuss their corresponding opto-electronic properties along with some device data.

3.2 Syntheses

Scheme 3-1 shows the general synthetic routes towards the target acceptors. In this section, the detailed syntheses of 3.1, 3.2 and 3.4 will be explored first before moving onto the final discussion of coupling between 3.1 and rhodanine derivatives.

3.2.1 5,5'-([1,1'-Binaphthalene]-2,2'-diyl)bis(thiophene-2-carbaldehyde) (3.1)

Compound 3.1 was synthesized via the Vilsmeier-Haack reaction (Scheme 3-2). Four optimizations were conducted. The best yield (79 %, entry 2, Table 3-1) was achieved with 40 eq. of DMF, 30 eq. of $POCl_3$ and a reaction temperature of 65 °C for 3 days. Lowering the relative amount of $POCl_3$ and shortening reaction time results in only mono-coupled side product 3.8 (entry 1, Table 3-1).



Scheme 3-2: Vilsmeier-Haack synthesis of 3.1.

Three days of reaction time is rather long, and therefore investigations were undertaken to see if a similar yield could be achieved with shorter reaction time but higher reaction temperature. Unfortunately, increasing reaction temperature while shortening reaction time (entry 3, Table 3-1) resulted in inferior yield, only 7.5 % isolated. The corresponding TLC showed an

additional product forming with greater polarity. This might potentially be an over-formylated BNT (3.9, Scheme 3-2).

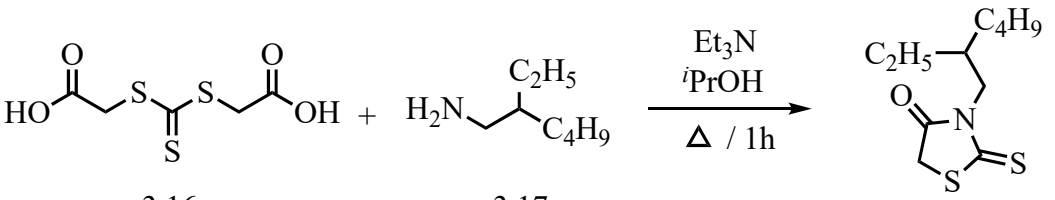
Another attempt keeping the same high temperature while lowering the relative amount of $POCl_3$ (entry 4, Table 3-1) eliminated 3.9 from the side products but with only 40 % isolated yield for the desired product. Therefore, increasing temperature in an attempt to shorten reaction time and maintain the same high yield was not a feasible approach in this case. The reaction for three days was therefore repeated as the best conditions.

Table 3-1: Optimization of the synthesis of 3.1.

DMF / eq.	$POCl_3$ / eq.	Reaction time	Temperature / °C	Yield[a] / %
40	5.0	12 h	65	--
40	30	3 days	65	79
40	30	2 days	reflux	7.5
40	15	2 days	reflux	40

a isolated yield of 3.1.

3.2.2 3-(2-Ethylhexyl)-2-thioxothiazolidin-4-one (3.2)



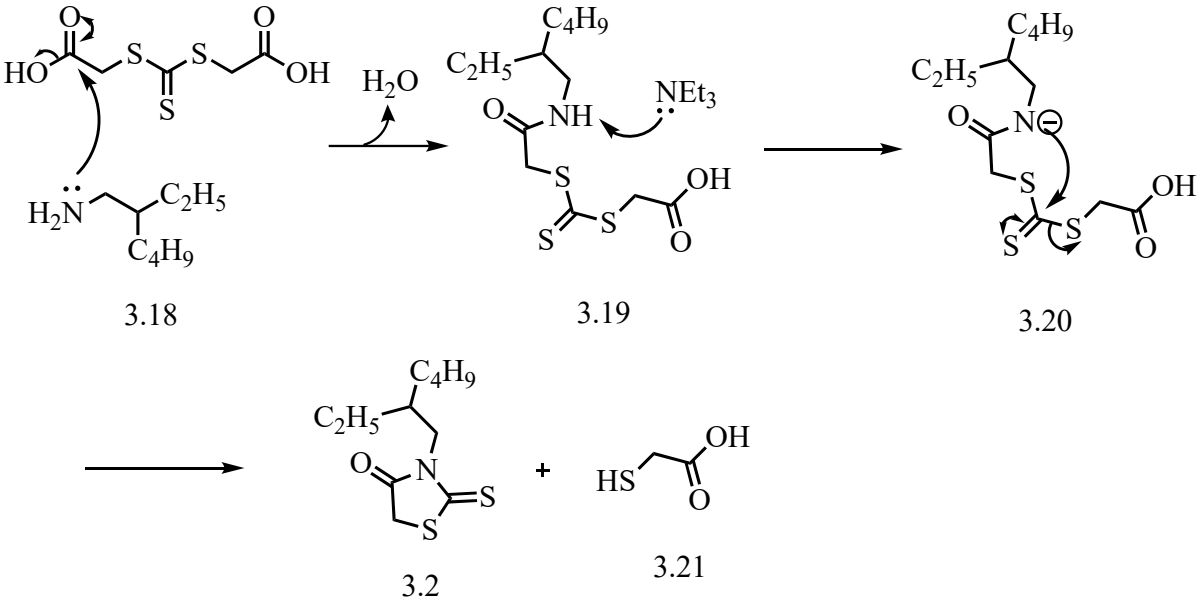
3.16 3.17 3.2

69 % (lit. 77 %)

Scheme 3-3: Synthesis of 3-(2-ethylhexyl)-2-thioxothiazolidin-4-one.

3-(2-Ethylhexyl)-2-thioxothiazolidin-4-one (3.2) was synthesized according to literature procedure[94] (Scheme 3-3). Scheme 3-4 depicts its corresponding mechanism. The amino group of 2-ethylhexylamine 3.18 attacks the carbonyl to form intermediate 3.19, followed by

deprotonation of the resulting amide by triethylamine and ring closure by attack at the thiocarbonyl and elimination of thioglycolic acid.

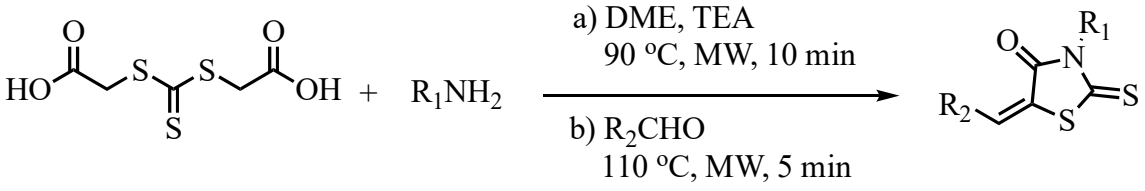


3.18 3.19 3.20 3.2 3.21

Scheme 3-4: Mechanism of the synthesis of 3.2.

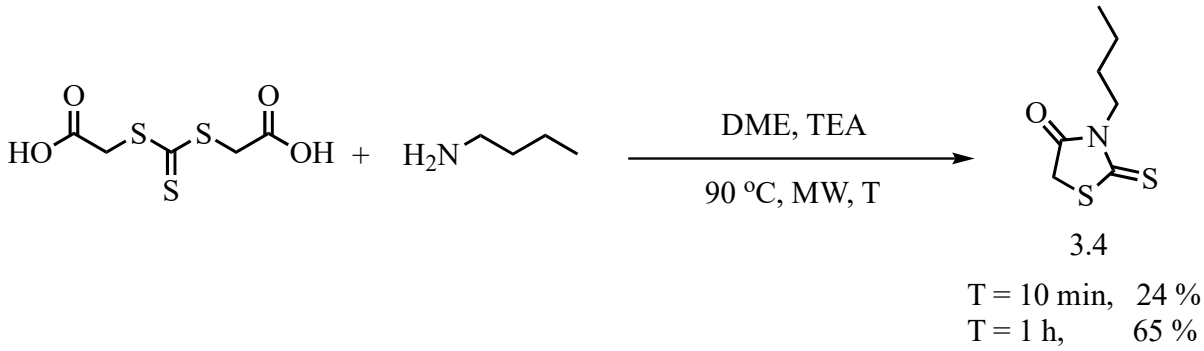
3.2.3 3-Butyl-2-thioxothiazolidin-4-one (3.4)

Botta et al.[95] synthesized 3-butyl-2-thioxothiazolidin-4-one (3.4) using the similar approach to that of 3.2. Nevertheless, his approach used 1,2–dimethoxyethane (DME) as solvent and the reaction mixture was heated at 90 °C in a microwave reactor for just 10 minutes. It is also worth mentioning that in his approach 3.4 was used in the next step of coupling directly without isolation (Scheme 3-5).



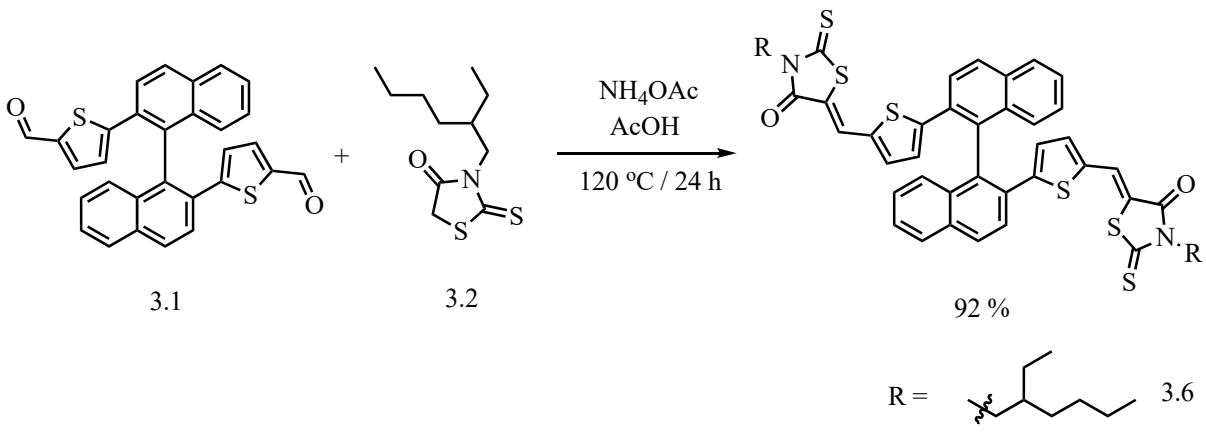
Scheme 3-5: Simplified reaction scheme for the work of Botta et al.[95]

As for this project, following the exact same literature procedure[95] but attempting to isolate 3.4 first resulted in only 24 % yield. The yield was successfully improved to 65 % by extending the reaction time to 1 hour (Scheme 3-6).



Scheme 3-6: Optimization of the synthesis of compound 3.4 by extending heating time to 1 h.

3.2.4 (5Z,5'E)-5,5'-(([1,1'-Binaphthalene]-2,2'-diylbis(thiophene-5,2-diyl))bis(methaneylylidene))bis(3-(2-ethylhexyl)-2-thioxothiazolidin-4-one) (3.6)



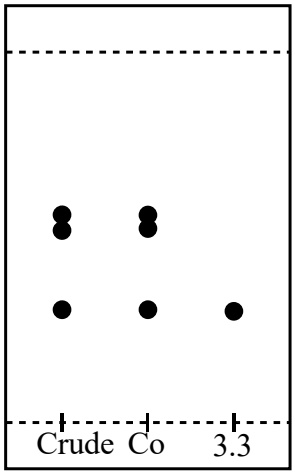
Scheme 3-7: Synthesis of (5Z,5'E)-5,5'-(([1,1'-binaphthalene]-2,2'-diylbis(thiophene-5,2-diyl))bis(methaneylylidene))bis(3-(2-ethylhexyl)-2-thioxothiazolidin-4-one) (3.6).

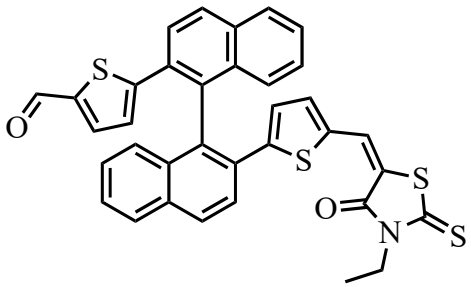
The synthesis of acceptor 3.6 was inspired by Martin et al. and McCulloch et al.'s work.[91,96] The initial attempt used 5 equivalents of 3.2 and 6.4 equivalents of ammonium acetate in hot acetic acid for 24 hours. The crude product was purified by column chromatography over silica

(eluent: DCM:hexane = 2:1) to afford a 92 % yield, with the desired product appearing as an orange-red solid (Scheme 3-7).

3.2.5 (5Z,5'E)-5,5'-(([1,1'-Binaphthalene]-2,2'-diylbis(thiophene-5,2-diyl))bis(methaneylylidene))bis(3-ethyl-2-thioxothiazolidin-4-one) (3.5) & (5Z,5'E)-5,5'-(([1,1'-binaphthalene]-2,2'-diylbis(thiophene-5,2-diyl))bis(methaneylylidene))bis(3-butyl-2-thioxothiazolidin-4-one) (3.7)

The syntheses of 3.5 and 3.7 are discussed here together as they form an interesting story of discovery and understanding through an iterative process.





3.22

Figure 3-2: a) TLC of the synthesis of 3.5 after 24 h reflux (Left: crude spot; Middle: co-spot; Right: compound 3.3 spot); b) possible mono-coupled side product.

Since the synthesis of 3.6 with branched ethylhexyl side chains was a great success with the first attempt achieving a 92 % yield, the same conditions were used for the synthesis of 3.5. However, the result was disappointing, since TLC of the crude reaction (Figure 3-2 a) obtained after 24 h of reflux showed two new spots, in addition to excess rhodanine. Our initial thoughts were that the reaction was not complete, and that mono-coupled side product 3.22 (Figure 3-2 b) was present. Given that 3.3 (5 eq.) and ammonium acetate (6.4 eq.) were in excess, the

reaction was continued for 60 h. During this time, the TLC did not change. In case that stopping and restarting the reaction had caused an unexpected problem, the reaction was repeated with more ammonium acetate (8 eq.) Again, the crude product appeared identical, with two spots apparent on TLC analysis. Increasing the amount of base used in the reaction clearly did not convert the suggested mono-coupled side product 3.22 into the desired one. Therefore, a new batch with different base (triethylamine) and solvent (chloroform) were attempted. However, the crude reaction still displayed two spots.

The two spots were very close running (R_f = 0.33, 0.32 with eluent: DCM:hexane = 2:1), nevertheless an attempt was made to separate them by column chromatography. Despite a long and tedious fractionation process, it appeared that every fraction still contained both spots, and that no separation had occurred.

If NMR analysis was performed at the time for the two dots coming off the column together, further attempts at optimisation would have stopped here. However, instead we believed the difficulty associated with purification was due to poor solubility of short ethyl chain on rhodanine 3.3, rendering the entire molecule less soluble comparing to 3.6. Therefore, in order to tackle with what we believed the solubility issue, additional two carbons were added to form 3.7.

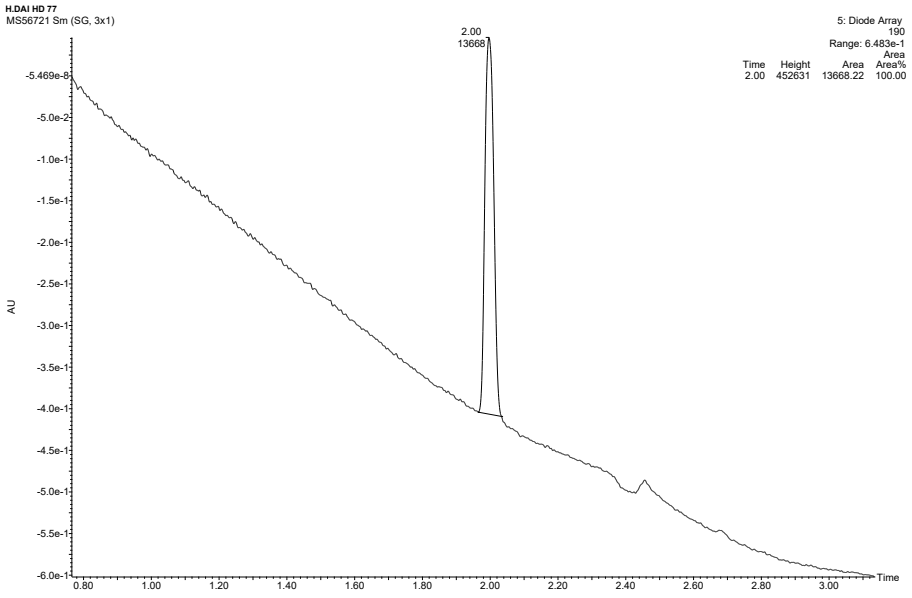


Figure 3-3: UV trace of LCMS of compound 3.7.

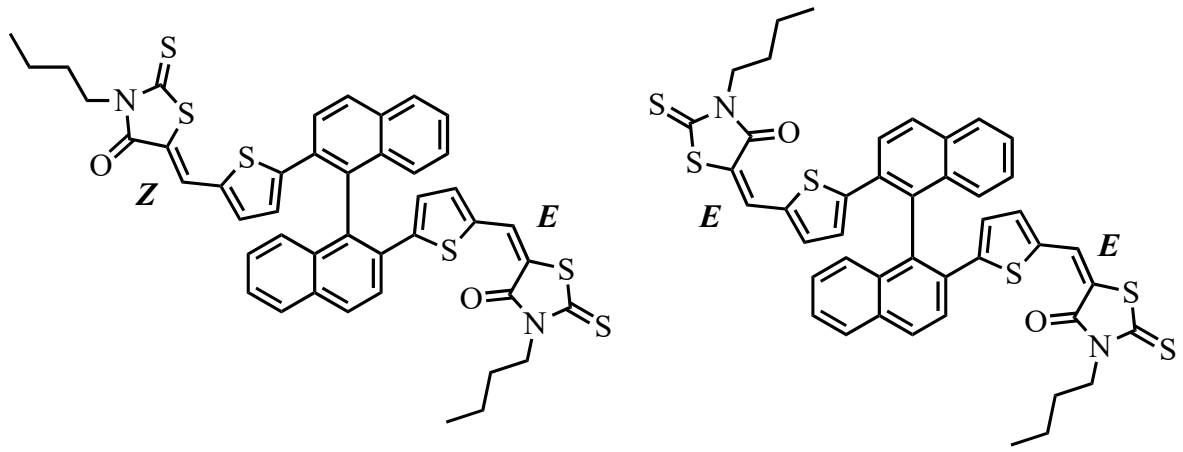


Figure 3-4: Possible different polarities due to different *E*-, *Z*- conformations of 3.7.

While synthesizing 3.7 under the same conditions as for 3.6, the identical problem was encountered as that for 3.5 (i.e. the first two dots on TLC could not be separated). However, it was noticed that there was a large amount of solid precipitate forming on the vessel wall after cooling the reaction mixture to room temperature. The solid was isolated via recrystallization in acetic acid and analysis by NMR and HRMS (see Appendix) appeared fully consistent with the expected product. Despite this, the TLC still exhibited two close running spots. Further evidence of the two dots being the same product comes from LCMS (Figure 3-3) where only one peak was shown, and melting point analysis gave a sharp transition (214 – 215 °C). A possible explanation for the observation of two spots on TLC was that a mixture of *E* and *Z* isomers was forming in the reaction (Figure 3-4). Due to the different configurations these isomers could have different polarities, and on TLC they appear to be separate. It is possible that even if they were separated on the column, they quickly interconvert under exposure to light.

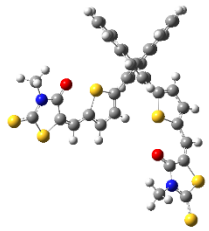
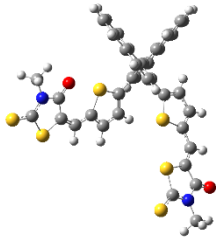
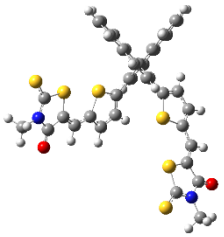
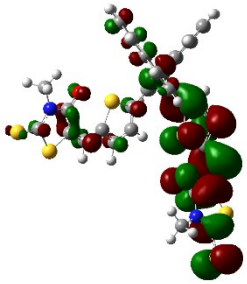
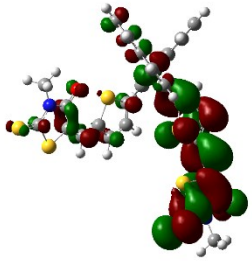
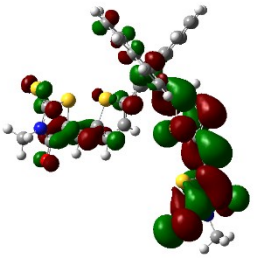
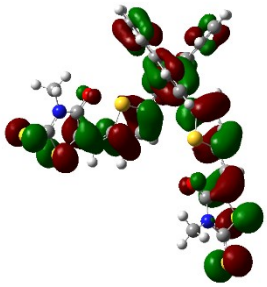
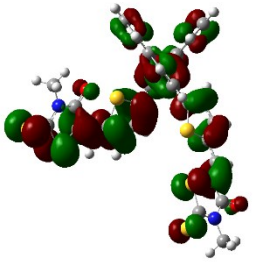
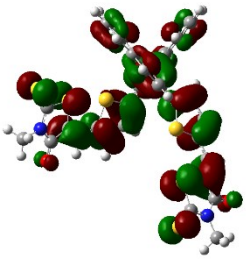
The synthesis of 3.5 was then revisited and pure 3.5 was successfully isolated with a sharp melting point (235 - 236 °C) and clean NMR spectra (see Appendix) even though TLC still existed as two dots.

On the other hand, acceptor 3.6 only showed one spot on TLC. This might be because ethyl-hexyl side chain is sterically bulky and only one conformation is favoured.

3.3 Opto-electric, thermal properties & computational simulation

3.3.1 DFT

Table 3-2: Comparison of *E, E*; *E, Z* and *Z, Z* isomers.

		
E, E	*E, Z*	*Z, Z*
-4111.6635	-4111.6685	-4111.6742
		
LUMO -2.65 eV	LUMO -2.67 eV	LUMO -2.68 eV
		
HOMO -5.60 eV	HOMO -5.64 eV	HOMO -5.68 eV

In this section, all the computational simulations were performed using DFT with the 6-31G(d, p) basis set and all the alkyl chains were replaced with methyl groups for the ease of calculation. Furthermore, all the simulations were conducted with the identical geometry for binaphthyl

core and thiophene, except the geometry for rhodanine units where different orientations (i.e. *E*, *E*; *E*, *Z* and *Z*, *Z*) will be examined.

Among all three geometries (Table 3-2), the *Z, Z* orientation has the lowest ground state energy with lowest lying HOMO and LUMO, which makes sense as the lowest lying HOMO and LUMO are also least susceptible to oxidation and reduction respectively, rendering it the most stable conformer.

3.3.2 Cyclic Voltammetry (CV)

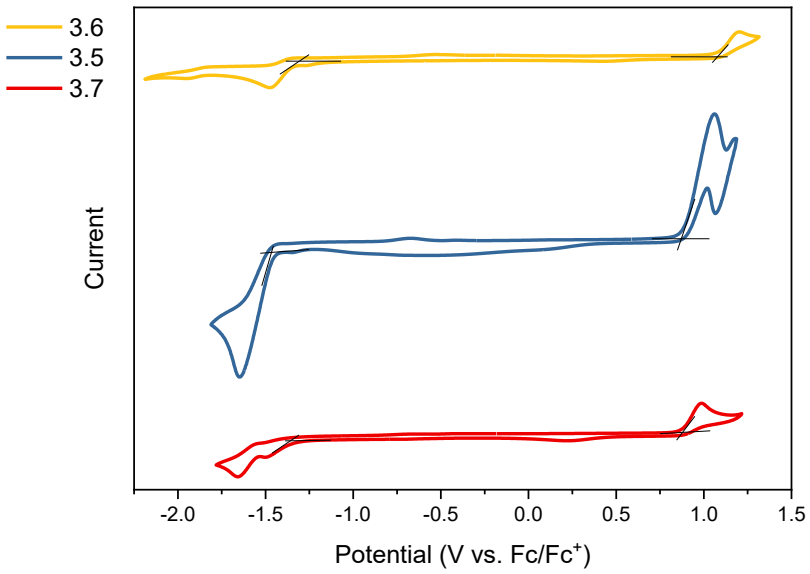


Figure 3-5: Cyclic voltammograms of 3.5, 3.6 and 3.7 in DCM solutions. Measurements were taken in DCM/[n-Bu_4N]PF_6 solutions (0.1 M) at a scan rate of 0.1 V s^{-1}.

Thin film cyclic voltammetry could not be obtained for the binaphthyl rhodanine series as they are too soluble in the acetonitrile solvent used for measurements. Therefore, solution CV was performed instead in dichloromethane, referenced against ferrocene/ferrocenium. The HOMO level of ferrocene was taken to be -4.8 eV. The onset of reduction and oxidation were used to extract the HOMO and LUMO levels. In all cases the reduction peaks were irreversible, and with the exception of 3.5 the oxidation was also irreversible. 3.5 showed a reversible oxidation peak. Interestingly both 3.5 and 3.7 with ethyl and butyl sidechains showed very similar profiles, however 3.6 with bulkier ethylhexyl sidechains cleared exhibited a higher onset of oxidation, suggesting a deeper HOMO level.

Table 3-3: Frontier molecular orbital energetics of 3.5, 3.6 and 3.7 calculated from solution CV.

	E_{HOMO} / eV	E_{LUMO} / eV	$E_{HOMO-LUMO}$ / eV
3.5 (Et)	- 5.67	- 3.35	2.32
3.6 (EH)	- 5.85	- 3.63	2.22
3.7 (Bu)	-5.64	- 3.49	2.15

The HOMO, LUMO energies were calculated by referencing against ferrocene/ferrocenium redox couple: $E_{HOMO/LUMO}$ = - ($E_{onset}^{ox/red}$ + 4.8) eV.

3.3.3 Ultraviolet-visible Spectroscopy (UV-Vis)

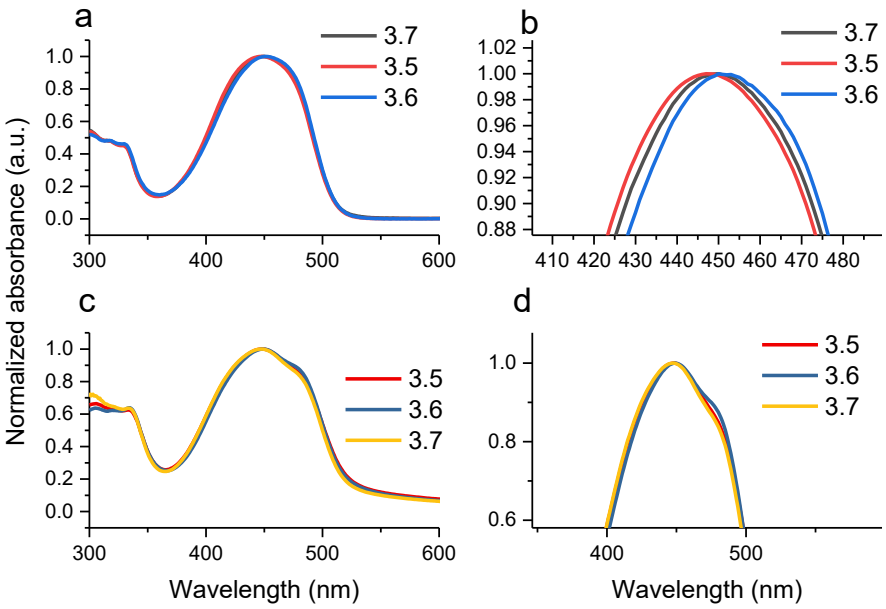


Figure 3-6: a) normalized solution UV-Vis; b) expanded plot of a; c) normalized thin film UV-Vis and d) expanded plot of c.

Table 3-4: Solution UV-Vis data of 3.5, 3.6 and 3.7.

	λ_{max} (nm)	λ_{onset} (nm)	ε (10^4 $M^{-1}cm^{-1}$)
3.5 (Et)	448	517	6.00
3.6 (EH)	452	517	6.61
3.7 (Bu)	450	517	6.42

Both solution and thin film UV-Vis of the three molecules have absorption maximum at ca. 450 nm. However, for solution UV-Vis, a small redshift in absorption maximum of 2 nm is observed for every increase in alkyl chain size from ethyl to butyl to ethylhexyl (Figure 3-6 b). All materials showed the same onset wavelength in solution at 517 nm, suggesting an identical optical band gap. This is different to the results of the CV measurements. Moving from solution to thin film does not change the absorption maxima, but a new shoulder peak at ca. 480 nm appears, likely as a result of molecular aggregation.

3.3.4 TGA & DSC

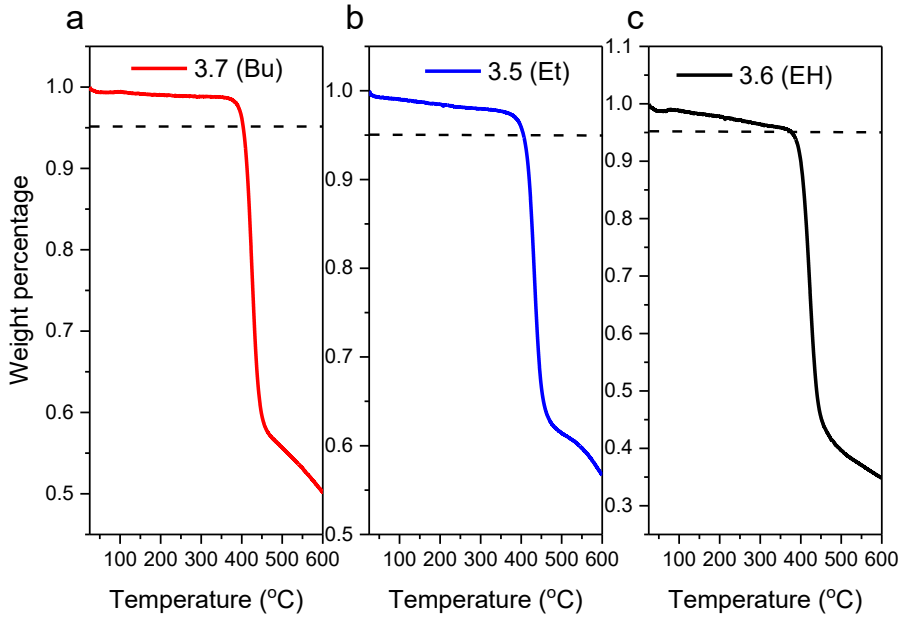


Figure 3-7: TGA analyses of 3.5, 3.6 and 3.7. under nitrogen atmosphere.

All three acceptors exhibited sufficient thermal stability to be incorporated into OPV devices, showing 5 % weight loss (T5d) at a temperature with average above 400 °C in thermogravimetric analysis (Figure 3-7). Their DSC analyses (Figure 3-8) showed a similar trend as that for BNTDPP(EH), with the first cycle showing a protruding melting peak and featureless second and third cycle, implying very slow crystallization possibly due to the twisted binaphthyl core.

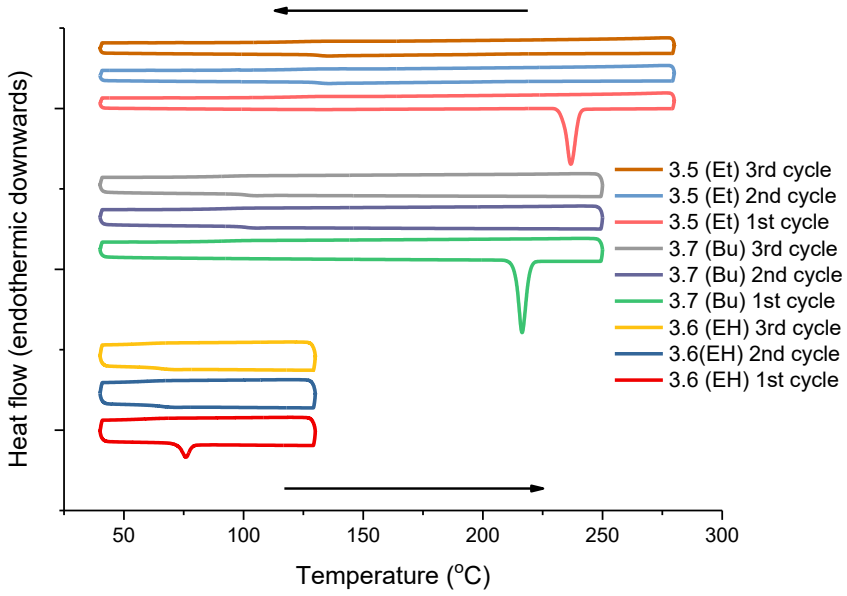


Figure 3-8: DSC analyses of 3.5, 3.6 and 3.7 at a heat rate of 10 °C min^{-1} under nitrogen atmosphere.

3.3.5 OPV device performance

The performance of 3.6 as an acceptor in OPV devices was investigated using two donors polymers, regioregular P3HT and a low bandgap donor-acceptor ADC2 (Figure 3-9), which was first reported by Zhang et al.[97] The device architecture was glass/ITO/ZnO/active layer/MoO_3/Ag, a so-called inverted device architecture.

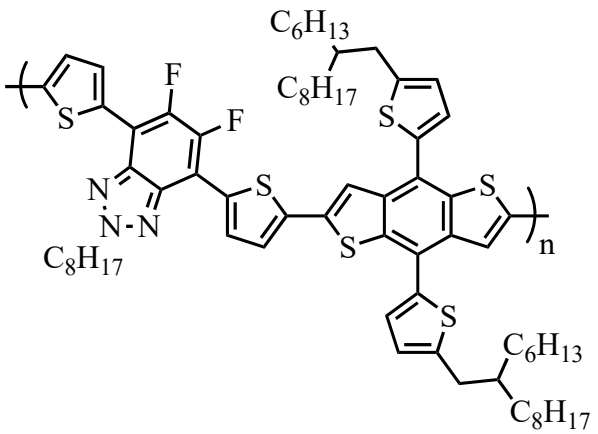


Figure 3-9: Chemical structure of ADC2.

For ADC2 and 3.6, the best power conversion efficiency of 1.22 % was achieved for the blend ratio of 1:1 after thermal annealing at 120 °C, with J_{sc} of 3.91 mA cm^{-2} and V_{oc} of 1.01 V (Figure 3-10 and Table 3-5).

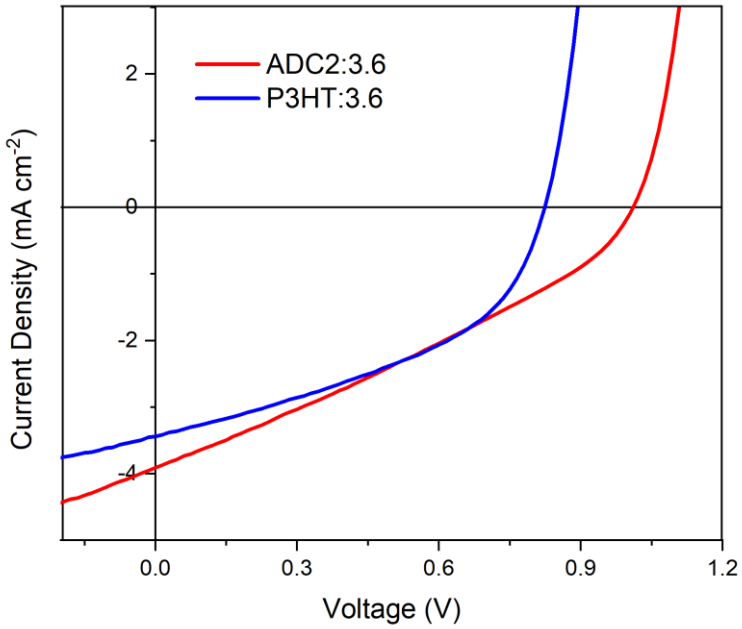


Figure 3-10: *J-V* curve of 3.6 with donor P3HT and ADC2 under standard testing conditions.

Table 3-5: Best solar cell device testing results for 3.6 with ADC2 and P3HT.

Blend (ratio)	Thermal annealing	J_{sc} (mA cm^{-2})	V_{oc} (V)	FF	PCE (%)
ADC2:3.6 (1:1)	120 °C	3.91	1.01	0.31	1.22
P3HT:3.6 (1:2)	120 °C	3.44	0.82	0.44	1.24

For P3HT and 3.6, the best power conversion efficiency of 1.24 % (via thermal annealing at 120 °C) was achieved for the blend ratio of 1:2 with J_{sc} of 3.44 mA cm^{-2} and V_{oc} of 0.82 V. In both cases the low fill factors obtained were limiting the performance, and possibly suggests that poor electron mobility is hindering charge extraction.

Even though the efficiencies are low compared to the state-of-art commonly reported in the literature with an average value of around 10 % from other acceptor materials, it is worth mentioning that they all show high open circuit voltage suggesting 3.6 can be a potential candidate for semi-transparent and/or tandem devices.

4. Binaphthyl Based Polymers

4.1 Overview

Circularly polarized (CP) light has attracted interest in fields like spintronics[20], high efficiency displays[19,22] and quantum optical computing.[50] Conventionally, for the field of light emitting displays, it was produced from a non-polarized light source using filters. However, such generation mechanism leads to loss in display brightness and efficiency,[98] and often requires complicated device architectures. Thus, to tackle those issues, direct generation of CP light from emissive source has been a focus of interest in light emitting display field such as OLEDs, which is the focus of this chapter.

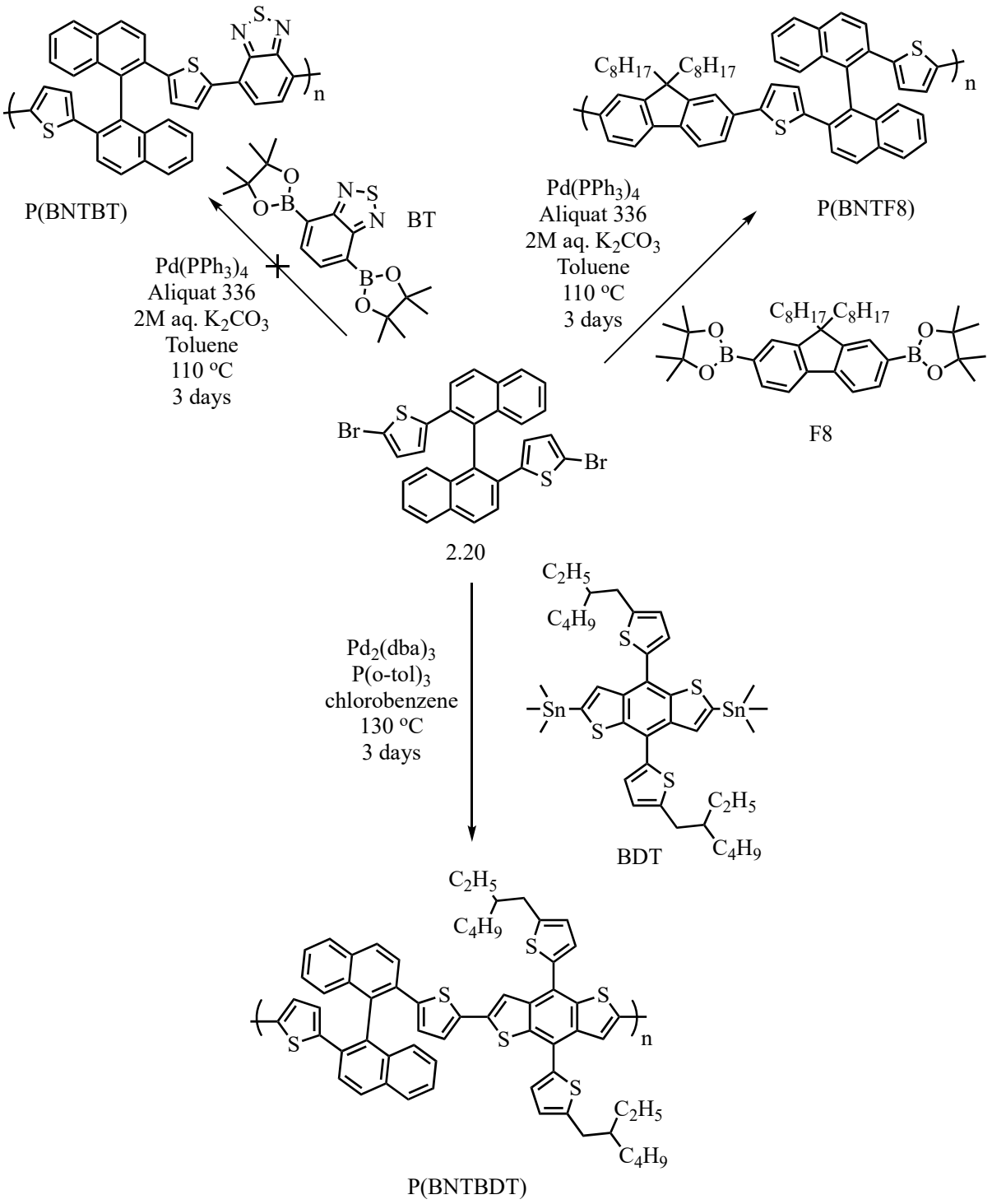
The dissymmetry factor (*g* factor), ranging from +2 to -2, is used to measure the relationship between right- and left- components of circularly polarized light. A *g* factor of +2 or -2 corresponds to fully left- or right-handed CP light respectively, whilst a *g* factor of zero corresponds to light with no circular polarization. The equation used for *g* factor calculation is defined by $= 2\frac{I_L - I_R}{I_L + I_R}$, where *I* refers to light intensity.

Organic materials that emit circularly polarized light directly often contain chiral components as mentioned earlier in Chapter 1. In this Chapter, the syntheses of three different 1,1'-binaphthyl based polymers were attempted (starting from racemic ones), and their corresponding optical properties and computational simulation were studied.

4.2 Synthesis

The synthetic route started from 2.20, as reported in Chapter 2. Three co-monomers were investigated, either benzothiadiazole (BT), benzodithiophene (BDT) or 9,9-dioctylfluorene (F8) (Scheme 4-1). The latter two co-monomers contained solubilizing side chains whereas the benzothiadiazole (BT) did not. We hypothesised that the contorted nature of the polymer might prevent close aggregation of the conjugated backbones and therefore promote solubility even without additional solubilizing groups, and therefore selected BT as a suitable co-monomer. The three co-monomers varied in terms of their electronic nature, from electron rich (BDT) to

neutral (fluorene) to electron poor (benzothiadiazole) in order to tune the optical band gap and emission wavelength of the resulting polymers.



Scheme 4-1: Preparation of three different polymers based on 1,1'-binaphthyl core.

The co-monomers were all commercially available. For the Suzuki polymerisation of BT and F8 co-monomers, the reactions were refluxed for three days in toluene in the presence of $Pd(PPh_3)_4$, 2M K_2CO_3 and a phase transfer catalyst to ensure good mixing between the organic and aqueous phase. For the Stille polymerisation of BDT, no additional base was required, and the polymerisation was performed in refluxing chlorobenzene. After reaction, the crude polymers were precipitated into methanol. Low weight oligomers and catalyst residues were removed by Soxhlet extraction with methanol, acetone and hexane. The final polymers were scraped off from the thimble, followed by drying under vacuum to afford 86%, 84% yield for P(BNTF8) and P(BNTBDT) respectively.

During the polymerisation with BT to afford P(BNTBT) it was observed that a precipitate began to form after a couple of hours, presumably due to poor solubility in the reaction solvent. After work-up the solid could not be redissolved in common solvents like chlorobenzene or 1,2-dichlorobenzene, even with heating. The poor observed solubility suggests that solubilizing side chains are required for processability. In the case of P(BNTF8) and P(BNTBDT) soluble materials were obtained in both cases. The molecular weight was measured by Gel Permeation Chromatography (GPC) in 1,2-dichlorobenzene against polystyrene standard. P(BNTF8) had a number average molecular weight ($\overline{M_n}$) of 8,400 Da with a weight average ($\overline{M_w}$) of 18,000 Da. P(BNTDBT) had a $\overline{M_n}$ of 17,000 Da, a $\overline{M_w}$ of 37,000 Da (Table 4-1).

Due to time constraint, the synthesis of enantioenriched/enantiomerically pure 1,1'-binaphthyl based polymers was not investigated.

Table 4-1: Weight average and number average molecular weights of the polymers.

	$\overline{M_n}$ / Da	$\overline{M_w}$ / Da	PDI
P(BNTF8)	8,400	18,000	2.14
P(BNTBDT)	17,000	37,000	2.15

4.3 Optical properties & Computational simulation

4.3.1 Ultraviolet-visible (UV-Vis) & Fluorescence Spectroscopy

The UV-Vis spectrum of P(BNTF8) in chloroform has an absorption maximum at 400 nm (Figure 4-1 a, c). Upon film formation (Figure 4-1 c) the spectra are very similar in shape, with

a maximum around 400 nm, although a new shoulder begins to emerge at longer wavelength. As for P(BNTBDT) (Figure 4-1 d), the peak at 423 nm becomes more protruding for thin film compared to its solution, which is possibly due to increased vibronic absorption at 423 nm as a result of change of aggregation at solid state. The similar solution and thin film UV-Vis absorption is a possible sign that the polymers cannot effectively planarise in the solid state, due to the twisting binaphthyl group in the backbone.

The solution emission spectrum of P(BNTF8) was measured with excitation wavelength of 400 nm (Figure 4-1 a), and its corresponding Stokes shift was 51 nm. As for P(BNTBDT) (Figure 4-1 b), the emission spectrum was measured with excitation wavelength of 440 nm, and its corresponding Stokes shift was 72 nm.

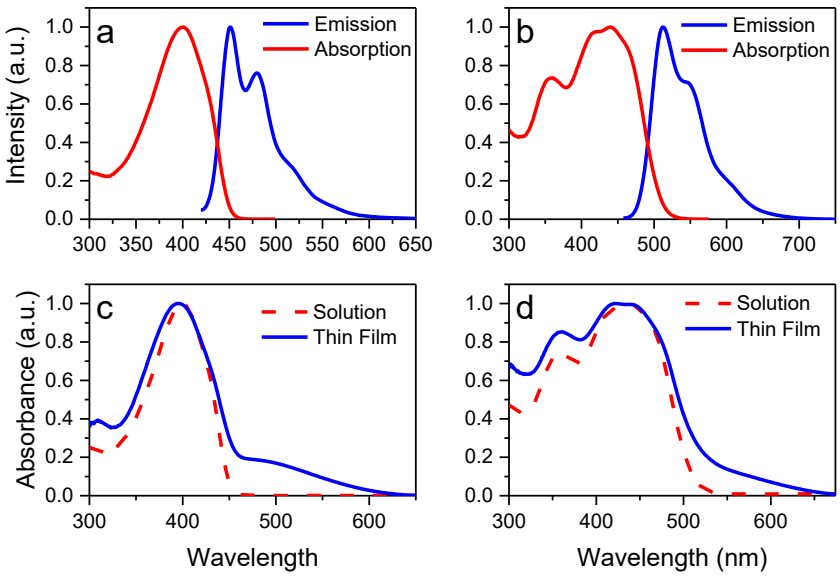


Figure 4-1: Normalized solution absorption and emission spectra of a) P(BNTF8) and b) P(BNTBDT) in chloroform; Normalized UV-Vis absorption spectra of c) P(BNTF8) and d) P(BNTBDT). All the films were made via spin coating with solution concentration of 10 mg/mL.

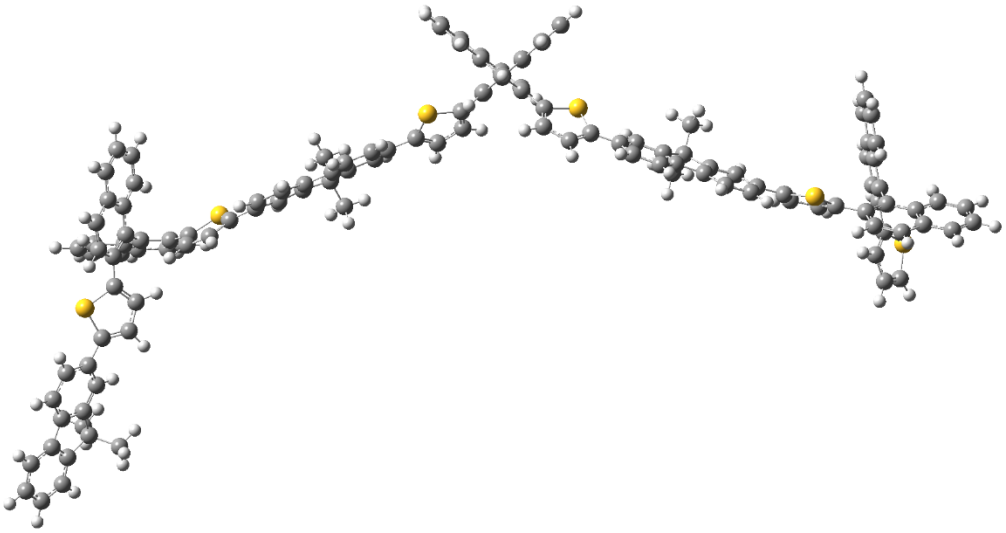
Table 4-2: Solution absorption and emission maxima of the polymers.

	$\lambda_{max,\ absorption}$ / nm	$\lambda_{max,\ emission}$ / nm
P(BNTF8)	400	451
P(BNTBDT)	440	512

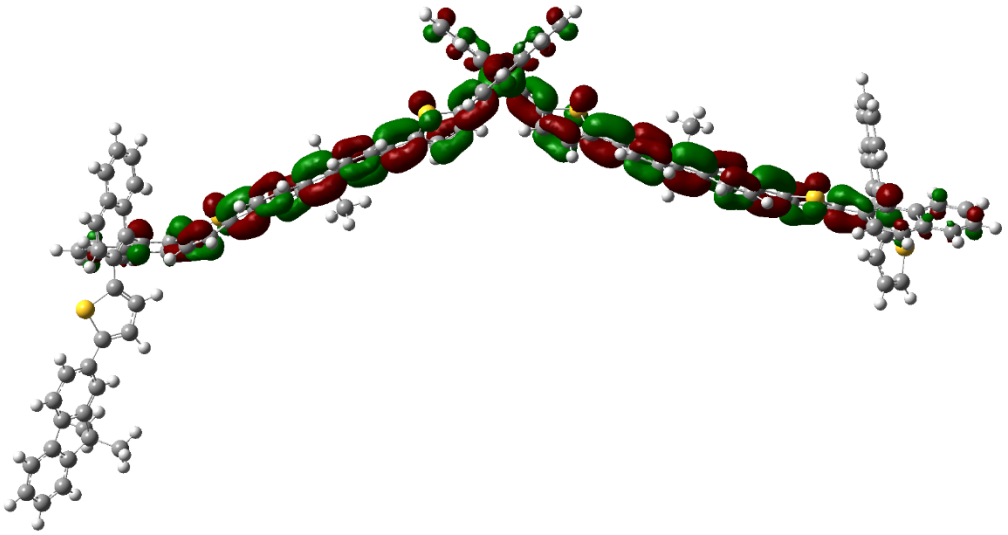
The absorption and emission maxima were measured in chloroform.

4.3.2 DFT

a)



b)

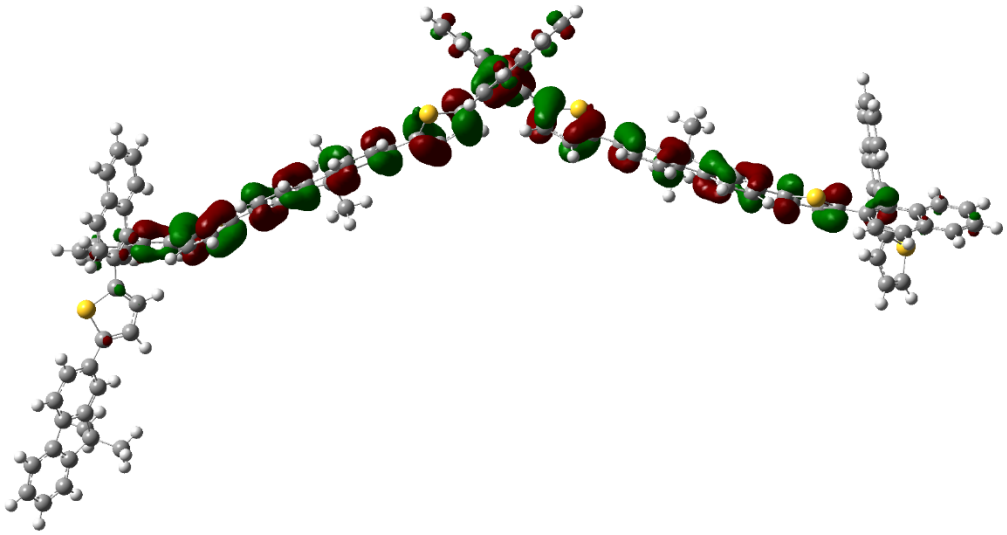


LUMO = -1.75 eV

Continued next page…

Continue of the previous

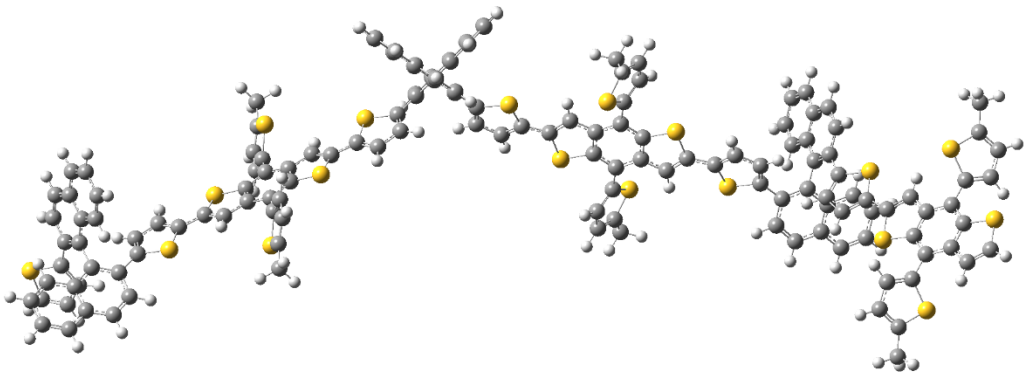
c)



HOMO = -4.98 eV

Figure 4-2: a) optimized ground state geometry, b) LUMO electron density plot and c) HOMO electron density plot of P(BNTF8).

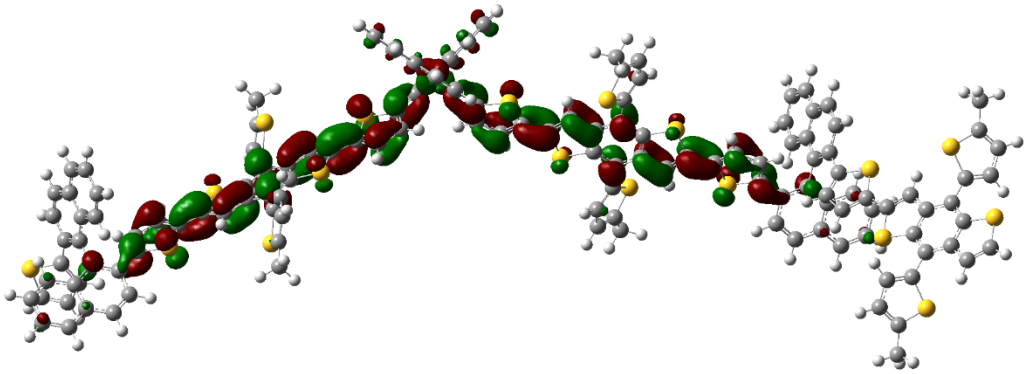
(a)



Continued next page…

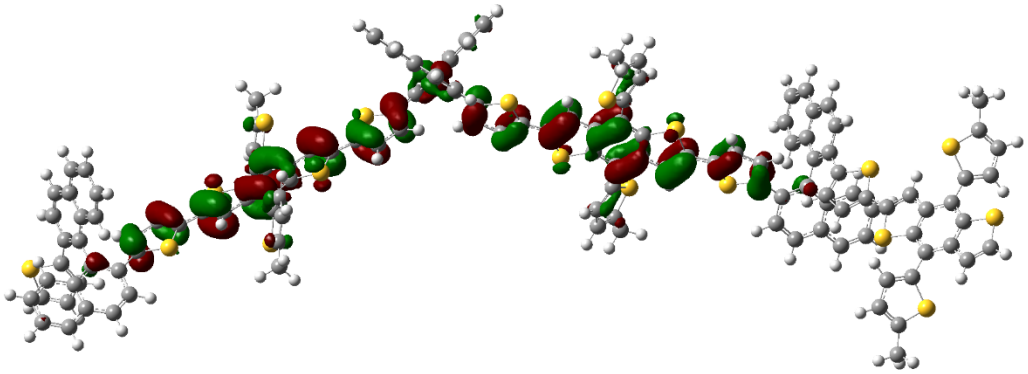
Continue of the previous

(b)



LUMO = -2.00 eV

c)



HOMO = -4.83 eV

Figure 4-3: a) optimized ground state geometry, b) LUMO electron density plot and c) HOMO electron density plot of P(BNTBDT).

DFT optimizations of P(BNTF8) and P(BNTBDT) were conducted using B3LYP with basis set of 6-31G (d, p) for finding the ground state geometry, followed by frequency analysis for verification. In order to simplify the calculations and reduce analysis time, three repeating units were used for each polymer with long alkyl chains substituted with methyl groups, and the relative geometry within each repeating unit was kept identical. Both polymers exhibit a highly contorted backbone, principally as a result of the binaphthyl group but additional twisting is observed between the other aromatic co-monomers.

The HOMO and LUMO were found to be - 4.98 eV and - 1.75 eV respectively for P(BNTF8). The HOMO of P(BNTBDT) was calculated to be – 4.83 eV and its LUMO was – 2.00 eV. Their corresponding HOMOs and LUMOs electron density plots are shown in Figure 4-2 and Figure 4-3. The contorted shape of optimized geometries is as expected due to twisted nature of binaphthyl core. Therefore, it is difficult for polymers to aggregate and planarize, rendering solution and thin film UV-Vis absorption spectra similar.

4.4 Conclusions

Two soluble polymers based on a racemic binaphthyl co-monomer were prepared. Both polymers exhibited very similar solution and solid-state UV-Vis absorption, likely as a result of their highly contorted backbone. These proof-of-concept synthetic studies suggest that the use of enantiomerically pure binaphthyl co-monomer is a valid strategy towards chirally pure polymers.

5. Conclusions

Chapter 2: Binaphthyl DPP Based Materials

Chapter 2 first looked at the material combination between 1,1'-binaphthyl core and DPP(EH). The syntheses of racemic BNDPP(EH) and BNTDPP(EH) were successful via Negishi cross-coupling with BNDPP(EH) had much lower yield (~ 5 %) compared to that of BNTDPP(EH) (~ 20 %). This improvement in yield is possibly due to relief of steric hindrance as a result of incorporation of an additional bridging thiophene unit for BNTDPP(EH) and is further justified by DFT analysis, where a smaller dihedral angle was observed for the binaphthyl core of BNTDPP, suggesting a greater degree of freedom. Opto-electronic properties of the materials were investigated with UV-Vis analysis and cyclic voltammetry. Solar cell device performance was tested for BNTDPP(EH) with negative feedback suggesting it is not a potential candidate in this field.

As for outlook, since the lab now has a preparative GPC, the syntheses of DPP boronic esters or its tin derivatives may deserve a revisit to investigate the possibility of having higher overall yields, so more devices and studies can be tested. In addition, the thin film morphology of solar cell blends is of interest to help to understand the lack of photocurrent for BNTDPP(EH).

The second part of Chapter 2 looked at the synthesis and characterisation of enantioenriched BNTDPP(BH) with potential application for circularly polarized light (CPL) detection or modification. DPP(BH) was synthesized first in the exact same manner as that for DPP(EH) to eliminate chirality on the ethylhexyl side chain, therefore allowing focus solely on the chirality of binaphthyl core. The same method used for the synthesis of BNTDPP(EH) did not work for BNTDPP(BH), and this problem was overcome by replacing $Pd(PPh_3)_4$ with sterically much less bulky $Pd(ACN)_2Cl_2$, which in turn gave a yield of ca. 15 %. Due to time constraint, further optimizations were not conducted for the improvement of the yield, and only UV-Vis and circular dichroism measurements were taken. The enantiomeric excess (ee) analysis for enantioenriched *S*-BNTDPP(BH) was not successful because it absorbs at sodium line and attempted analytical chiral HPLC analysis failed to separate. Therefore, as for outlook, one could carry on more optimizations, and possibly try a polarimeter with longer wavelength (800 nm) or different HPLC columns if possible, for ee determination. In addition, more characterisations such as making a device for tests in CPL applications.

Chapter 3: Binaphthyl Rhodanine Based Small Molecule Acceptors

First section of chapter 3 looked at the syntheses of binaphthyl rhodanine based acceptors 3.5 (Et), 3.6 (EH) and 3.7 (Bu). In which, 3.5 and 3.7 displayed an interesting phenomenon on TLC showing dumbbell liked two dots as a result of different polarities due to possible fast inter-converting stereo-configurations. NMR, mass spectroscopy and LCMS techniques were used for validation of the purity of the compounds. For 3.6, only one dot was observed on TLC, possibly because of steric clash imposed by bulky ethylhexyl chains.

The second section of chapter 3 looked at the opto-electric (UV-Vis and CV) and thermal properties of the compounds, where TGA analyses of all three compounds displayed great thermal stability with average T5d (temperature with 5 % weight loss) temperature of greater than 400 °C. DSC analyses displayed similar outcome as that for BNTDPP(EH), where first cycle showed a very pronounced melting peak followed by featureless second and third cycle, suggesting very slow rate of crystallization, which is possibly correlated to the nature of twisted binaphthyl core. DFT computational simulation with B3LYP, 6-31G(d, p) basis set and simplified alkyl chain suggested *Z*, *Z* - configuration has the lowest ground state energy at gaseous state. Moving to device performance test for 3.6 (EH), ADC-2 and regio-regular P3HT as donors showed best power conversion efficiencies around 1.2 % after thermal annealing at 120 °C with high open circuit voltage but low short circuit current compared to other common high-performance non-fullerene acceptors in literature.

As for outlook, more OPV device testing could be conducted to further optimize efficiencies. Furthermore, since the test results showed high open circuit voltage, it may be good to test out for tandem or semi-transparent devices.

Chapter 4: Binaphthyl Based Polymers

The original objective of chapter 4 was to synthesize and analysis of enantiomerically pure / enantioenriched 1, 1'- binaphthyl based polymers for potential application in detection/modification of circularly polarized light. However, due to time constraint, only racemic versions were synthesized from test runs. Three different polymers were attempted, P(BNTF8), P(BNTBDT) and P(BNTBT), in which P(BNTBT) could not be synthesized due to poor solubility, and P(BNTF8), P(BNTBDT) were synthesized successfully via Suzuki and Stille polymerization respectively. Opto-properties via UV-Vis absorption spectroscopy and photoluminescence spectroscopy were studied with corresponding stoke shift values calculated.

Furthermore, DFT simulations with B3LYP, 6-31G(d, p) basis set were also conducted for the two successful polymers.

As for outlook, the synthesis of enantioenriched version can be attempted. A comparison can then be drawn between racemic and enantioenriched compounds to further elucidate the differences in molecular packing and opto-electronic properties.

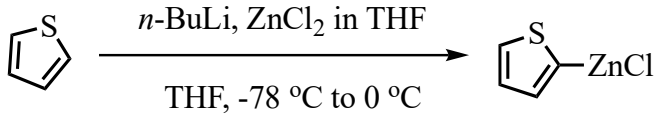
6. Experimental

General Experimental Techniques

All reactions were conducted in oven-dried glassware under inert atmosphere unless otherwise stated. All reagents and solvents were used directly without further purification unless otherwise stated. Commercially available 2,2'-(9,9-dioctyl-9H-fluorene-2,7-diyl)bis(4,4,5,5-tetramethyl-1,3,2-dioxaborolane) was purified by recrystallization (acetone). Reaction progress was monitored by analytical thin layer chromatography (TLC) on silica gel coated aluminium oxide F254 plates. Developed TLCs were visualized under UV light and/or stained with iodine. Column chromatography was performed employing silica gel 60 Å, particle size 40 - 63 μm. All ^{1}H and ^{13}C NMR spectra were recorded at 400 MHz and 101 MHz respectively at ambient temperature in $CDCl_3$ (with / without TMS as internal standard) unless otherwise noted and chemical shifts were reported in ppm. IR spectra are reported in cm^{-1}. Mass spectra were obtained from the Imperial College Mass Spectrometry Service or Swansea National Mass Spectrometry Facility. Melting points were uncorrected. Number-average ($\overline{M_n}$) and weight-average ($\overline{M_w}$) were determined by Agilent Technologies 1200 series GPC running in 1,2-dichlorobenzene at 80 °C, using two PL mixed B columns in series, and calibrated against narrow polydispersity polystyrene standards. UV-vis spectra were recorded on a UV-1601 Shimadzu UV-vis spectrometer. Cyclic voltammetry (CV) was carried out with a standard three-electrode cell in a 0.1 M tetrabutylammonium hexafluorophosphate ((TBA)PF6) solution in dichloromethane at room temperature with a scanning rate of 0.1 V s^{-1}. A Pt rod working electrode (1.6 mm diameter), a Pt wire counter electrode, and an Ag/AgCl reference electrode were used. The oxidation / reduction potentials were calibrated with respect to a standard ferrocene/ferrocenium (FOC) redox system (assuming the energy level of FOC is 4.8 eV below vacuum) for estimating the energy levels of molecules.

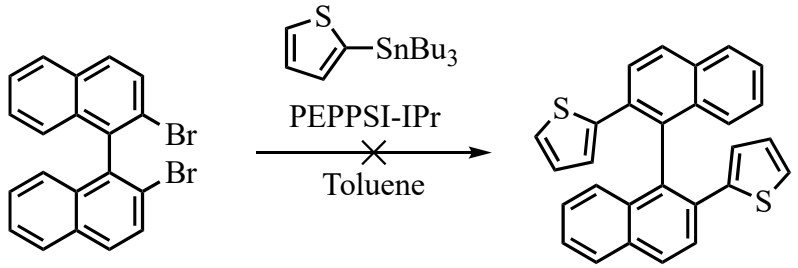
6.1 Chapter 2

Thiophen-2-ylzinc(II) chloride (~ 0.3 M in THF)



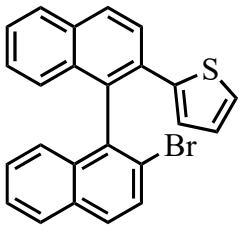
To a solution of thiophene (2.1 g, 25.0 mmol) in anhydrous THF (14 mL) at 0 ℃ was added *n*-BuLi (9 mL, 2.5 M in hexane, 22.5 mmol) dropwise, followed by stirring at 0 ℃ for 30 min. The mixture was then cooled to - 78 ℃, $ZnCl_2$ (43.8 mL, 0.7 M in THF, 30.0 mmol) was added dropwise. The resulting mixture was warmed to R.T. and used as it is.

2,2'-Di(thiophen-2-yl)-1,1'-binaphthalene (BNT)



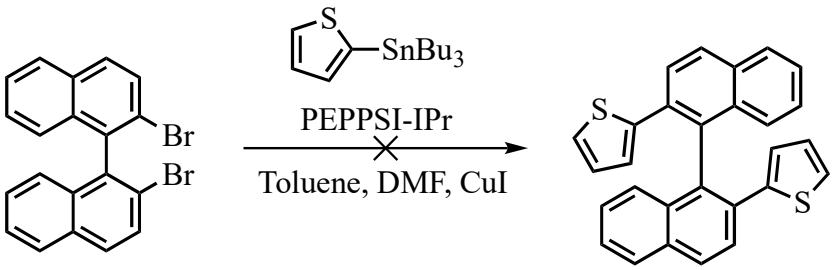
To a solution of 2,2′-dibromo-1,1′-binaphthyl (100 mg, 0.24 mmol), PEPPSI-IPr (8.26 mg, 0.012 mmol) in anhydrous toluene (3 mL) was added 2-(tributylstannyl)thiophene (0.17 mL, 0.53 mmol). The mixture was stirred overnight at room temperature. Reaction monitored by TLC (eluent: hexane/$CHCl_3$ = 3/1) showed majority being starting material (Rf = 0.4) and mono-coupled side product (Rf = 0.33):

2-(2'-Bromo-[1,1'-binaphthalen]-2-yl)thiophene

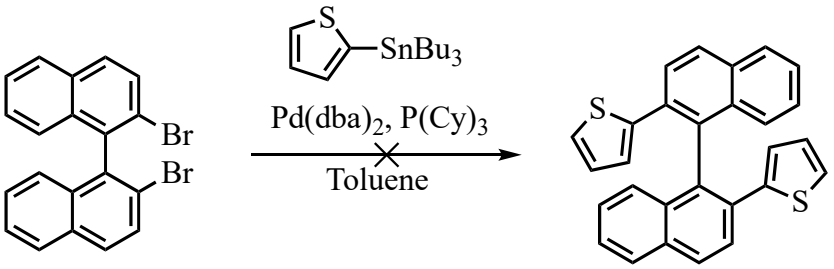


mp 169 – 170 °C. ^{1}H NMR (400 MHz, $CDCl_3$) δ 8.04 (d, *J* = 8.6 Hz, 1H), 7.99 – 7.82 (m, 4H), 7.77 (d, *J* = 8.8 Hz, 1H), 7.52 – 7.43 (m, 2H), 7.34 – 7.22 (m, 2H), 7.19 (d, *J* = 8.5 Hz, 1H), 7.13 (d, *J* = 8.5 Hz, 1H), 7.05 (dd, *J* = 5.1, 1.2 Hz, 1H), 6.87 (dd, *J* = 3.7, 1.2 Hz, 1H), 6.77

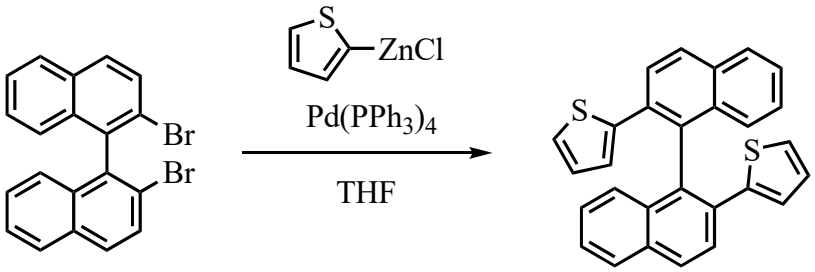
(dd, J = 5.1, 3.7 Hz, 1H). ^{13}C NMR (101 MHz, $CDCl_3$) δ 142.5, 136.9, 134.7, 133.9, 132.9, 132.6, 132.4, 131.8, 130.2, 129.9, 128.9, 128.3, 128.2, 127.6, 127.4, 127.1, 126.7, 126.5-126.3 (6 C), 124.3. HRMS (pAPCI) *m/z* calcd for $C_{24}H_{16}BrS$ $[M+H]^+$ 415.0151, found 415.0142.



To a solution of 2,2′-dibromo-1,1′-binaphthyl (100 mg, 0.24 mmol), PEPPSI-IPr (16.5 mg, 0.024 mmol) in anhydrous toluene (3 mL) was added 2-(tributylstannyl)thiophene (0.17 mL, 0.53 mmol), DMF (0.6 mL) and CuI (9.26 mg, 0.049 mmol). The mixture was stirred overnight at 100 ℃. TLC showed majority being starting material and mono-coupled side product.



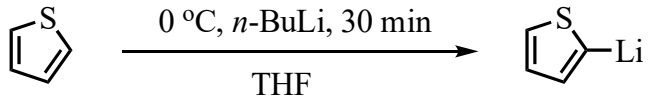
To a solution of 2,2′-dibromo-1,1′-binaphthyl (100 mg, 0.24 mmol), $Pd(dba)_2$ (14.0mg, 0.024 mmol) in anhydrous toluene (3 mL) was added 2-(tributylstannyl)thiophene (0.17 mL, 0.53 mmol), $P(Cy)_3$ (27.3 mg, 0.097 mmol). The mixture was stirred overnight at room temperature. TLC showed majority being starting material and mono-coupled side product.



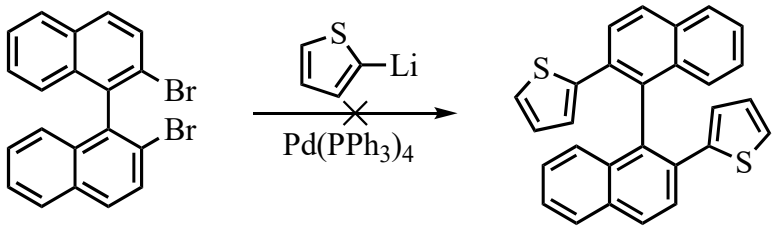
To a solution of 2,2'-dibromo-1,1'-binaphthalene (1 g, 2.43 mmol) and $Pd(PPh_3)_4$ (0.14 g, 0.121 mmol, 5 mol%) in anhydrous THF (30 mL) was added thiophen-2-ylzinc(II) chloride (45.5 mL, 0.3 M in THF, 14.6 mmol). The resulting mixture was refluxed for 2 days. The mixture was cooled to room temperature and filtered through a silica pad using THF as eluent. The filtrate was concentrated in *vacuo* and subjected to silica gel column chromatography (eluent: hexane/$CHCl_3$ = 3:1) to afford the product as a light yellow-green solid (0.94 g, 92 %). mp 196 – 200 °C (lit.[54] mp 195 – 200 °C). ^{1}H NMR (400 MHz, $CDCl_3$) δ 8.01 (d, *J* = 8.6 Hz, 2H), 7.92 (d, *J* = 8.3 Hz, 2H), 7.86 (d, *J* = 8.6 Hz, 2H), 7.48 – 7.41 (m, 2H), 7.25 – 7.21 (m, 4H), 6.99 (dd, *J* = 4.9, 1.4 Hz, 2H), 6.74 – 6.66 (m, 4H). ^{13}C NMR (101 MHz, $CDCl_3$) δ 142.7, 134.1, 133.3, 132.7 (2 C), 128.8, 128.0, 127.6, 126.9, 126.8, 126.5, 126.2, 126.1, 126.1. MS (EI) *m/z* 418.1 (M^+, 100%).

The reaction was repeated as above using 2,2'-dibromo-1,1'-binaphthalene (5.0 g, 12.1 mmol), $Pd(PPh_3)_4$ (0.705 g, 0.610 mmol, 5 mol%), anhydrous THF (95 mL) and thiophen-2-ylzinc(II) chloride (242 mL, 0.3 M in THF, 72.6 mmol) to afford the product as a light yellow-green solid (4.8 g, 95 %).

Thiophen-2-yllithium (~ 0.9 M in THF)



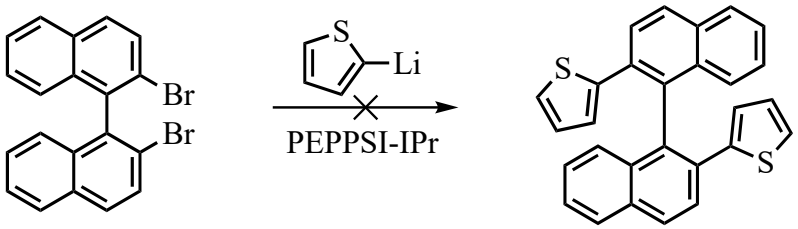
To a solution of thiophene (2.1 g, 25.0 mmol) in anhydrous THF (14 mL) at 0 °C was added *n*-BuLi (9 mL, 2.5 M in hexane, 22.5 mmol) dropwise, followed by stirring at 0 °C for 30 min. It was then warmed to room temperature and used as it is.



To 2,2'-dibromo-1,1'-binaphthalene (100 mg, 0.243 mmol) and $Pd(PPh_3)_4$ (14.0 mg, 0.012 mmol, 5 mol%) in an oven-dried 20 mL high-pressure microwave reactor vial at room temperature was added thiophen-2-yllithium (1.6 mL, 0.9 M in THF, 1.46 mmol). The resulting

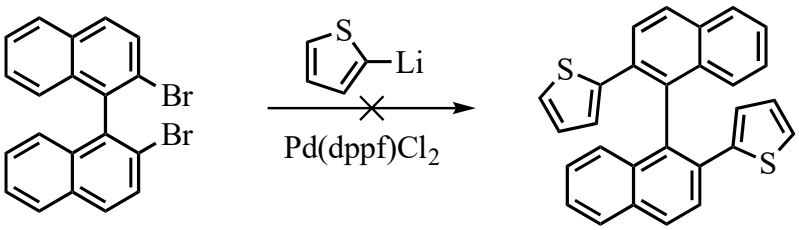
mixture was stirred at R.T for up to 3 days (TLC every overnight). TLC showed majority being starting material and mono-coupled side product.

Repeated as above with $Pd(PPh_3)_4$ (28.0 mg, 0.024 mmol, 10 mol%) and $Pd(PPh_3)_4$ (42.0 mg, 0.036 mmol, 15 mol%) with identical results.

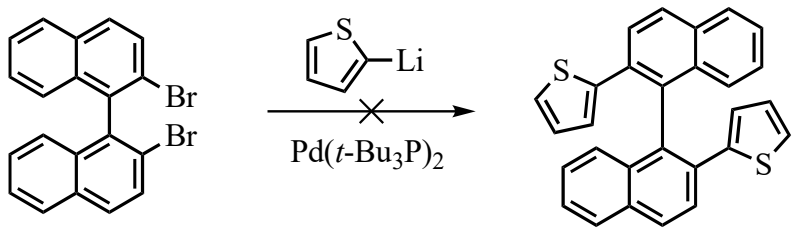


To 2,2'-dibromo-1,1'-binaphthalene (100 mg, 0.243 mmol) and PEPPSI-IPr (8.2 mg, 0.012 mmol, 5 mol%) in an oven-dried 20 mL high-pressure microwave reactor vial at room temperature was added thiophen-2-yllithium (1.6 mL, 0.9 M in THF, 1.46 mmol). The resulting mixture was stirred at R.T overnight. TLC showed majority being starting material and small amount of mono-coupled side product.

Repeated as above with PEPPSI-IPr (16.4 mg, 0.024 mmol, 10 mol%) with identical results.



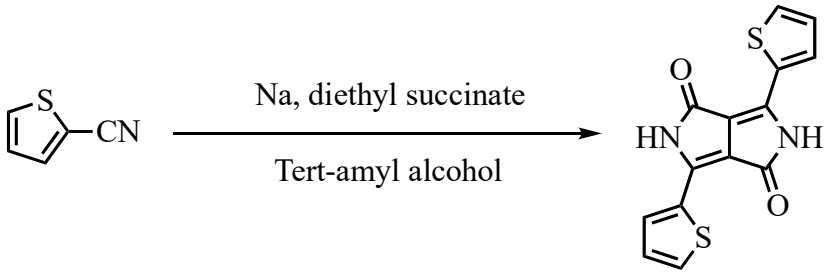
To 2,2'-dibromo-1,1'-binaphthalene (100 mg, 0.243 mmol) and $Pd(dppf)Cl_2$ (8.8 mg, 0.012 mmol, 5 mol%) in an oven dried 20 mL high-pressure microwave reactor vial at room temperature was added thiophen-2-yllithium (1.6 mL, 0.9 M in THF, 1.46 mmol). The resulting mixture was stirred at R.T overnight. TLC showed only starting material.



To 2,2'-dibromo-1,1'-binaphthalene (100 mg, 0.243 mmol) and Pd(*t*-$Bu_3P)_2$ (2.5 mg, 4.8 x 10^{-3} mmol, 2 mol%) in an oven dried 20 mL high-pressure microwave reactor vial at room temperature was added thiophen-2-yllithium (1.6 mL, 0.9 M in THF, 1.46 mmol). The resulting mixture was stirred at R.T overnight. TLC showed only starting material.

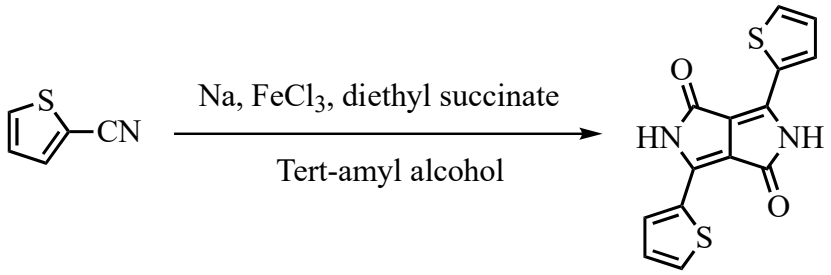
Repeated as above with Pd(*t*-$Bu_3P)_2$ (6.1 mg, 0.012 mmol, 5 mol%) and Pd(*t*-$Bu_3P)_2$ (12.2 mg, 0.024 mmol, 10 mol%) with identical results.

3,6-Di(thiophen-2-yl)-2,5-dihydropyrrolo[3,4-c]pyrrole-1,4-dione



Sodium (3.32 g, 144.3 mmol) was added to 2-methylbutan-2-ol (75 mL), the mixture was stirred at 110 °C until complete dissolution. The temperature was then lowered to 90 °C and 2-thiophenecarbonitrile (8.0 mL, 86.6 mmol) was added in one portion, affording a brown medium. A solution of diethyl succinate (4.8 mL, 28.9 mmol) in 2-methylbutan-2-ol (18 mL) was added dropwise and the solution was stirred at 110 °C overnight. A solution of acetic acid (20 mL) in methanol (100 mL) was added to the medium, resulting in the precipitation of a deep purple solid, collected via vacuum filtration. Several washes with hot methanol were carried out until filtrate is reasonably colourless. The crude product was dried to afford a purple powder (4.0 g, 46 %) and it was used as it was without further purification.

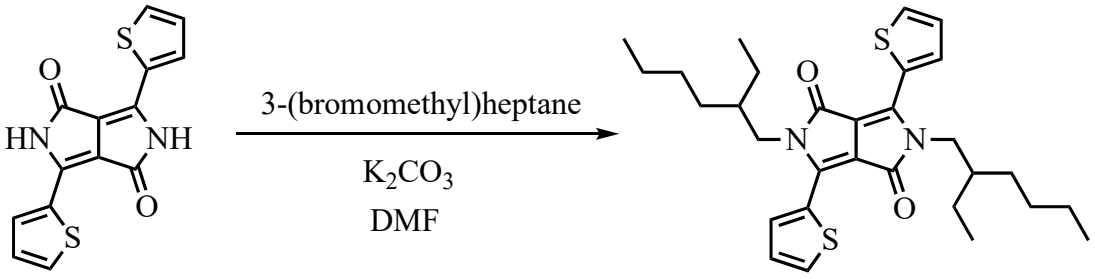
The reaction was repeated using sodium (9.96 g, 432.8 mmol),2-methylbutan-2-ol (200 mL), 2-thiophenecarbonitrile (24.0 mL, 259.7 mmol) under identical conditions to above to afford a purple powder (20.0 g, 76.9 %) and it was used as it was without further purification.



Alternative Procedure

Sodium (6.36 g, 276.5 mmol) and trace amount of $FeCl_3$ were added to 2-methylbutan-2-ol (150 mL), the mixture was stirred at 110 °C until complete dissolution. The temperature was then lowered to 90 °C and 2-thiophenecarbonitrile (16 mL, 171.7 mmol) was added in one portion, affording a brown medium. A solution of diethyl succinate (9.6 mL, 57.3 mmol) in 2-methylbutan-2-ol (36 mL) was added dropwise and the solution was stirred at 110 °C overnight. A solution of acetic acid (40 mL) in methanol (200 mL) was added to the medium, resulting in the precipitation of a deep purple solid, collected via vacuum filtration. Several washes with hot methanol were carried out until filtrate is reasonably colourless. The crude product was dried to offer a purple powder (12.6 g, 73.1%) and it was used as it was without further purification.

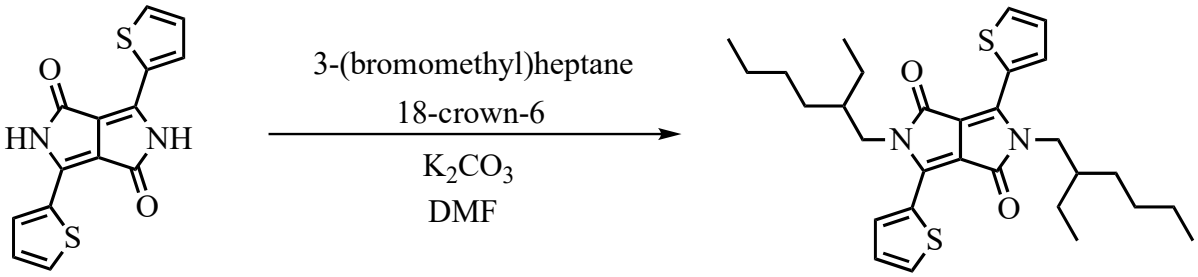
2,5-Bis(2-ethylhexyl)-3,6-di(thiophen-2-yl)-2,5-dihydropyrrolo[3,4-c]pyrrole-1,4-dione {DPP(EH)}



To a solution of 3,6-dithiophen-2-yl-2,5-dihydropyrrolo[3,4-c]pyrrole-1,4-(2H,5H)-dione (3.92 g, 13.1 mmol) in anhydrous DMF (65 mL) was added anhydrous potassium carbonate (7.23 g, 52.3 mmol). The mixture was stirred at 145 °C for 10 min resulting in a deep purple

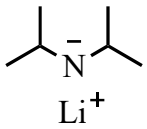
colour solution. It was then cooled to 100 °C and 2-ethylhexylbromide (11.6 mL, 65.2 mmol) was added slowly. The resulting mixture was stirred at 145 °C overnight, cooled to RT and was quenched with an ice/water solution (150 mL). Extraction with DCM (3 x), the combined organic phases were washed with water, brine, dried over Na_2SO_4, filtered and concentrated in *vacuo*. Purification by silica chromatography (eluent: hexane/DCM = 1:2) to afford the desired product as a purple solid (1.5 g, 21 %). mp 124 – 128 °C (lit.[99] mp 127 °C). ^{1}H NMR (400 MHz, $CDCl_3$) δ 8.89 (d, *J* = 3.9 Hz, 2H), 7.63 (d, *J* = 5.0 Hz, 2H), 7.27 (dd, *J* = 5.0, 3.9 Hz, 2H), 4.10 – 3.95 (m, 4H), 1.95 – 1.76 (m, 2H), 1.41 – 1.17 (m, 16H), 0.91 – 0.80 (m, 12H). ^{13}C NMR (101 MHz, $CDCl_3$) δ 161.4, 140.9, 135.6, 130.8, 129.8, 128.5, 108.1, 45.9, 39.1, 30.2, 28.3, 23.5, 23.1, 14.0, 10.5. HRMS (ES+) *m/z* calcd for $C_{30}H_{41}N_2O_2S_2$ [M^+] 525.2609, found 525.2623.

Repeated as above using 3,6-dithiophen-2-yl-2,5-dihydropyrrolo[3,4-c]pyrrole-1,4-(2H,5H)-dione (12.0 g, 40.0 mmol), potassium carbonate (22.1 g, 159.8 mmol),DMF (195 mL) to afford the desired product as a purple solid (6.93 g, 33 %).



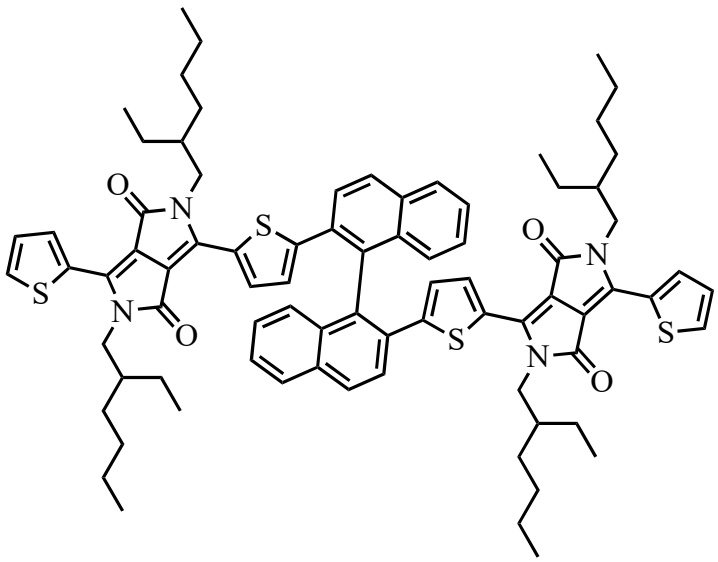
To a solution of 3,6-dithiophen-2-yl-2,5-dihydro-pyrrolo[3,4-c]pyrrole-1,4-dione (5.0 g, 16.6 mmol) in anhydrous N,N-dimethylformamide (DMF, 120 mL) was added anhydrous K_2CO_3 (7.60 g, 55.0 mmol). The mixture was heated at 120 °C for 1 h. 3-(bromomethyl)heptane (9.80 g, 50.7 mmol) was then added dropwise, followed by a small amount of 18-crown-6. The reaction mixture was further stirred at 150 °C overnight, before being cooled to room temperature and poured into distilled water (400 mL). The resulting suspension was stirred at room temperature for 1 h, collected by vacuum filtration, washed with several portions of distilled water and methanol, dried under vacuum. The crude product was purified via silica gel column chromatography (eluent: hexane/DCM = 1:1) to afford a dark red solid (2.37 g, 27 %).

General method for preparing lithium diisopropylamide (LDA) freshly:



To a solution of diisopropylamine (1 eq.) in anhydrous THF at – 78 °C was added *n*-BuLi (2.5 M in hexane, 0.9 eq.) dropwise and the resulting solution was stirred at – 78 °C for 1 min. The resulting mixture was warmed to room temperature and used as it is.

6,6'-([1,1'-Binaphthalene]-2,2'-diylbis(thiophene-5,2-diyl))bis(2,5-bis(2-ethylhexyl)-3-(thiophen-2-yl)-2,5-dihydropyrrolo[3,4-c]pyrrole-1,4-dione) {BNDPP(EH)}



With 5 mol% $Pd(PPh_3)_4$ and 3 eq. of DPP(EH).

To a solution of DPP(EH) (382 mg, 0.73 mmol) in THF (25 mL) at – 78 °C was added LDA (0.87 mmol) dropwise. After stirring for 30 min at – 78 °C. $ZnCl_2$ (0.7 M in THF, 1.5 mL, 1.02 mmol) was added and the mixture was stirred for another 30 min before warming to room temperature. 2,2'-Dibromo-1,1'-binaphthalene (100 mg, 0.243 mmol) and $Pd(PPh_3)_4$ (14.0 mg, 0.012 mmol, 5 mol%) in THF (7 mL) were added and the resulting mixture was refluxed overnight. The reaction was cooled to RT, saturated NH_4Cl solution was added and the mixture extracted with $CHCl_3$ (3 x 15 mL). The combined organic phases were washed with water, brine, dried over Na_2SO_4, filtered and concentrated in *vacuo*. The crude was purified by column

chromatography over silica (eluent: DCM) to give the desired product as a black-purple solid (15 mg, 4 %). ^{1}H NMR (400 MHz, $CDCl_3$) δ 8.84 – 8.70 (m, 4H), 8.13 – 8.02 (m, 2H), 7.94 (dd, *J* = 8.3, 3.9 Hz, 4H), 7.58 (d, *J* = 4.7 Hz, 2H), 7.52 – 7.42 (m, 2H), 7.25 – 7.13 (m, 6H), 6.99 – 6.86 (m, 2H), 4.10 – 3.84 (m, 4H), 3.80 – 3.49 (m, 4H), 1.93 – 1.69 (m, 2H), 1.62 – 1.49 (m, 2H), 1.41 – 0.97 (m, 32H), 0.89 – 0.55 (m, 24H). ^{13}C NMR (101 MHz, $CDCl_3$) δ 161.8, 161.6, 148.1, 140.6, 139.8, 136.2, 135.1, 133.8, 133.6, 133.4, 131.8, 130.4, 130.0, 129.8, 128.4, 128.1, 127.67, 127.0, 126.7, 108.2, 107.9, 46.0, 39.2, 39.0, 30.3, 30.0, 28.5, 24.6, 23.2, 14.2, 10.6. HRMS (ESI+) *m/z* calcd for $C_{88}H_{95}O_4N_4S_6$ $[M+H]^+$ 1463.5672, found 1463.5651.

With 7.5 mol% $Pd(PPh_3)_4$ and 3 eq. of DPP(EH):

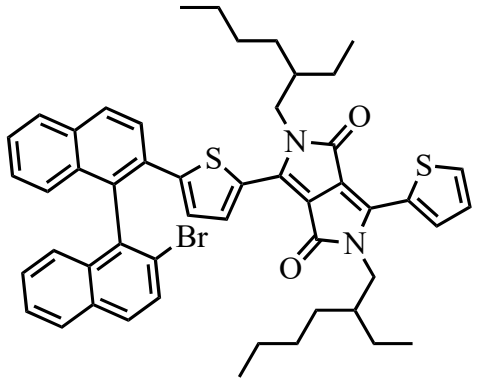
Repeated as above using DPP(EH) (382 mg, 0.73 mmol), THF (25 mL), LDA (0.87 mmol), $ZnCl_2$ (0.7 M in THF, 1.5 mL, 1.02 mmol), 2,2'-dibromo-1,1'-binaphthalene (100 mg, 0.243 mmol) and $Pd(PPh_3)_4$ (21.0 mg, 0.018 mmol, 7.5 mol%) to give desired product as a black-purple solid (15 mg, 4 %).

With 5 mol% $Pd(PPh_3)_4$ and 6 eq. of DPP(EH):

Repeated as above using DPP(EH) (764 mg, 1.46 mmol), THF (50 mL), LDA (1.74 mmol), $ZnCl_2$ (0.7 M in THF, 3.0 mL, 2.04 mmol), 2,2'-dibromo-1,1'-binaphthalene (100 mg, 0.243 mmol) and $Pd(PPh_3)_4$ (14.0 mg, 0.012 mmol, 5 mol%) to give desired product as a black-purple solid (16 mg, 5 %).

Side product:

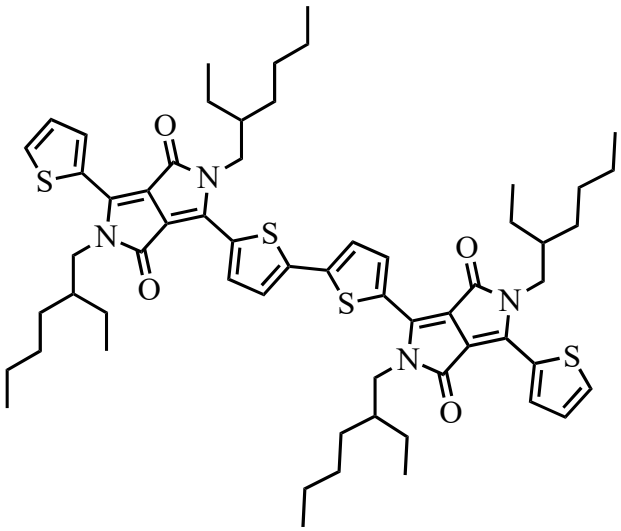
3-(5-(2'-Bromo-[1,1'-binaphthalen]-2-yl)thiophen-2-yl)-2,5-bis(2-ethylhexyl)-6-(thiophen-2-yl)-2,5-dihydropyrrolo[3,4-c]pyrrole-1,4-dione



^{1}H NMR (400 MHz, $CDCl_3$) δ 8.82 (d, *J* = 3.9 Hz, 1H), 8.76 (dd, *J* = 6.1, 4.2 Hz, 1H), 8.07 (d, *J* = 8.7 Hz, 1H), 8.00 – 7.84 (m, 4H), 7.77 (d, *J* = 8.8 Hz, 1H), 7.59 (d, *J* = 5.1 Hz, 1H), 7.55 – 7.40 (m, 2H), 7.36 – 7.29 (m, 1H), 7.26 – 7.20 (m, 2H), 7.17 – 7.09 (m, 2H), 7.03 – 6.96 (m, 1H), 4.08 – 3.90 (m, 2H), 3.80 – 3.62 (m, 2H), 1.89 – 1.75 (m, 1H), 1.73 – 1.63 (m, 1H), 1.40 – 0.99 (m, 16H), 0.94 – 0.67 (m, 12H). ^{13}C NMR (101 MHz, $CDCl_3$) δ 161.9, 161.7, 148.3, 140.9, 139.8, 136.2, 135.1, 134.6, 133.4, 132.6, 132.4, 130.6, 130.4-130.15 (multiple C), 130.0, 129.3, 128.5, 128.3, 128.1, 127.7, 127.4, 127.05-126.92 (multiple C), 126.6, 126.2, 124.3, 108.3, 107.8, 46.1, 39.2, 39.0, 30.3, 30.1, 28.5, 23.6, 23.3, 14.2, 10.6. HRMS (ES+) *m/z* calcd for $C_{50}H_{52}N_2O_2S_2Br$ [M^+] 855.2654, found 855.2664.

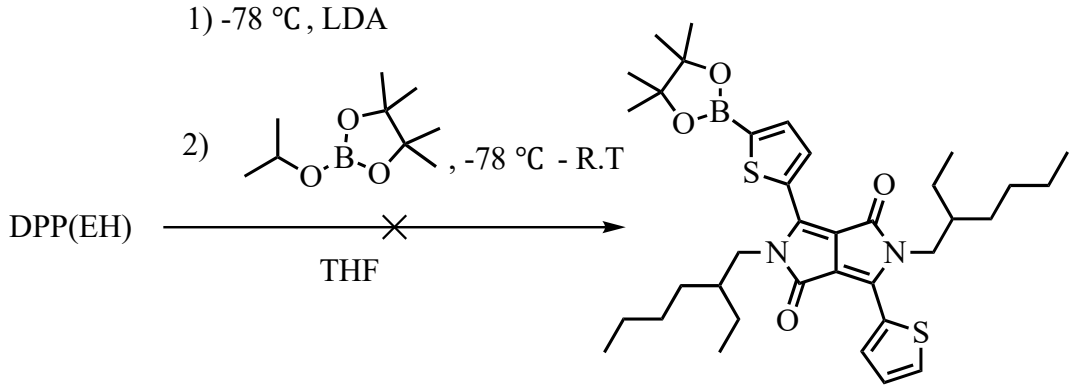
Side product:

6,6'-([2,2'-Bithiophene]-5,5'-diyl)bis(2,5-bis(2-ethylhexyl)-3-(thiophen-2-yl)-2,5-dihydropyrrolo[3,4-*c*]pyrrole-1,4-dione)



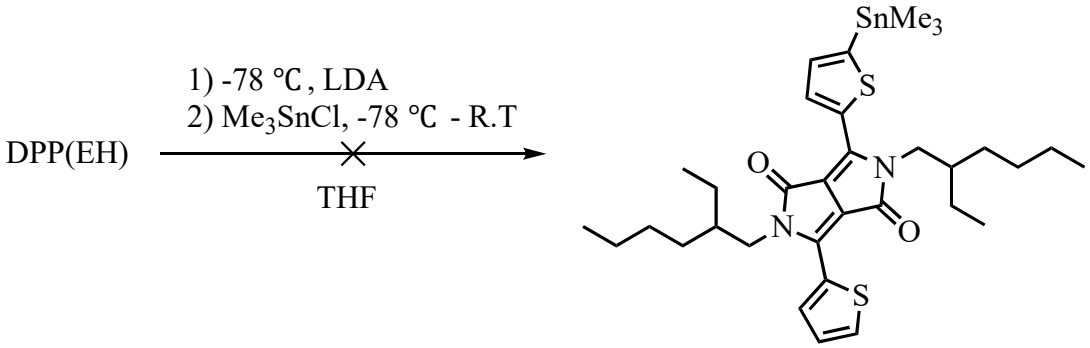
^{1}H NMR (400 MHz, $CDCl_3$) δ 8.96 (d, *J* = 4.2 Hz, 2H), 8.92 (dd, *J* = 4.0, 0.9 Hz, 2H), 7.64 (dd, *J* = 4.9, 0.9 Hz, 2H), 7.43 (d, *J* = 4.2 Hz, 2H), 7.28 (dd, *J* = 4.9, 4.0 Hz, 2H), 4.14 – 3.92 (m, 8H), 1.99 – 1.81 (m, 4H), 1.49 – 1.11 (m, 32H), 1.02 – 0.77 (m, 24H).

2,5-Bis(2-ethylhexyl)-3-(5-(4,4,5,5-tetramethyl-1,3,2-dioxaborolan-2-yl)thiophen-2-yl)-6-(thiophen-2-yl)-2,5-dihydropyrrolo[3,4-*c*]pyrrole-1,4-dione



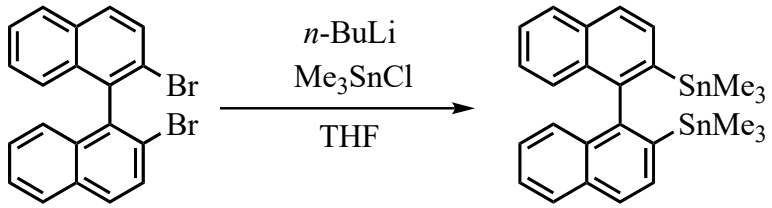
To a solution of DPP(EH) (100 mg, 0.19 mmol) in THF (15 mL) at -78 ºC was added LDA (0.19 mmol) dropwise, the resulting mixture was stirred at -78 ºC for 30 min before addition of 2-isopropoxy-4,4,5,5-tetramethyl-1,3,2-dioxaborolane (42.5 mg, 0.23 mmol). The resulting mixture was stirred overnight allowing warm to ambient temperature. Water was added followed by extraction with DCM 3x, the combined organic phases were washed with water, brine, dried over sodium sulphate, and concentrated in *vacuo*. The crude product could not be purified by column chromatography due to protodeboronation.

2,5-Bis(2-ethylhexyl)-3-(thiophen-2-yl)-6-(5-(trimethylstannyl)thiophen-2-yl)-2,5-dihydropyrrolo[3,4-*c*]pyrrole-1,4-dione



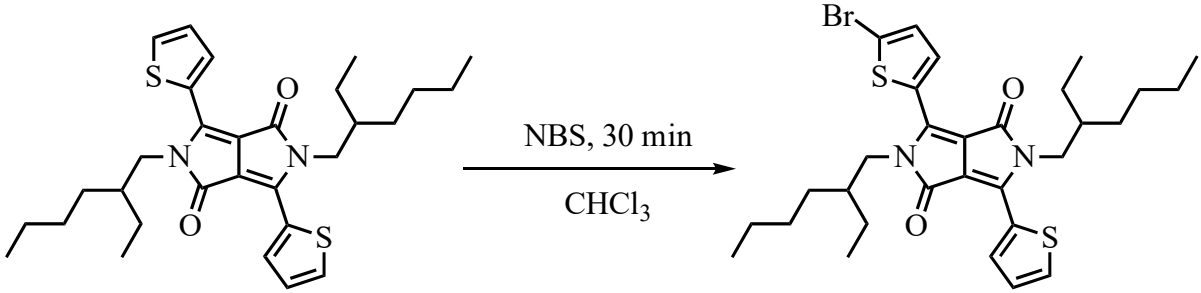
To a solution of DPP(EH) (100 mg, 0.19 mmol) in THF at -78 ºC was added LDA (0.19 mmol) dropwise, the resulting mixture was stirred at -78 ºC for 30 min before addition of chlorotrimethylstannane (45.4 mg, 0.23 mmol). The resulting mixture was stirred overnight allowing warm to ambient temperature. Water was added followed by extraction with DCM 3x, the combined organic phases were washed with water, brine, dried over sodium sulphate, and concentrated in *vacuo*. The crude product could not be purified by column chromatography due to degradation.

2,2'-Bis(trimethylstannyl)-1,1'-binaphthalene



To a solution of 2,2'-dibromo-1,1'-binaphthalene (300 mg, 0.727 mmol) in anhydrous THF (10 mL) at -45 °C was added *n*-BuLi (2.5 M in hexane, 1.2 mL, 2.91 mmol) dropwise. The resulting mixture was stirred at - 45 °C for 1 h then cooled to – 78 °C. Trimethyltin chloride solution (1M in THF, 4.4 mL, 4.4 mmol) was added dropwise. The mixture was allowed to warm to room temperature with stirring overnight. Water (5 mL) was added and the mixture was extracted with hexane (3 x 15 mL). The combined organic phases were washed with saturated aqueous NH_4Cl, brine, dried over $MgSO_4$, filtered and concentrated in *vacuo*. The crude was purified by column chromatography over silica (eluent: hexane:Et_2O = 49:1) to give the desire product as a colourless oil (98.8 mg, 23.4 %). ^{1}H NMR (400 MHz, $CDCl_3$) δ 7.97 – 7.89 (m, 4H), 7.75 (d, *J* = 8.1 Hz, 2H), 7.45 (ddd, *J* = 8.1, 5.3, 2.7 Hz, 2H), 7.27 – 7.21 (m, 4H), -0.27 (s, 18H). ^{13}C NMR (101 MHz, $CDCl_3$) δ 147.6, 142.6, 133.7, 133.3, 132.1, 127.9, 127.0, 126.9, 126.0, 125.9, -8.62.

3-(5-Bromothiophen-2-yl)-2,5-bis(2-ethylhexyl)-6-(thiophen-2-yl)-2,5-dihydropyrrolo[3,4-c]pyrrole-1,4-dione

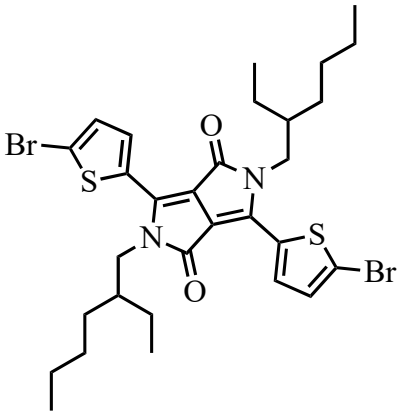


To a solution of 2,5-bis(2-ethylhexyl)-3,6-di(thiophen-2-yl)-2,5-dihydropyrrolo[3,4-c]pyrrole-1,4-dione (7.11 g, 13.5 mmol) in anhydrous $CHCl_3$ (150 mL) was added NBS (2.89 g, 16.3 mmol) in one portion. The mixture was stirred in the dark at room temperature for 30 min. The

solution was concentrated in *vacuo* and the residue was taken up in CH_2Cl_2, washed with water, brine, dried over Na_2SO_4, filtered and concentrated in *vacuo*. Purification via column chromatography over silica (eluent: DCM:hexane = 3:2) to afford the desired product as a fushia-purple solid (4.09 g, 50 %). mp 127 – 129 °C. ^{1}H NMR (400 MHz, $CDCl_3$) δ 8.90 (dd, *J* = 3.9, 1.0 Hz, 1H), 8.63 (d, *J* = 4.2 Hz, 1H), 7.64 (dd, *J* = 5.0, 1.0 Hz, 1H), 7.27 (dd, *J* = 5.0, 3.9 Hz, 1H), 7.22 (d, *J* = 4.2 Hz, 1H), 4.08 – 3.88 (m, 4H), 1.91 – 1.77 (m, 2H), 1.44 – 1.15 (m, 16H), 0.98 – 0.76 (m, 12H). HRMS (ES+) *m/z* calcd for $C_{30}H_{40}N_2O_2S_2$ [M^+] 603.1715, found 603.1704.

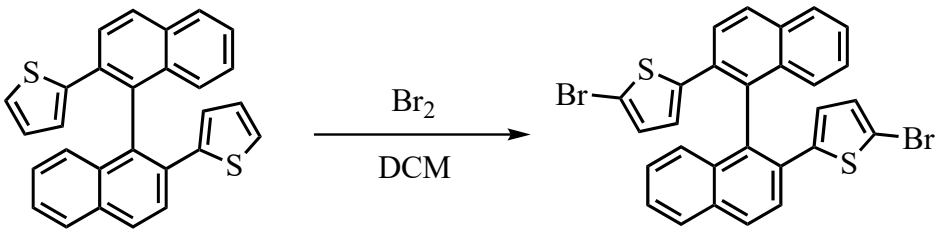
Side product of the above NBS bromination procedure:

3,6-Bis(5-bromothiophen-2-yl)-2,5-bis(2-ethylhexyl)-2,5-dihydropyrrolo[3,4-*c*]pyrrole-1,4-dione



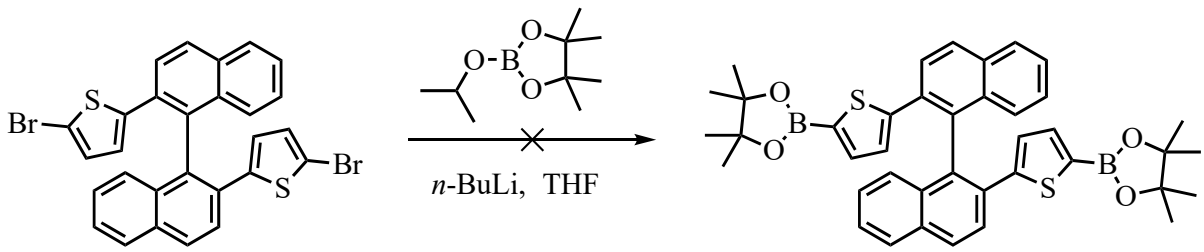
mp 164 – 165 ºC (lit[100] mp 164.6 – 166.3 ºC) ^{1}H NMR (400 MHz, $CDCl_3$) δ 8.64 (d, *J* = 4.2 Hz, 2H), 7.22 (d, *J* = 4.2 Hz, 2H), 4.01 – 3.83 (m, 4H), 1.93 – 1.73 (m, 2H), 1.42 – 1.12 (m, 16H), 0.96 – 0.71 (m, 12H). MS (ES+) *m/z* 683.1 (M^+).

2,2'-Bis(5-bromothiophen-2-yl)-1,1'-binaphthalene

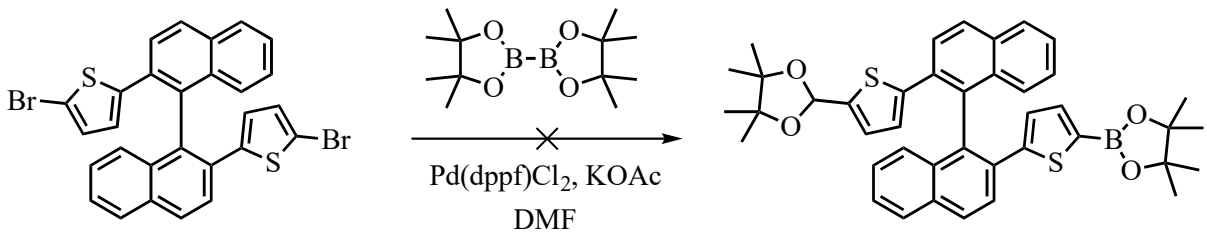


To a solution of 2,2'-di(thiophen-2-yl)-1,1'-binaphthalene (200 mg, 0.48 mmol) in anhydrous DCM (75 mL) at 0 °C was added Br_2 (0.28 mL, 3.3 M in DCM, 0.95 mmol) dropwise. The resulting mixture was stirred strongly at 0 °C - R.T for 3 hrs. It was then washed with saturated aqueous solution of $Na_2S_2O_5$ (2 x 15 mL), water, brine, dried over $MgSO_4$, filtered and concentrated in *vacuo*. The crude was purified by column chromatography over silica (eluent: hexane:$CHCl_3$ = 5:1) to afford desired product as a white solid (0.20 g, 72 %). mp 201-202 °C (lit.[53] mp 200-202 °C). ^{1}H NMR (400 MHz, $CDCl_3$) δ 8.02 (d, *J* = 8.7 Hz, 1H), 7.92 (d, *J* = 8.5 Hz, 2H), 7.79 (d, *J* = 8.7 Hz, 2H), 7.46 (t, *J* = 7.4 Hz, 2H), 7.24 (t, *J* = 7.4 Hz, 2H), 7.13 (d, *J* = 8.5 Hz, 2H), 6.68 (d, *J* = 3.9 Hz, 2H), 6.52 (d, *J* = 3.9 Hz, 2H). ^{13}C NMR (101 MHz, $CDCl_3$) δ 144.0, 133.9, 132.9, 132.6, 132.0, 129.4, 129.3, 128.1, 127.1, 126.7, 126.5, 126.4, 126.4, 113.2. MS (EI+) *m/z* 576 (M^+, 100%).

4,4,5,5-Tetramethyl-2-(5-(2'-(5-(4,4,5,5-tetramethyl-1,3-dioxolan-2-yl)thiophen-2-yl)-[1,1'-binaphthalen]-2-yl)thiophen-2-yl)-1,3,2-dioxaborolane

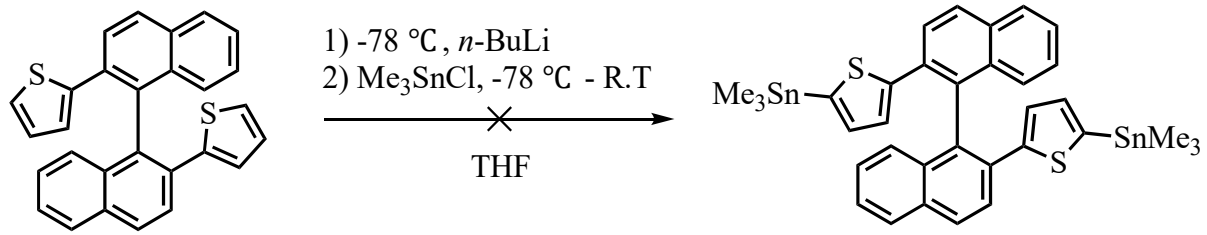


To a solution of 2,2'-bis(5-bromothiophen-2-yl)-1,1'-binaphthalene (200 mg, 0.35 mmol) in anhydrous THF (15 mL) at – 78 °C was added *n*-BuLi (1.6 M in hexane, 0.5 mL, 0.80 mmol) dropwise. The mixture was stirred vigorously at – 78 °C for 1.5 hrs then 2-isopropoxy-4,4,5,5-tetramethyl-1,3,2-dioxaborolane (0.3 mL, 1.4 mmol) was added in one portion. The resulting mixture was allowed to warm to ambient temperature with stirring overnight. Water (6 mL) was added and the mixture was extracted with EtOAc (3 x 15 mL). The combined organic phases were washed with brine, dried over Na_2SO_4, filtered and concentrated in *vacuo*. Isolation of desired product via silica column chromatography failed due to protodeboronation.



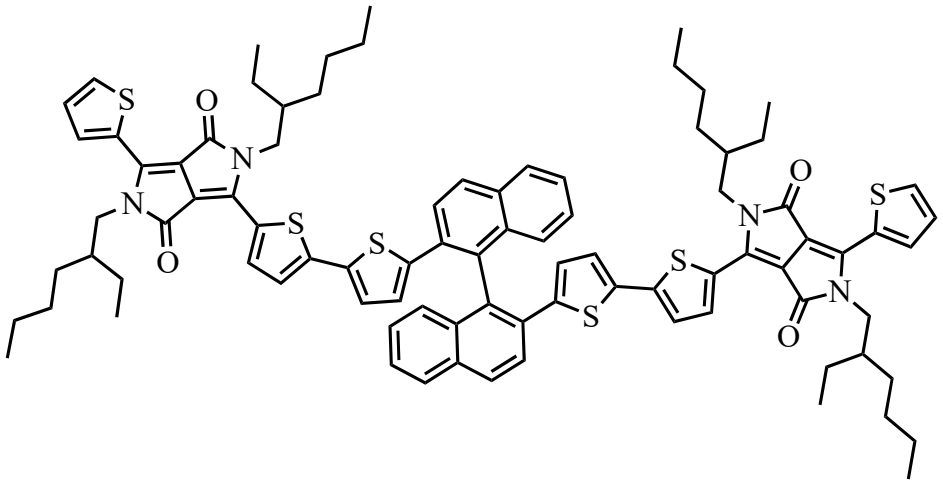
A solution of 2,2'-bis(5-bromothiophen-2-yl)-1,1'-binaphthalene (200 mg, 0.35 mmol), bis(pinacolato)diboron (353 mg, 1.39 mmol), Pd(dppf)Cl_2 (25.4 mg, 0.035 mmol, 10 mol%) and potassium acetate (409 mg, 4.16 mmol) in anhydrous DMF (35 mL) was refluxed for 5 hrs. TLC (eluent: hexane:$CHCl_3$ = 5:1)was used to monitor the reaction. Once starting materials was consumbed (5 h) , the reaction was cooled and water (5 mL) was added. The mixture was extracted with DCM (3 x 20 mL), the combined organic phases were washed with water (5 x 35 mL), brine, dried over Na_2SO_4, filtered and concentrated in *vacuo*. NMR of crude suggested the presence of both mono- and di-coupled products. Attempted purification by column chromatography over silica (eluent: hexane:$CHCl_3$ = 2:1) resulted in protodeboronation. Isolation of desired product was not successful.

2,2'-Bis(5-(trimethylstannyl)thiophen-2-yl)-1,1'-binaphthalene



To a solution of 2,2'-di(thiophen-2-yl)-1,1'-binaphthalene (100 mg, 0.24 mmol) in THF (7 mL) at -78 ºC was added *n*-BuLi(2.5 M in hexane, 0.4 mL) dropwise. The resulting mixture was stirred at -78 ºC for 1 h before addition of chlorotrimethylstannane (1M in THF, 1.4 mL). The mixture was warmed to room temperature with stirring overnight. It was then quenched with water, extracted with DCM 3 x 7 mL. The combined organic phases were washed with water, brine, dried over sodium sulfate, filtered and concentrated in *vacuo*. Attempted purification via column chromatography over silica (eluent: hexane:$CHCl_3$ = 3:1) resulted in degradation. Isolation of desired product was not successful.

6,6'-([1,1'-Binaphthalene]-2,2'-diylbis([2,2'-bithiophene]-5',5-diyl))bis(2,5-bis(2-ethylhexyl)-3-(thiophen-2-yl)-2,5-dihydropyrrolo[3,4-c]pyrrole-1,4-dione) {BNTDPP(EH)}



To 2,2'-di(thiophen-2-yl)-1,1'-binaphthalene (300 mg, 0.717 mmol) in anhydrous THF (18 mL) at -78 ℃ was added *n*-BuLi (0.86 mL, 2.5 M in hexane, 2.15 mmol) dropwise. After stirring for 2 hrs, the reaction mixture was treated with solution of $ZnCl_2$ in THF (4.1 mL, 0.7 M in THF, 2.87 mmol), kept stirring at -78 ℃ for 30 min, and then warmed up to RT. Stirring was continued for 2 hrs. $Pd(PPh_3)_4$ (41.4 mg, 0.036 mmol, 5 mol%) and 3-(5-bromothiophen-2-yl)-2,5-bis(2-ethylhexyl)-6-(thiophen-2-yl)-2,5-dihydropyrrolo[3,4-c]pyrrole-1,4-dione (2.6 g, 4.30 mmol) were dissolved in anhydrous THF (40 mL) under protection of nitrogen and transferred to the reaction mixture under nitrogen flow. The resulting mixture was refluxed for 2 days, cooled to room temperature and quenched by filtering through a silica pad using THF as eluent. The filtrate was concentrated in *vacuo* and subjected to silica gel column chromatography (eluent: DCM) followed by recrystallization ($CHCl_3$-MeOH) to provide the desired product as a black-purple solid (150 mg, 14.3 %). mp 242 – 243 °C. ^{1}H NMR (400 MHz, $CDCl_3$) δ 8.84 (d, *J* = 3.9 Hz, 4H), 8.07 (d, *J* = 8.7 Hz, 2H), 7.95 (d, *J* = 8.2 Hz, 2H), 7.91 (d, *J* = 8.7 Hz, 2H), 7.59 (d, *J* = 5.0 Hz, 2H), 7.48 (t, *J* = 7.4 Hz, 2H), 7.34 – 7.11 (m, 6H), 7.02 (d, *J* = 4.2 Hz, 2H), 6.94 (d, *J* = 3.9 Hz, 2H), 6.68 (d, *J* = 2.9 Hz, 2H), 4.13 – 3.77 (m, 8H), 1.94 – 1.73 (m, 4H), 1.44 – 1.08 (m, 32H), 0.98 – 0.61 (m, 24H). ^{13}C NMR (101 MHz, $CDCl_3$) δ 161.8, 161.5, 143.6, 142.7, 140.0, 139.7, 136.8, 135.0, 134.0, 133.1, 131.9, 130.3, 130.0, 129.3, 128.4, 128.1, 127.8, 127.4, 126.8, 126.6, 124.8, 124.5, 108.2, 108.0, 45.91, 39.13, 30.25, 28.38, 23.57, 23.05, 14.00, 10.49. HRMS (ES+) *m/z* calcd for $C_{88}H_{95}N_4O_4S_6$ [M^+] 1463.5672, found 1463.5651.

The reaction was repeated using 2,2'-di(thiophen-2-yl)-1,1'-binaphthalene (100 mg, 0.239 mmol), THF (7 mL), *n*-BuLi (0.30 mL, 2.5 M in hexane, 0.75 mmol), $ZnCl_2$ in THF (1.4 mL, 0.7 M in THF, 0.98 mmol), $Pd(PPh_3)_4$ (27.6 mg, 0.024 mmol, 10 mol%), 3-(5-bromothiophen-2-yl)-2,5-bis(2-ethylhexyl)-6-(thiophen-2-yl)-2,5-dihydropyrrolo[3,4-c]pyrrole-1,4-dione (865.1 mg, 1.43 mmol) and anhydrous THF (50 mL) to afford the desired product as a black-purple solid (52 mg, 15 %).

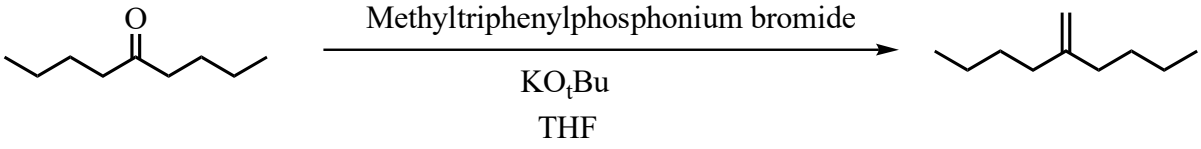
The reaction was repeated using 2,2'-di(thiophen-2-yl)-1,1'-binaphthalene (100 mg, 0.239 mmol), anhydrous THF (7 mL), *n*-BuLi (0.30 mL, 2.5 M in hexane, 0.75 mmol), $ZnCl_2$ in THF (1.4 mL, 0.7 M in THF, 0.98 mmol), $Pd(PPh_3)_4$ (41.4 mg, 0.036 mmol, 15 mol%), 3-(5-bromothiophen-2-yl)-2,5-bis(2-ethylhexyl)-6-(thiophen-2-yl)-2,5-dihydropyrrolo[3,4-c]pyrrole-1,4-dione (865.1 mg, 1.43 mmol) and anhydrous THF (50 mL) to afford the desired product as a black-purple solid (44 mg, 12.6 %).

The reaction was repeated using 2,2'-di(thiophen-2-yl)-1,1'-binaphthalene (100 mg, 0.239 mmol), THF (7 mL), *n*-BuLi (0.6 mL, 2.5 M in hexane, 1.43 mmol), $ZnCl_2$ in THF (2.7 mL, 0.7 M in THF, 1.91 mmol), $Pd(PPh_3)_4$ (41.4 mg, 0.036 mmol, 15 mol%), 3-(5-bromothiophen-2-yl)-2,5-bis(2-ethylhexyl)-6-(thiophen-2-yl)-2,5-dihydropyrrolo[3,4-c]pyrrole-1,4-dione (863 mg, 1.43 mmol) and anhydrous THF (50 mL) to afford the desired product as a black-purple solid (65 mg, 18.6 %).

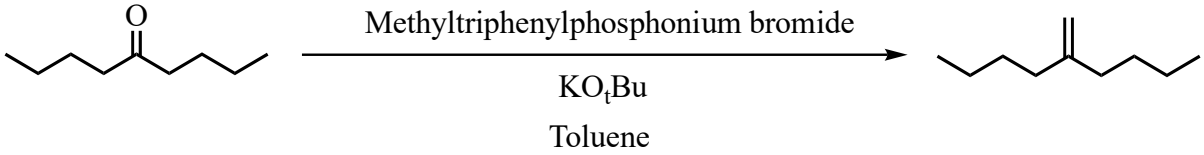
Reverse polarity approach

To a solution of DPP(EH) (517 mg, 1.02 mmol) in THF (30 mL) at -78 °C was added LDA (1.02 mmol) dropwise. The mixture was stirred at -78 °C for 30 min. $ZnCl_2$ (0.7 M in THF, 1.7 mL) was added dropwise, the resulting mixture was stirred at -78 °C for 30 min before warming to room temperature. 2,2'-Bis(5-bromothiophen-2-yl)-1,1'-binaphthalene (100 mg, 0.17 mmol) and $Pd(PPh_3)_4$ (9.8 mg, 5 mol%) in THF were added to the organo-zinc reagent, followed by reflux for 2 days. After cooling to room temperature, the mixture was filtered through a pad of silica, concentrated in *vacuo*, and purified by column chromatography over silica (eluent: DCM) to give the desired product as a black-purple solid (36 mg, 15 %).

5-Methylenenonane[71]



KO^{t}Bu (0.62 g, 5.53 mmol) was added in four portions to a mixture of methyltriphenylphosphonium bromide (1.67 g, 4.68 mmol) in anhydrous THF (30 mL) at room temperature. The mixture was refluxed for 1 h under argon atmosphere before cooling to room temperature. Nonan-5-one (0.500 g, 3.52 mmol) in dry THF (2.5 mL) was added dropwise and then stirred for 30 min. Saturated aqueous NH_4Cl solution (15 mL) was added to the reaction mixture. Aqueous phase was extracted with diethyl ether (3 x). The combined organic phases were washed with brine (2 x), dried over $MgSO_4$, filtered and concentrated in *vacuo*. The crude mixture was purified via flash silica chromatography (eluent: n-pentane) to offer the corresponding methylene product as a colourless oil (0.107 g, 22 %). ^{1}H NMR (400 MHz, $CDCl_3$) δ 4.69 (s, 2H), 2.00 (t, *J* = 7.2 Hz, 4H), 1.46 – 1.23 (m, 8H), 0.91 (t, *J* = 7.2 Hz, 6H). MS (+EI) *m/z* 140.1 (M^+).



Using the same amount of toluene as literature:[71]

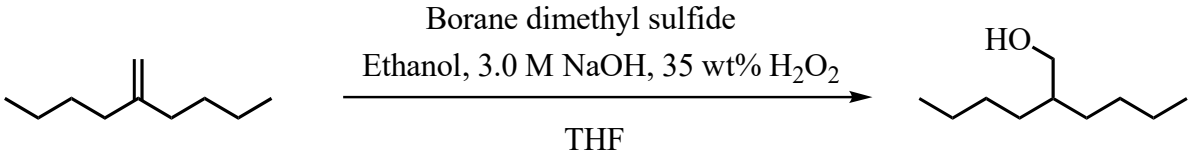
KO^{t}Bu (12 g, 110 mmol) was added in four portions to a mixture of methyltriphenylphosphonium bromide (33 g, 92.5 mmol) in anhydrous toluene (700 mL) at room temperature. The mixture was refluxed for 1 h under argon atmosphere before cooled to room temperature. Nonan-5-one (10 g, 70.5 mmol) in dry toluene (50 mL) was added dropwise and then stirred for 30 min. Saturated aqueous NH_4Cl solution (150 mL) was added to the reaction mixture. Aqueous phase was extracted with diethyl ether (3 x). The combined organic phases were washed with brine (2 x), dried over $MgSO_4$. The drying agent was filtered off and the filtrate was concentrated in the presence of excess silica to avoid stopping of the column

by the remaining organic salts. The silica mixture was subjected to a flash silica column (eluent: n-pentane) to offer the corresponding methylene product as a colourless oil (6.1 g, 62 %).

The above was repeated under identical conditions but with less toluene (500 mL) to afford (7.2 g, 73 %).

The above was repeated using KO_tBu (24 g, 220 mmol), methyltriphenylphosphonium bromide (66 g, 185 mmol), toluene (1 L) and nonan-5-one (20 g, 141 mmol) in dry toluene (100 mL) to afford the corresponding methylene product as a colourless oil (25.2 g, 64 %).

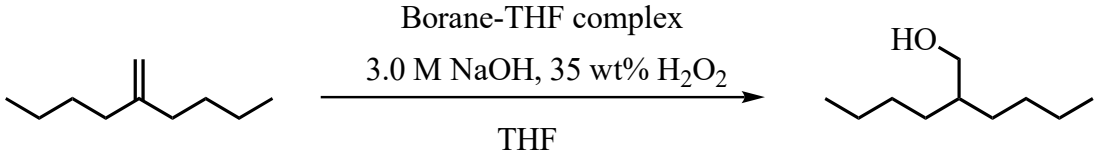
2-Butylhexan-1-ol[71]



To a solution of 5-methylenenonane (2.638 g, 18.8 mmol) in THF (200 mL) at 0 °C was added borane dimethyl sulfide complex solution (2.0 M in toluene, 5.9 mL, 11.8 mmol) dropwise. After 2 h of stirring at 0 °C, the reaction mixture was warmed to room temperature and stirred for an additional 2.5 h. The reaction was cooled to 0 °C and ethanol (39.6 mL), aqueous 3.0 M NaOH (231 mL) and 35 wt% aqueous H_2O_2 (231 mL) were added. After 30 min of stirring, the reaction mixture was warmed to RT and stirred overnight. The basic mixture was treated with aqueous 1 M HCl (204 mL), the organic layer was separated, and the aqueous layer was extracted with diethyl ether (3 x 100 mL). The combined organic phases were washed with brine (2 x 70 mL), dried over $MgSO_4$, filtered, and concentrated in *vacuo*. The crude product was purified via silica gel chromatography (eluent: hexane:Et_2O = 2:1) to afford the desired product as a light-yellow tinted oil (1.99 g, 67 %). ^{1}H NMR (400 MHz, $CDCl_3$) δ 3.54 (t, J = 5.5 Hz, 2H), 1.51 – 1.40 (m, 1H), 1.40 – 1.21 (m, 12H), 1.17 (t, J = 5.7 Hz, 1H), 0.97 – 0.81 (m, 6H). FTIR $\bar{\nu}_{max}$ (cm^{-1}): 3314 (br, OH).

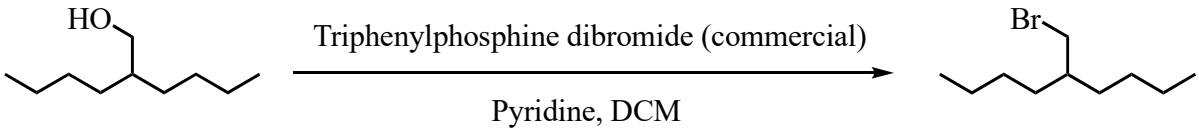
Repeated as above using 5-methylenenonane (400 mg, 2.85 mmol) in THF (30 mL), borane dimethyl sulfide complex solution (2.0 M in toluene, 0.9 mL, 1.8 mmol), ethanol (1.2 mL),

aqueous 3.0 M NaOH (7 mL), 35 wt% aqueous H_2O_2 (7 mL) and aqueous 1 M HCl (5 mL) to afford the desired product as a light-yellow tinted oil (0.13 g, 29 %).



To a solution of 5-methylenenonane (5 g, 35.6 mmol) in THF (120 mL) at 0 °C was added borane tetrahydrofuran complex solution (1.0 M in THF, 17.8 mL, 17.8 mmol) slowly. The solution was stirred at RT for 2 h. Water (10 mL), 3.0 M NaOH (15.4 mL) were added dropwise and the resulting mixture was stirred at room temperature for another 1.5 h. The mixture was cooled to 0 °C again and 35 wt% H_2O_2 (13 mL) was added dropwise and stirred at 0 °C for 2 h. It was warmed to ambient temperature and stirred overnight. Extraction with Et_2O (3 x 40 mL), the combined organic phases were washed with brine (2 x), dried over $MgSO_4$, filtered and concentrated in *vacuo*. The residue was purified by silica gel chromatography (eluent: hexane:Et_2O = 2:1) to afford the product as a light- yellow tinted oil (3.8 g, 67.4%).

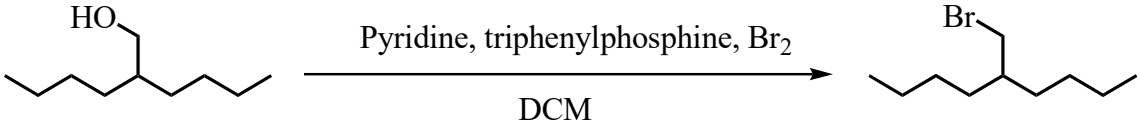
5-(Bromomethyl)nonane[72]



With commercial triphenylphosphine dibromide:

To a solution of triphenylphosphine dibromide (commercially available, 0.886 g, 2.1 mmol) in anhydrous dichloromethane (9 mL) at 0 °C was added a solution of 2-butylhexan-1-ol (0.25 g, 1.6 mmol) and pyridine (0.4 mL, 5.0 mmol) in anhydrous dichloromethane (2 mL). The mixture was stirred at 0 °C for 15 min and for 1 h at room temperature. It was neutralized with 10% aqueous sodium bisulfite.The organic layer was separated, and the aqueous layer was extracted with dichloromethane (2 x 5 mL) and diethyl ether (1 x 5mL). The combined organic phases were washed with brine, dried over $MgSO_4$, filtered and concentrated in the presence of excess

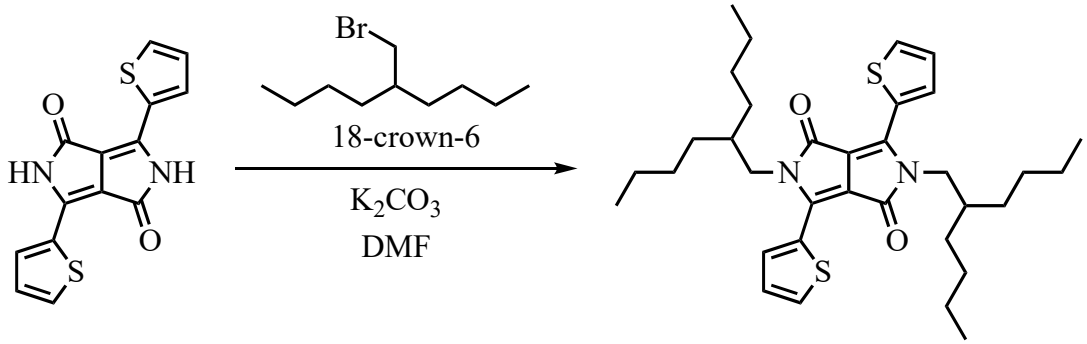
of silica to avoid stopping of column by remaining organic salts. The silica mixture was purified by column chromatography over silica (eluent: hexane) to give 5-(bromomethyl)nonane as a colourless oil (0.141 g, 40 %). ^{1}H NMR (400 MHz, $CDCl_3$) δ 3.45 (d, J = 4.8 Hz, 2H), 1.64 – 1.56 (m, 1H), 1.45 – 1.17 (m, 12H), 0.95 – 0.87 (m, 6H).



As above with freshly made triphenylphosphine dibromide. A solution of brominating agent was prepared as follows:

To a solution of triphenylphosphine (0.55 g, 2.1 mmol) in anhydrous dichloromethane (9 mL) at 0 ℃ was added Br_2 (0.11 mL, 2.1 mmol) dropwise. The addition of Br_2 caused the solution to become cloudy initially but became clear again once addition was complete. The reaction was completed as above to afford 5-(bromomethyl)nonane as a colourless oil (0.30 g, 86 %).

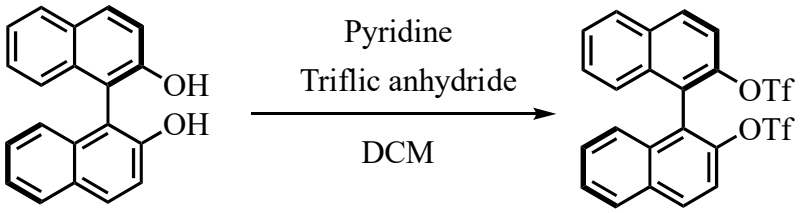
2,5-Bis(2-butylhexyl)-3,6-di(thiophen-2-yl)-2,5-dihydropyrrolo[3,4-c]pyrrole-1,4-dione {DPP(BH)}



A solution of 3,6-dithiophen-2-yl-2,5-dihydro-pyrrolo[3,4-c]pyrrole-1,4-dione (7.5 g, 25.0 mmol) and anhydrous K_2CO_3 (11.04 g, 79.9 mmol) in anhydrous N,N-dimethylformamide (DMF, 180 mL) were stirred at 120 ℃ for 1 h. 5-(Bromomethyl)nonane (16.56 g, 74.9 mmol) was added dropwise, followed by a catalytic amount of 18-crown-6 (spatula tip). The reaction

mixture was further stirred at 150 °C overnight, cooled to room temperature and poured into water (600 mL). After stirring the resulting suspension at room temperature for 1 h, the solid was collected by vacuum filtration, washed with several portions of water and methanol and dried under vacuum. The crude product was purified by silica gel column chromatography (eluent: DCM:hexane = 2:1) to afford a dark red solid (4.31 g, 30%). mp 153 – 155 °C. ^{1}H NMR (400 MHz, $CDCl_3$) δ 8.85 (dd, *J* = 3.9, 1.1 Hz, 2H), 7.62 (dd, *J* = 5.0, 1.1 Hz, 2H), 7.29 – 7.25 (dd, *J* = 5.0 Hz, 3.9 Hz, 2H), 4.02 (d, *J* = 7.8 Hz, 4H), 2.00 – 1.82 (m, 2H), 1.39 – 1.07 (m, 24H), 0.84 (t, *J* = 7.0 Hz, 12H). ^{13}C NMR (101 MHz, $CDCl_3$) δ 161.8, 140.4, 135.1, 130.5, 129.9, 128.4, 108.0, 46.2, 37.7, 30.9, 28.4, 23.1, 14.0. HRMS (ES+) *m/z* calcd for $C_{34}H_{49}N_2O_2S_2$ [M^+] 581.3230, found 581.3221.

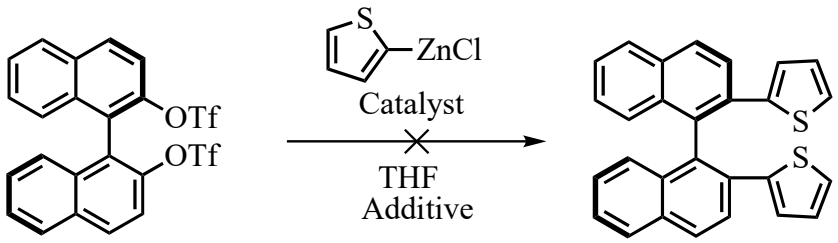
(*R*)-(−)-1,1′-Bi-2-naphthol bis(trifluoromethanesulfonate)[101]



To a solution of (*R*)-(+)-1,1′-bi(2-naphthol) (2 g, 6.98 mmol) in anhydrous DCM (70 mL) at 0 °C was added pyridine (2 mL, 24.6 mmol) slowly and the mixture was stirred at 0 °C for 15 min before dropwise addition of triflic anhydride (4.0 mL, 23.8 mmol). The mixture allowed warm to ambient temperature with stirring overnight. Upon completion of the reaction (TLC checked, eluent DCM, Rf = 0.35 for the desired product), it was quenched with 1.5 N HCl and ice water. The layers were separated, and the aqueous layer was extracted with ethyl acetate (3 x 20 mL). The combined organic phases were washed with brine, dried over sodium sulphate, filtered and concentrated in *vacuo*. It was filtered through a silica pad (eluent: DCM) and the filtrate was concentrated in *vacuo,* followed by recrystallization from hexane to give desired product as white crystals (3.60 g, 94 %). mp 82 – 83 °C (lit.[102] mp 82 – 83 °C). $[\alpha]^{25}_{D}$ = -155.4 (*c* = 1.01, $CHCl_3$) (lit.[74] $[\alpha]^{20}_{D}$ = -147.7 (*c* = 1.01, $CHCl_3$)). ^{1}H NMR (400 MHz, $CDCl_3$) δ 8.14 (d, *J* = 9.0 Hz, 2H), 8.01 (d, *J* = 8.3 Hz, 2H), 7.67 – 7.55 (m, 4H), 7.46 – 7.37 (m, 2H), 7.29 – 7.23 (m, 2H). ^{13}C NMR (101 MHz, $CDCl_3$) δ 145.6, 133.3, 132.5, 132.1, 128.5, 128.1, 127.5,

126.9, 123.6, 119.9, 119.5. ^{19}F NMR (377 MHz, $CDCl_3$) δ -74.6. MS (pAPCI) *m/z* 551.0 (M^+, 5 %).

(*R*)-2,2'-di(thiophen-2-yl)-1,1'-binaphthalene



Catalyst = $Pd(amphos)Cl_2$ / PEPPSI-IPr / $Pd(PPh_3)_4$
Additive = LiOAc

$Pd(PPh_3)_4$ without additive:

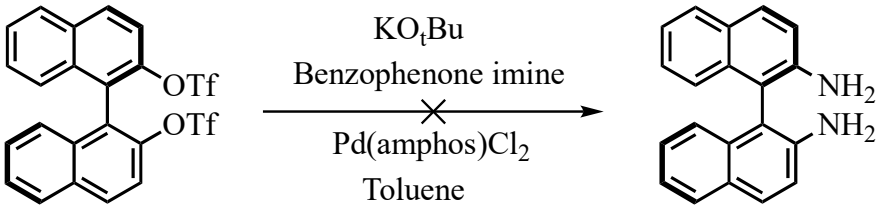
To a solution of (*R*)-(−)-1,1′-bi-2-naphthol bis(trifluoromethanesulfonate) (100 mg, 0.182 mmol), tetrakis(triphenylphosphine)palladium(0) (10.5 mg, 9.1 x 10^{-3} mmol, 5 mol%) in THF (15 mL) in an oven-dried 20 mL high-pressure microwave reactor vial was added 2-thienyl zinc chloride (0.3 M in THF, 3.6 mL, 1.08 mmol). The entire reaction mass was heated in a microwave reactor under following conditions: 30 s pre-stirring, 90 °C for 1 min and 120 °C for 30 min. TLC (eluent: hexane:DCM = 4:1) showed no product formation with majority still being starting material.

Repeated as above but with addition of lithium acetate (36 mg, 0.546 mmol). TLC showed no product formation. The mixture was then put back to react for another 30 min at 120 °C and afterwards there was still no product spot on TLC.

Repeated as above with PEPPSI-IPr (6.2 mg, 9.1 x 10^{-3} mmol, 5 mol%). TLC showed only starting material and no product formation.

Repeated as above with bis(di-tert-butyl(4-dimethylaminophenyl)-phosphine)dichloropalladium(II) (6.4 mg, 9.1 x 10^{-3} mmol, 5 mol%). TLC showed only starting material and no product formation.

(*R*)-(+)-1,1′-Binaphthyl-2,2′-diamine[76,77]



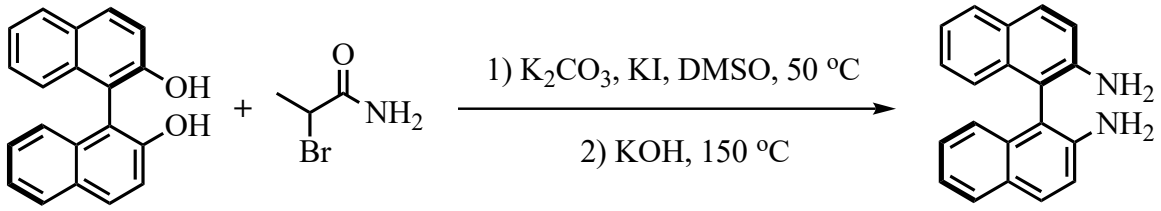
To a solution of (*R*)-(−)-1,1′-bi-2-naphthol bis(trifluoromethanesulfonate) (200 mg, 0.363 mmol) and benzophenone imine (0.14 mL,0.83 mmol) in toluene (18 mL) was purged with argon for 10 min. Potassium tert-butoxide (81.3 mg, 0.726 mmol) and catalytic amount of bis(di-tert-butyl(4-dimethylaminophenyl)-phosphine)dichloropalladium(II) (spatula tip) were added. The reaction mixture was heated at 95 °C for two days (TLC (eluent: DCM) checked at each overnight) before being poured into 1.5 N HCl solution. Sodium hydroxide solution (3 M) was then added for basification. The mixture was extracted with ethyl acetate, washed with brine, dried over sodium sulphate, filtered and concentrated in *vacuo*. TLC showed no product formation.

Repeated as above with bis(di-tert-butyl(4-dimethylaminophenyl)-phosphine)dichloropalladium(II) (12.9 mg, 0.018 mmol, 5 mol%). TLC showed no product formation.

Repeated as above with (*R*)-(−)-1,1′-bi-2-naphthol bis(trifluoromethanesulfonate) (100 mg, 0.182 mmol), benzophenone imine (0.11 mL, 0.636 mmol) in toluene (18 mL), potassium tert-butoxide (61.3 mg, 0.546 mmol) and bis(di-tert-butyl(4-dimethylaminophenyl)-phosphine)dichloropalladium(II) (6.4 mg, 9.1 x 10^{-3} mmol, 5 mol%). TLC showed no product formation.

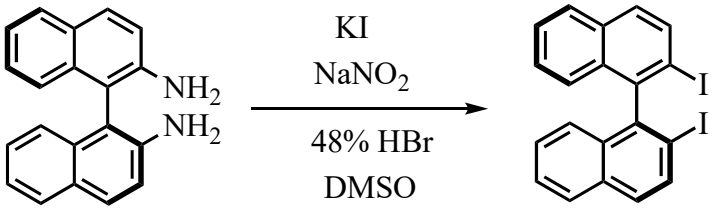
Repeated as above with (*R*)-(−)-1,1′-bi-2-naphthol bis(trifluoromethanesulfonate) (100 mg, 0.182 mmol) and benzophenone imine (0.11 mL,0.636 mmol) in toluene (18 mL), potassium tert-butoxide (61.3 mg, 0.546 mmol) and bis(di-tert-butyl(4-dimethylaminophenyl)-phosphine)dichloropalladium(II) (12.9 mg, 1.8 x 10^{-2} mmol, 10 mol%). TLC showed no product formation.

Repeated as above with (*R*)-(−)-1,1′-bi-2-naphthol bis(trifluoromethanesulfonate) (100 mg, 0.182 mmol) and benzophenone imine (0.18 mL, 1.09 mmol) in toluene (18 mL), potassium tert-butoxide (122 mg, 1.09 mmol) and bis(di-tert-butyl(4-dimethylaminophenyl)-phosphine)dichloropalladium(II) (12.9 mg, 0.018 mmol, 10 mol%) TLC showed no product formation.



Under normal air condition, (*R*)-(+)-1,1′-Bi(2-naphthol) (0.229 g, 0.8 mmol), 2-bromopropionamide (0.365 g, 2.4 mmol), K_2CO_3 (0.332 g, 2.4 mmol), KI (0.013 g, 0.08 mmol) and anhydrous DMSO (8 mL) were added to an oven-dried 20 mL high-pressure microwave reactor vial. The vial was capped with a suba-seal and stirred at 50 °C for 48 hrs. KOH (0.561 g, 10.0 mmol) was added followed by stirring at 150 °C for 4 hrs. It was quenched with water (50 mL), extracted with DCM (3 x 8 mL). The combined organic phases were washed with water (5 x 15 mL), brine, dried over Na_2SO_4, filtered and concentrated in *vacuo*. The crude product was subjected to silica gel column chromatography (eluent: hexane/EtOAc = 3/2) to give the desired product as an off-white solid (0.050 g, 22 %). mp 237 – 239 °C (lit.[103] mp 244.5 – 247 °C). $[\alpha]^{25}_D$ = + 76.3 (*c* = 0.5, $CHCl_3$) (lit.[78] $[\alpha]^{20}_D$ = + 244 (*c* = 0.5, $CHCl_3$)) ^{1}H NMR (400 MHz, $CDCl_3$) δ 7.91 – 7.65 (m, 4H), 7.39 – 6.92 (m, 8H), 3.67 (s, 4H). ^{13}C NMR (101 MHz, $CDCl_3$) δ 142.7, 133.7, 129.5, 128.4, 128.1, 126.8, 123.9, 122.4, 118.3, 112.6. HRMS (pAPCI) *m/z* calcd for $C_{20}H_{17}N_2$ [M^+] 285.1386, found 285.1378.

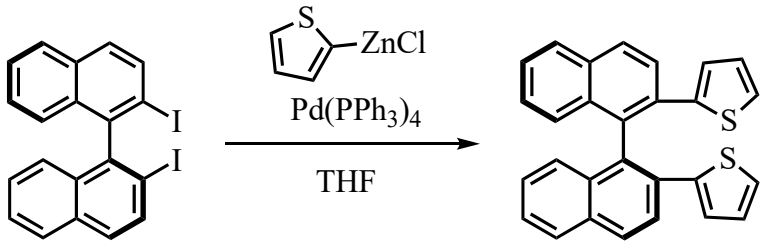
(*S*)-2,2'-Diiodo-1,1'-binaphthalene[82]



To a solution of (*S*)-1,1'-binaphthyl-2,2'-diamine (0.25 g, 0.879 mmol), potassium iodide (1.46 g, 8.80 mmol), and sodium nitrite (0.49 g, 7.10 mmol) in anhydrous DMSO (15 mL) at room temperature (using water bath) was added 48% aqueous HBr (1.2 mL, 22.1 mmol) dropwise. The addition of acid led to a darkening in colour and visible gas evolution. The water bath was removed, and the mixture was stirred for 1 h. It was then poured into half diluted saturated aqueous $NaHCO_3$ solution (90 mL) and extracted with DCM (3 x 5 mL). The combined organic phases were washed with 10% aq. $Na_2S_2O_3$, then water, dried over Na_2SO_4, filtered and concentrated in *vacuo*. The crude was subjected to silica gel chromatography (eluent: DCM:hexane = 1:20) to give the product as off-white crystals (0.071 g, 16 %). mp 202 – 205 °C (lit.[81] mp 205 – 207 °C). $[\alpha]^{25}_D$ = - 16 (*c* = 1.75, pyridine) (lit.[104] $[\alpha]^{23}_D$ = - 16.2 (*c* = 1.75, pyridine)). ^{1}H NMR (400 MHz, $CDCl_3$) δ 8.06 (d, *J* = 8.7 Hz, 2H), 7.93 (d, *J* = 8.2 Hz, 2H), 7.71 (d, *J* = 8.7 Hz, 2H), 7.51 (ddd, *J* = 8.2, 6.8, 1.2 Hz, 2H), 7.29 (ddd, *J* = 8.3, 6.8, 1.3 Hz, 2H), 7.08 (dd, *J* = 8.3, 1.3 Hz, 2H). ^{13}C NMR (101 MHz, $CDCl_3$) δ 144.8, 135.6, 133.0, 129.6, 128.2, 127.3, 126.6, 126.4, 99.7. MS (pAPCI) *m/z* 505.9 (M^+, 5 %).

Repeated as above with (*S*)-1,1'-binaphthyl-2,2'-diamine (1.50 g, 5.27 mmol), potassium iodide (8.76 g, 52.8 mmol), and sodium nitrite (2.94 g, 42.6 mmol) in anhydrous DMSO (90 mL), 48% aqueous HBr (7.2 mL, 133 mmol) to afford the product as off-white crystals (2.4 g, 45 %).

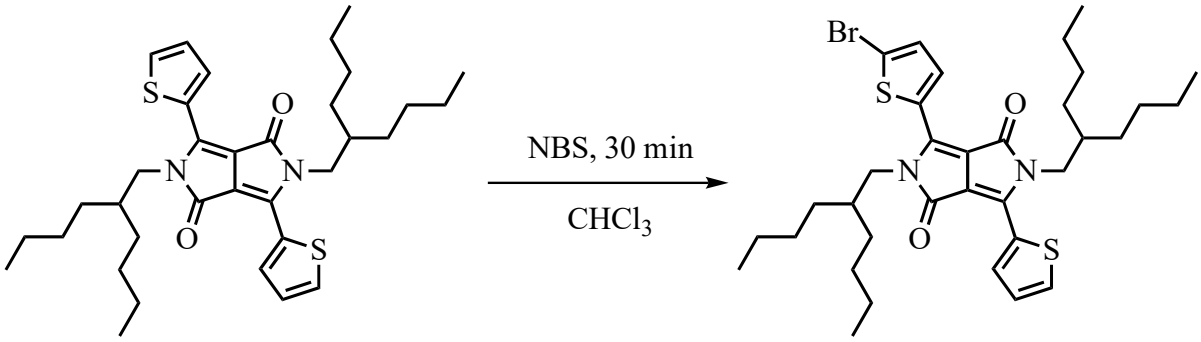
(*S*)-2,2'-Di(thiophen-2-yl)-1,1'-binaphthalene



To a solution of (*S*)-2,2'-diiodo-1,1'-binaphthalene (1.0 g, 1.98 mmol) and tetrakis(triphenylphosphine)palladium(0) (114 mg, 0.10 mmol, 5 mol%) in anhydrous THF (45 mL) was added 2-thienyl zinc chloride (0.3 M in THF, 39.5 mL, 11.9 mmol) followed by refluxing for 30 min. The mixture was cooled to room temperature and filtered through a pad

of silica, the filtrate was concentrated in *vacuo* and purified by column chromatography over silica (eluent: hexane:chloroform = 2:1) to afford an off-white solid (0.79 g, 96 %). $[\alpha]^{25}_{D}$ = + 17.0 (*c* = 1.0, chloroform) (lit.[54] $[\alpha]^{21}_{D}$ = -15.7 (*c* = 1.0, chloroform) for its *R* – enantiomer).

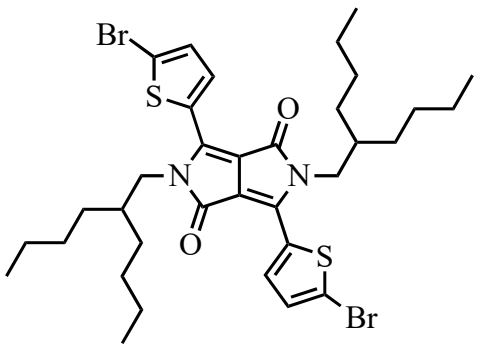
3-(5-Bromothiophen-2-yl)-2,5-bis(2-butylhexyl)-6-(thiophen-2-yl)-2,5-dihydropyrrolo[3,4-c]pyrrole-1,4-dione



To a solution of 2,5-bis(2-butylhexyl)-3,6-di(thiophen-2-yl)-2,5-dihydropyrrolo[3,4-c]pyrrole-1,4-dione (0.25 g, 0.430 mmol) in anhydrous $CHCl_3$ (25 mL) was added NBS (0.092 g, 0.516 mmol) in one portion. The mixture was stirred in the dark at RT for 30 min. The solution was concentrated in *vacuo* and the residue was taken up in CH_2Cl_2, washed with water, brine, dried over Na_2SO_4, filtered and concentrated in *vacuo*. The crude was purified by column chromatography over silica repeatedly (eluent: DCM:hexane = 4:3) to afford the desired product as a fushia-purple solid (0.126 g, 44.4 %). mp 155 – 157 °C. ^{1}H NMR (400 MHz, $CDCl_3$) δ 8.86 (d, *J* = 3.8 Hz, 1H), 8.59 (d, *J* = 4.1 Hz, 1H), 7.64 (d, *J* = 4.9 Hz, 1H), 7.27 (d, *J* = 4.1 Hz, 1H), 7.22 (d, *J* = 3.8 Hz, 1H), 4.01 (d, *J* = 7.7 Hz, 2H), 3.94 (d, *J* = 7.6 Hz, 2H), 2.00 – 1.81 (m, 2H), 1.41 – 1.02 (m, 24H), 1.00 – 0.69 (m, 12H). ^{13}C NMR ^{13}C NMR (101 MHz, $CDCl_3$) δ 161.7, 140.9, 138.9, 135.4, 134.9, 131.3, 130.7, 129.8, 128.4, 118.5, 108.3, 46.3, 37.7, 30.9, 28.4, 23.0, 14.0. HRMS (ES+) *m/z* calcd for $C_{34}H_{47}BrN_2O_2S_2$ [M^+] 659.2335, found 659.2325.

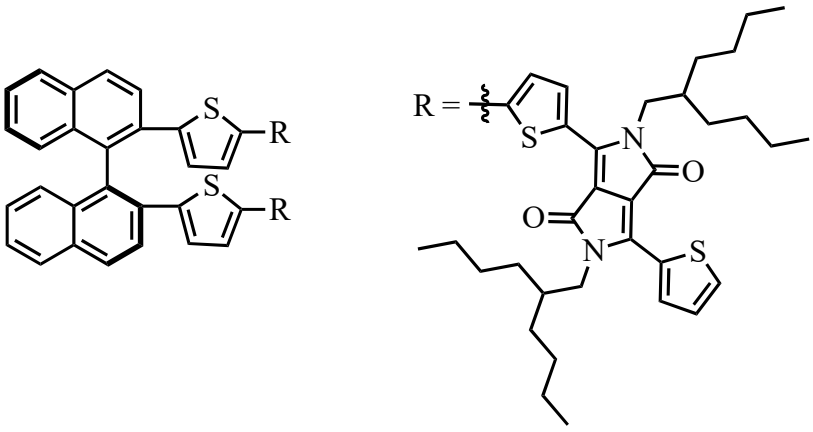
The dibrominated by-product was also isolated (112 mg) during column with Rf value of 0.36.

3,6-Bis(5-bromothiophen-2-yl)-2,5-bis(2-butylhexyl)-2,5-dihydropyrrolo[3,4-c]pyrrole-1,4-dione



mp 194 – 195 °C. ^{1}H NMR (400 MHz, $CDCl_3$) δ 8.60 (d, *J* = 4.2 Hz, 2H), 7.21 (d, *J* = 3.9 Hz, 2H), 3.92 (d, *J* = 7.7 Hz, 4H), 1.94 – 1.79 (m, 2H), 1.40 – 1.05 (m, 24H), 0.85 (t, *J* = 6.8 Hz, 12H). ^{13}C NMR (101 MHz, $CDCl_3$) δ 161.4, 139.4, 135.2, 131.4, 131.2, 118.9, 108.1, 46.3, 37.7, 30.9, 28.4, 23.0, 14.0. HRMS (ES+) *m/z* calcd for $C_{34}H_{46}Br_2N_2O_2S_2$ [M^+] 737.1440, found 737.1436.

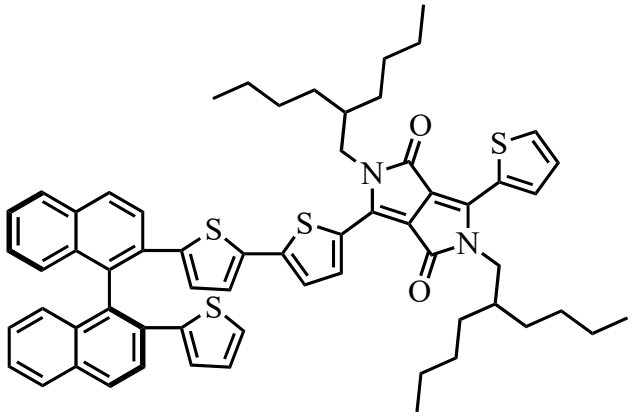
(S)-6,6'-([1,1'-Binaphthalene]-2,2'-diylbis([2,2'-bithiophene]-5',5-diyl))bis(2,5-bis(2-butylhexyl)-3-(thiophen-2-yl)-2,5-dihydropyrrolo[3,4-c]pyrrole-1,4-dione)



n-BuLi (0.57 mL, 2.5 M in hexane, 1.43 mmol) was added dropwise to (S)-2,2'-di(thiophen-2-yl)-1,1'-binaphthalene (100 mg, 0.239 mmol) in anhydrous THF (7 mL) at -78 °C. After stirring for 2 hrs, the reaction mixture was treated with solution of $ZnCl_2$ in THF (2.7 mL, 0.7 M in THF, 1.91 mmol), kept stirring at -78 °C for 30 min, and then warmed to RT. Stirring was continued for 2 hrs. $Pd(PPh_3)_4$ (41.4 mg, 0.036 mmol, 15 mol%) and 3-(5-bromothiophen-2-yl)-2,5-bis(2-butylhexyl)-6-(thiophen-2-yl)-2,5-dihydropyrrolo[3,4-c]pyrrole-1,4-dione (946 mg, 1.43 mmol) were dissolved in anhydrous THF (50 mL) under protection of nitrogen and

transferred to the reaction mixture under nitrogen flow. The resulting mixture was refluxed for 2 days, cooled to RT and quenched by filtering through a silica pad using THF as eluent. The filtrate was concentrated in *vacuo* and subjected to silica gel column chromatography (eluent: DCM). The only product isolated was the mono-coupled product (25 mg) with starting material also observed on TLC.

(S)-2,5-Bis(2-butylhexyl)-3-(thiophen-2-yl)-6-(5'-(2'-(thiophen-2-yl)-[1,1'-binaphthalen]-2-yl)-[2,2'-bithiophen]-5-yl)-2,5-dihydropyrrolo[3,4-c]pyrrole-1,4-dione



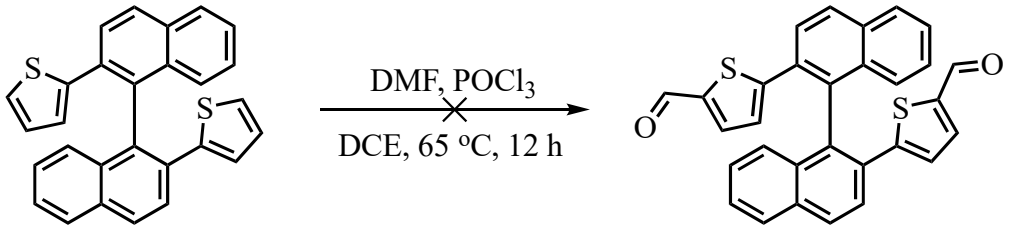
^{1}H NMR (400 MHz, $CDCl_3$) δ 8.85 (dd, *J* = 4.0, 1.5 Hz, 2H), 8.06 (dd, *J* = 10.5, 8.7 Hz, 2H), 8.00 – 7.84 (m, 4H), 7.62 (dd, *J* = 5.0, 1.1 Hz, 1H), 7.54 – 7.43 (m, 2H), 7.35 – 7.19 (m, 5H), 7.09 – 7.00 (m, 2H), 6.93 (d, *J* = 3.9 Hz, 1H), 6.80 – 6.70 (m, 2H), 6.61 (d, *J* = 3.9 Hz, 1H), 4.02 (dd, *J* = 20.3, 7.7 Hz, 4H), 2.01 – 1.86 (m, 2H), 1.52 – 1.13 (m, 24H), 1.06 – 0.69 (m, 12H). ^{13}C NMR (101 MHz, $CDCl_3$) δ 161.8, 161.6, 143.9, 142.9, 142.5, 140.1, 139.7, 136.8, 136.4, 134.9, 134.1, 133.9, 133.6, 132.8, 131.8, 130.3, 130.0, 129.0, 128.4, 128.1, 127.7, 127.3, 127.1, 126.8, 126.5, 126.4, 126.2, 124.9, 124.4, 108.2, 108.0, 46.2, 37.8, 30.9, 28.5, 23.1, 14.1. HRMS (FTMS + p APCI) *m/z* calcd for $C_{62}H_{65}N_2O_2S_4$ [M^+] 997.3923, found 997.3904.

Repeated as above with $Pd(ACN_2)Cl_2$ (3.1 mg, 0.012 mmol, 5 mol%) and 3-(5-bromothiophen-2-yl)-2,5-bis(2-butylhexyl)-6-(thiophen-2-yl)-2,5-dihydropyrrolo[3,4-c]pyrrole-1,4-dione (631 mg, 0.956 mmol) to afford the desired product as a black-purple solid (0.011 g, 5 %). ^{1}H NMR (400 MHz, $CDCl_3$) δ 8.84 – 8.78 (m, 4H), 8.08 (d, *J* = 8.7 Hz, 2H), 7.95 (d, *J* = 8.1 Hz, 2H), 7.91 (d, *J* = 8.7 Hz, 2H), 7.59 (dd, *J* = 5.0, 1.2 Hz, 2H), 7.51 – 7.45 (m, 2H), 7.30 – 7.19 (m, 6H), 7.00 (d, *J* = 4.2 Hz, 2H), 6.93 (d, *J* = 3.9 Hz, 2H), 6.68 (d, *J* = 3.9 Hz, 2H), 4.00 (d, *J* = 7.7 Hz, 4H), 3.94 (d, *J* = 7.6 Hz, 4H), 1.95 – 1.81 (m, 4H), 1.39 – 1.08 (m, 48H), 0.91 – 0.70 (m, 24H). ^{13}C NMR (101 MHz, $CDCl_3$) δ 161.8, 161.6, 143.6, 142.7, 140.0, 139.7, 136.7,

134.9, 133.9, 133.1, 131.9, 130.3, 129.9, 129.3, 128.4, 128.1, 127.8, 127.4, 127.3, 126.8, 126.6, 124.8, 124.46, 108.2, 108.1, 46.2, 37.7, 30.9, 29.7, 28.4, 23.1, 14.0. HRMS (FTMS + p APCI) *m/z* calcd for $C_{96}H_{111}N_4O_4S_6$ [M^+] 1575.6910, found 1576.6910.

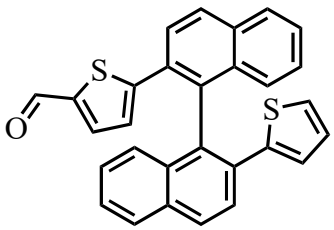
6.2 Chapter 3

5,5'-([1,1'-Binaphthalene]-2,2'-diyl)bis(thiophene-2-carbaldehyde)

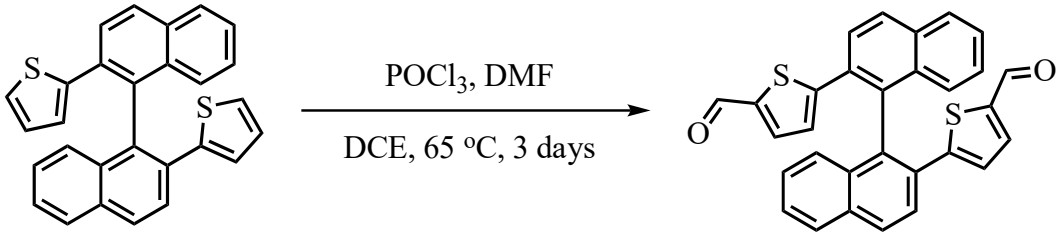


To a solution of 2,2'-di(thiophen-2-yl)-1,1'-binaphthalene (0.200 g, 0.478 mmol) in anhydrous 1,2-dichloroethane (80 mL) and anhydrous DMF (1.5 mL, 19.1 mmol) at 0 °C was added $POCl_3$ (0.22 mL, 2.39 mmol) dropwise followed by stirring at 0 °C for 30 min. The reaction was then stirred at 65 °C for 12 hrs. After cooling to RT, water (35 mL) and saturated aqueous Na_2CO_3 (25 mL) were added and layers were separated. The aqueous layer was extracted with DCM (3 x 35 mL). The combined organic phases were washed with water (4 x 10 mL), brine, dried over Na_2SO_4, filtered and concentrated in *vacuo*. The crude was purified by column chromatography over silica (eluent: $CHCl_3$:EtOAc = 100:1). It did not give any desired product but only mono-coupled.

5-(2'-(Thiophen-2-yl)-[1,1'-binaphthalen]-2-yl)thiophene-2-carbaldehyde

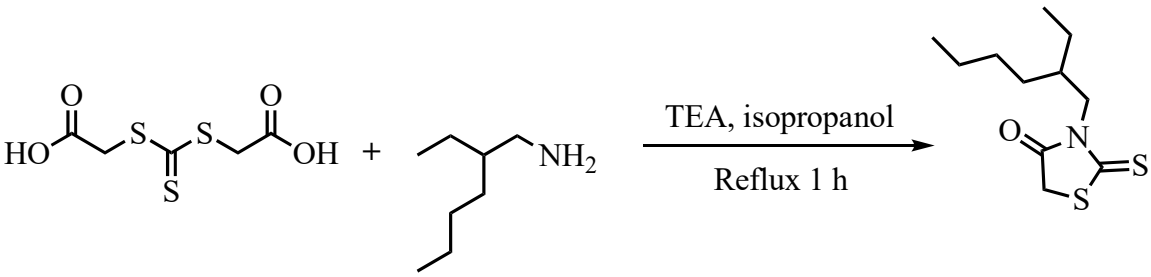


^{1}H NMR (400 MHz, $CDCl_3$) δ 9.64 (s, 1H), 8.03 (dd, *J* = 13.3, 8.6 Hz, 2H), 7.94 (t, *J* = 9.1 Hz, 2H), 7.81 (dd, *J* = 15.0, 8.6 Hz, 2H), 7.53 – 7.41 (m, 2H), 7.32 (d, *J* = 4.0 Hz, 1H), 7.29 – 7.22 (m, 2H), 7.16 (d, *J* = 8.6 Hz, 2H), 7.00 (dd, *J* = 5.1, 1.2 Hz, 1H), 6.70 (dd, *J* = 5.1, 3.7 Hz, 1H), 6.64 – 6.57 (m, 2H).



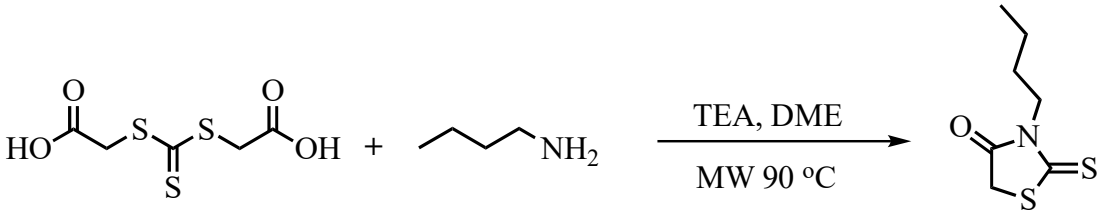
Repeated as above with $POCl_3$ (1.3 mL, 14.3 mmol) and stirring at 65 °C for 3 days to afford the desired product as a light-yellow fluffy solid (0.179 g, 79 %). ^{1}H NMR (400 MHz, $CDCl_3$) δ 9.67 (s, 2H), 8.09 (d, *J* = 8.6 Hz, 2H), 7.98 (d, *J* = 8.0 Hz, 2H), 7.83 (d, *J* = 8.6 Hz, 2H), 7.53 (t, *J* = 7.4 Hz, 2H), 7.37 (d, *J* = 4.0 Hz, 2H), 7.34 – 7.27 (m, 2H), 7.22 (d, *J* = 8.4 Hz, 2H), 6.68 (d, *J* = 4.0 Hz, 2H). ^{13}C NMR (101 MHz, $CDCl_3$) δ 182.7, 152.5, 143.4, 135.8, 133.9, 133.6, 133.4, 131.4, 129.7, 128.3, 127.5, 127.4, 127.1, 127.1, 126.1. HRMS (ASAP+) *m/z* calcd for $C_{30}H_{19}O_2S_2$ [M^+] 475.0826, found 475.0829. FTIR $\bar{\nu}_{max}$ (cm^{-1}): 2804 (CH, aldehyde), 1656 (C=O, aldehyde).

3-(2-Ethylhexyl)-2-thioxothiazolidin-4-one[96]



A solution of bis(carboxymethyl)trithiocarbonate (0.500 g, 2.21 mmol), 2-ethylhexan-1-amine (0.36 mL, 2.21 mmol) and triethylamine (1.35 mL, 9.68 mmol) in isopropanol (5 mL) was refluxed for 1 h. After cooling to room temperature, solvent was evaporated under reduced pressure and the residue was purified by column chromatography over silica (eluent: hexane:DCM = 1:1) to afford the desired product as a colorless oil (0.372 g, 68.6 %). ^{1}H NMR (400 MHz, $CDCl_3$) δ 3.97 (s, 2H), 3.89 (d, *J* = 7.3 Hz, 2H), 2.03 – 1.90 (m, 1H), 1.37 – 1.14 (m, 8H), 0.95 – 0.82 (m, 6H). MS (EI) *m/z* 245 (M^+).

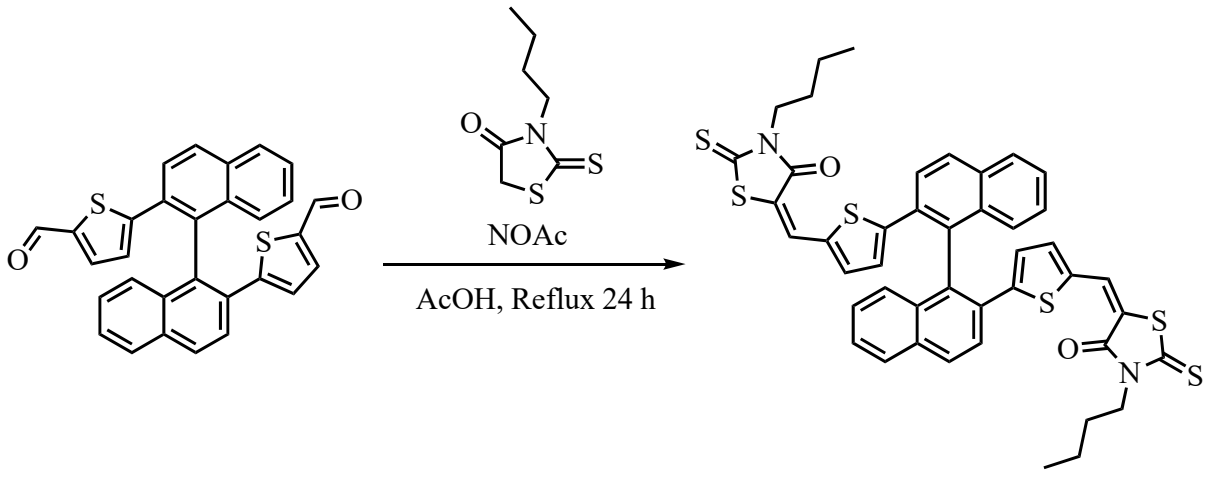
3-Butyl-2-thioxothiazolidin-4-one



A solution of bis(carboxymethyl)trithiocarbonate (0.200 g, 0.884 mmol), butan-1-amine (0.09 mL, 0.884 mmol) and triethylamine (0.54 mL, 3.87 mmol) in anhydrous DME (18 mL) in an oven-dried 20 mL high-pressure microwave reactor vial was heated in a microwave reactor under the following conditions: 30 s pre-stirring, 90 °C for 10 min. After cooling to room temperature, DME was evaporated under reduced pressure and the residue was purified by column chromatography over silica (eluent: hexane:DCM = 1:1) to afford the desired product as a light-yellow oil (0.040 g, 23.9 %). ^{1}H NMR (400 MHz, $CDCl_3$) δ 4.02 – 3.93 (m, 4H), 1.66 – 1.56 (m, 2H), 1.41 – 1.29 (m, 2H), 0.94 (t, *J* = 7.3 Hz, 3H). HRMS (pAPCI) *m/z* calcd for $C_7H_{12}NOS_2$ [M^+] 190.0355, found 190.0349.

The reaction was repeated with 1 h heating time to afford the product (0.122 g, 64.5 %).

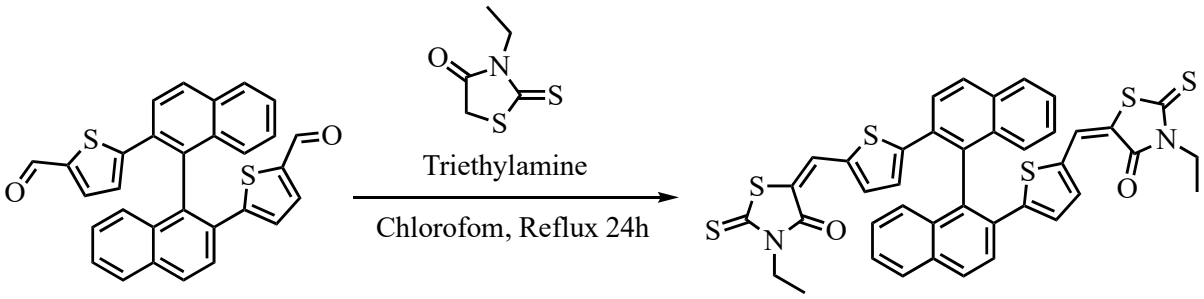
(5E,5'E)-5,5'-(([1,1'-Binaphthalene]-2,2'-diylbis(thiophene-5,2-diyl))bis(methaneylylidene))bis(3-butyl-2-thioxothiazolidin-4-one)



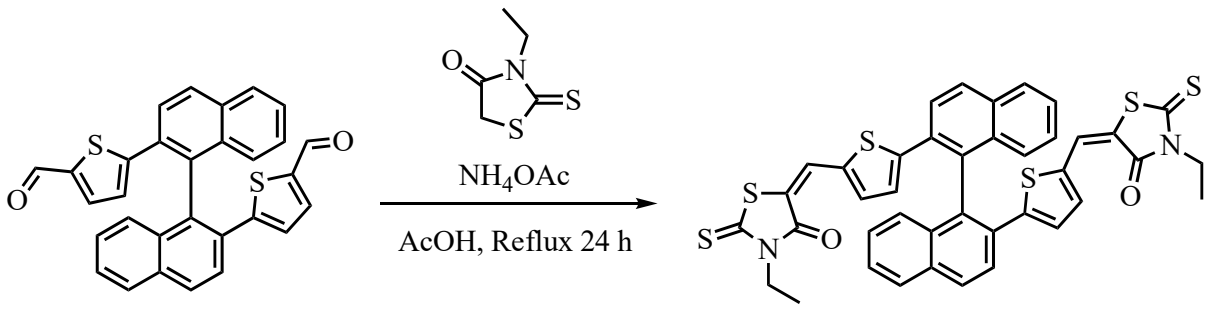
A solution of 5,5'-([1,1'-binaphthalene]-2,2'-diyl)bis(thiophene-2-carbaldehyde) (100 mg, 0.211 mmol), 3-butyl-2-thioxothiazolidin-4-one (198.8 mg, 1.05 mmol) and NH_4OAc (195 mg, 2.53 mmol) in glacial acetic acid (40 mL) was refluxed for 48 hrs (TLC check every 24 hrs). After cooling to room temperature, the reaction was diluted with chloroform and repeatedly

washed with saturated $NaHCO_3$ solution until no more bubbling was observed. The organic phase was washed with brine, dried over Na_2SO_4, filtered and concentrated in *vacuo*. The crude mixture was purified by column chromatography over silica (eluent: DCM:hexane = 2:1) followed by recrystallization in acetic acid to give the desired product as an orange-red crystal (0.12 g, 70 %). mp 214 – 215 °C. ^{1}H NMR (400 MHz, $CDCl_3$) δ 8.14 (d, *J* = 8.7 Hz, 2H), 8.03 (d, *J* = 8.2 Hz, 2H), 7.92 (d, *J* = 8.7 Hz, 2H), 7.59 (s, 2H), 7.57 – 7.52 (m, 2H), 7.36 – 7.29 (m, 2H), 7.26 (d, *J* = 7.3 Hz, 2H), 7.03 (d, *J* = 4.0 Hz, 2H), 6.84 (d, *J* = 4.0 Hz, 2H), 4.04 (t, *J* = 7.4 Hz, 4H), 1.70 – 1.58 (m, 4H), 1.42 – 1.28 (m, 4H), 0.94 (t, *J* = 7.3 Hz, 6H). ^{13}C NMR (101 MHz, $CDCl_3$) δ 192.5, 167.4, 150.0, 138.9, 134.1, 133.5, 133.4, 131.5, 130.15, 128.5, 127.8, 127.7, 127.2, 126.6, 126.5, 125.0, 120.8, 118.4, 44.5, 29.1, 20.1, 13.7. HRMS (ASAP+) *m/z* calcd for $C_{44}H_{37}N_2O_2S_6$ [M^+] 817.1179, found 817.1180.

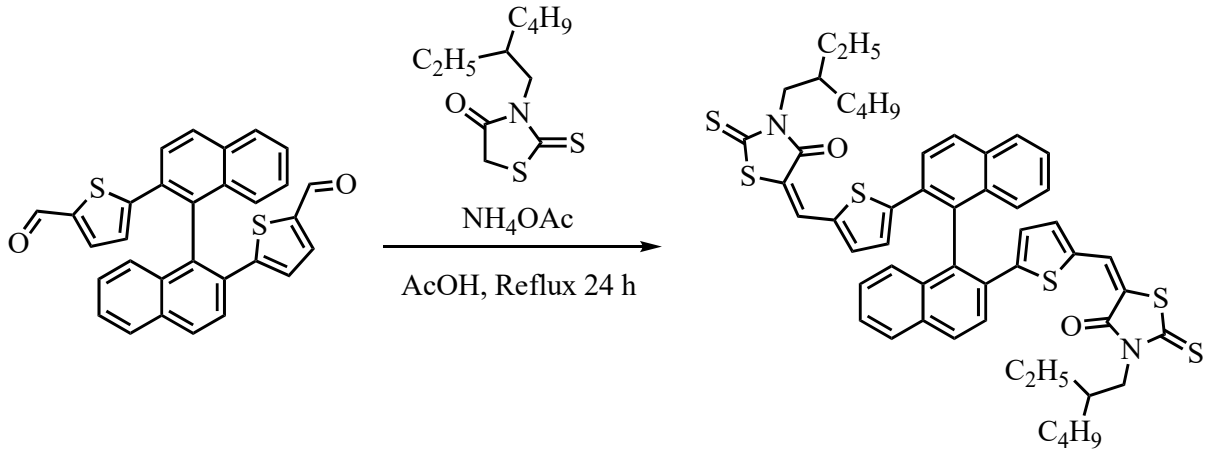
(5E,5'E)-5,5'-(([1,1'-Binaphthalene]-2,2'-diylbis(thiophene-5,2-diyl))bis(methaneylylidene))bis(3-ethyl-2-thioxothiazolidin-4-one)



To a solution of 5,5'-([1,1'-binaphthalene]-2,2'-diyl)bis(thiophene-2-carbaldehyde) (150 mg, 0.316 mmol), 3-ethyl-2-thioxothiazolidin-4-one (509.6 mg, 3.16 mmol) in anhydrous chloroform (40 mL) was added triethylamine (3.2 mL, 22.9 mmol) and the mixture was refluxed for 24 hrs. After cooling to room temperature, water (20 mL) was added and layers were separated. The organic layer was washed with water, brine, dried over Na_2SO_4, filtered and concentrated in *vacuo*. The crude was purified by column chromatography over silica (eluent: DCM:hexane = 3:1) to give trace of desired product.



A solution of 5,5'-([1,1'-binaphthalene]-2,2'-diyl)bis(thiophene-2-carbaldehyde) (300 mg, 0.632 mmol), 3-ethyl-2-thioxothiazolidin-4-one (509.6 mg, 3.16 mmol) and NH_4OAc (584.6 mg, 7.58 mmol) in glacial acetic acid (50 mL) was refluxed for 24 hrs. After cooling to room temperature, the reaction was diluted with chloroform and repeatedly washed with saturated $NaHCO_3$ solution until no more bubbling was observed. The organic phase was washed with brine, dried over Na_2SO_4, filtered and concentrated in *vacuo*. The crude mixture was purified by column chromatography (eluent: DCM:hexane = 2:1) followed by recrystallization in acetic acid to afford the desired product as an orange-red crystal (0.33 g, 68.6 %). mp 235 – 236 °C. ^{1}H NMR (400 MHz, $CDCl_3$) δ 8.14 (d, *J* = 8.7 Hz, 2H), 8.04 (d, *J* = 8.2 Hz, 2H), 7.91 (d, *J* = 8.7 Hz, 2H), 7.60 (s, 2H), 7.59 – 7.52 (m, 2H), 7.36 – 7.30 (m, 2H), 7.27 (d, *J* = 8.6 Hz, 2H), 7.03 (dd, *J* = 4.0, 0.6 Hz, 2H), 6.81 (d, *J* = 4.0 Hz, 2H), 4.11 (q, *J* = 7.1 Hz, 4H), 1.23 (t, *J* = 7.1 Hz, 6H). ^{13}C NMR (101 MHz, $CDCl_3$) δ 192.3, 167.2, 150.1, 138.8, 134.1, 133.5, 133.5, 133.4, 131.5, 130.1, 128.5, 127.8, 127.7, 127.2, 126.7, 126.5, 125.0, 120.9, 39.8, 12.3. HRMS (ASAP+) *m/z* calcd for $C_{40}H_{29}N_2O_2S_6$ [M^+] 761.0553, found 761.0556.

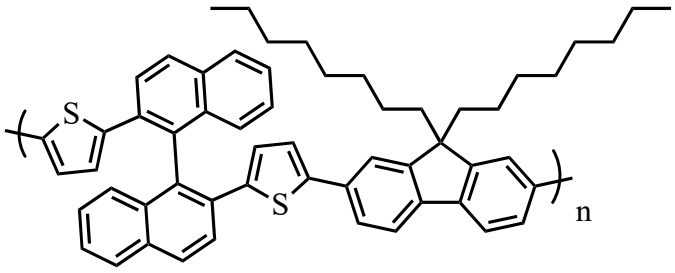


A solution of 5,5'-([1,1'-binaphthalene]-2,2'-diyl)bis(thiophene-2-carbaldehyde) (300 mg, 0.632 mmol), 3-(2-ethylhexyl)-2-thioxothiazolidin-4-one (776 mg, 3.16 mmol) and NH_4OAc (312 mg, 4.04 mmol) in glacial acetic acid (45 mL) was refluxed for 24 hrs. After cooling to

room temperature, the reaction was diluted with chloroform and repeatedly washed with saturated $NaHCO_3$ solution until no more bubbling was observed. The organic phase was washed with brine, dried over Na_2SO_4, filtered and concentrated in *vacuo*. The crude mixture was purified by column chromatography (eluent: DCM:hexane = 2:1) to afford the desired product as an orange-red solid (0.54 g, 92.4 %). mp 90 – 91 °C. ^{1}H NMR (400 MHz, $CDCl_3$) δ 8.15 (d, *J* = 8.7 Hz, 2H), 8.04 (d, *J* = 8.2 Hz, 2H), 7.94 (d, *J* = 8.7 Hz, 2H), 7.57 (s, 2H), 7.54 (d, *J* = 7.2 Hz, 2H), 7.38 – 7.29 (m, 2H), 7.26 (d, *J* = 8.0 Hz, 2H), 7.03 (d, *J* = 4.0 Hz, 2H), 6.90 (d, *J* = 7.2 Hz, 4H), 3.95 (d, *J* = 7.2 Hz, 4H), 2.08 – 1.94 (m, 2H), 1.45 – 1.05 (m, 16H), 0.88 (t, *J* = 7.2 Hz, 12H). ^{13}C NMR (101 MHz, $CDCl_3$) δ 192.9, 167.9, 149.9, 138.9, 134.1, 133.5, 133.4, 133.3, 131.6, 130.2, 128.5, 127.9, 127.7, 127.2, 126.6, 126.4, 125.0, 120.7, 48.7, 37.0, 30.5, 28.5, 23.9, 23.0, 14.1, 10.5. HRMS (ASAP+) *m/z* calcd for $C_{52}H_{53}N_2O_2S_6$ [M^+] 929.2431, found 929.2429.

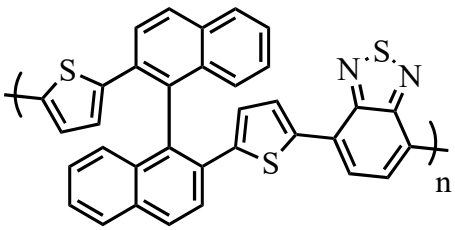
6.3 Chapter 4

Poly{2-(9,9-dioctyl-9H-fluoren-2-yl)-5-(2'-(thiophen-2-yl)-[1,1'-binaphthalen]-2-yl)thiophene}P(BNTF8)



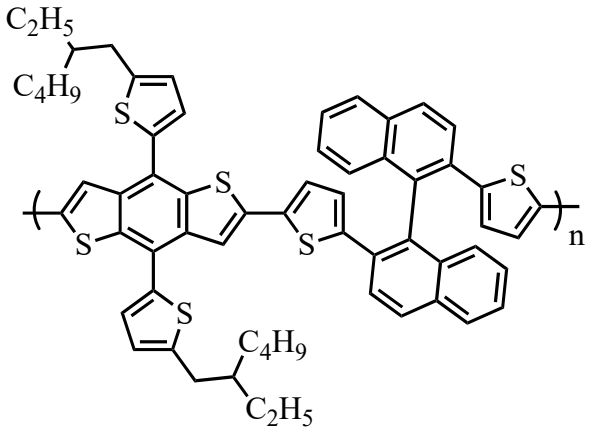
2,2'-Bis(5-bromothiophen-2-yl)-1,1'-binaphthalene (100 mg, 0.174 mmol), 2,2'-(9,9-dioctyl-9H-fluorene-2,7-diyl)bis(4,4,5,5-tetramethyl-1,3,2-dioxaborolane) (111.5 mg, 0.174 mmol),$Pd(PPh_3)_4$ (4.0 mg, 3.47 x 10^{-3} mmol, 2 mol%) and aliquat 336 (2 pipette drops) were added to an oven-dried 5 mL high-pressure microwave reactor vial. Anhydrous toluene was added, and the solution was heated to dissolve the 2,2'-bis(5-bromothiophen-2-yl)-1,1'-binaphthalene. 2M aqueous K_2CO_3 solution (0.35 mL) was added and the resulting mixture was stirred at 120 °C (oil bath) for 3 days. The mixture was cooled, precipitated into methanol (100 mL) and filtered through a Soxhlet thimble. It was extracted (Soxhlet) with methanol, acetone and then hexane. The residue from the thimble was collected and dried under vacuum (72 mg, 86 %). M_n 8.4 kDa, M_w 18 kDa. ^{1}H NMR (400 MHz, $CDCl_3$) δ 8.04 (d, J = 8.6 Hz, 2H), 7.98 (d, J = 8.8 Hz, 2H), 7.91 (d, J = 7.6 Hz, 2H), 7.47 (d, J = 7.9 Hz, 2H), 7.44 – 7.39 (m, 2H), 7.30 – 7.20 (m, 8H), 6.97 (d, J = 3.6 Hz, 2H), 6.72 (d, J = 3.9 Hz, 2H), 1.85 (br, 4H), 1.21 – 0.92 (m, 20H), 0.81 – 0.70 (m, 6H), 0.54 (br, 4H).

Poly{4-(5-(2'-(thiophen-2-yl)-[1,1'-binaphthalen]-2-yl)thiophen-2-yl)benzo[c][1,2,5]thiadiazole} P(BNTBT)



2,2'-Bis(5-bromothiophen-2-yl)-1,1'-binaphthalene (60 mg, 0.104 mmol), 4,7-bis(4,4,5,5-tetramethyl-1,3,2-dioxaborolan-2-yl)benzo[c][1,2,5]thiadiazole (40.4 mg, 0.104 mmol) and $Pd(PPh_3)_4$ (2.4 mg, 2.08 x 10^{-3} mmol, 2 mol%), aliquat 336 (2 pipette drops) were added to an oven-dried 5 mL high-pressure microwave reactor vial. Anhydrous toluene was added, and the vial was heated to dissolve the 2,2'-bis(5-bromothiophen-2-yl)-1,1'-binaphthalene. 2M aqueous K_2CO_3 solution (0.21 mL) was added and the resulting mixture was stirred at 120 °C (oil bath) for 3 days. However, solid started precipitating out after a few hours of heating, and it could not be re-dissolved, which in turn resulted in the failure of the reaction.

Poly{4,8-bis(5-(2-ethylhexyl)thiophen-2-yl)-2-(5-(2'-(thiophen-2-yl)-[1,1'-binaphthalen]-2-yl)thiophen-2-yl)benzo[1,2-*b*:4,5-*b'*]dithiophene} P(BNTBDT)



A solution of 2,2'-bis(5-bromothiophen-2-yl)-1,1'-binaphthalene (100 mg, 0.174 mmol), (4,8-bis(5-(2-ethylhexyl)thiophen-2-yl)benzo[1,2-*b*:4,5-*b'*]dithiophene-2,6-diyl)bis(trimethylstannane) (156.9 mg, 0.174 mmol), Pd_2dba_3 (3.2 mg, 3.47 x 10^{-3} mmol, 2 mol%), $P(o\text{-}tol)_3$ (4.2 mg, 0.014 mmol) in chlorobenzene (5 mL) in an oven-dried 5 mL high-pressure microwave reactor vial. was stirred at 130 °C (oil bath) for 3 days. The mixture was cooled, precipitated into methanol (100 mL) and filtered through a Soxhlet thimble. It was extracted (Soxhlet) with methanol, acetone and hexane. The residue from the thimble was collected and dried under vacuum (145 mg, 84 %). M_n 17 kDa, M_w 37 kDa. ^{1}H NMR (400 MHz, $CDCl_3$) δ 8.04 – 7.55 (m, 6H), 7.36 (br, 4H), 7.14 (br, 6H), 6.80 (br, 4H), 6.41 (br, 2H), 2.80 (br, 4H), 1.64 (br, 2H), 1.31 (br, 16H), 1.00 – 0.72 (m, 12H).

7. References

(1) Dimitrakopoulos, C. D.; Brown, A. R.; Pomp, A. Molecular Beam Deposited Thin Films of Pentacene for Organic Field Effect Transistor Applications. *J. Appl. Phys.* **1996**, *80* (4), 2501–2508. https://doi.org/10.1063/1.363032.

(2) Takeya, J.; Yamagishi, M.; Tominari, Y.; Hirahara, R.; Nakazawa, Y.; Nishikawa, T.; Kawase, T.; Shimoda, T.; Ogawa, S. Very High-Mobility Organic Single-Crystal Transistors with in-Crystal Conduction Channels. *Appl. Phys. Lett.* **2007**, *90* (10), 102120. https://doi.org/10.1063/1.2711393.

(3) Köhler, A.; Bässler, H. *Electronic Processes in Organic Semiconductors*; Wiley-VCH Verlag GmbH & Co. KGaA: Weinheim, Germany, 2015. https://doi.org/10.1002/9783527685172.

(4) Li, C.; Bo, Z. CHAPTER 1. New Chemistry for Organic Photovoltaic Materials; pp 1–31. https://doi.org/10.1039/9781782622307-00001.

(5) Scharber, M. C.; Sariciftci, N. S. Efficiency of Bulk-Heterojunction Organic Solar Cells. *Prog. Polym. Sci.* **2013**, *38* (12), 1929–1940. https://doi.org/10.1016/j.progpolymsci.2013.05.001.

(6) Mikhnenko, O. V.; Kuik, M.; Lin, J.; van der Kaap, N.; Nguyen, T.-Q.; Blom, P. W. M. Trap-Limited Exciton Diffusion in Organic Semiconductors. *Adv. Mater.* **2014**, *26* (12), 1912–1917. https://doi.org/10.1002/adma.201304162.

(7) Watkins, P. K.; Walker, A. B.; Verschoor, G. L. B. Dynamical Monte Carlo Modelling of Organic Solar Cells: The Dependence of Internal Quantum Efficiency on Morphology. *Nano Lett.* **2005**, *5* (9), 1814–1818. https://doi.org/10.1021/nl051098o.

(8) Nielsen, C. B.; Holliday, S.; Chen, H.; Cryer, S. J.; McCulloch, I. Non-Fullerene Electron Acceptors for Use in Organic Solar Cells. *Acc. Chem. Res.* **2015**, *48* (11), 2803–2812. https://doi.org/10.1021/acs.accounts.5b00199.

(9) Andrews, D. L. *Photonics*; Andrews, D. L., Ed.; John Wiley & Sons, Inc.: Hoboken, NJ, USA, 2015. https://doi.org/10.1002/9781119011781.

(10) Grynberg, G.; Aspect, A.; Fabre, C.; Cohen-Tannoudji, C. *Introduction to Quantum*

Optics : From the Semi-Classical Approach to Quantized Light; Cambridge University Press: Cambridge, UNITED KINGDOM, 2010.

(11) *Chirality*; Janoschek, R., Ed.; Springer Berlin Heidelberg: Berlin, Heidelberg, 1991. https://doi.org/10.1007/978-3-642-76569-8.

(12) Brmtain, H. G. Excited-State Optical Activity, 1987-1995. *Chirality* **1996**, *8* (5), 357–363.

(13) Riehl, J. P.; Richardson, F. S. Circularly Polarized Luminescence Spectroscopy. *Chem. Rev.* **1986**, *86* (1), 1–16. https://doi.org/10.1021/cr00071a001.

(14) *Comprehensive Chiroptical Spectroscopy*; Berova, N., Polavarapu, P. L., Nakanishi, K., Woody, R. W., Eds.; John Wiley & Sons, Inc.: Hoboken, NJ, USA, 2011. https://doi.org/10.1002/9781118120187.

(15) *Luminescence of Lanthanide Ions in Coordination Compounds and Nanomaterials*; de Bettencourt-Dias, A., Ed.; John Wiley & Sons Ltd: Chichester, United Kingdom, 2014. https://doi.org/10.1002/9781118682760.

(16) Zinna, F.; Di Bari, L. Lanthanide Circularly Polarized Luminescence: Bases and Applications. *Chirality* **2015**, *27* (1), 1–13. https://doi.org/10.1002/chir.22382.

(17) Peeters, E.; Christiaans, M. P. T.; Janssen, R. A. J.; Schoo, H. F. M.; Dekkers, H. P. J. M.; Meijer, E. W. Circularly Polarized Electroluminescence from a Polymer Light-Emitting Diode. *J. Am. Chem. Soc.* **1997**, *119* (41), 9909–9910. https://doi.org/10.1021/ja971912c.

(18) Kawai, T.; Kawamura, K.; Tsumatori, H.; Ishikawa, M.; Naito, M.; Fujiki, M.; Nakashima, T. Circularly Polarized Luminescence of a Fluorescent Chiral Binaphtylene–Perylenebiscarboxydiimide Dimer. *ChemPhysChem* **2007**, *8* (10), 1465–1468. https://doi.org/10.1002/cphc.200600747.

(19) Schadt, M. LIQUID CRYSTAL MATERIALS AND LIQUID CRYSTAL DISPLAYS. *Annu. Rev. Mater. Sci.* **1997**, *27* (1), 305–379. https://doi.org/10.1146/annurev.matsci.27.1.305.

(20) Farshchi, R.; Ramsteiner, M.; Herfort, J.; Tahraoui, A.; Grahn, H. T. Optical Communication of Spin Information between Light Emitting Diodes. *Appl. Phys. Lett.* **2011**, *98* (16), 162508. https://doi.org/10.1063/1.3582917.

(21) Heffern, M. C.; Matosziuk, L. M.; Meade, T. J. Lanthanide Probes for Bioresponsive Imaging. *Chem. Rev.* **2014**, *114* (8), 4496–4539. https://doi.org/10.1021/cr400477t.

(22) Singh, R.; Narayanan Unni, K. N.; Solanki, A.; Deepak. Improving the Contrast Ratio of OLED Displays: An Analysis of Various Techniques. *Opt. Mater. (Amst).* **2012**, *34* (4), 716–723. https://doi.org/10.1016/j.optmat.2011.10.005.

(23) Farnum, D. G.; Mehta, G.; Moore, G. G. I.; Siegal, F. P. Attempted Reformatskii Reaction of Benzonitrile, 1,4-Diketo-3,6-Diphenylpyrrolo[3,4-C]Pyrrole. A Lactam Analogue of Pentalene. *Tetrahedron Lett.* **1974**, *15* (29), 2549–2552. https://doi.org/10.1016/S0040-4039(01)93202-2.

(24) Iqbal, A.; Jost, M.; Kirchmayr, R.; Pfenninger, J.; Rochat, A.; Wallquist, O. The Synthesis and Properties of 1,4-Diketo-Pyrrolo[3,4-C]Pyrroles. *Bull. des Sociétés Chim. Belges* **2010**, *97* (8–9), 615–644. https://doi.org/10.1002/bscb.19880970804.

(25) Hao, Z.; Iqbal, A. Some Aspects of Organic Pigments. *Chem. Soc. Rev.* **1997**, *26* (3), 203. https://doi.org/10.1039/cs9972600203.

(26) Lenz, R.; Wallquist, O. DPP Chemistry — Continuous Innovation. *Surf. Coatings Int. Part B Coatings Trans.* **2002**, *85* (1), 19–26. https://doi.org/10.1007/BF02699738.

(27) Wallquist, O.; Lenz, R. Diketopyrrolopyrrole (DPP) Pigments. In *High Performance Pigments*; Wiley-VCH Verlag GmbH & Co. KGaA: Weinheim, Germany; pp 165–194. https://doi.org/10.1002/9783527626915.ch11.

(28) Zollinger, H. *Color Chemistry: Syntheses, Properties, and Applications of Organic Dyes and Pigments*; Wiley, 2003.

(29) Potrawa, T.; Langhals, H. Fluoreszenzfarbstoffe Mit Großen Stokes-Shifts - Lösliche Dihydropyrrolopyrroldione. *Chem. Ber.* **1987**, *120* (7), 1075–1078. https://doi.org/10.1002/cber.19871200702.

(30) Colonna, G.; Pilati, T.; Rusconi, F.; Zecchi, G. Synthesis and Properties of Some New N,N′-Disubstituted 2,5-Dihydro-1,4-Dioxo-3,6-Diphenylpyrrolo[3,4-c]Pyrroles. *Dye. Pigment.* **2007**, *75* (1), 125–129. https://doi.org/10.1016/j.dyepig.2006.05.024.

(31) Grzybowski, M.; Gryko, D. T. Diketopyrrolopyrroles: Synthesis, Reactivity, and Optical Properties. *Adv. Opt. Mater.* **2015**, *3* (3), 280–320. https://doi.org/10.1002/adom.201400559.

(32) Tieke, B.; Rabindranath, A. R.; Zhang, K.; Zhu, Y. Conjugated Polymers Containing Diketopyrrolopyrrole Units in the Main Chain. *Beilstein J. Org. Chem.* **2010**, *6*, 830–845. https://doi.org/10.3762/bjoc.6.92.

(33) Qu, S.; Tian, H. Diketopyrrolopyrrole (DPP)-Based Materials for Organic Photovoltaics. *Chem. Commun.* **2012**, *48* (25), 3039–3051. https://doi.org/10.1039/c2cc17886a.

(34) Nielsen, C. B.; Turbiez, M.; McCulloch, I. Recent Advances in the Development of Semiconducting DPP-Containing Polymers for Transistor Applications. *Adv. Mater.* **2013**, *25* (13), 1859–1880. https://doi.org/10.1002/adma.201201795.

(35) Chandran, D.; Lee, K.-S. Diketopyrrolopyrrole: A Versatile Building Block for Organic Photovoltaic Materials. *Macromol. Res.* **2013**, *21* (3), 272–283. https://doi.org/10.1007/s13233-013-1141-3.

(36) Li, Y. N.; Sonar, P.; Murphy, L.; Hong, W. High Mobility Diketopyrrolopyrrole (DPP)-Based Organic Semiconductor Materials for Organic Thin Film Transistors and Photovoltaics. *Energy Environ. Sci.* **2013**, *6* (6), 1684–1710. https://doi.org/10.1039/c3ee00015j.

(37) Kaur, M.; Choi, D. H. Diketopyrrolopyrrole: Brilliant Red Pigment Dye-Based Fluorescent Probes and Their Applications. *Chem. Soc. Rev.* **2015**, *44* (1), 58–77. https://doi.org/10.1039/C4CS00248B.

(38) Liu, J.; Zhang, Y.; Phan, H.; Sharenko, A.; Moonsin, P.; Walker, B.; Promarak, V.; Nguyen, T.-Q. Effects of Stereoisomerism on the Crystallization Behavior and Optoelectrical Properties of Conjugated Molecules. *Adv. Mater.* **2013**, *25* (27), 3645–3650. https://doi.org/10.1002/adma.201300255.

(39) Zerdan, R. B.; Shewmon, N. T.; Zhu, Y.; Mudrick, J. P.; Chesney, K. J.; Xue, J.; Castellano, R. K. The Influence of Solubilizing Chain Stereochemistry on Small Molecule Photovoltaics. *Adv. Funct. Mater.* **2014**, *24* (38), 5993–6004. https://doi.org/10.1002/adfm.201401030.

(40) Li, S.; Liu, W.; Shi, M.; Mai, J.; Lau, T. K.; Wan, J.; Lu, X.; Li, C. Z.; Chen, H. A Spirobifluorene and Diketopyrrolopyrrole Moieties Based Non-Fullerene Acceptor for Efficient and Thermally Stable Polymer Solar Cells with High Open-Circuit Voltage. *Energy Environ. Sci.* **2016**, *9* (2), 604–610. https://doi.org/10.1039/c5ee03481g.

(41) Luo, Z.; Liu, T.; Cheng, W.; Wu, K.; Xie, D.; Huo, L.; Sun, Y.; Yang, C. A Three-Dimensional Thiophene-Annulated Perylene Bisimide as a Fullerene-Free Acceptor for a High Performance Polymer Solar Cell with the Highest PCE of 8.28% and a V OC over 1.0 V. *J. Mater. Chem. C* **2018**, *6* (5), 1136–1142. https://doi.org/10.1039/C7TC05261H.

(42) Wu, Q.; Zhao, D.; Schneider, A. M.; Chen, W.; Yu, L. Covalently Bound Clusters of Alpha-Substituted PDI—Rival Electron Acceptors to Fullerene for Organic Solar Cells. *J. Am. Chem. Soc.* **2016**, *138* (23), 7248–7251. https://doi.org/10.1021/jacs.6b03562.

(43) Zhong, Y.; Trinh, M. T.; Chen, R.; Purdum, G. E.; Khlyabich, P. P.; Sezen, M.; Oh, S.; Zhu, H.; Fowler, B.; Zhang, B.; et al. Molecular Helices as Electron Acceptors in High-Performance Bulk Heterojunction Solar Cells. *Nat. Commun.* **2015**, *6* (1), 8242. https://doi.org/10.1038/ncomms9242.

(44) Zhong, H.; Wu, C. H.; Li, C. Z.; Carpenter, J.; Chueh, C. C.; Chen, J. Y.; Ade, H.; Jen, A. K. Y. Rigidifying Nonplanar Perylene Diimides by Ring Fusion Toward Geometry-Tunable Acceptors for High-Performance Fullerene-Free Solar Cells. *Adv. Mater.* **2016**, *28* (5). https://doi.org/10.1002/adma.201504120.

(45) Liang, N.; Meng, D.; Ma, Z.; Kan, B.; Meng, X.; Zheng, Z.; Jiang, W.; Li, Y.; Wan, X.; Hou, J.; et al. Triperylene Hexaimides Based All-Small-Molecule Solar Cells with an Efficiency over 6% and Open Circuit Voltage of 1.04 V. *Adv. Energy Mater.* **2017**, *7* (6), 1601664. https://doi.org/10.1002/aenm.201601664.

(46) Zhang, J.; Li, Y.; Huang, J.; Hu, H.; Zhang, G.; Ma, T.; Chow, P. C. Y.; Ade, H.; Pan, D.; Yan, H. Ring-Fusion of Perylene Diimide Acceptor Enabling Efficient Nonfullerene Organic Solar Cells with a Small Voltage Loss. *J. Am. Chem. Soc.* **2017**, *139* (45), 16092–16095. https://doi.org/10.1021/jacs.7b09998.

(47) Wan, L.; Wade, J.; Salerno, F.; Arteaga, O.; Laidlaw, B.; Wang, X.; Penfold, T.; Fuchter, M. J.; Campbell, A. J. Inverting the Handedness of Circularly Polarized Luminescence from Light-Emitting Polymers Using Film Thickness. *ACS Nano* **2019**, *13* (7), 8099–8105. https://doi.org/10.1021/acsnano.9b02940.

(48) Brandt, J. R.; Wang, X.; Yang, Y.; Campbell, A. J.; Fuchter, M. J. Circularly Polarized Phosphorescent Electroluminescence with a High Dissymmetry Factor from PHOLEDs Based on a Platinahelicene. *J. Am. Chem. Soc.* **2016**, *138* (31), 9743–9746.

https://doi.org/10.1021/jacs.6b02463.

(49) Yang, Y.; Da Costa, R. C.; Smilgies, D. M.; Campbell, A. J.; Fuchter, M. J. Induction of Circularly Polarized Electroluminescence from an Achiral Light-Emitting Polymer via a Chiral Small-Molecule Dopant. *Adv. Mater.* **2013**, *25* (18), 2624–2628. https://doi.org/10.1002/adma.201204961.

(50) Wagenknecht, C.; Li, C.-M.; Reingruber, A.; Bao, X.-H.; Goebel, A.; Chen, Y.-A.; Zhang, Q.; Chen, K.; Pan, J.-W. Experimental Demonstration of a Heralded Entanglement Source. *Nat. Photonics* **2010**, *4* (8), 549–552. https://doi.org/10.1038/nphoton.2010.123.

(51) Inoue, Y. Asymmetric Photochemical Reactions in Solution. *Chem. Rev.* **1992**, *92* (5), 741–770. https://doi.org/10.1021/cr00013a001.

(52) Richardson, R. D.; Baud, M. G. J.; Weston, C. E.; Rzepa, H. S.; Kuimova, M. K.; Fuchter, M. J. Dual Wavelength Asymmetric Photochemical Synthesis with Circularly Polarized Light. *Chem. Sci.* **2015**, *6* (7), 3853–3862. https://doi.org/10.1039/C4SC03897E.

(53) Li, J.; Rajca, A.; Rajca, S. Synthesis and Conductivity of Binaphthyl-Based Conjugated Polymers. *Synth. Met.* **2003**, *137* (1–3), 1507–1508. https://doi.org/10.1016/S0379-6779(02)01205-5.

(54) Krascsenicsová, K.; Walla, P.; Kasák, P.; Uray, G.; Kappe, C. O.; Putala, M. Stereoconservative Negishi Arylation and Alkynylation as an Efficient Approach to Enantiopure 2,2′-Diarylated 1,1′-Binaphthyls. *Chem. Commun.* **2004**, No. 22, 2606–2607. https://doi.org/10.1039/B410185E.

(55) O'Brien, C. J.; Kantchev, E. A. B.; Valente, C.; Hadei, N.; Chass, G. A.; Lough, A.; Hopkinson, A. C.; Organ, M. G. Easily Prepared Air- and Moisture-Stable Pd–NHC (NHC=N-Heterocyclic Carbene) Complexes: A Reliable, User-Friendly, Highly Active Palladium Precatalyst for the Suzuki–Miyaura Reaction. *Chem. - A Eur. J.* **2006**, *12* (18), 4743–4748. https://doi.org/10.1002/chem.200600251.

(56) Organ, M. G.; Avola, S.; Dubovyk, I.; Hadei, N.; Kantchev, E. A. B.; O'Brien, C. J.; Valente, C. A User-Friendly, All-Purpose Pd–NHC (NHC=N-Heterocyclic Carbene) Precatalyst for the Negishi Reaction: A Step Towards a Universal Cross-Coupling Catalyst. *Chem. - A Eur. J.* **2006**, *12* (18), 4749–4755.

https://doi.org/10.1002/chem.200600206.

(57) Pinxterhuis, E. B.; Giannerini, M.; Hornillos, V.; Feringa, B. L. Fast, Greener and Scalable Direct Coupling of Organolithium Compounds with No Additional Solvents. *Nat. Commun.* **2016**, *7* (1), 11698. https://doi.org/10.1038/ncomms11698.

(58) Grzybowski, M.; Glodkowska-Mrowka, E.; Hugues, V.; Brutkowski, W.; Blanchard-Desce, M.; Gryko, D. T. Polar Diketopyrrolopyrrole-Imidazolium Salts as Selective Probes for Staining Mitochondria in Two-Photon Fluorescence Microscopy. *Chem. - A Eur. J.* **2015**, *21* (25), 9101–9110. https://doi.org/10.1002/chem.201500738.

(59) Ripaud, E.; Demeter, D.; Rousseau, T.; Boucard-Cétol, E.; Allain, M.; Po, R.; Leriche, P.; Roncali, J. Structure–Properties Relationships in Conjugated Molecules Based on Diketopyrrolopyrrole for Organic Photovoltaics. *Dye. Pigment.* **2012**, *95* (1), 126–133. https://doi.org/10.1016/j.dyepig.2012.03.021.

(60) BASF, S.; GRZYBOWSKI, M.; GRYKO, D. T. NOVEL HETEROCYCLIC FLUORESCENT DYES AND METHOD OF PRODUCTION THEREOF. WO2013/92474, 2013.

(61) Heyer, E.; Ziessel, R. Panchromatic Push-Pull Dyes of Elongated Form from Triphenylamine, Diketopyrrolopyrrole, and Tetracyanobutadiene Modules. *Synlett* **2015**, *26* (15), 2109–2116. https://doi.org/10.1055/s-0034-1378818.

(62) Yoon, W. S.; Park, S. K.; Cho, I.; Oh, J. A.; Kim, J. H.; Park, S. Y. High-Mobility n-Type Organic Transistors Based on a Crystallized Diketopyrrolopyrrole Derivative. *Adv. Funct. Mater.* **2013**, *23* (28), 3519–3524. https://doi.org/10.1002/adfm.201203065.

(63) Sahu, D.; Tsai, C.-H.; Wei, H.-Y.; Ho, K.-C.; Chang, F.-C.; Chu, C.-W. Synthesis and Applications of Novel Low Bandgap Star-Burst Molecules Containing a Triphenylamine Core and Dialkylated Diketopyrrolopyrrole Arms for Organic Photovoltaics. *J. Mater. Chem.* **2012**, *22* (16), 7945. https://doi.org/10.1039/c2jm16760c.

(64) Stas, S.; Sergeyev, S.; Geerts, Y. Synthesis of Diketopyrrolopyrrole (DPP) Derivatives Comprising Bithiophene Moieties. *Tetrahedron* **2010**, *66* (10), 1837–1845. https://doi.org/10.1016/j.tet.2010.01.027.

(65) Challis, B. G.; Challis, J. A. Reactions of the Carboxamide Group. In *Amides (1970)*;

John Wiley & Sons, Ltd.: Chichester, UK; pp 731–857. https://doi.org/10.1002/9780470771235.ch13.

(66) Jin, L.; Lei, A. Insights into the Elementary Steps in Negishi Coupling through Kinetic Investigations. *Org. Biomol. Chem.* **2012**, *10* (34), 6817. https://doi.org/10.1039/c2ob25650a.

(67) Más-Montoya, M.; Janssen, R. A. J. The Effect of H- and J-Aggregation on the Photophysical and Photovoltaic Properties of Small Thiophene-Pyridine-DPP Molecules for Bulk-Heterojunction Solar Cells. *Adv. Funct. Mater.* **2017**, *27* (16), 1605779. https://doi.org/10.1002/adfm.201605779.

(68) Wawrzinek, R.; Zhou, X.; Ullah, M.; Namdas, E. B.; Lo, S.-C. Aggregates of Diketopyrrolopyrrole Dimers in Solution. *Dye. Pigment.* **2017**, *136* (22), 678–685. https://doi.org/10.1016/j.dyepig.2016.08.064.

(69) Raychev, D.; Seifert, G.; Sommer, J.; Guskova, O. A Comparative Analysis of Symmetric Diketopyrrolopyrrole-cored Small Conjugated Molecules with Aromatic Flanks: From Geometry to Charge Transport. *J. Comput. Chem.* **2018**, *39* (30), 2526–2538. https://doi.org/10.1002/jcc.25609.

(70) Groom, C. R.; Bruno, I. J.; Lightfoot, M. P.; Ward, S. C. The Cambridge Structural Database. *Acta Crystallogr. Sect. B Struct. Sci. Cryst. Eng. Mater.* **2016**, *72* (2), 171–179. https://doi.org/10.1107/S2052520616003954.

(71) Deutman, A. B. C.; Varghese, S.; Moalin, M.; Elemans, J. A. A. W.; Rowan, A. E.; Nolte, R. J. M. Slippage of a Porphyrin Macrocycle over Threads of Varying Bulkiness: Implications for the Mechanism of Threading Polymers through a Macrocyclic Ring. *Chem. - A Eur. J.* **2015**, *21* (1), 360–370. https://doi.org/10.1002/chem.201403740.

(72) Meakin, B. J.; Mumford, F. R.; Ward, E. R. THE SYNTHESIS OF SOME POTENTIAL ANTIMETABOLITES OF PHENYLALANINE. *J. Pharm. Pharmacol.* **1960**, *12* (1), 400–410. https://doi.org/10.1111/j.2042-7158.1960.tb12681.x.

(73) Price of (R)-(+)-1,1′-Bi(2-naphthol) http://www.fluorochem.co.uk/Products/Search?searchType=C&searchText=18531-94-7 (accessed Sep 10, 2019).

(74) Page, P. C. B.; Farah, M. M.; Buckley, B. R.; Blacker, A. J. New Chiral Binaphthalene-

Derived Iminium Salt Organocatalysts for Asymmetric Epoxidation of Alkenes. *ChemInform* **2007**, *38* (42). https://doi.org/10.1002/chin.200742093.

(75) Sumida, Y.; Sumida, T.; Hosoya, T. Nickel-Catalyzed Reductive Cross-Coupling of Aryl Triflates and Nonaflates with Alkyl Iodides. *Synthesis (Stuttg).* **2017**, *49* (16), 3590–3601. https://doi.org/10.1055/s-0036-1588464.

(76) Ashokkumar, V.; Chithiraikumar, C.; Siva, A. Binaphthyl-Based Chiral Bifunctional Organocatalysts for Water Mediated Asymmetric List-Lerner-Barbas Aldol Reactions. *Org. Biomol. Chem.* **2016**, *14* (38), 9021–9032. https://doi.org/10.1039/c6ob01558a.

(77) Guo, C.; Chang, X.; Zhang, Q. Chiral Aromatic Amine Compounds and Preparation Method Thereof. CN107814729, 2018.

(78) Quideau, S.; Lyvinec, G.; Marguerit, M.; Bathany, K.; Ozanne-Beaudenon, A.; Buffeteau, T.; Cavagnat, D.; Chénedé, A. Asymmetric Hydroxylative Phenol Dearomatization through In Situ Generation of Iodanes from Chiral Iodoarenes and m -CPBA. *Angew. Chemie Int. Ed.* **2009**, *48* (25), 4605–4609. https://doi.org/10.1002/anie.200901039.

(79) Bekkaye, M.; Masson, G. Synthesis of New Axially Chiral Iodoarenes. *Synthesis (Stuttg).* **2015**, *48* (02), 302–312. https://doi.org/10.1055/s-0035-1560512.

(80) Brown, K. J.; Berry, M. S.; Murdoch, J. R. Synthesis of Optically Active 2,2'-Dihalo-1,1'-Binaphthyls via Stable Diazonium Salts. *J. Org. Chem.* **1985**, *50* (22), 4345–4349. https://doi.org/10.1021/jo00222a029.

(81) Kasák, P.; Brath, H.; Krascsenicsová-Poláková, K.; Kicková, A.; Moldovan, N.; Putala, M. Chiral Binaphthalenes Bearing Two Pyridine Ligands Attached Via Acetylene Spacers. Synthesis and Coordination Study. *Collect. Czechoslov. Chem. Commun.* **2007**, *72* (8), 1139–1157. https://doi.org/10.1135/cccc20071139.

(82) Shimoda, Y.; Yamamoto, H. New Oxazaborolidine Catalysts for the Diels–Alder Reaction. *Synthesis (Stuttg).* **2016**, *49* (01), 175–180. https://doi.org/10.1055/s-0036-1588082.

(83) Pushkara Rao, V.; K.-Y. Jen, A.; Caldwell, J. B. Rhodanine-Methine as π-Electron Acceptor in Second-Order Nonlinear Optical Chromophores. *Tetrahedron Lett.* **1994**, *35* (23), 3849–3852. https://doi.org/10.1016/S0040-4039(00)76683-4.

(84) Marinado, T.; Hagberg, D. P.; Hedlund, M.; Edvinsson, T.; Johansson, E. M. J.; Boschloo, G.; Rensmo, H.; Brinck, T.; Sun, L.; Hagfeldt, A. Rhodaninedyes for Dye-Sensitized Solar Cells : Spectroscopy, Energy Levels and Photovoltaic Performance. *Phys. Chem. Chem. Phys.* **2009**, *11* (1), 133–141. https://doi.org/10.1039/B812154K.

(85) Insuasty, A.; Ortiz, A.; Tigreros, A.; Solarte, E.; Insuasty, B.; Martín, N. 2-(1,1-Dicyanomethylene)Rhodanine: A Novel, Efficient Electron Acceptor. *Dye. Pigment.* **2011**, *88* (3), 385–390. https://doi.org/10.1016/j.dyepig.2010.08.011.

(86) Li, Z.; He, G.; Wan, X.; Liu, Y.; Zhou, J.; Long, G.; Zuo, Y.; Zhang, M.; Chen, Y. Solution Processable Rhodanine-Based Small Molecule Organic Photovoltaic Cells with a Power Conversion Efficiency of 6.1%. *Adv. Energy Mater.* **2012**, *2* (1), 74–77. https://doi.org/10.1002/aenm.201100572.

(87) Zhou, J.; Zuo, Y.; Wan, X.; Long, G.; Zhang, Q.; Ni, W.; Liu, Y.; Li, Z.; He, G.; Li, C.; et al. Solution-Processed and High-Performance Organic Solar Cells Using Small Molecules with a Benzodithiophene Unit. *J. Am. Chem. Soc.* **2013**, *135* (23), 8484–8487. https://doi.org/10.1021/ja403318y.

(88) Zhou, J.; Wan, X.; Liu, Y.; Zuo, Y.; Li, Z.; He, G.; Long, G.; Ni, W.; Li, C.; Su, X.; et al. Small Molecules Based on Benzo[1,2-b:4,5-B′]Dithiophene Unit for High-Performance Solution-Processed Organic Solar Cells. *J. Am. Chem. Soc.* **2012**, *134* (39), 16345–16351. https://doi.org/10.1021/ja306865z.

(89) Liu, Y.; Chen, C.-C.; Hong, Z.; Gao, J.; (Michael) Yang, Y.; Zhou, H.; Dou, L.; Li, G.; Yang, Y. Solution-Processed Small-Molecule Solar Cells: Breaking the 10% Power Conversion Efficiency. *Sci. Rep.* **2013**, *3* (1), 3356. https://doi.org/10.1038/srep03356.

(90) Kim, Y.; Song, C. E.; Moon, S.-J.; Lim, E. Rhodanine Dye-Based Small Molecule Acceptors for Organic Photovoltaic Cells. *Chem. Commun.* **2014**, *50* (60), 8235–8238. https://doi.org/10.1039/C4CC01695E.

(91) Holliday, S.; Ashraf, R. S.; Nielsen, C. B.; Kirkus, M.; Röhr, J. A.; Tan, C.-H.; Collado-Fregoso, E.; Knall, A.-C.; Durrant, J. R.; Nelson, J.; et al. A Rhodanine Flanked Nonfullerene Acceptor for Solution-Processed Organic Photovoltaics. *J. Am. Chem. Soc.* **2015**, *137* (2), 898–904. https://doi.org/10.1021/ja5110602.

(92) Koh, C.; Lim, E. Synthesis and Characterization of a 2-(1,1-Dicyanomethylene)

Rhodanine-Based Nonfullerene Acceptor for OPVs. *Bull. Korean Chem. Soc.* **2018**, *39* (4), 555–558. https://doi.org/10.1002/bkcs.11435.

(93) Qu, J.; Mu, Z.; Lai, H.; Chen, H.; Liu, T.; Zhang, S.; Chen, W.; He, F. Alkyl Chain End Group Engineering of Small Molecule Acceptors for Non-Fullerene Organic Solar Cells. *ACS Appl. Energy Mater.* **2018**, *1* (9), 4724–4730. https://doi.org/10.1021/acsaem.8b00851.

(94) Sandoval-Torrientes, R.; Calbo, J.; García-Fresnadillo, D.; Santos, J.; Ortí, E.; Martín, N. Rhodanine-Based Dyes Absorbing in the Entire Visible Spectrum. *Org. Chem. Front.* **2017**, *4* (6), 1024–1028. https://doi.org/10.1039/C6QO00760K.

(95) Radi, M.; Botta, L.; Casaluce, G.; Bernardini, M.; Botta, M. Practical One-Pot Two-Step Protocol for the Microwave-Assisted Synthesis of Highly Functionalized Rhodanine Derivatives. *J. Comb. Chem.* **2010**, *12* (1), 200–205. https://doi.org/10.1021/cc9001789.

(96) Sandoval-Torrientes, R.; Calbo, J.; García-Fresnadillo, D.; Santos, J.; Ortí, E.; Martín, N. Rhodanine-Based Dyes Absorbing in the Entire Visible Spectrum. *Org. Chem. Front.* **2017**, *4* (6), 1024–1028. https://doi.org/10.1039/c6qo00760k.

(97) Zhang, Y.; Xu, X.; Lu, J.; Zhang, S. Effect of Polymer Molecular Weight on J51 Based Organic Solar Cells. *RSC Adv.* **2019**, *9* (26), 14657–14661. https://doi.org/10.1039/C9RA02022E.

(98) Grell, M.; Oda, M.; Whitehead, K. S.; Asimakis, A.; Neher, D.; Bradley, D. D. C. A Compact Device for the Efficient, Electrically Driven Generation of Highly Circularly Polarized Light. *Adv. Mater.* **2001**, *13* (8), 577–580. https://doi.org/10.1002/1521-4095(200104)13:8<577::AID-ADMA577>3.0.CO;2-K.

(99) Lucarelli, J.; Lessi, M.; Manzini, C.; Minei, P.; Bellina, F.; Pucci, A. "N-Alkyl Diketopyrrolopyrrole-Based Fluorophores for Luminescent Solar Concentrators: Effect of the Alkyl Chain on Dye Efficiency." *Dye. Pigment.* **2016**, *135*, 154–162. https://doi.org/10.1016/j.dyepig.2016.03.036.

(100) Szabadai, R. S.; Roth-Barton, J.; Ghiggino, K. P.; White, J. M.; Wilson, D. J. D. Solvatochromism in Diketopyrrolopyrrole Derivatives: Experimental and Computational Studies. *Aust. J. Chem.* **2014**, *67* (9), 1330. https://doi.org/10.1071/CH14057.

(101) Fujii, K.; Todani, H.; Ito, S.; Mikami, K. Design of Phosphinic Acid Catalysts with the Closest Stereogenicity at the α-Position: Synthesis and Application of α-Stereogenic Perfluoroalkyl Phosphinic Acid Catalysts. *Org. Lett.* **2019**, *21* (9), 3387–3391. https://doi.org/10.1021/acs.orglett.9b01131.

(102) Wöste, T. H.; Oestreich, M. BINAP versus BINAP(O) in Asymmetric Intermolecular Mizoroki-Heck Reactions: Substantial Effects on Selectivities. *Chem. - A Eur. J.* **2011**, *17* (42), 11914–11918. https://doi.org/10.1002/chem.201101695.

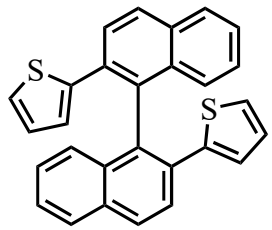
(103) Mislow, K.; Grasemann, P. Notes - Absolute Configuration of 1,1'-Bi-2-Naphthylamine. *J. Org. Chem.* **1958**, *23* (12), 2027–2028. https://doi.org/10.1021/jo01106a628.

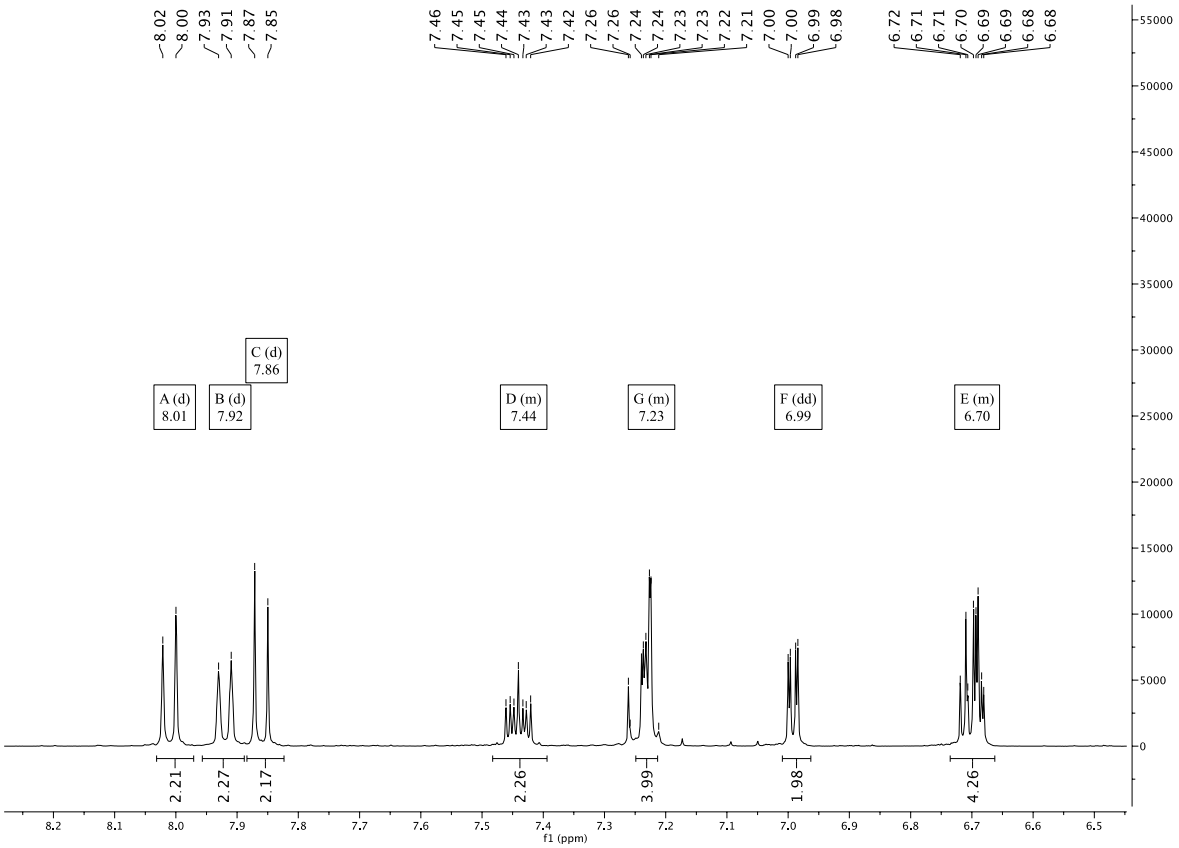
(104) Brath, H.; Dubovská, M.; Juríček, M.; Kasák, P.; Putala, M. Novel Route to Enantiopure 2,2'-Diaryl-1,1'-Binaphthalenes by Stereoconservative Suzuki Arylation at Positions 2 and 2'. *Collect. Czechoslov. Chem. Commun.* **2004**, *69* (7), 1517–1536. https://doi.org/10.1135/cccc20041517.

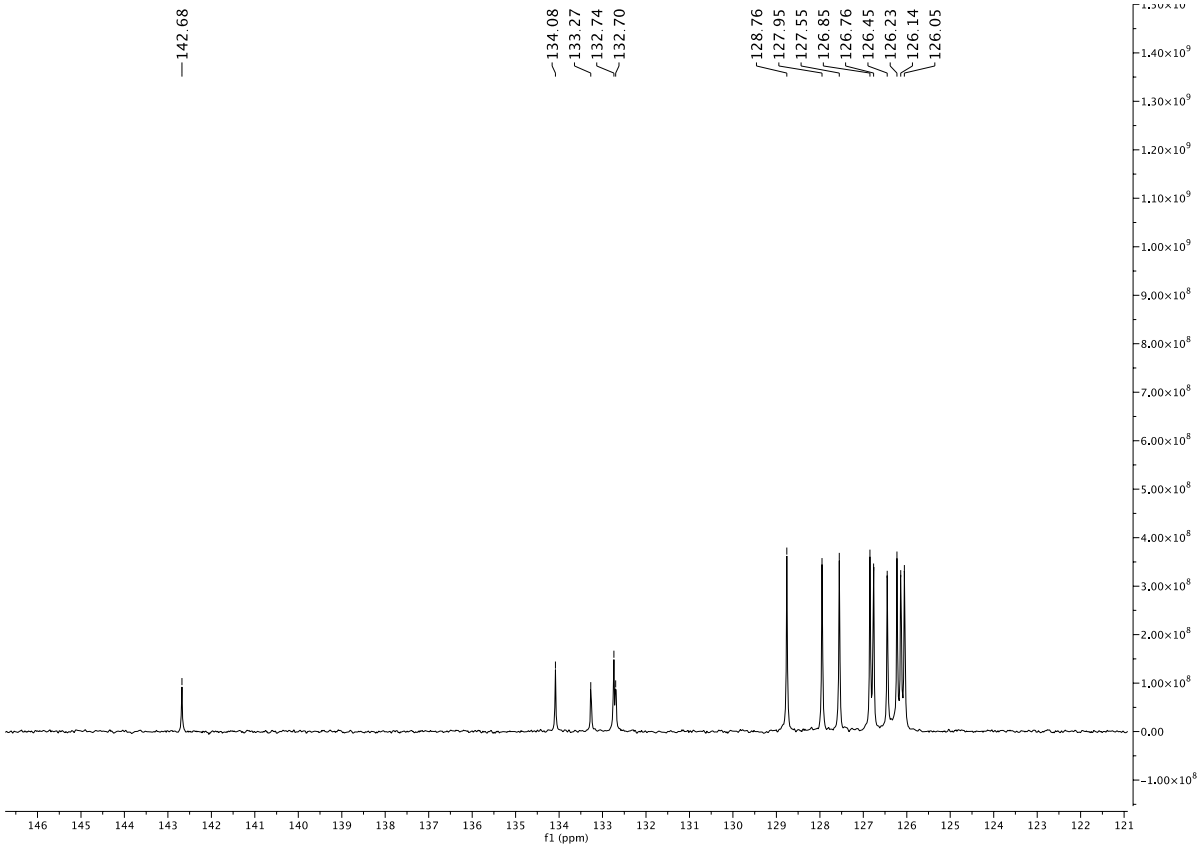
8. Appendix

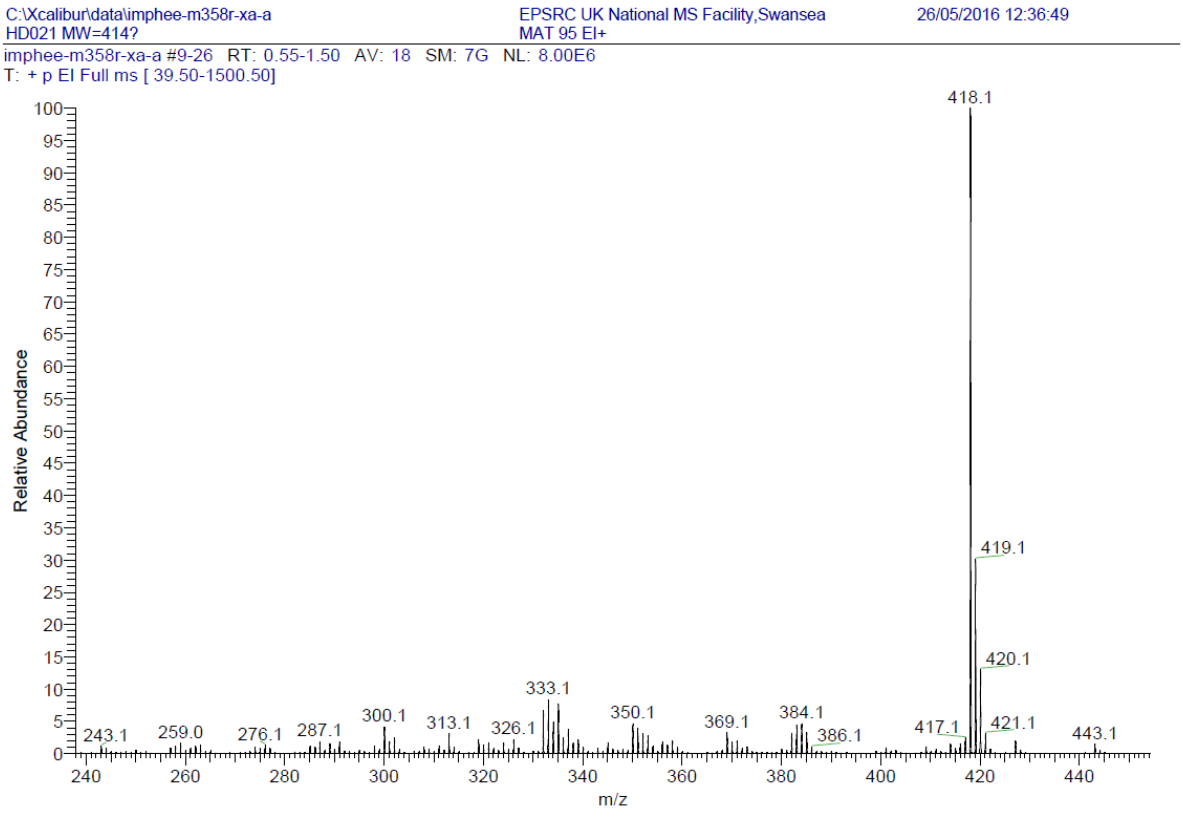
8.1 Chapter 2

2,2'-Di(thiophen-2-yl)-1,1'-binaphthalene

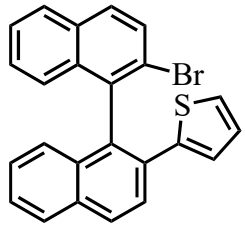


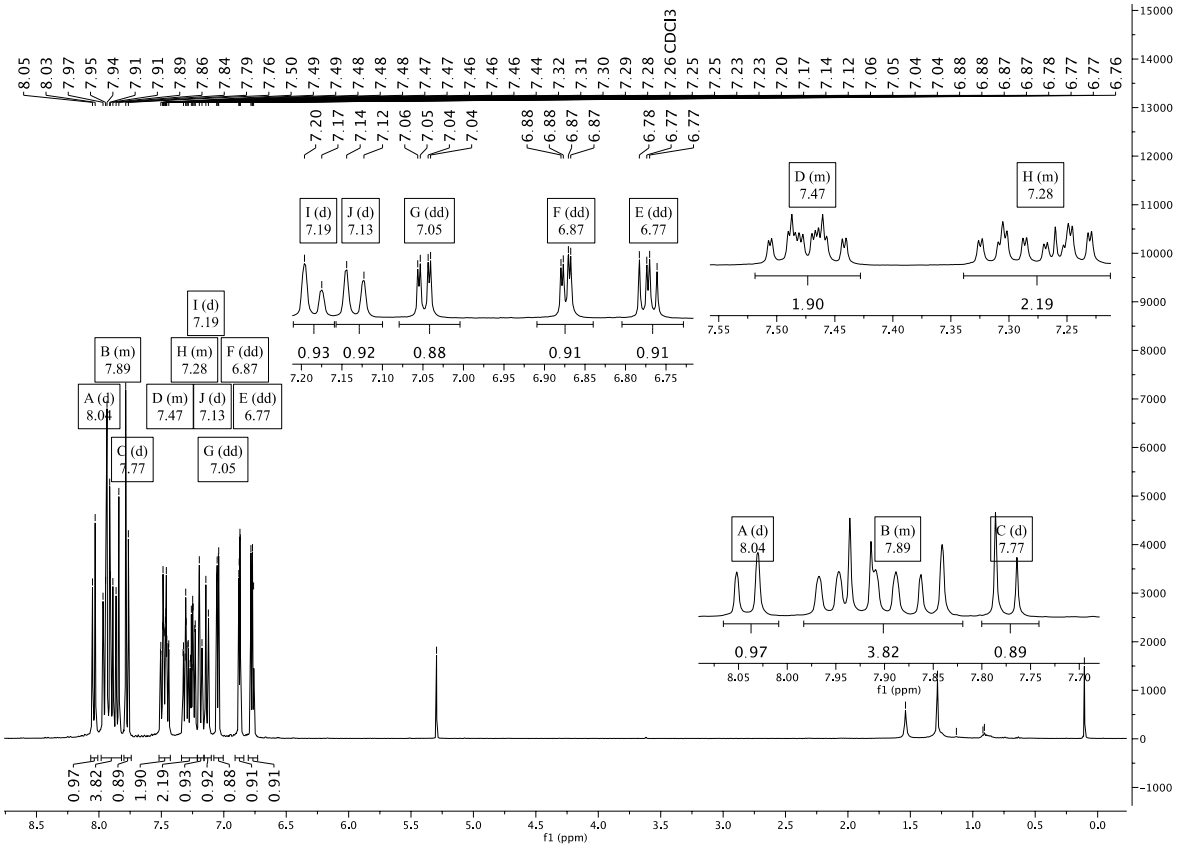


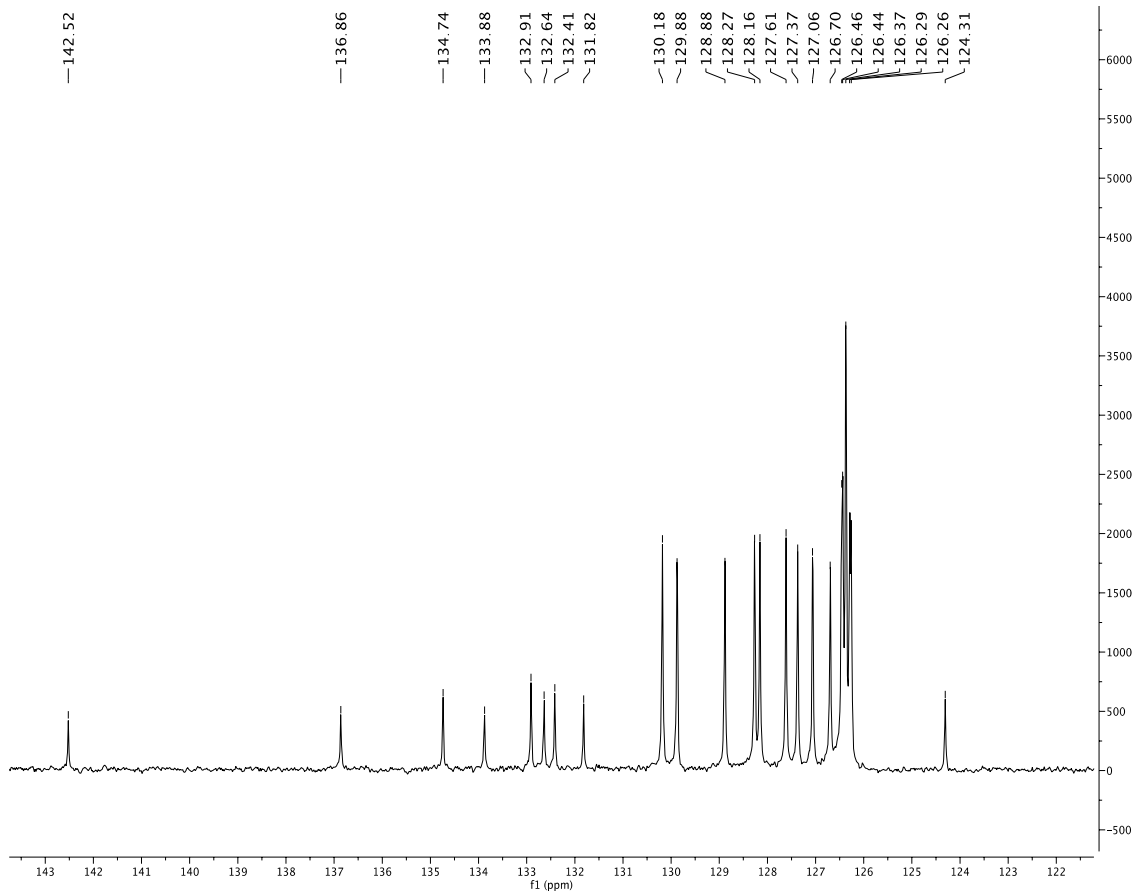

142.68
134.08
133.27
132.74
132.70
128.76
127.95
127.55
126.85
126.76
126.45
126.23
126.14
126.05
f1 (ppm)

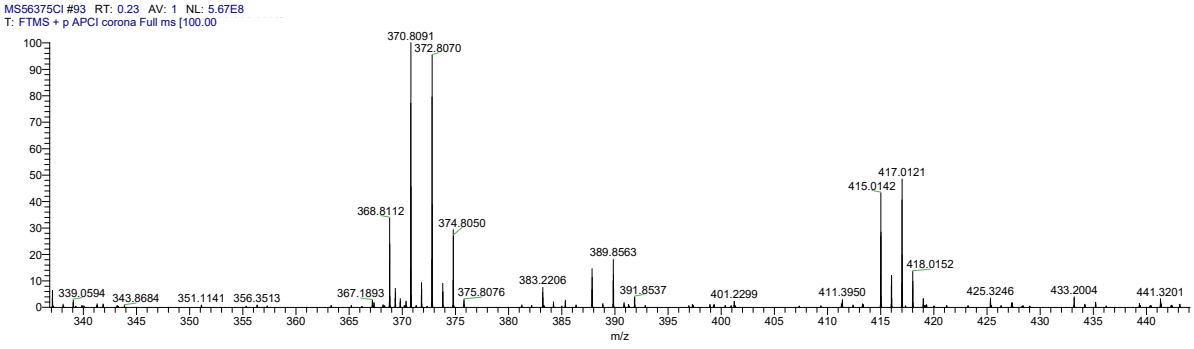

C:\Xcalibur\data\imphee-m358r-xa-a
HD021 MW=414?
EPSRC UK National MS Facility,Swansea
MAT 95 EI+
26/05/2016 12:36:49
imphee-m358r-xa-a #9-26 RT: 0.55-1.50 AV: 18 SM: 7G NL: 8.00E6
T: + p EI Full ms [39.50-1500.50]
Relative Abundance
m/z
418.1
419.1
420.1
421.1
333.1
350.1
384.1
369.1
300.1
313.1
326.1
243.1
259.0
276.1
287.1
386.1
417.1
443.1

2-(2'-Bromo-[1,1'-binaphthalen]-2-yl)thiophene

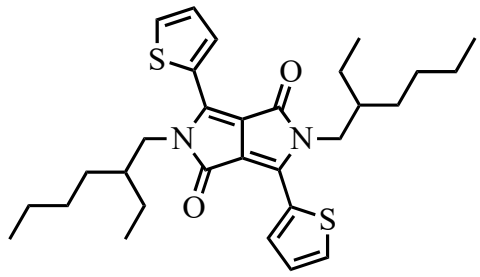


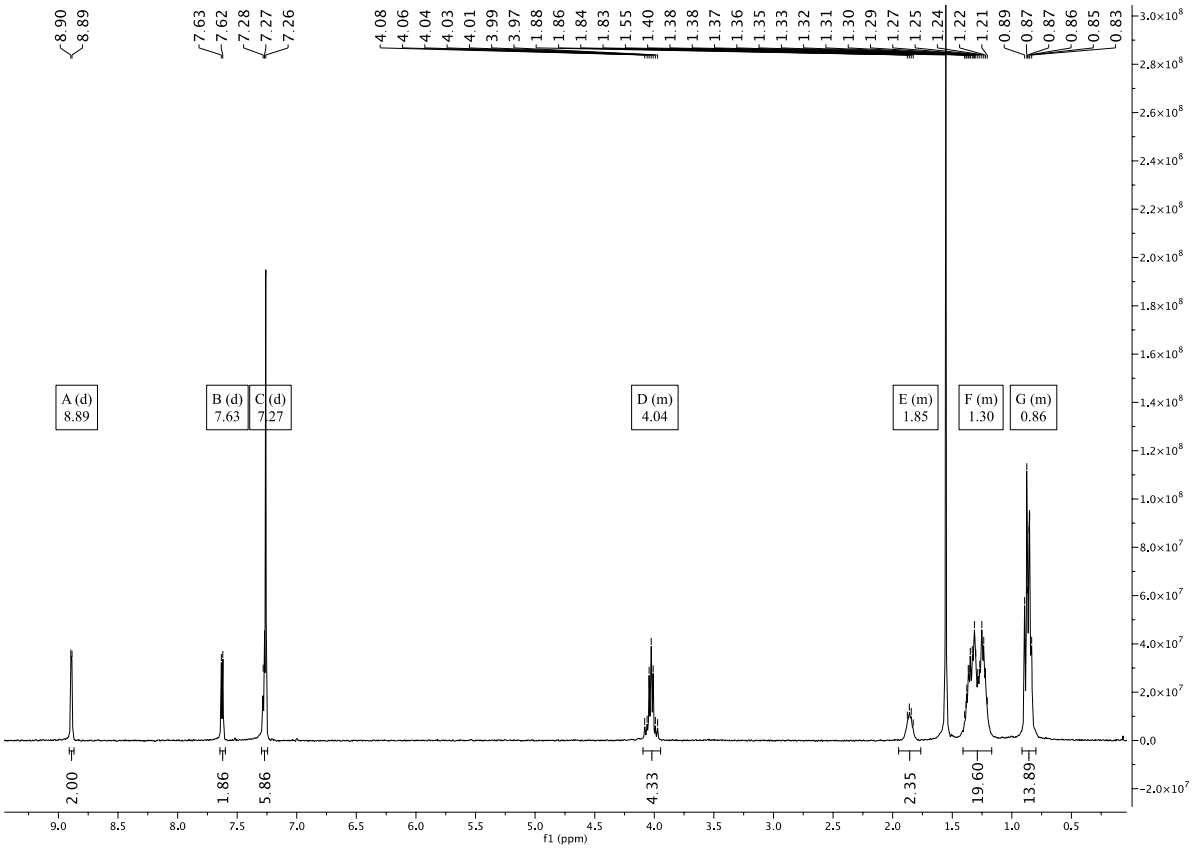


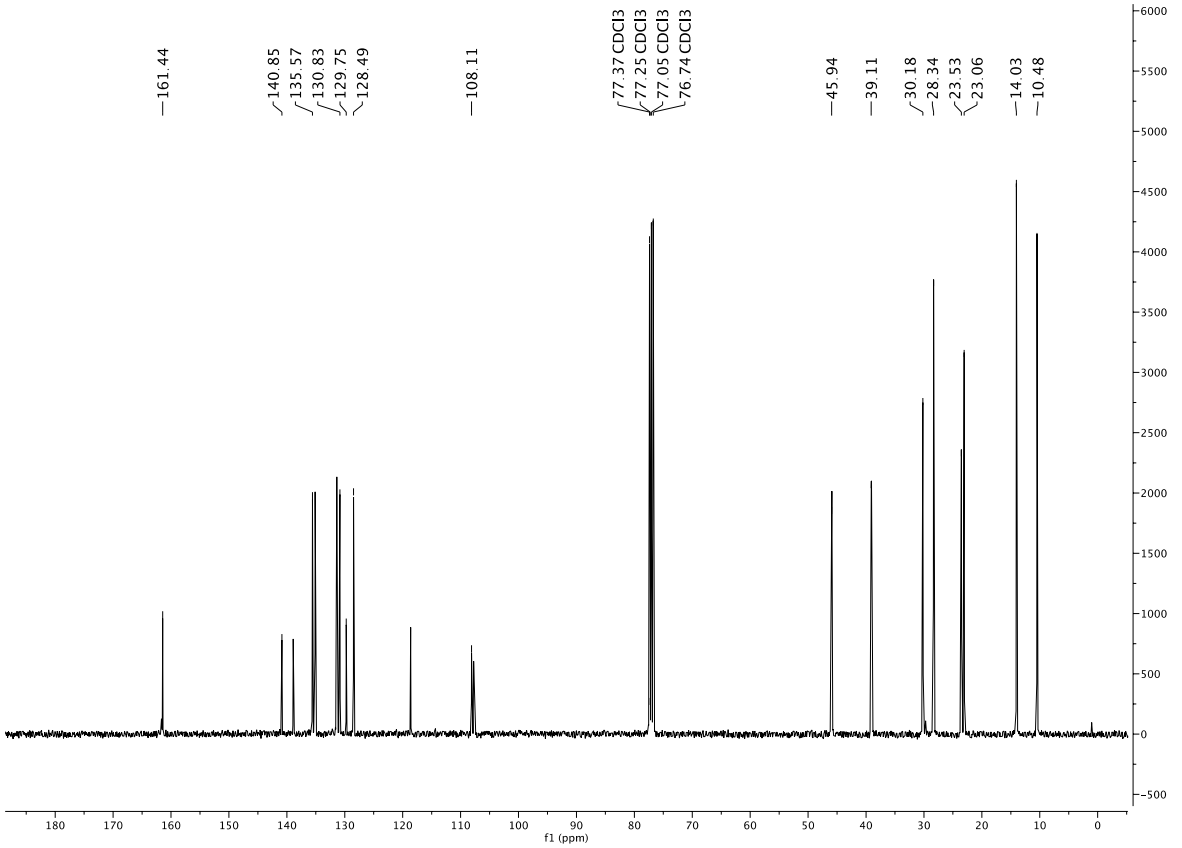

142.52
136.86
134.74
133.88
132.91
132.64
132.41
131.82
130.18
129.88
128.88
128.27
128.16
127.61
127.37
127.06
126.70
126.46
126.44
126.37
126.29
126.26
124.31
f1 (ppm)

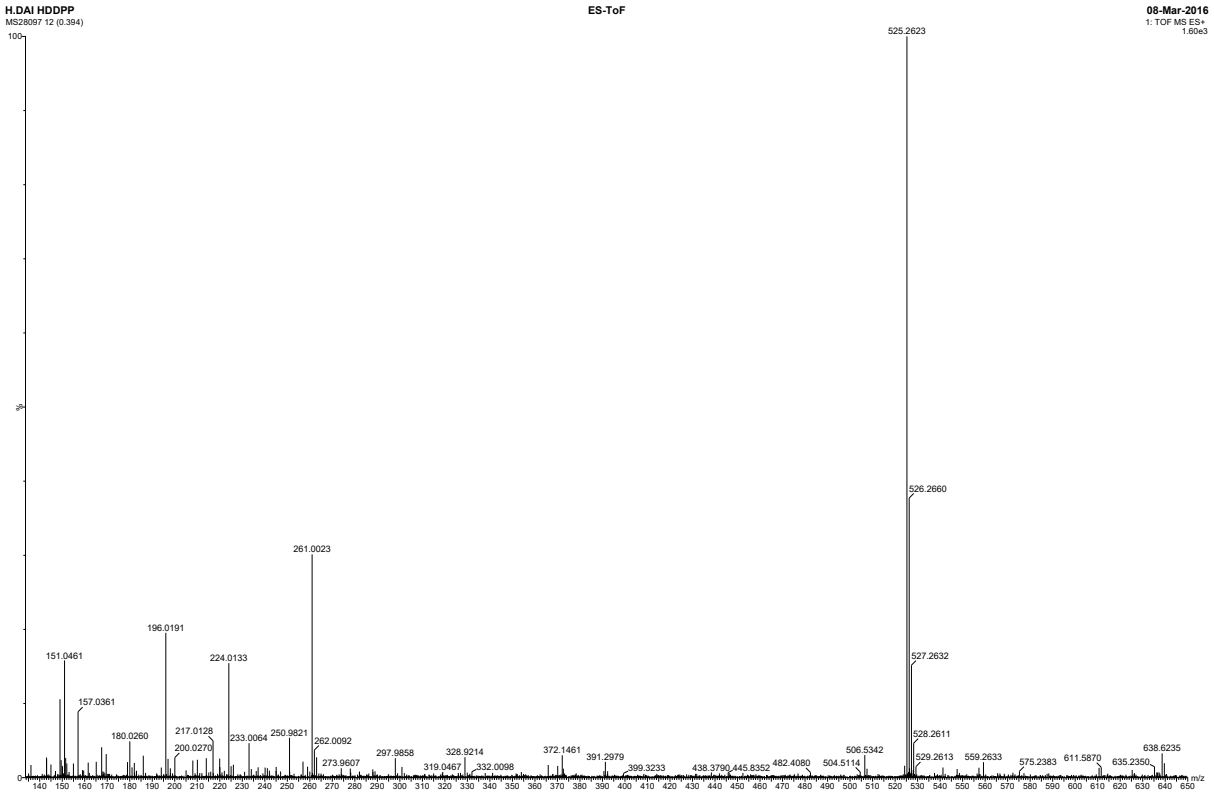

MS56375Cl #93 RT: 0.23 AV: 1 NL: 5.67E8
T: FTMS + p APCI corona Full ms [100.00
370.8091
372.8070
417.0121
415.0142
368.8112
374.8050
389.8563
418.0152
339.0594
343.8684
351.1141
356.3513
367.1893
375.8076
383.2206
391.8537
401.2299
411.3950
425.3246
433.2004
441.3201
m/z

2,5-Bis(2-ethylhexyl)-3,6-di(thiophen-2-yl)-2,5-dihydropyrrolo[3,4-*c*]pyrrole-1,4-dione

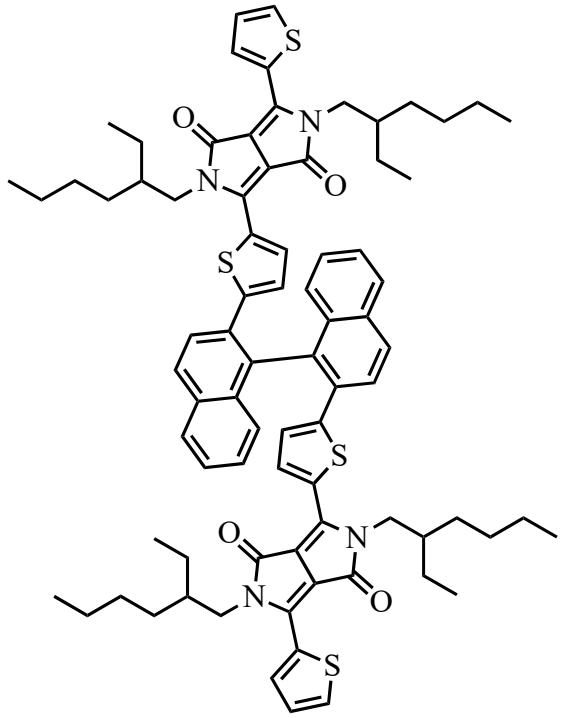


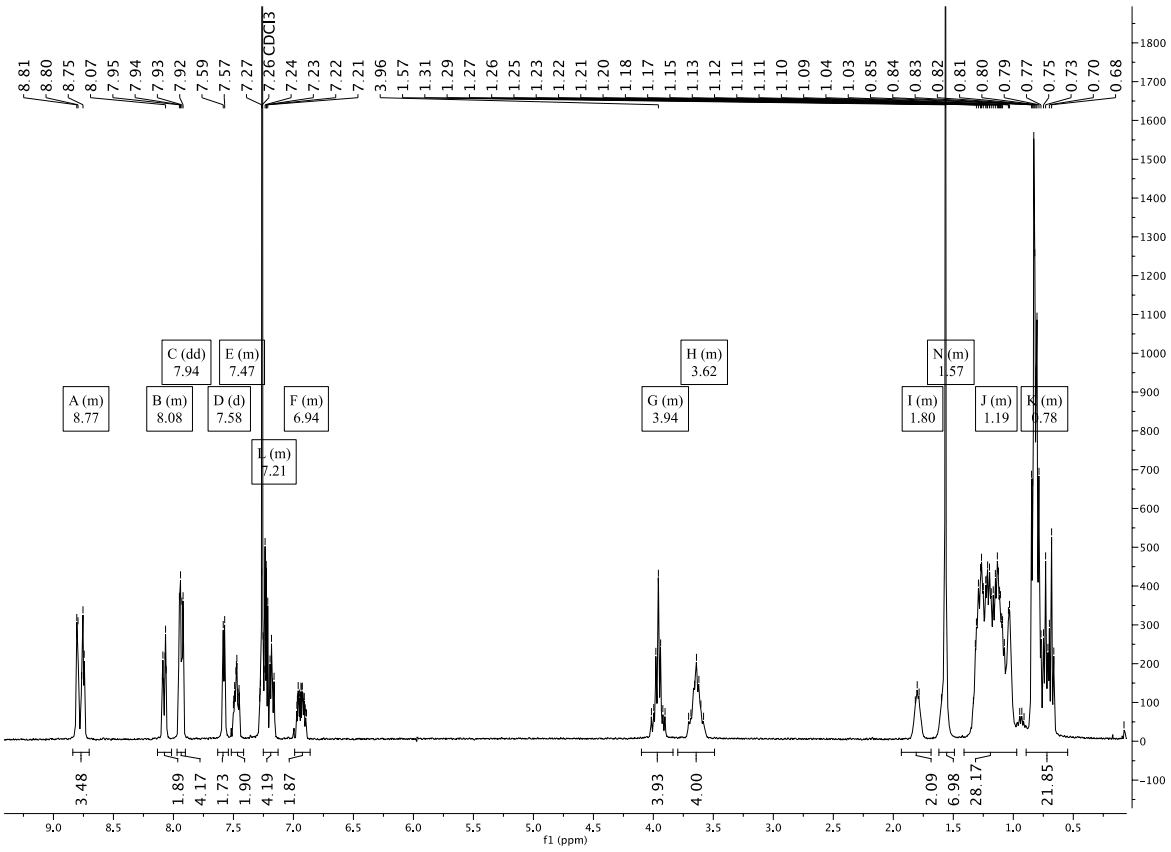


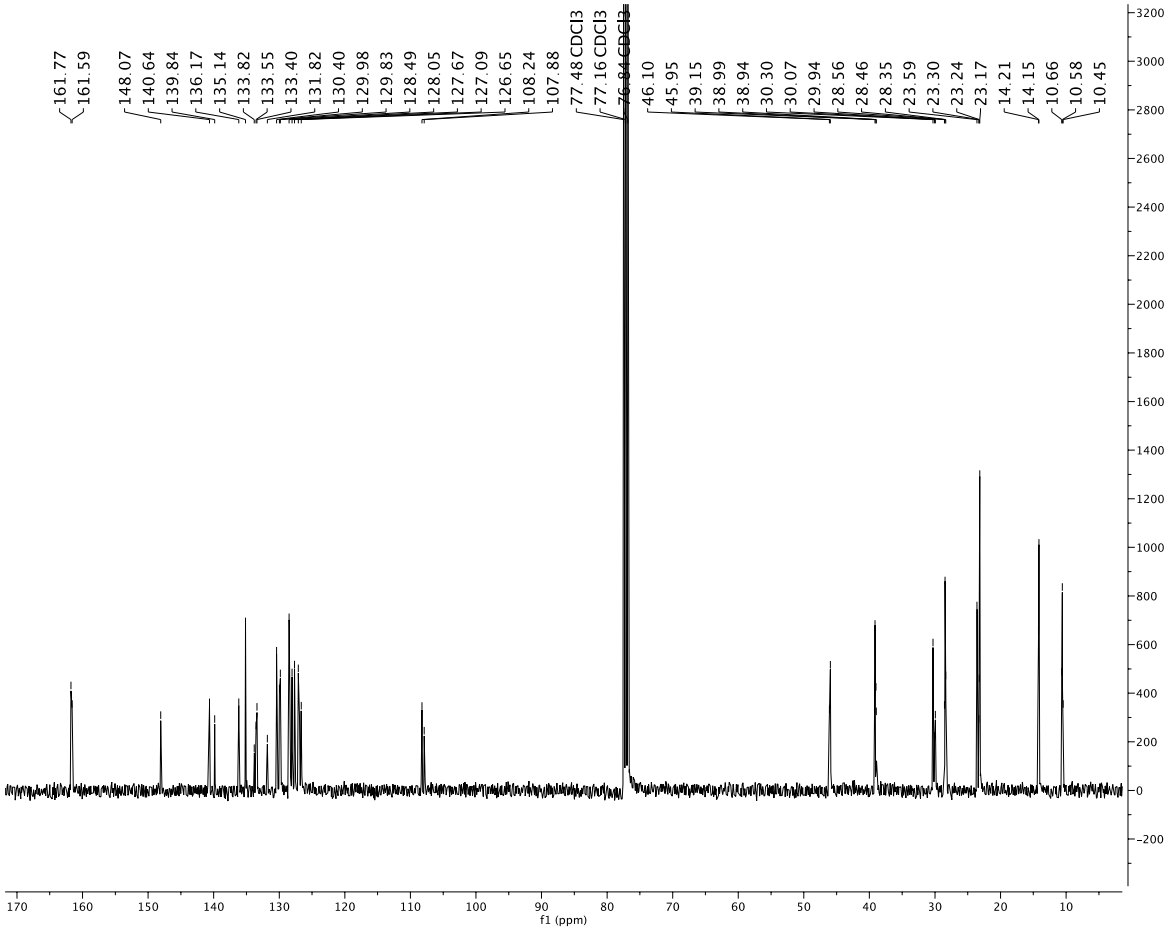

161.44
140.85
135.57
130.83
129.75
128.49
108.11
77.37 CDCl3
77.25 CDCl3
77.05 CDCl3
76.74 CDCl3
45.94
39.11
30.18
28.34
23.53
23.06
14.03
10.48
f1 (ppm)

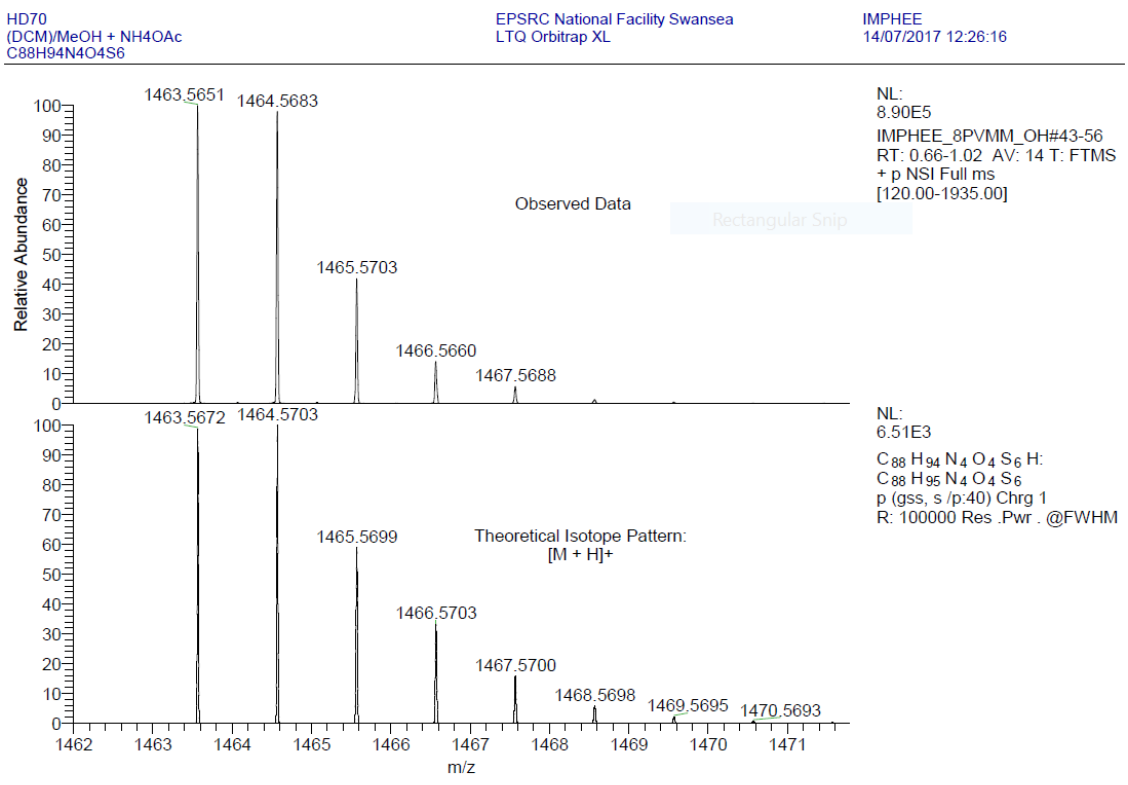

H.DAI HDDPP
MS28097 12 (0.394)
ES-ToF
08-Mar-2016
1: TOF MS ES+
1.60e3
%
m/z
525.2623
526.2660
527.2632
528.2611
261.0023
196.0191
151.0461
224.0133
157.0361
180.0260
217.0128
200.0270
233.0064
250.9821
262.0092
273.9607
297.9858
328.9214
319.0467
332.0098
372.1461
391.2979
399.3233
438.3790
445.8352
482.4080
504.5114
506.5342
529.2613
559.2633
575.2383
611.5870
635.2350
638.6235

6,6'-([1,1'-Binaphthalene]-2,2'-diylbis(thiophene-5,2-diyl))bis(2,5-bis(2-ethylhexyl)-3-(thiophen-2-yl)-2,5-dihydropyrrolo[3,4-*c*]pyrrole-1,4-dione)

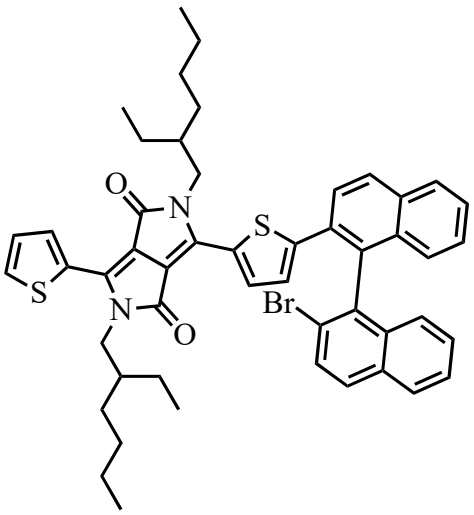


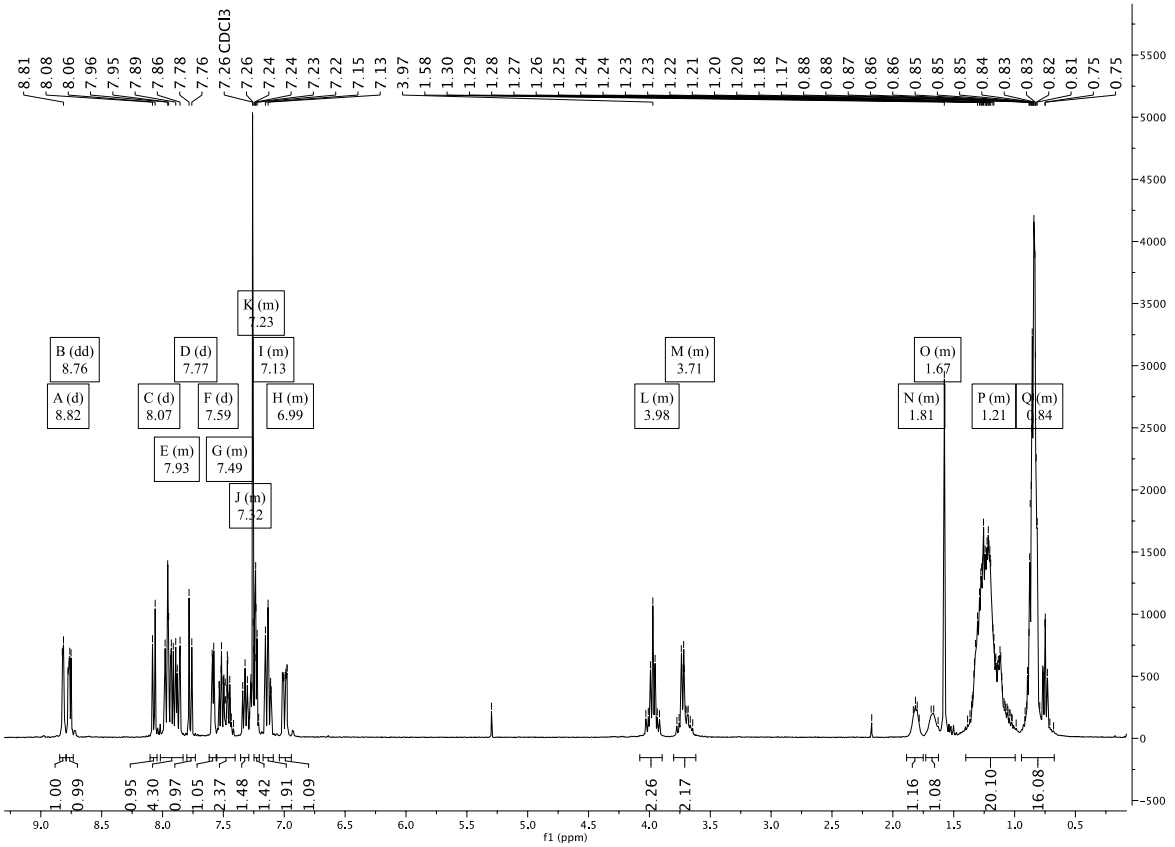


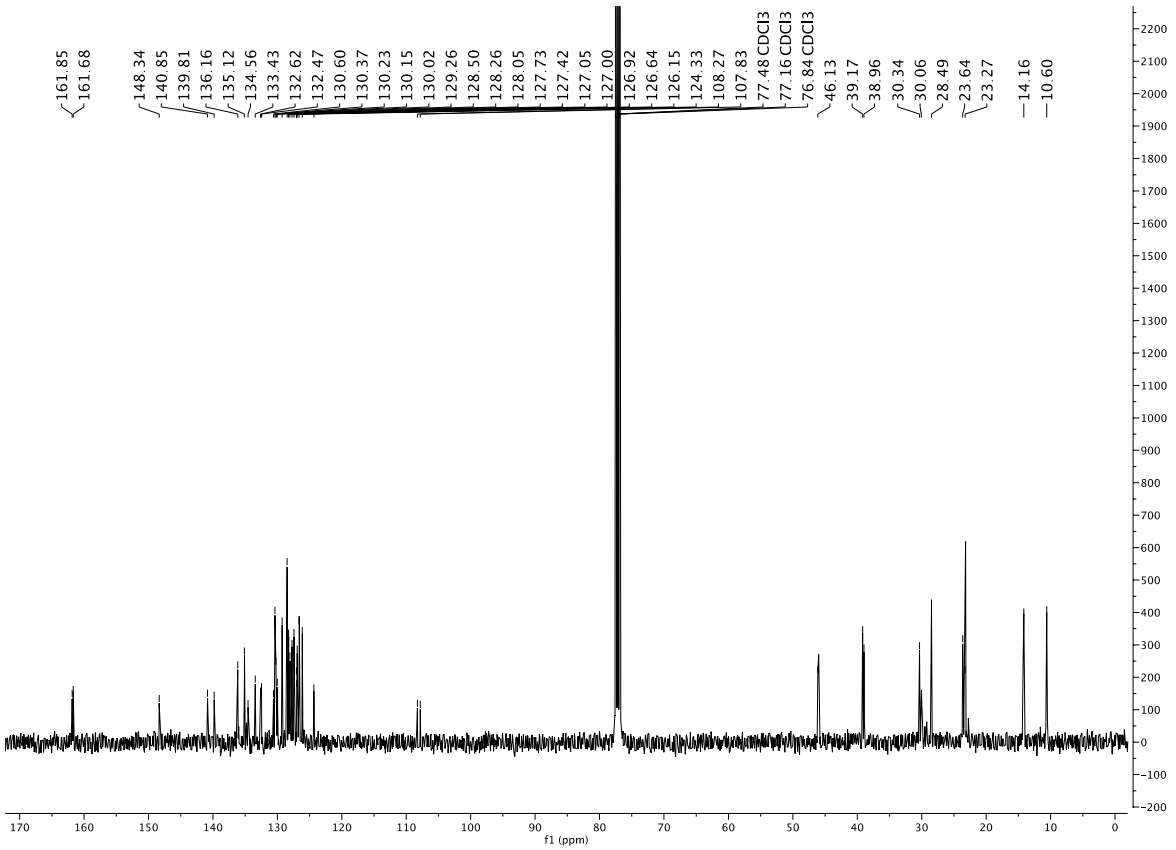

161.77
161.59
148.07
140.64
139.84
136.17
135.14
133.82
133.55
133.40
131.82
130.40
129.98
129.83
128.49
128.05
127.67
127.09
126.65
108.24
107.88
77.48 CDCl3
77.16 CDCl3
76.84 CDCl3
46.10
45.95
39.15
38.99
38.94
30.30
30.07
29.94
28.56
28.46
28.35
23.59
23.30
23.24
23.17
14.21
14.15
10.66
10.58
10.45
f1 (ppm)

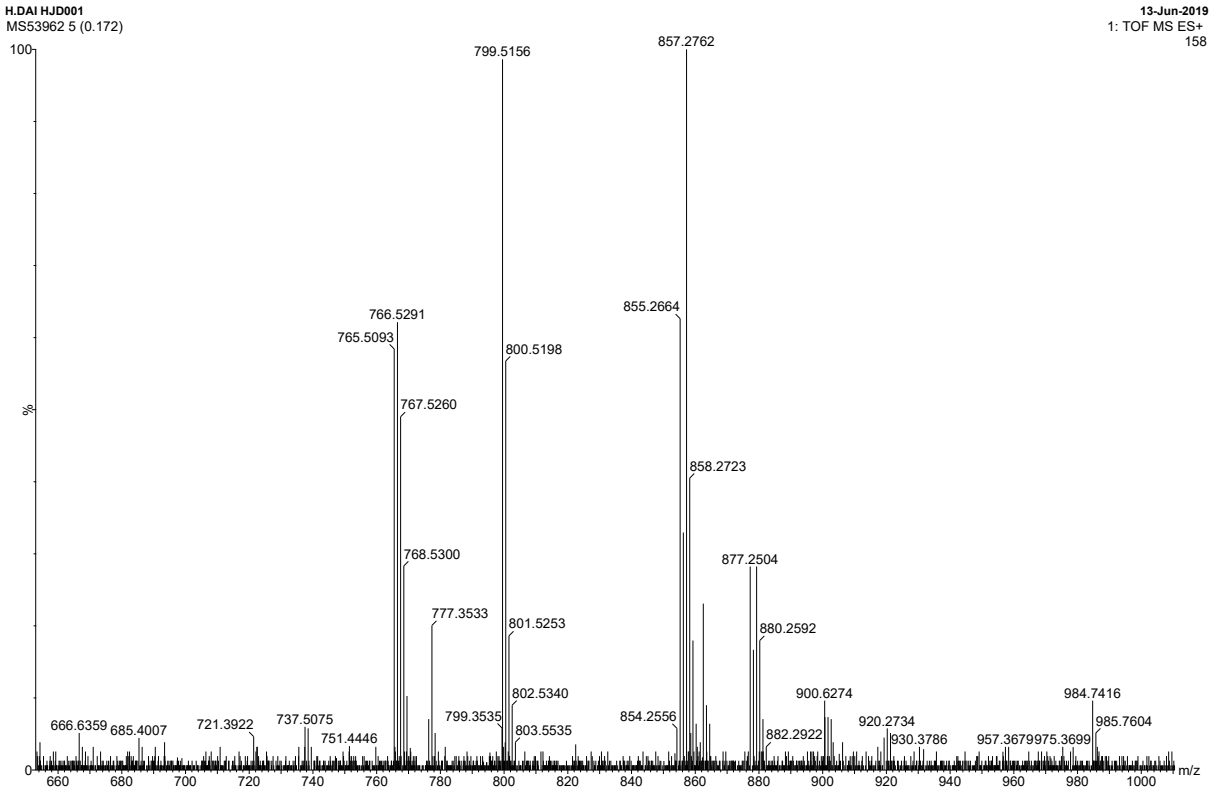

HD70
(DCM)/MeOH + NH4OAc
C88H94N4O4S6
EPSRC National Facility Swansea
LTQ Orbitrap XL
IMPHEE
14/07/2017 12:26:16
NL:
8.90E5
IMPHEE_8PVMM_OH#43-56
RT: 0.66-1.02 AV: 14 T: FTMS
+ p NSI Full ms
[120.00-1935.00]
Observed Data
1463.5651
1464.5683
1465.5703
1466.5660
1467.5688
Relative Abundance
NL:
6.51E3
C88 H94 N4 O4 S6 H:
C88 H95 N4 O4 S6
p (gss, s /p:40) Chrg 1
R: 100000 Res .Pwr . @FWHM
Theoretical Isotope Pattern:
[M + H]+
1463.5672
1464.5703
1465.5699
1466.5703
1467.5700
1468.5698
1469.5695
1470.5693
m/z

3-(5-(2'-Bromo-[1,1'-binaphthalen]-2-yl)thiophen-2-yl)-2,5-bis(2-ethylhexyl)-6-(thiophen-2-yl)-2,5-dihydropyrrolo[3,4-*c*]pyrrole-1,4-dione

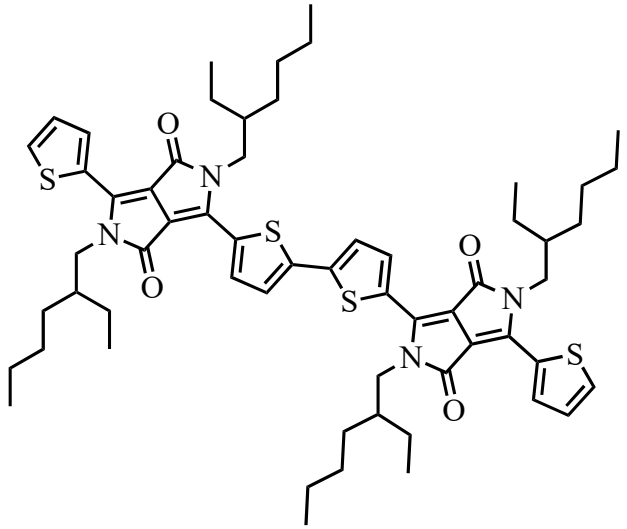


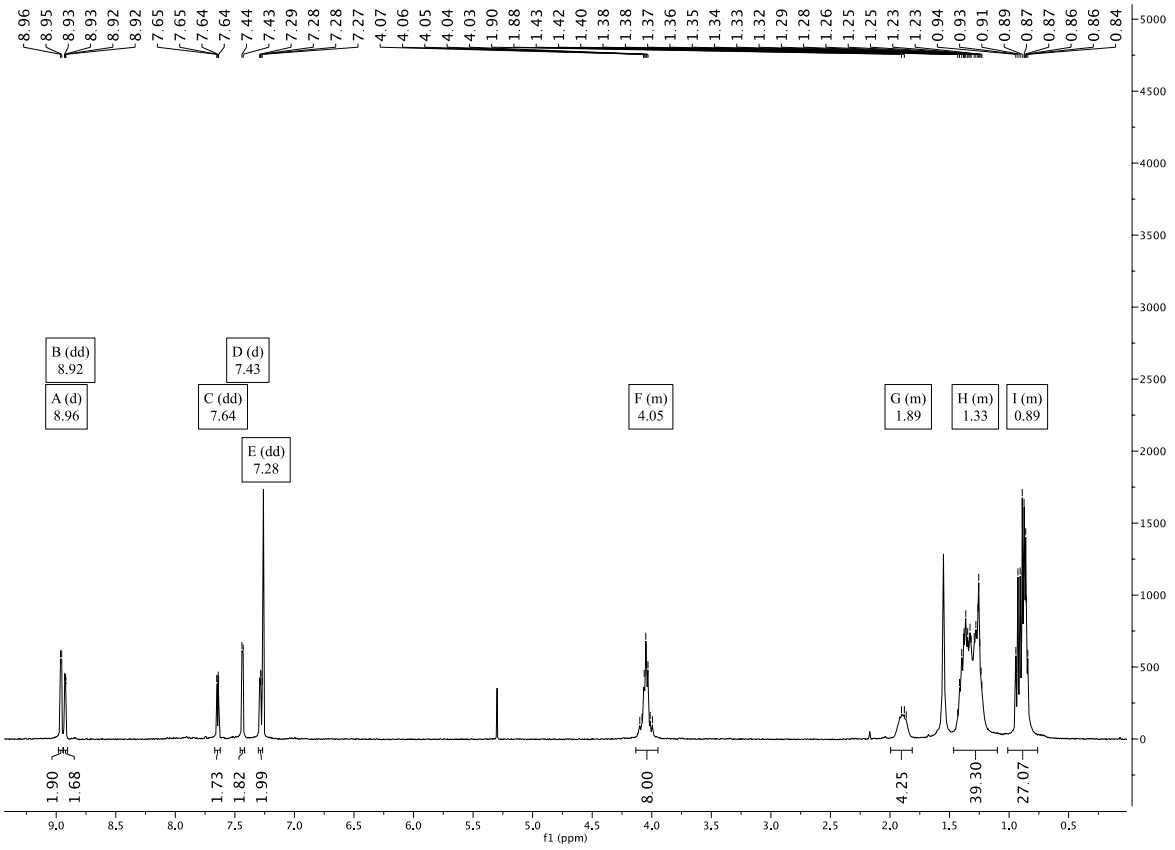



161.85
161.68
148.34
140.85
139.81
136.16
135.12
134.56
133.43
132.62
132.47
130.60
130.37
130.23
130.15
130.02
129.26
128.50
128.26
128.05
127.73
127.42
127.05
127.00
126.92
126.64
126.15
124.33
108.27
107.83
77.48 CDCl3
77.16 CDCl3
76.84 CDCl3
46.13
39.17
38.96
30.34
30.06
28.49
23.64
23.27
14.16
10.60
f1 (ppm)

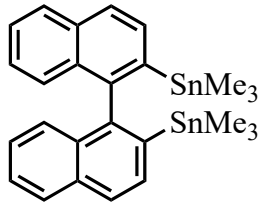

H.DAI HJD001
MS53962 5 (0.172)
13-Jun-2019
1: TOF MS ES+
158
799.5156
857.2762
766.5291
765.5093
855.2664
800.5198
767.5260
858.2723
768.5300
877.2504
777.3533
801.5253
880.2592
802.5340
900.6274
984.7416
666.6359
685.4007
721.3922
737.5075
751.4446
799.3535
803.5535
854.2556
882.2922
920.2734
930.3786
957.3679975.3699
985.7604
%
m/z

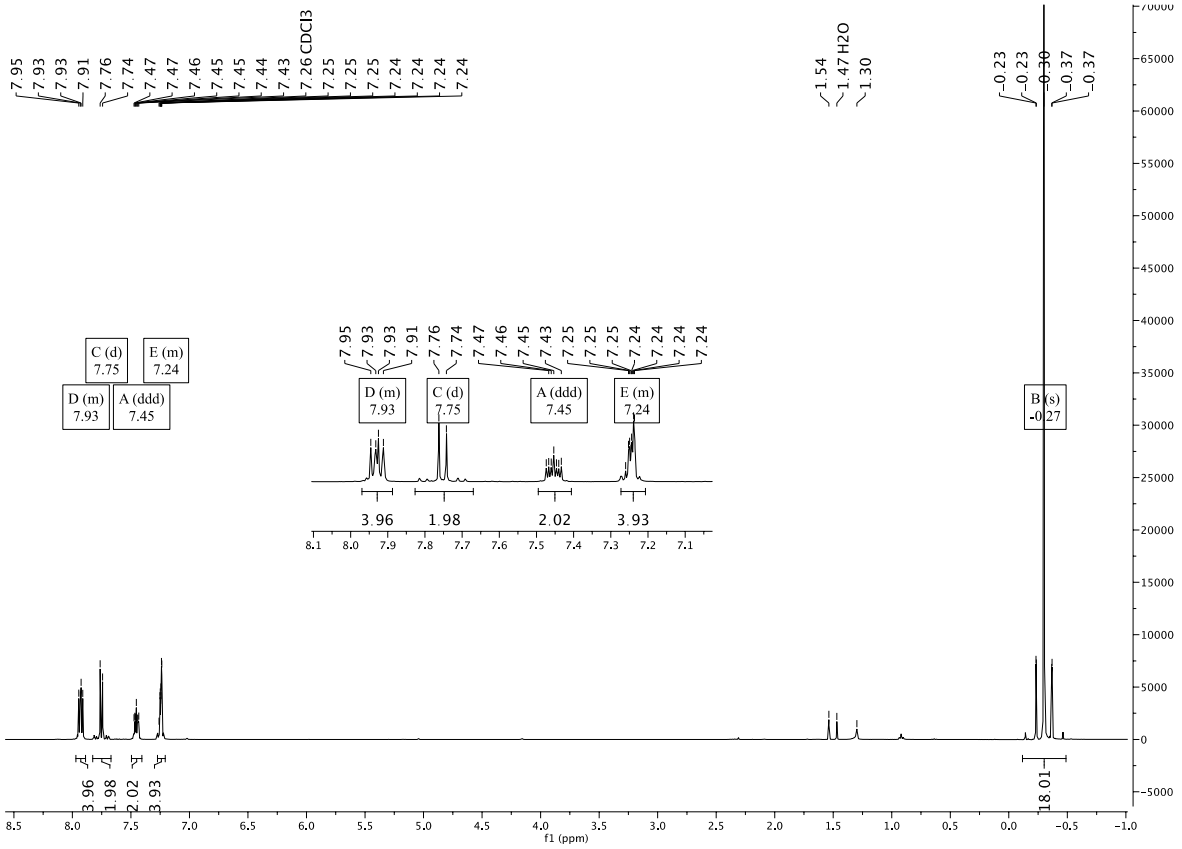
6,6'-([2,2'-Bithiophene]-5,5'-diyl)bis(2,5-bis(2-ethylhexyl)-3-(thiophen-2-yl)-2,5-dihydropyrrolo[3,4-*c*]pyrrole-1,4-dione)

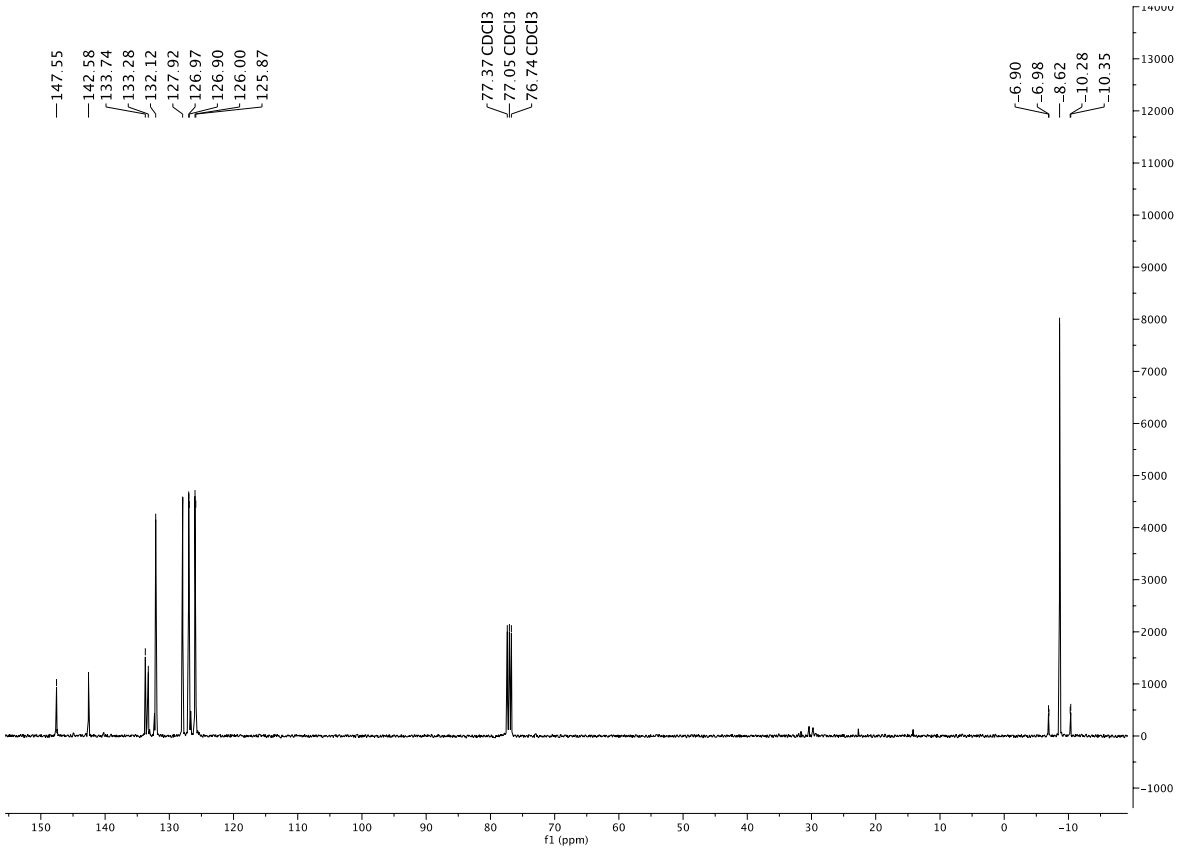




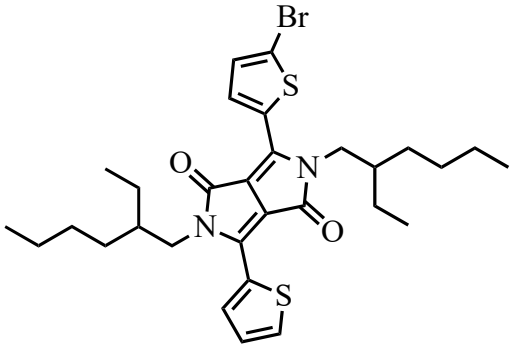
2,2'-Bis(trimethylstannyl)-1,1'-binaphthalene

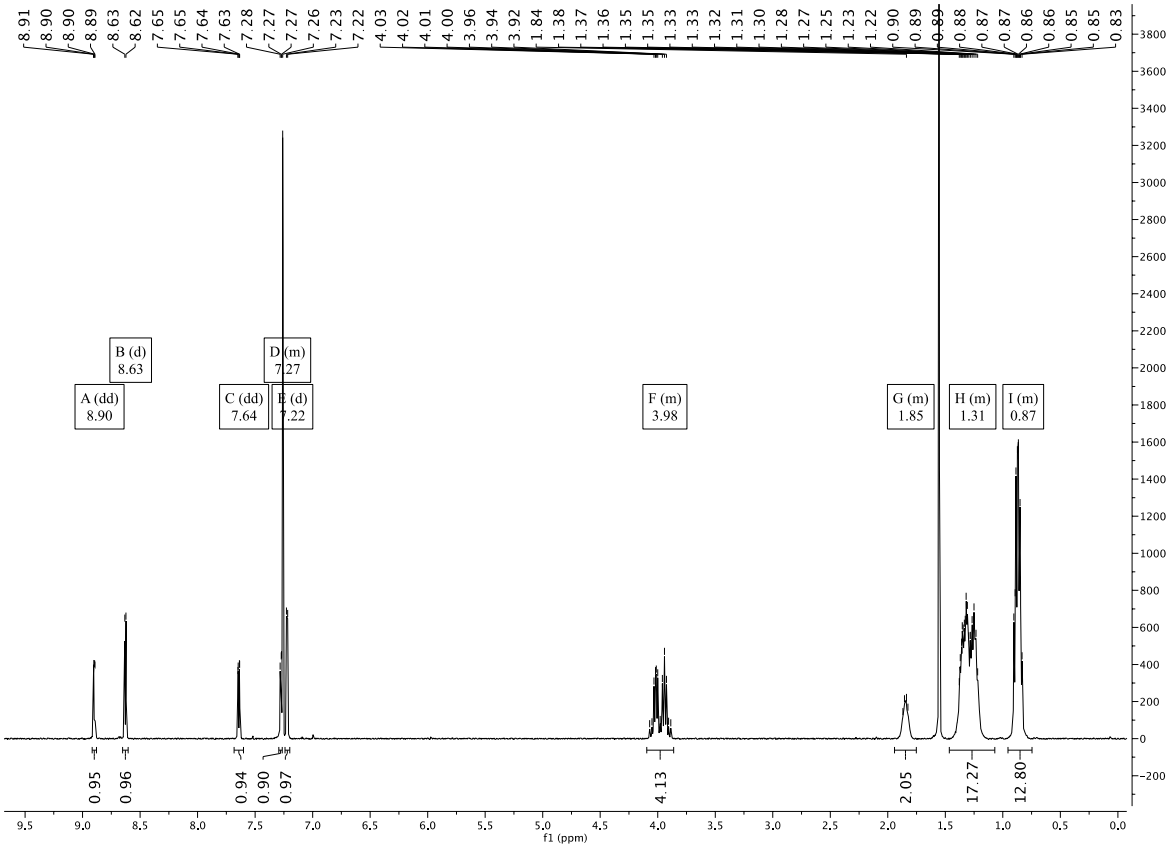


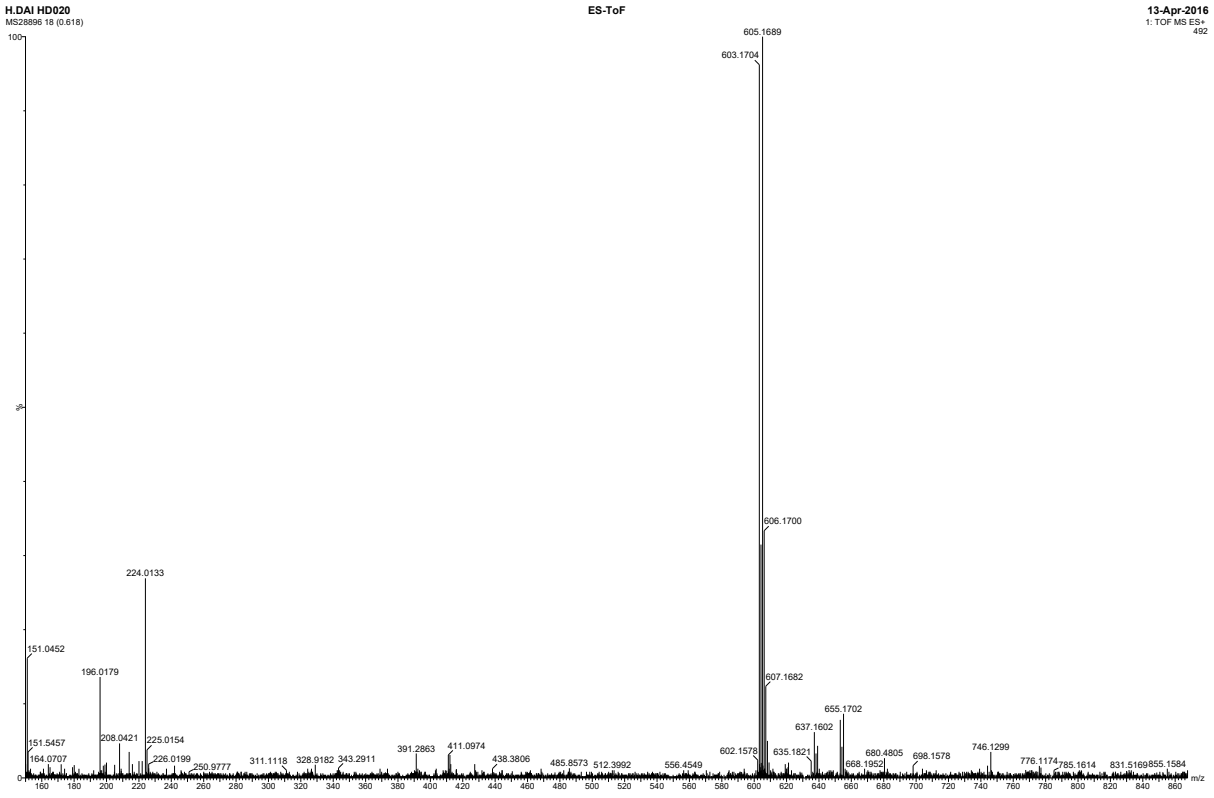



147.55
142.58
133.74
133.28
132.12
127.92
126.97
126.90
126.00
125.87
77.37 CDCl3
77.05 CDCl3
76.74 CDCl3
6.90
6.98
8.62
10.28
10.35
f1 (ppm)

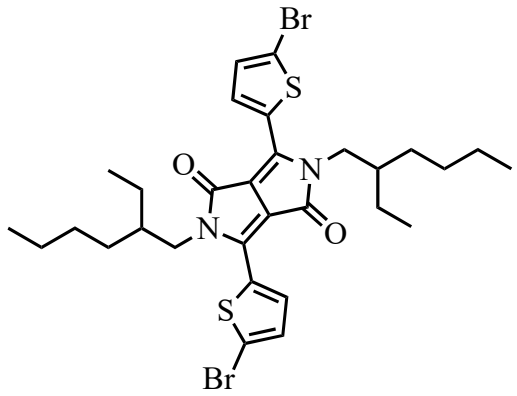
3-(5-Bromothiophen-2-yl)-2,5-bis(2-ethylhexyl)-6-(thiophen-2-yl)-2,5-dihydropyrrolo[3,4-*c*]pyrrole-1,4-dione

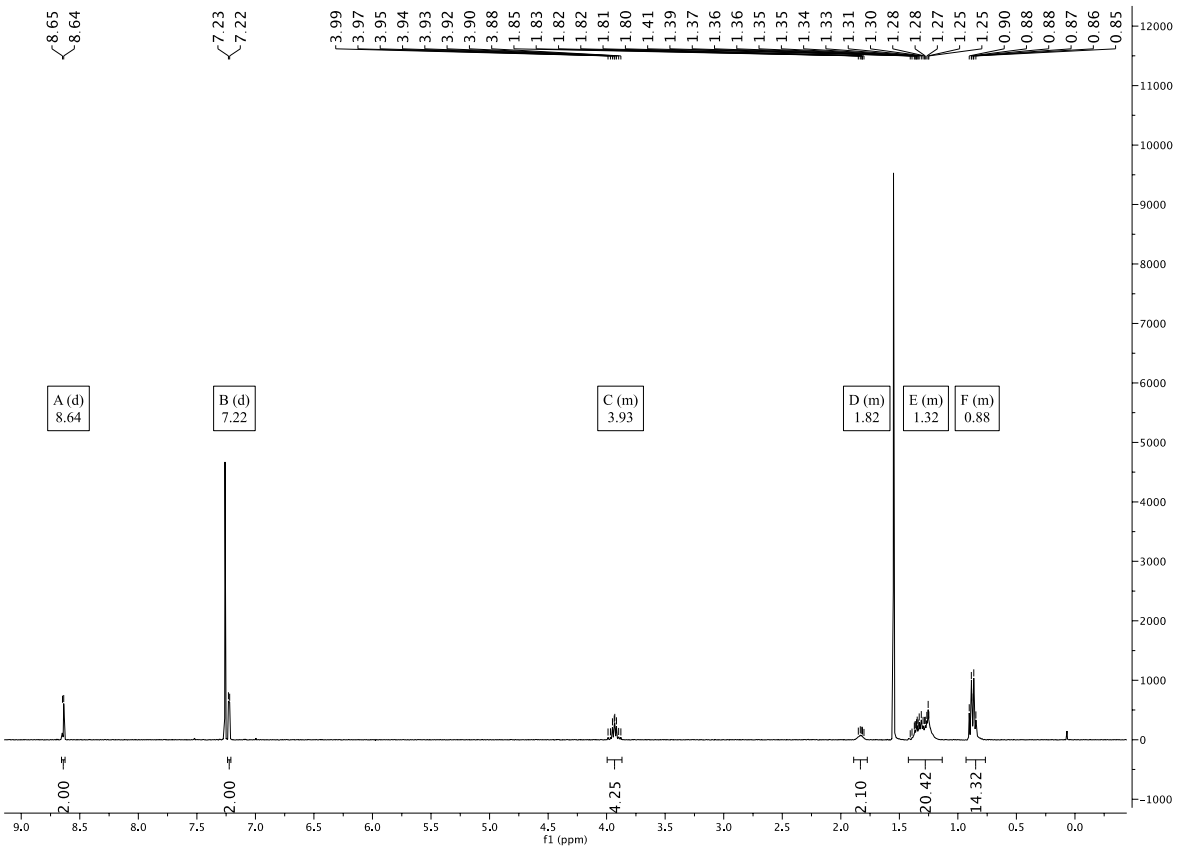


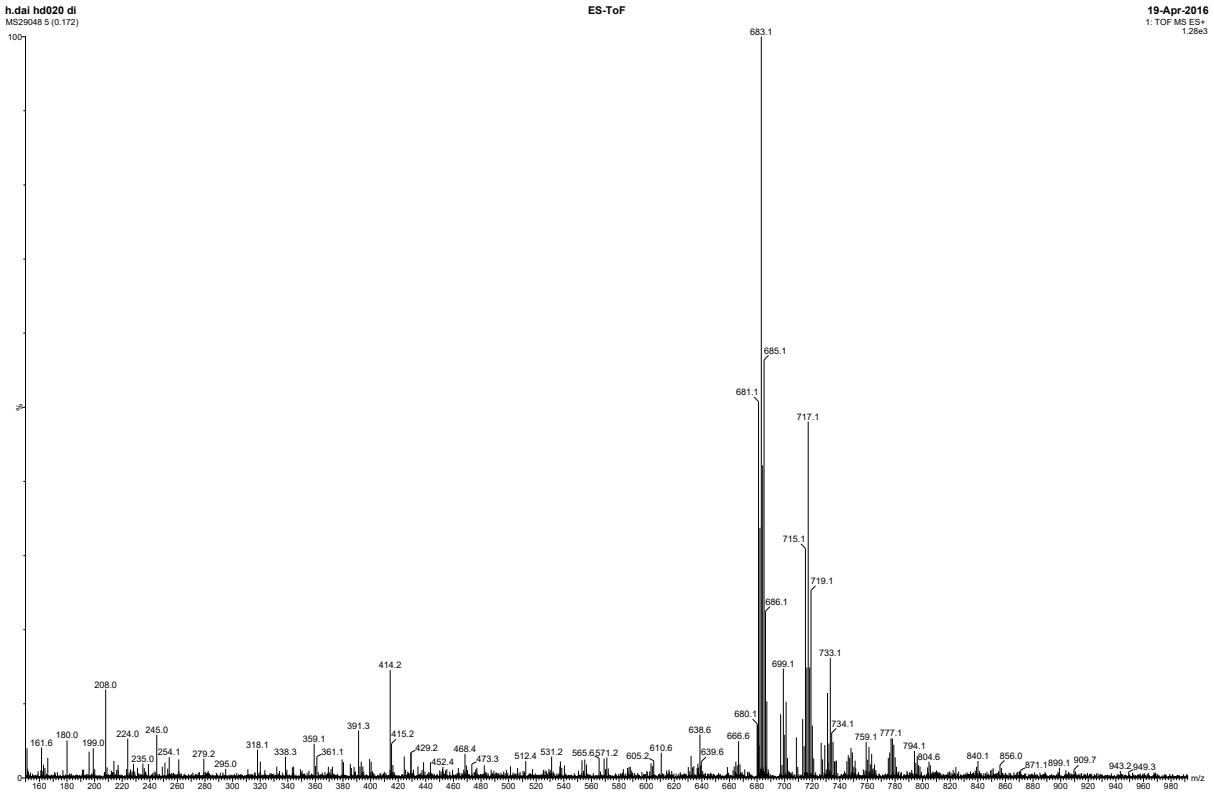



H.DAI HD020
MS28896 18 (0.618)
ES-ToF
13-Apr-2016
1: TOF MS ES+
492
100
%
0
605.1689
603.1704
606.1700
224.0133
151.0452
196.0179
607.1682
655.1702
637.1602
208.0421
225.0154
151.5457
164.0707
226.0199
250.9777
311.1118
328.9182
343.2911
391.2863
411.0974
438.3806
485.8573
512.3992
556.4549
602.1578
635.1821
680.4805
668.1950
698.1578
746.1299
776.1174
785.1614
831.5169
855.1584
160 180 200 220 240 260 280 300 320 340 360 380 400 420 440 460 480 500 520 540 560 580 600 620 640 660 680 700 720 740 760 780 800 820 840 860
m/z

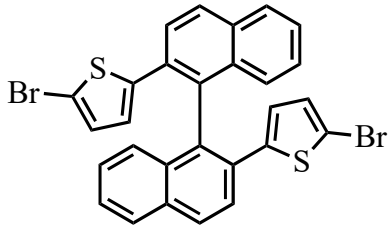
3,6-Bis(5-bromothiophen-2-yl)-2,5-bis(2-ethylhexyl)-2,5-dihydropyrrolo[3,4-*c*]pyrrole-1,4-dione

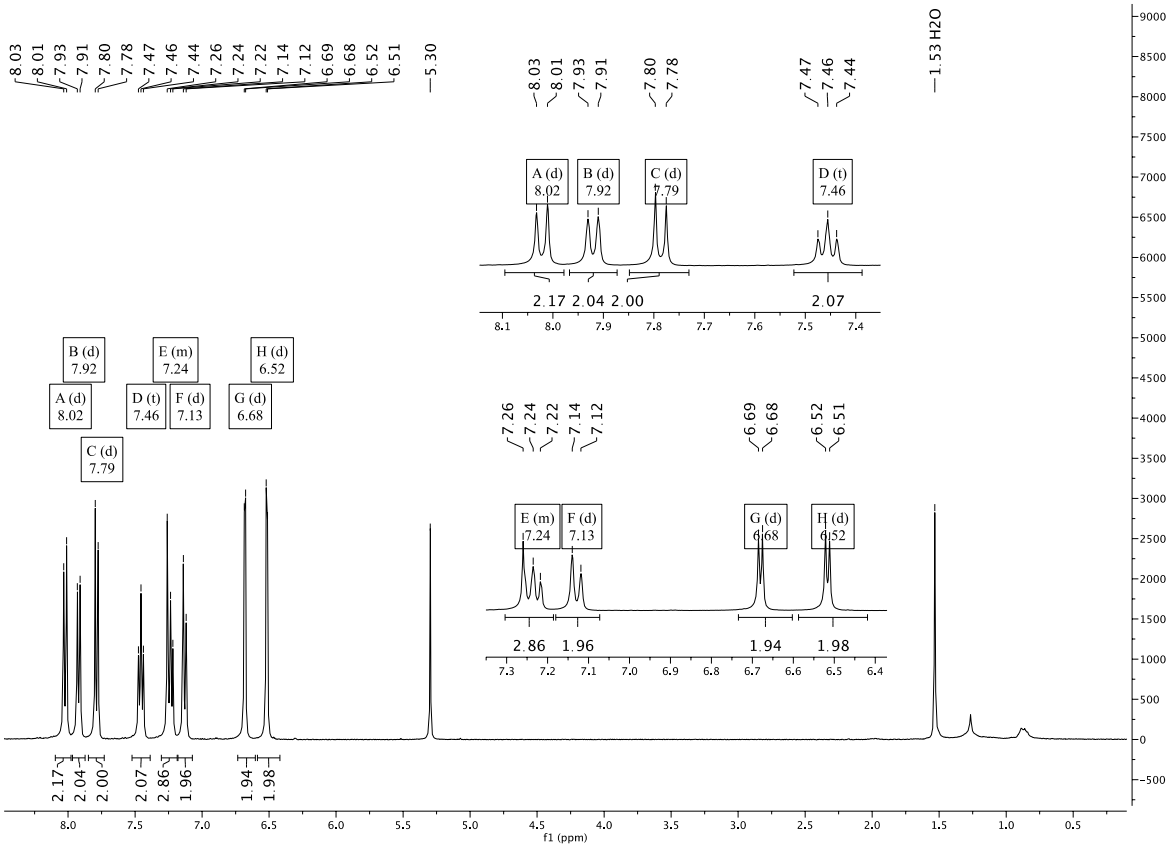


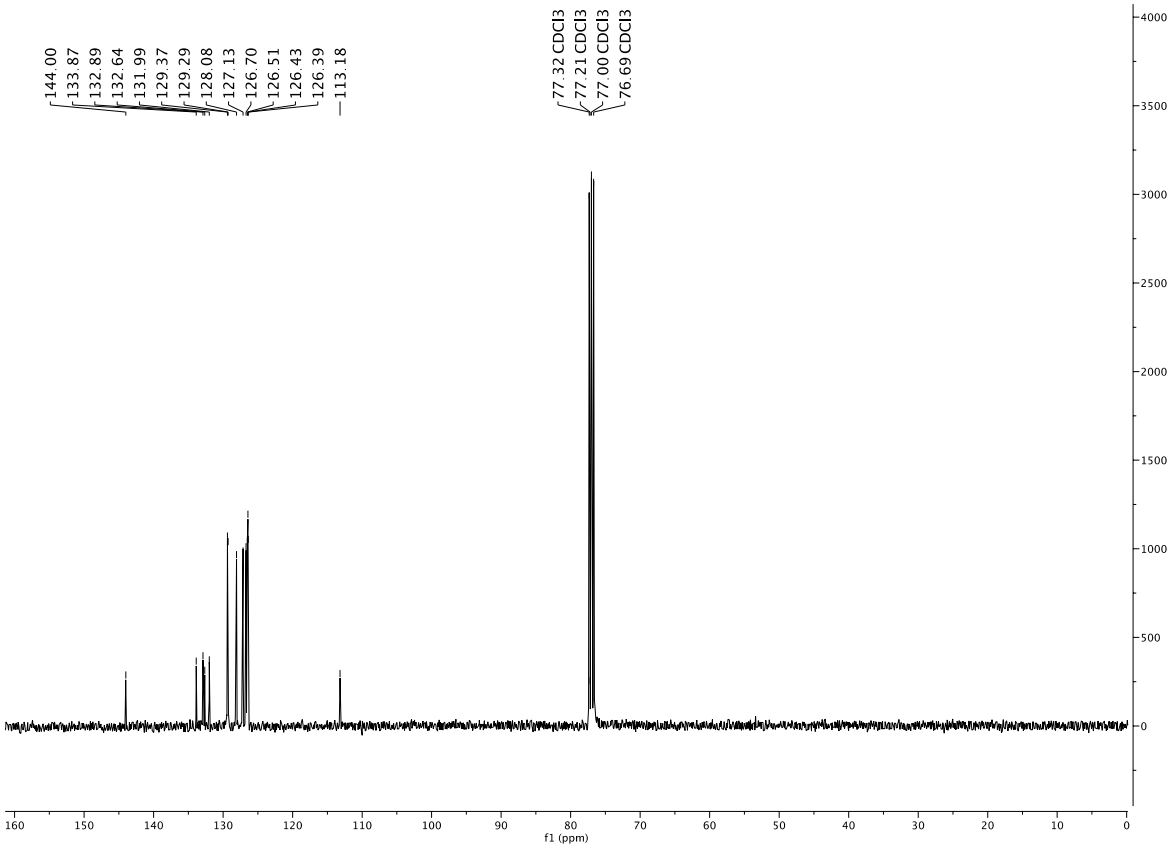


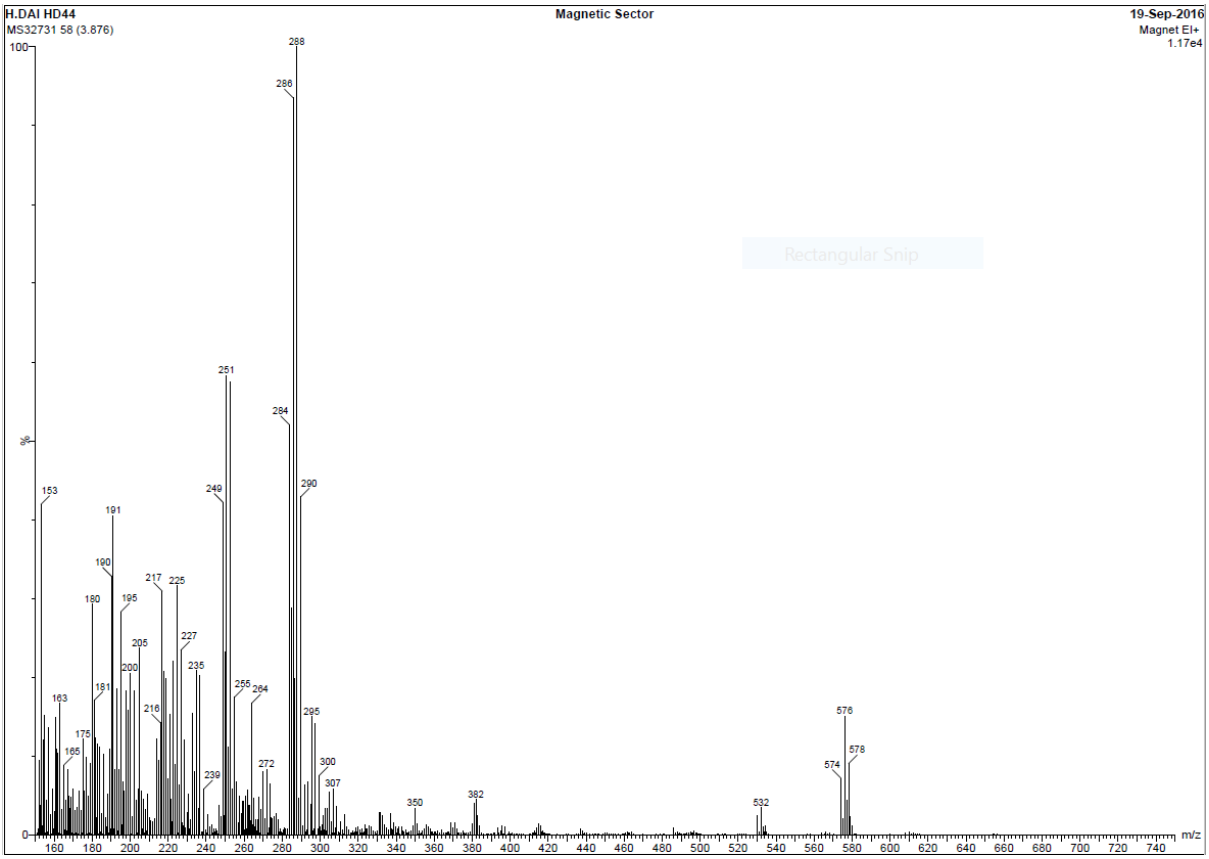

h.dai hd020 di
MS29048 5 (0.172)
ES-ToF
19-Apr-2016
1: TOF MS ES+
1.28e3
100
%
0
683.1
685.1
681.1
717.1
715.1
719.1
686.1
733.1
699.1
414.2
208.0
680.1
734.1
759.1
777.1
794.1
391.3
638.6
666.6
224.0
245.0
180.0
161.6
199.0
254.1
235.0
279.2
295.0
318.1
338.3
359.1
361.1
415.2
429.2
452.4
468.4
473.3
512.4
531.2
565.6
571.2
605.2
610.6
639.6
804.6
840.1
856.0
871.1
899.1
909.7
943.2
949.3
160 180 200 220 240 260 280 300 320 340 360 380 400 420 440 460 480 500 520 540 560 580 600 620 640 660 680 700 720 740 760 780 800 820 840 860 880 900 920 940 960 980
m/z

2,2'-Bis(5-bromothiophen-2-yl)-1,1'-binaphthalene

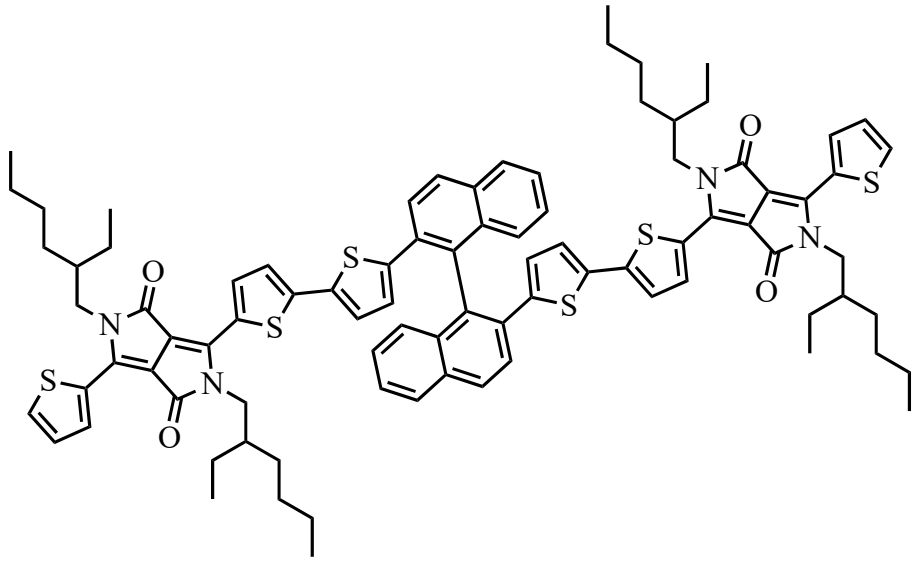


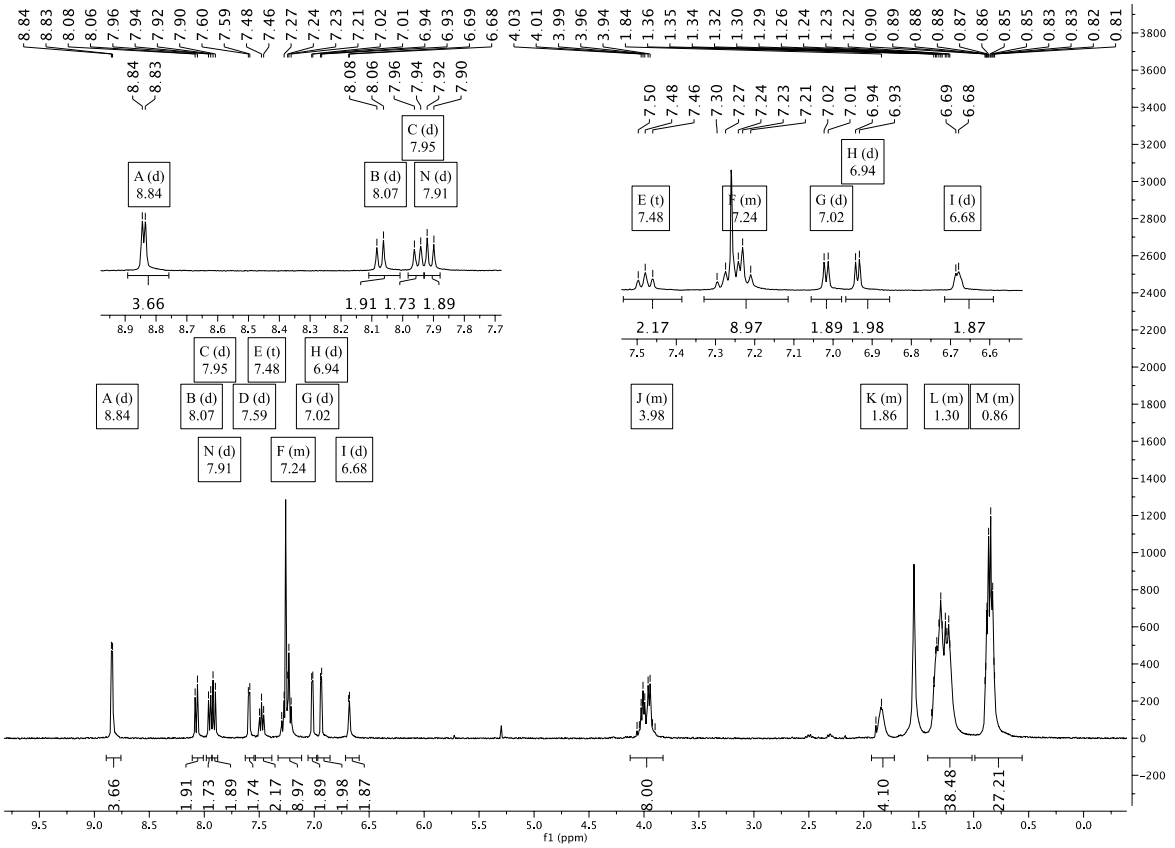


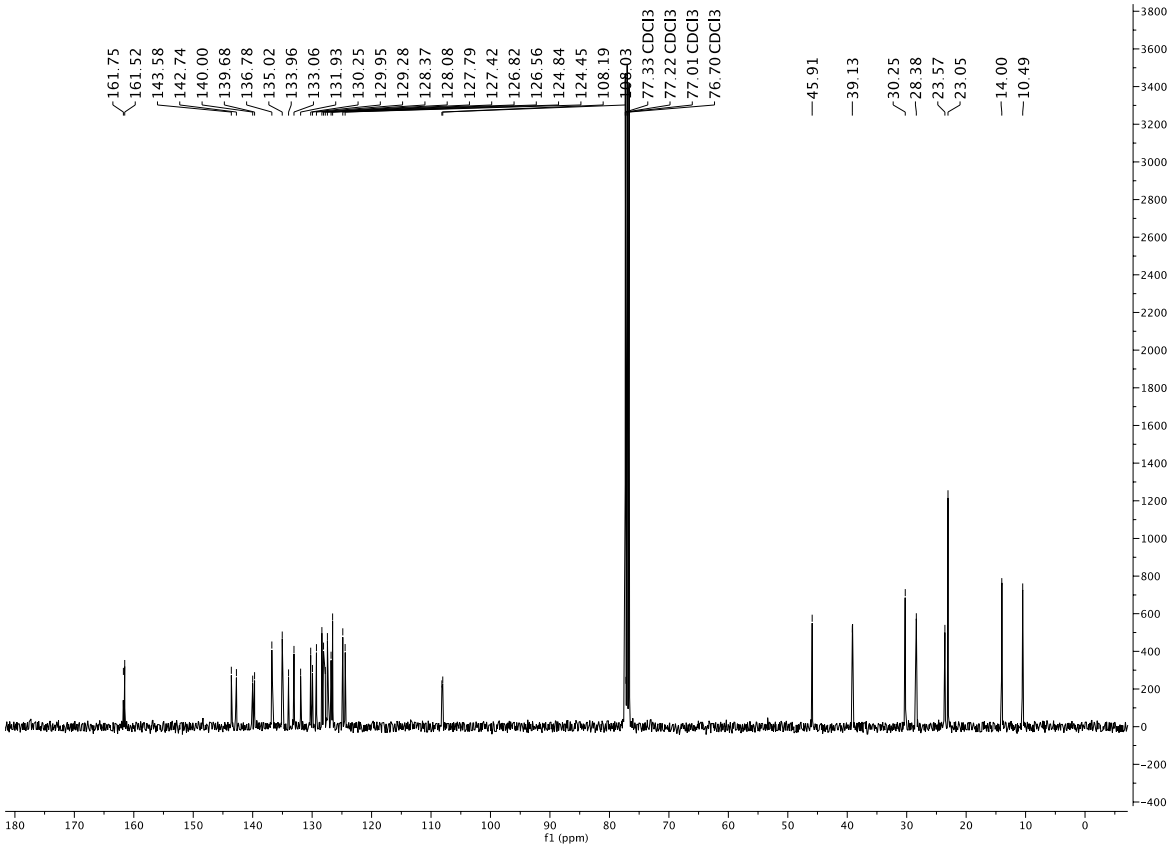

144.00
133.87
132.89
132.64
131.99
129.37
129.29
128.08
127.13
126.70
126.51
126.43
126.39
113.18
77.32 CDCl3
77.21 CDCl3
77.00 CDCl3
76.69 CDCl3
f1 (ppm)

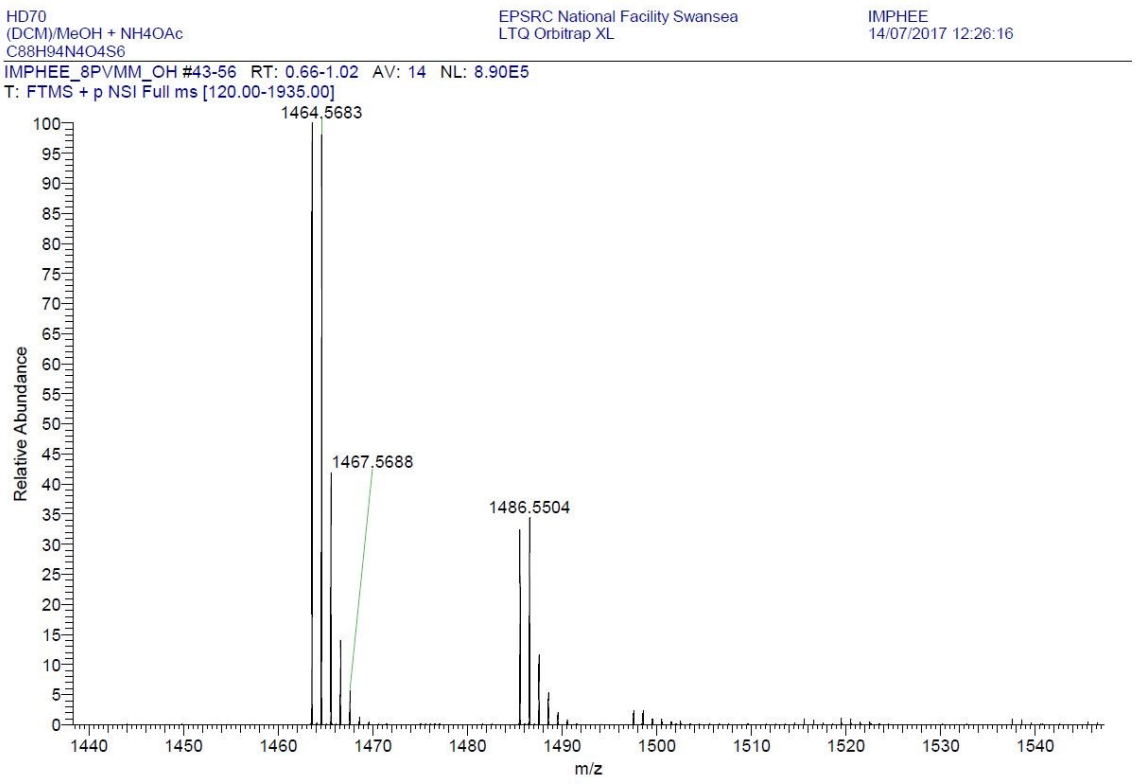

H.DAI HD44
MS32731 58 (3.876)
Magnetic Sector
19-Sep-2016
Magnet EI+
1.17e4
%
m/z

6,6'-([1,1'-Binaphthalene]-2,2'-diylbis([2",2"'-bithiophene]-5',5"-diyl))bis(2,5-bis(2-ethylhexyl)-3-(thiophen-2-yl)-2,5-dihydropyrrolo[3,4-*c*]pyrrole-1,4-dione)

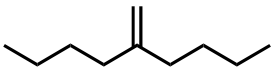


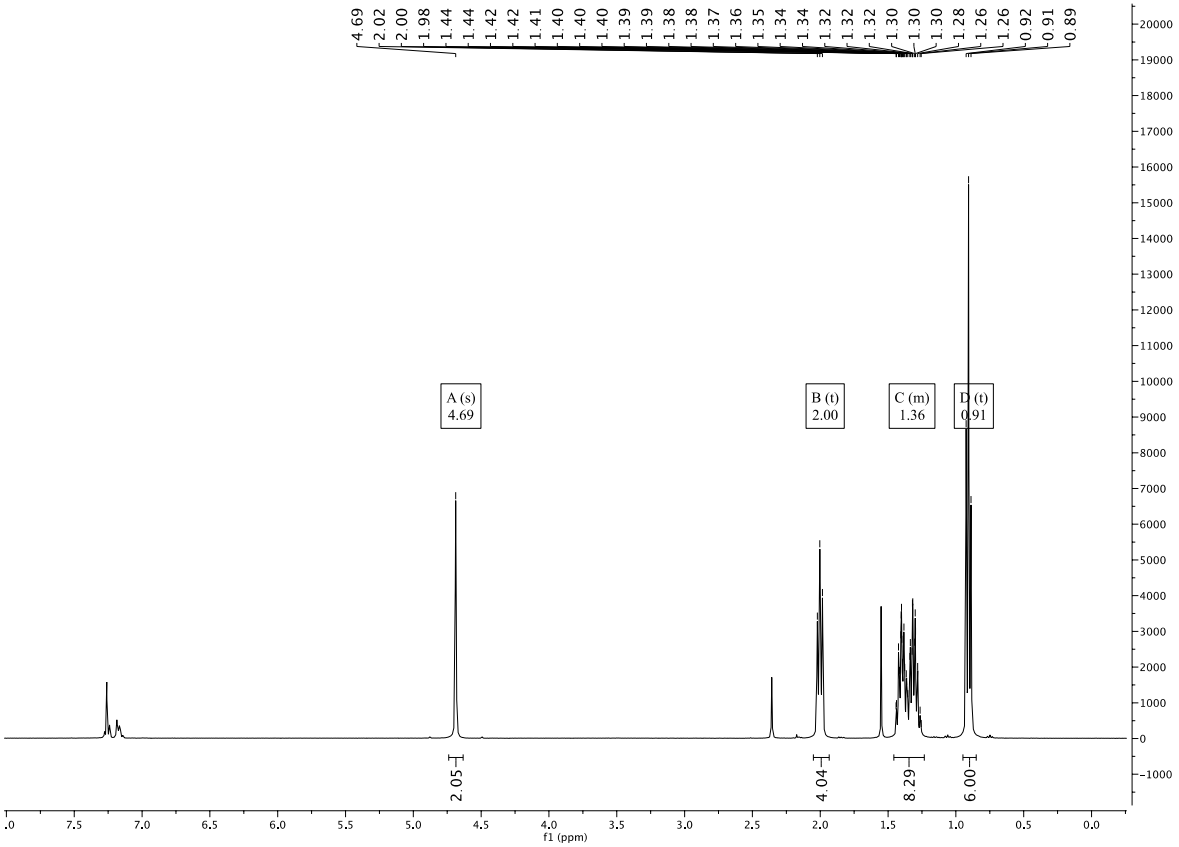


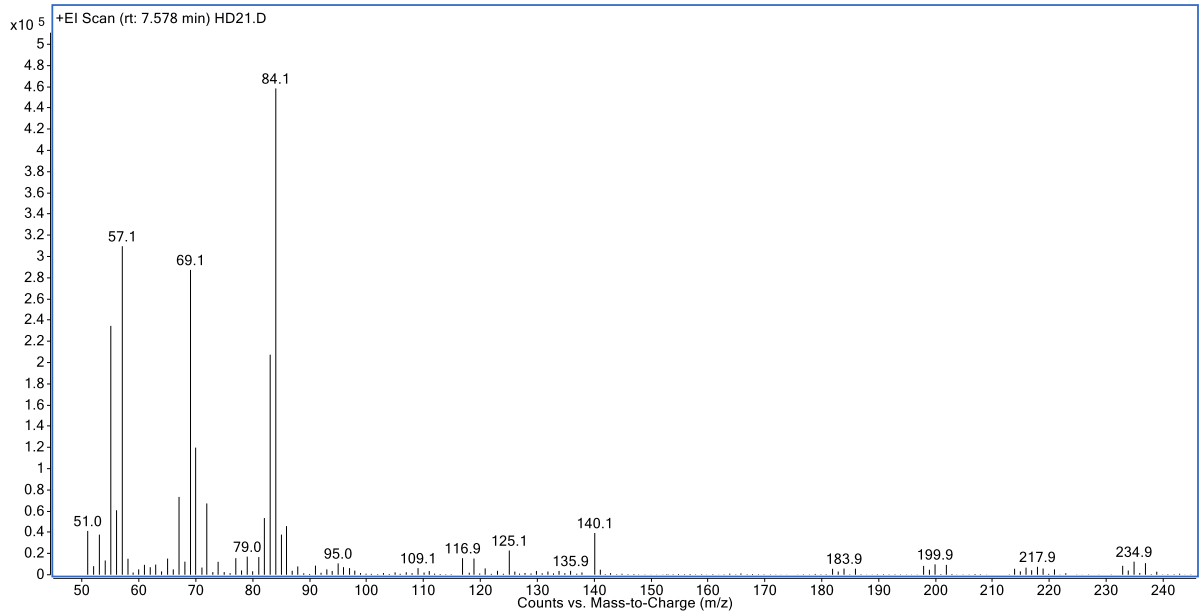

161.75
161.52
143.58
142.74
140.00
139.68
136.78
135.02
133.96
133.06
131.93
130.25
129.95
129.28
128.37
128.08
127.79
127.42
126.82
126.56
124.84
124.45
108.19
77.33 CDCl3
77.22 CDCl3
77.01 CDCl3
76.70 CDCl3
45.91
39.13
30.25
28.38
23.57
23.05
14.00
10.49
f1 (ppm)


HD70
(DCM)/MeOH + NH4OAc
C88H94N4O4S6
EPSRC National Facility Swansea
LTQ Orbitrap XL
IMPHEE
14/07/2017 12:26:16
IMPHEE_8PVMM_OH #43-56 RT: 0.66-1.02 AV: 14 NL: 8.90E5
T: FTMS + p NSI Full ms [120.00-1935.00]
1464.5683
1467.5688
1486.5504
Relative Abundance
m/z

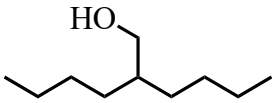
5-Methylenenonane

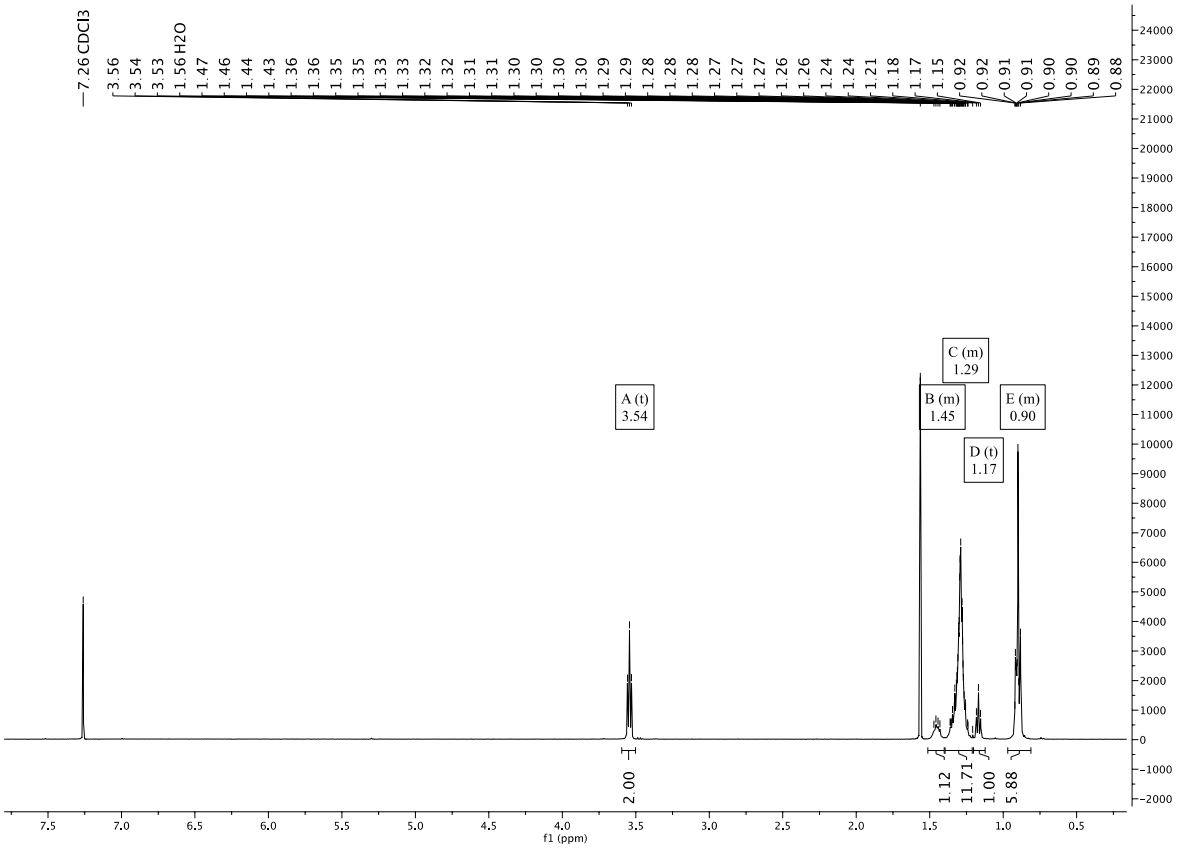


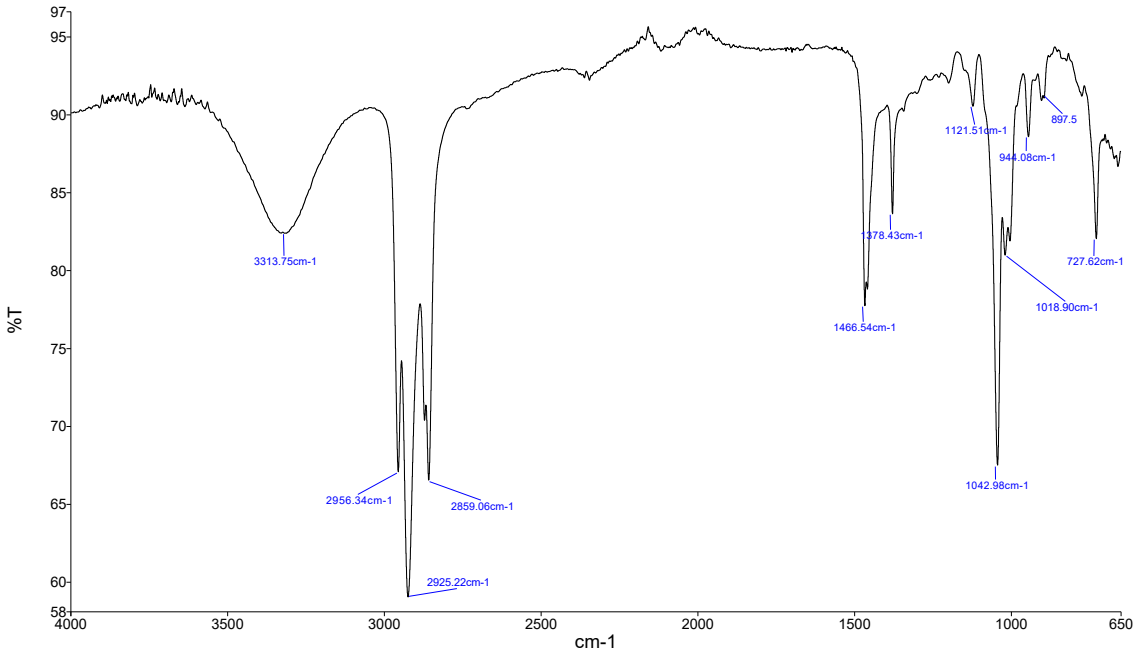




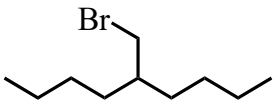
2-Butylhexan-1-ol

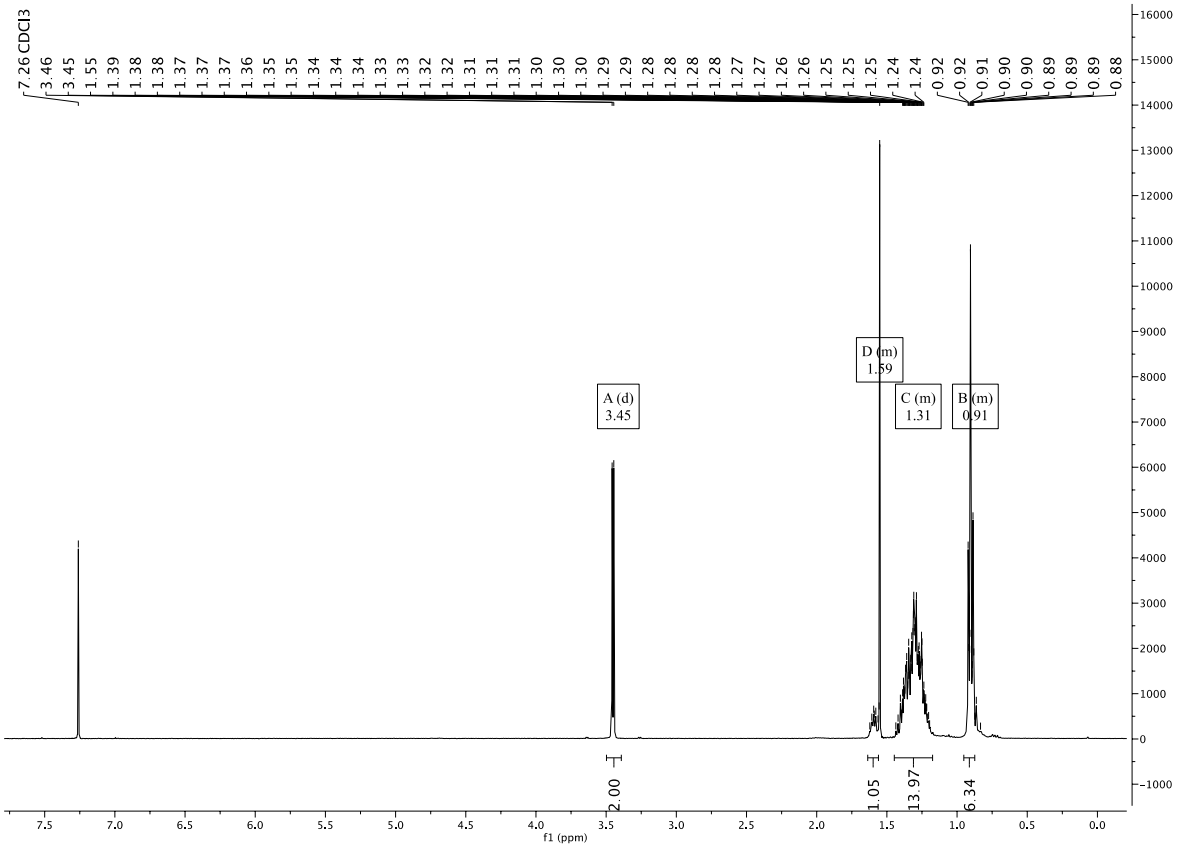




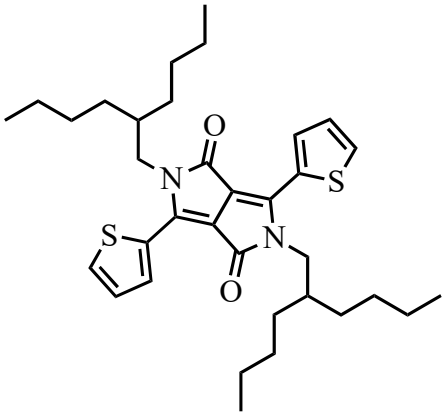


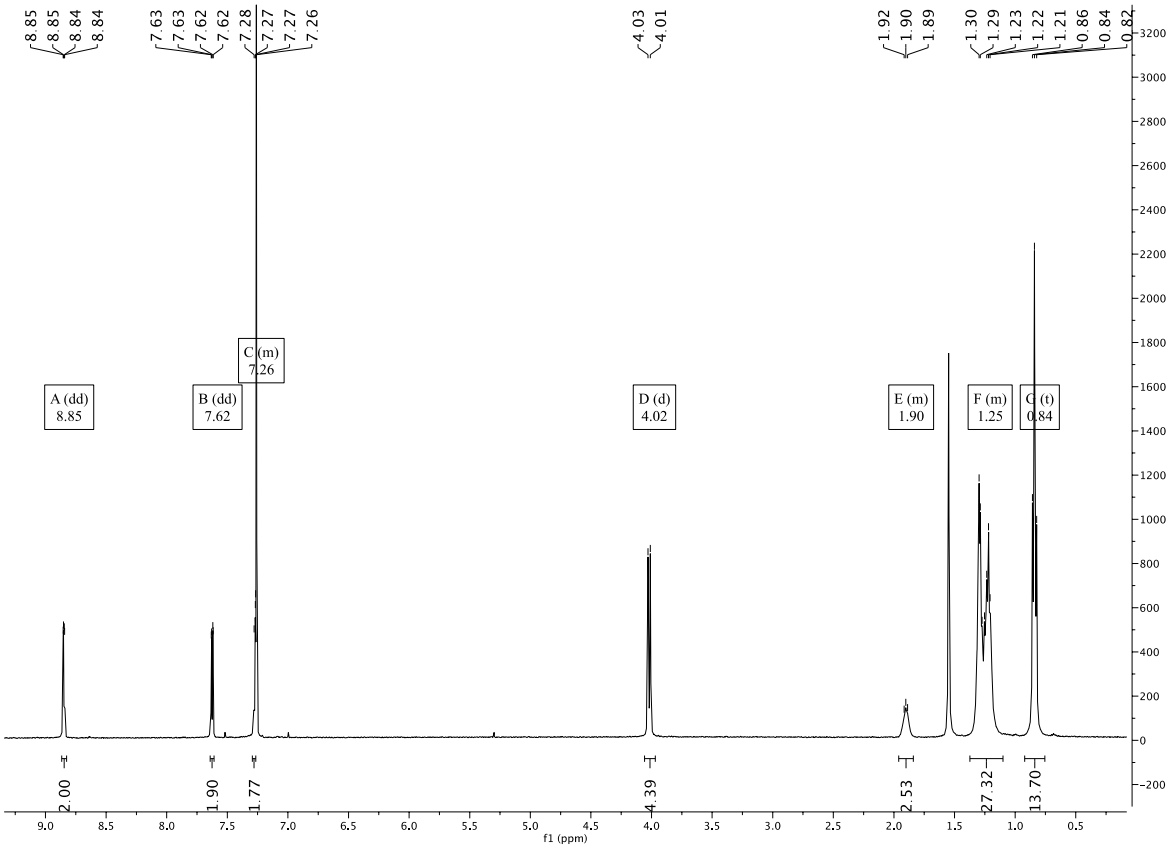
5-(Bromomethyl)nonane

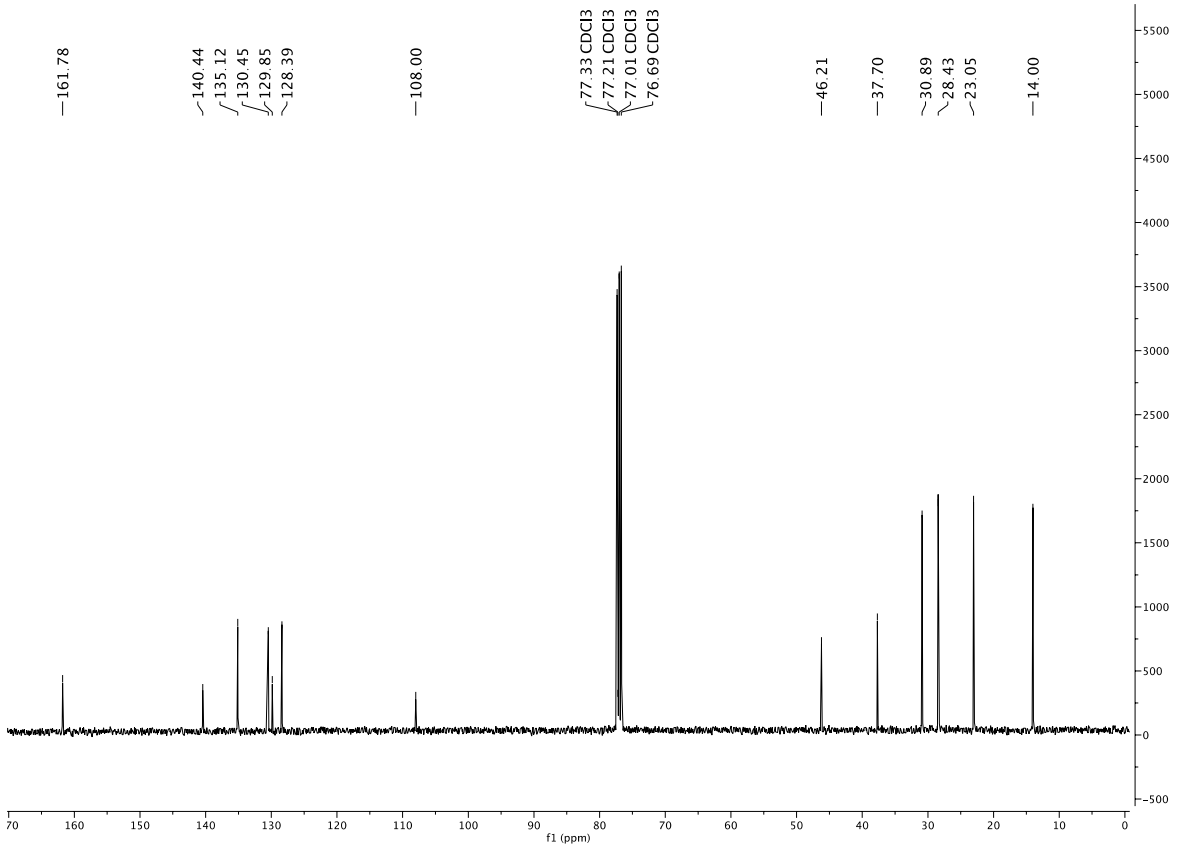


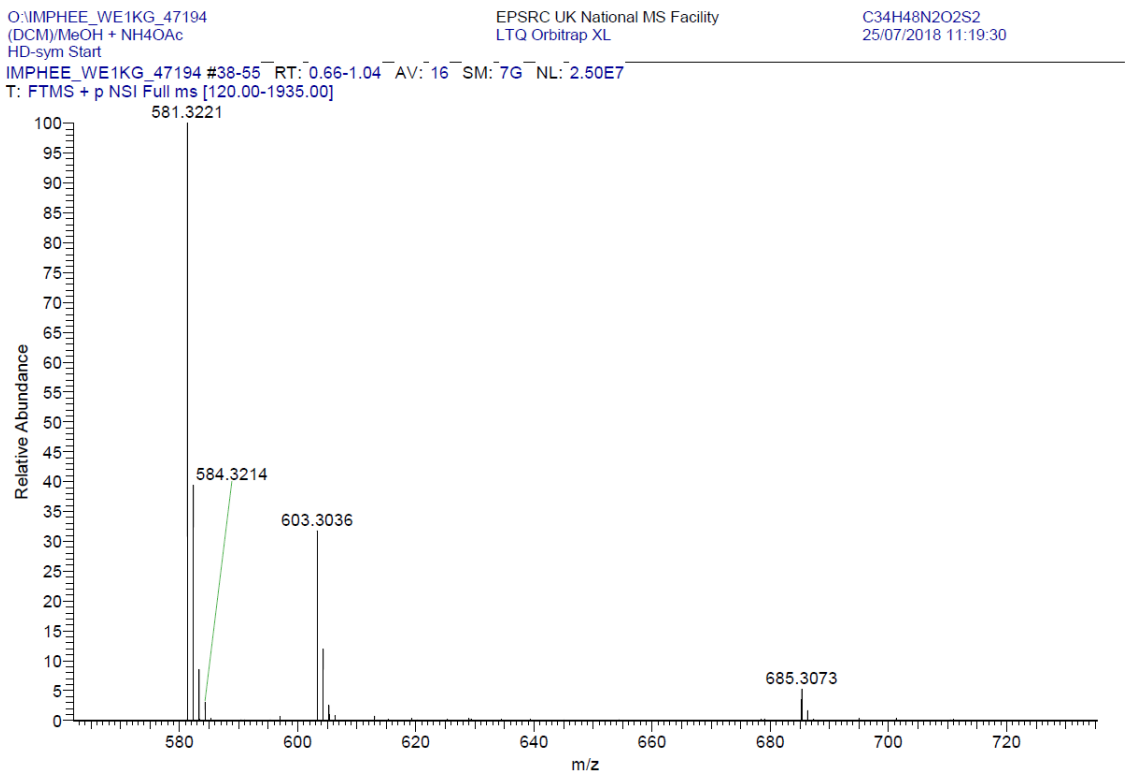


2,5-Bis(2-butylhexyl)-3,6-di(thiophen-2-yl)-2,5-dihydropyrrolo[3,4-*c*]pyrrole-1,4-dione

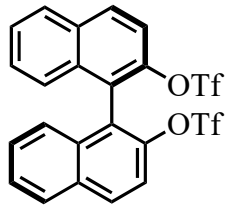


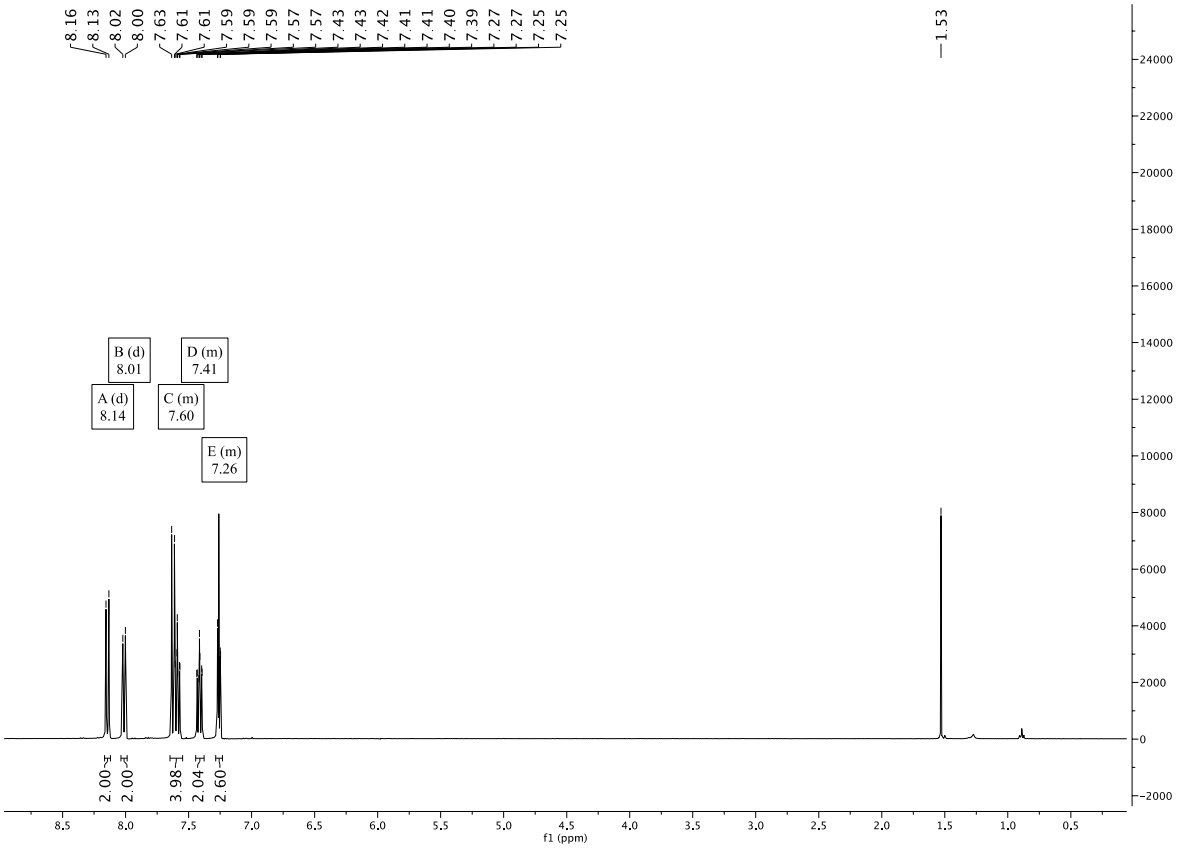


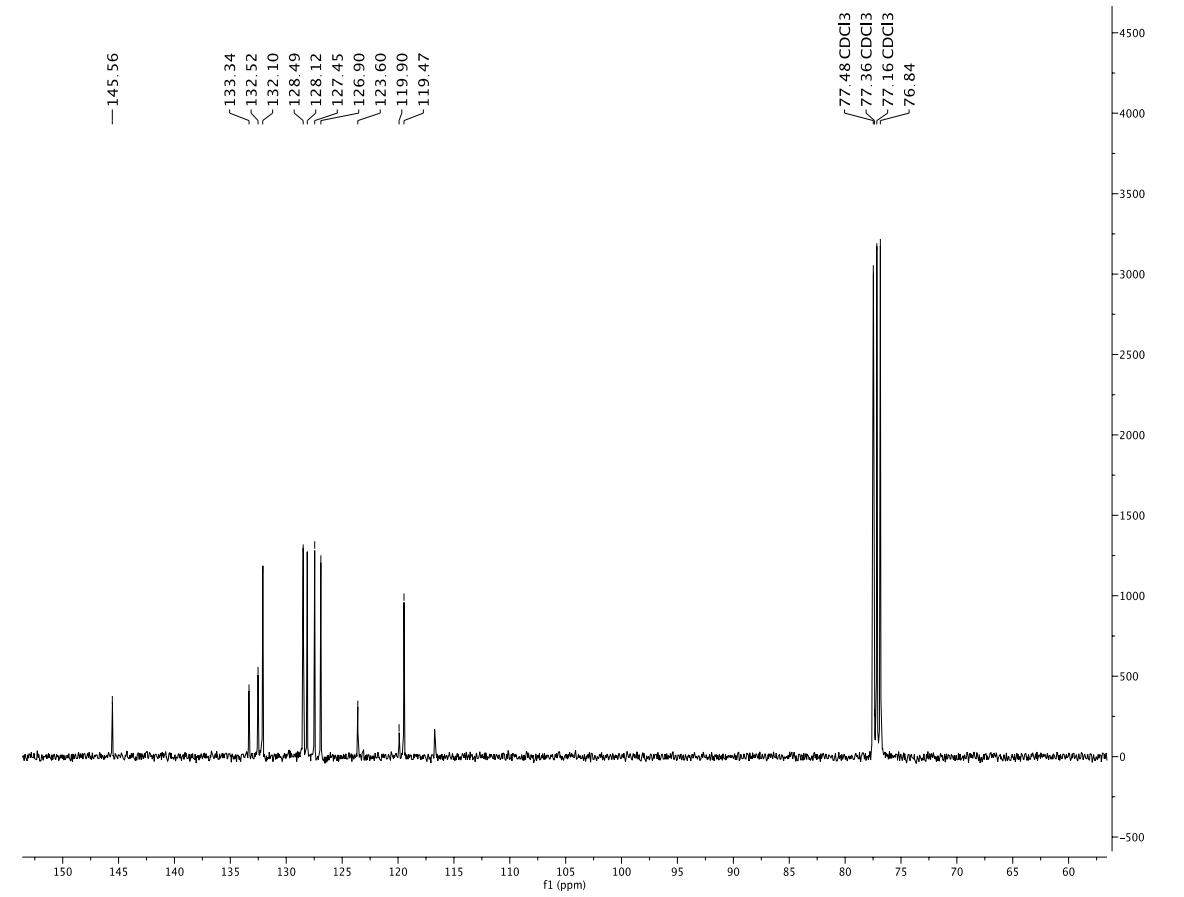

161.78
140.44
135.12
130.45
129.85
128.39
108.00
77.33 CDCl3
77.21 CDCl3
77.01 CDCl3
76.69 CDCl3
46.21
37.70
30.89
28.43
23.05
14.00
f1 (ppm)

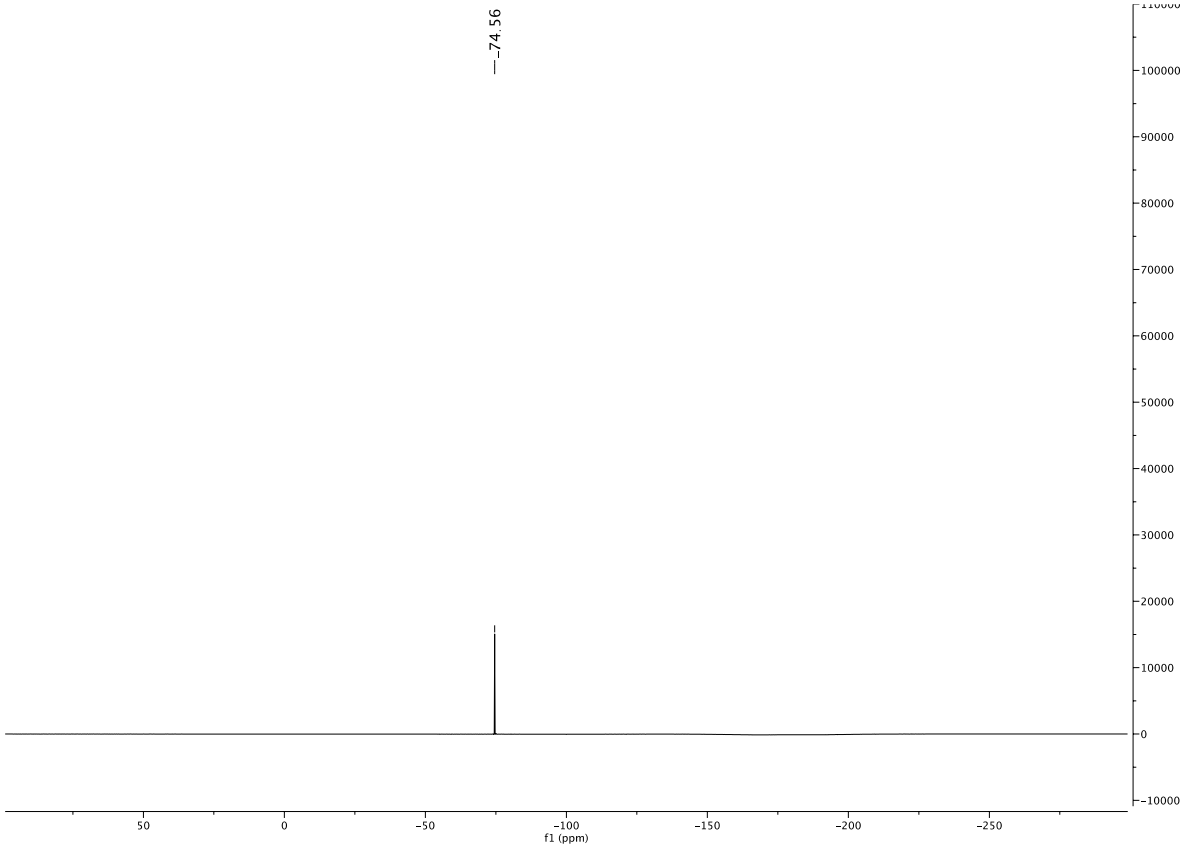

O:\IMPHEE_WE1KG_47194
(DCM)/MeOH + NH4OAc
HD-sym Start
EPSRC UK National MS Facility
LTQ Orbitrap XL
C34H48N2O2S2
25/07/2018 11:19:30
IMPHEE_WE1KG_47194 #38-55 RT: 0.66-1.04 AV: 16 SM: 7G NL: 2.50E7
T: FTMS + p NSI Full ms [120.00-1935.00]
581.3221
584.3214
603.3036
685.3073
Relative Abundance
m/z

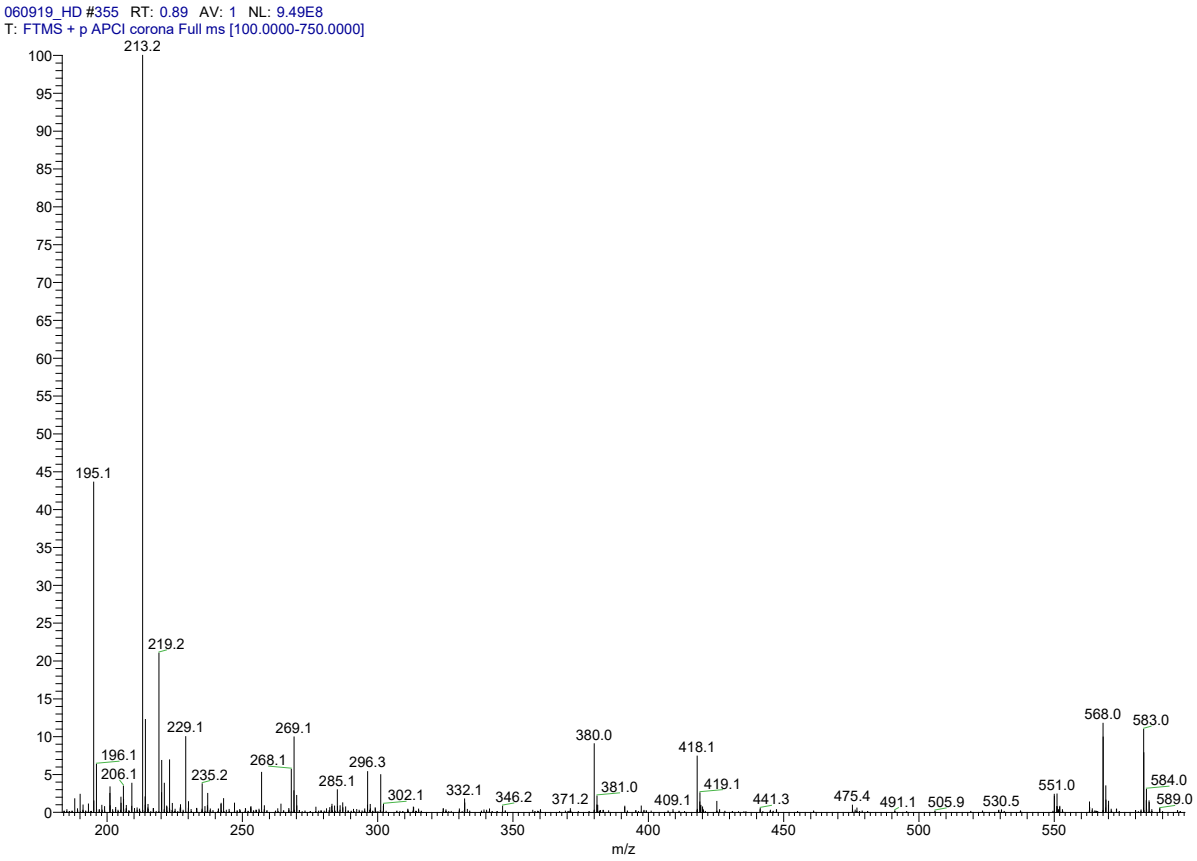
R-[1,1'-Binaphthalene]-2,2'-diyl bis(trifluoromethanesulfonate)



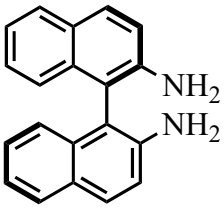



145.56
133.34
132.52
132.10
128.49
128.12
127.45
126.90
123.60
119.90
119.47
77.48 CDCl3
77.36 CDCl3
77.16 CDCl3
76.84
f1 (ppm)

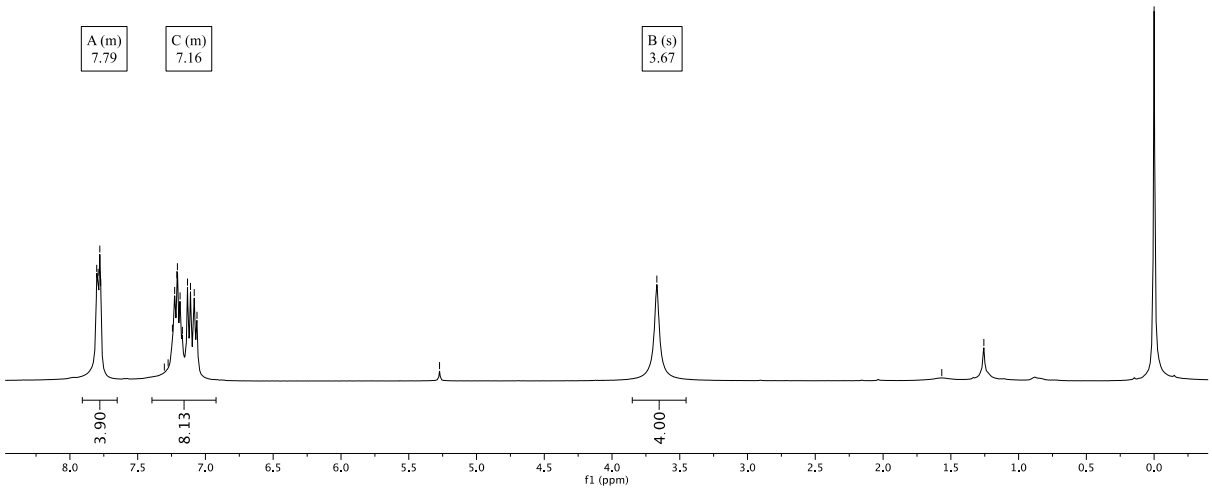

74.56
f1 (ppm)

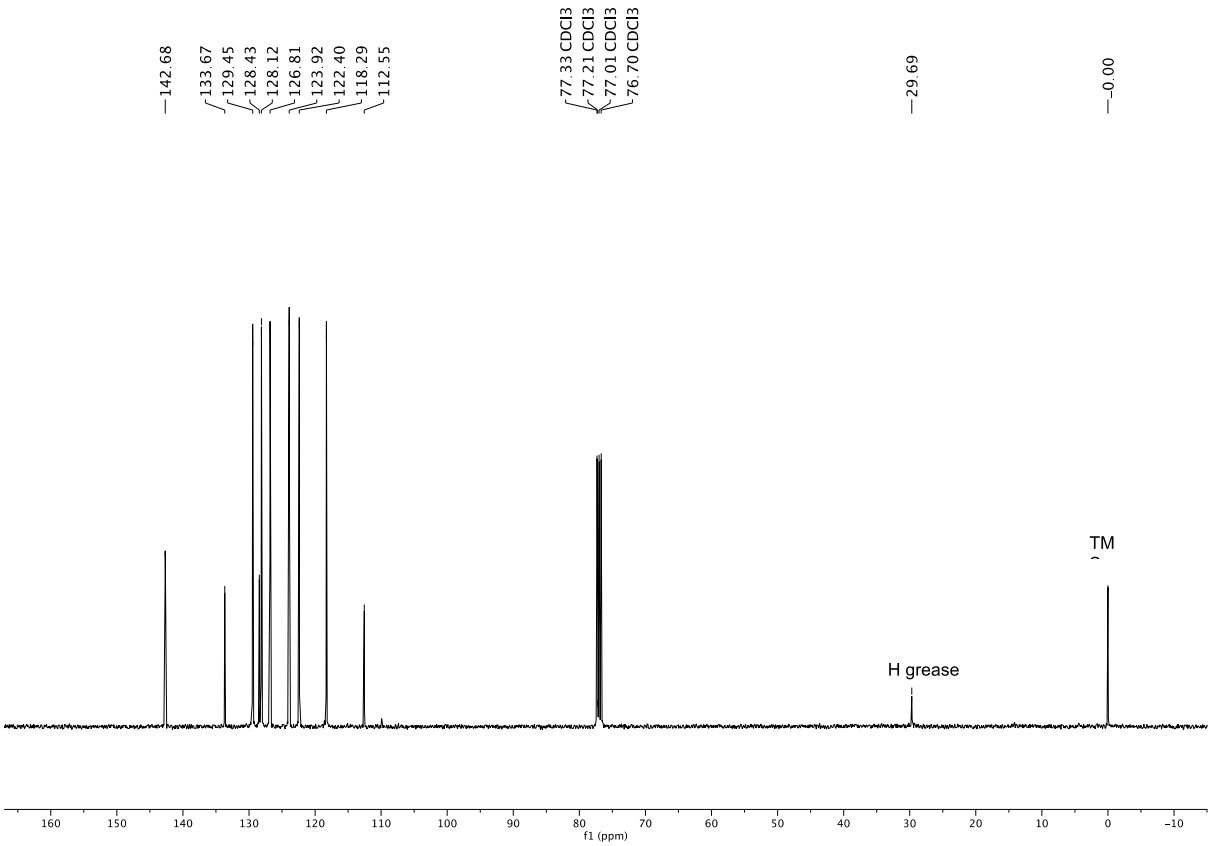

060919_HD #355 RT: 0.89 AV: 1 NL: 9.49E8
T: FTMS + p APCI corona Full ms [100.0000-750.0000]
213.2
195.1
219.2
229.1
269.1
196.1
206.1
235.2
268.1
296.3
285.1
302.1
332.1
346.2
371.2
380.0
381.0
409.1
418.1
419.1
441.3
475.4
491.1
505.9
530.5
551.0
568.0
583.0
584.0
589.0
m/z

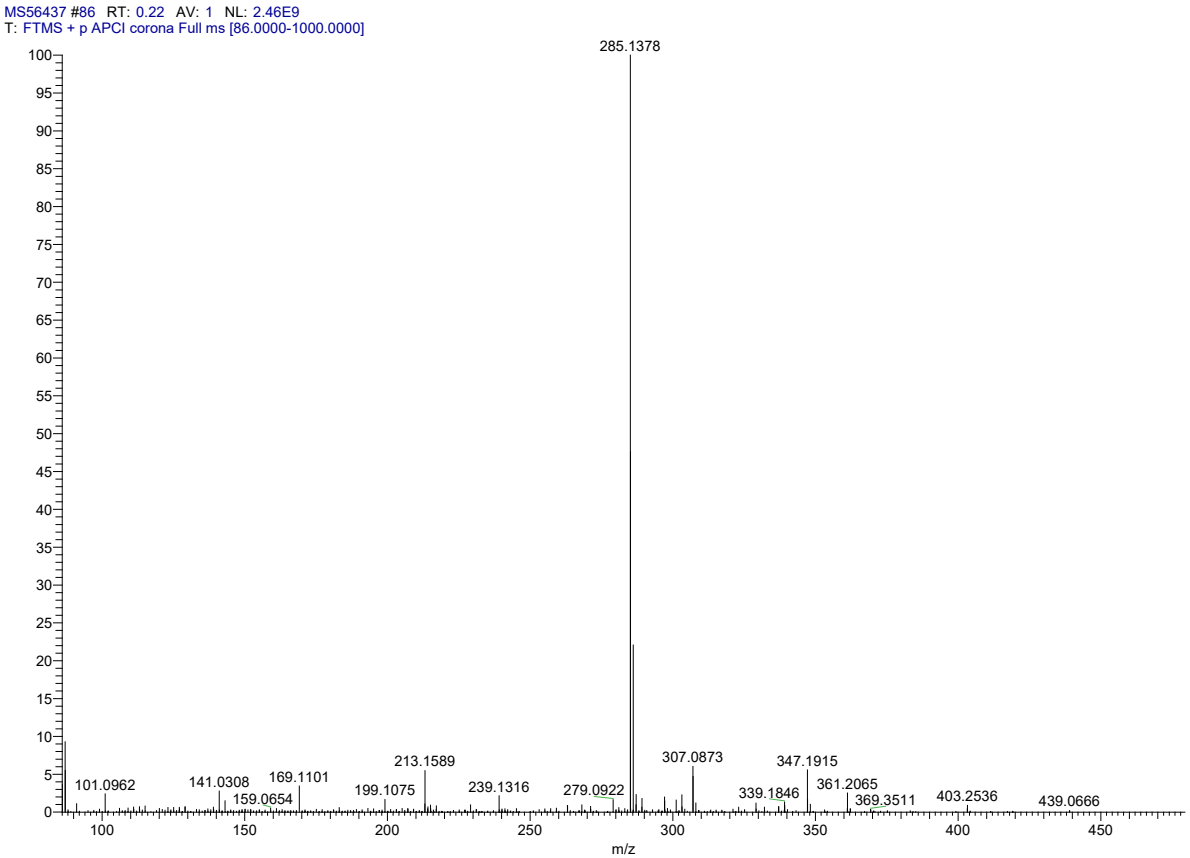
R-[1,1'-Binaphthalene]-2,2'-diamine



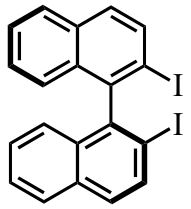


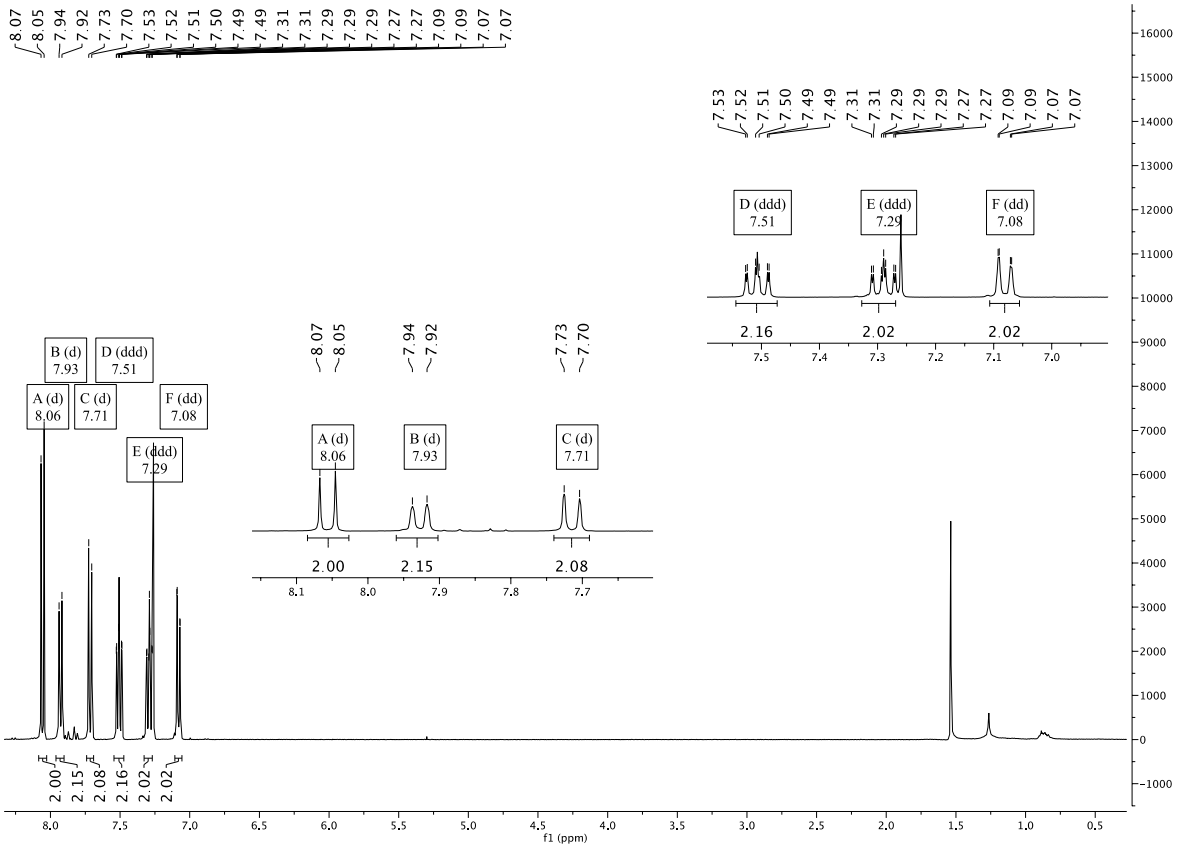


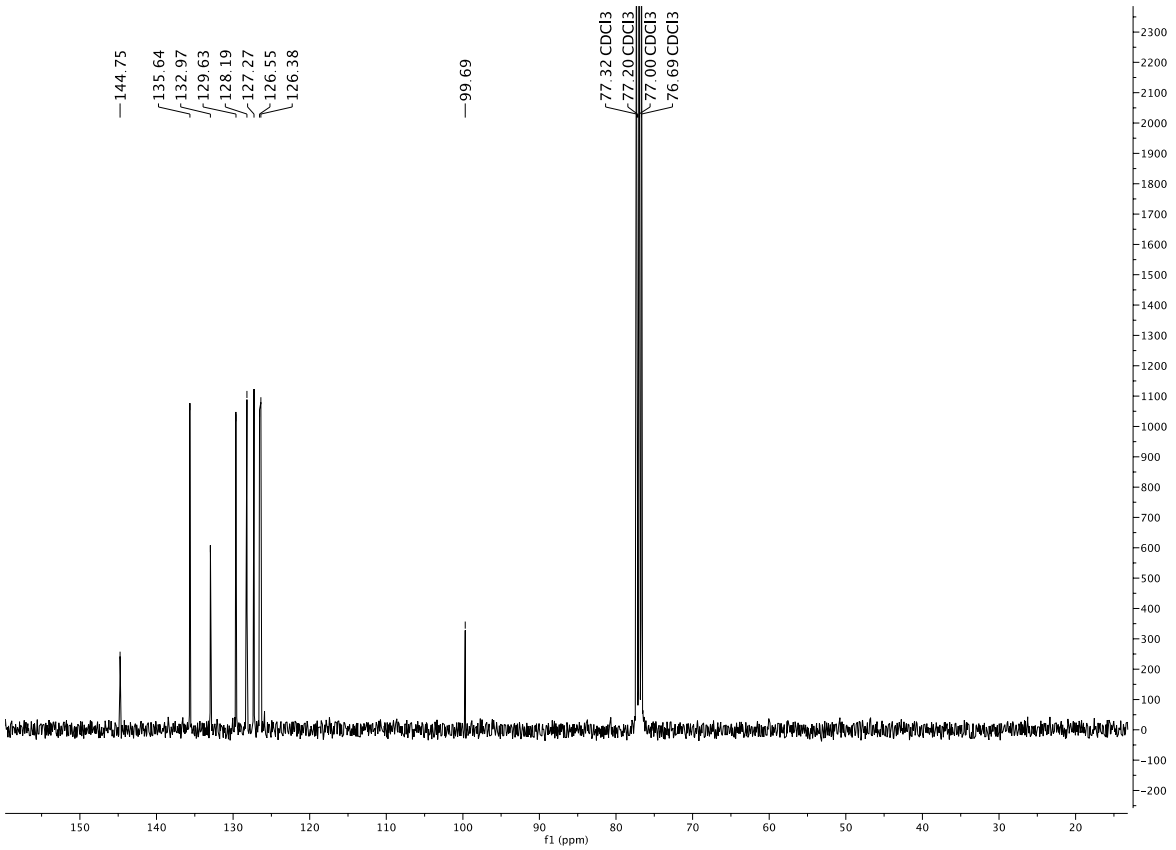

142.68
133.67
129.45
128.43
128.12
126.81
123.92
122.40
118.29
112.55
77.33 CDCl3
77.21 CDCl3
77.01 CDCl3
76.70 CDCl3
29.69
0.00
TM
H grease
f1 (ppm)

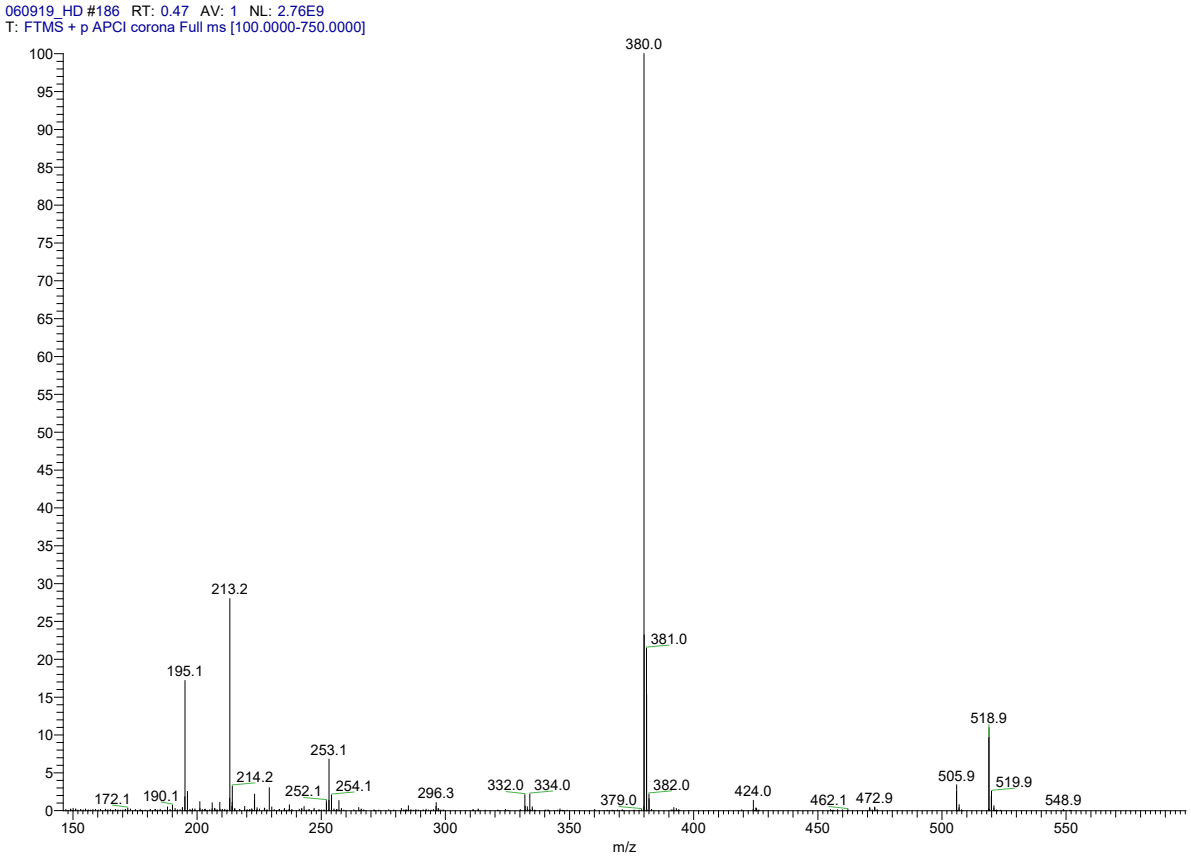

MS56437 #86 RT: 0.22 AV: 1 NL: 2.46E9
T: FTMS + p APCI corona Full ms [86.0000-1000.0000]
285.1378
307.0873
347.1915
213.1589
169.1101
361.2065
101.0962
141.0308
159.0654
199.1075
239.1316
279.0922
339.1846
369.3511
403.2536
439.0666
m/z

(*S*)-2,2'-Diiodo-1,1'-binaphthalene

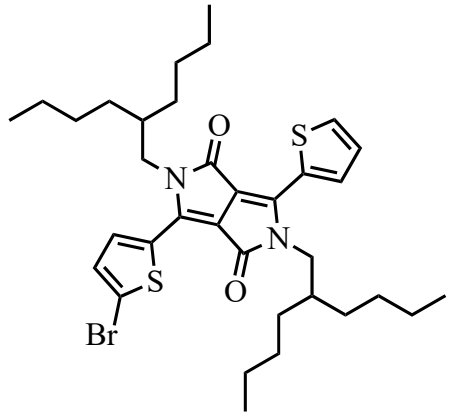


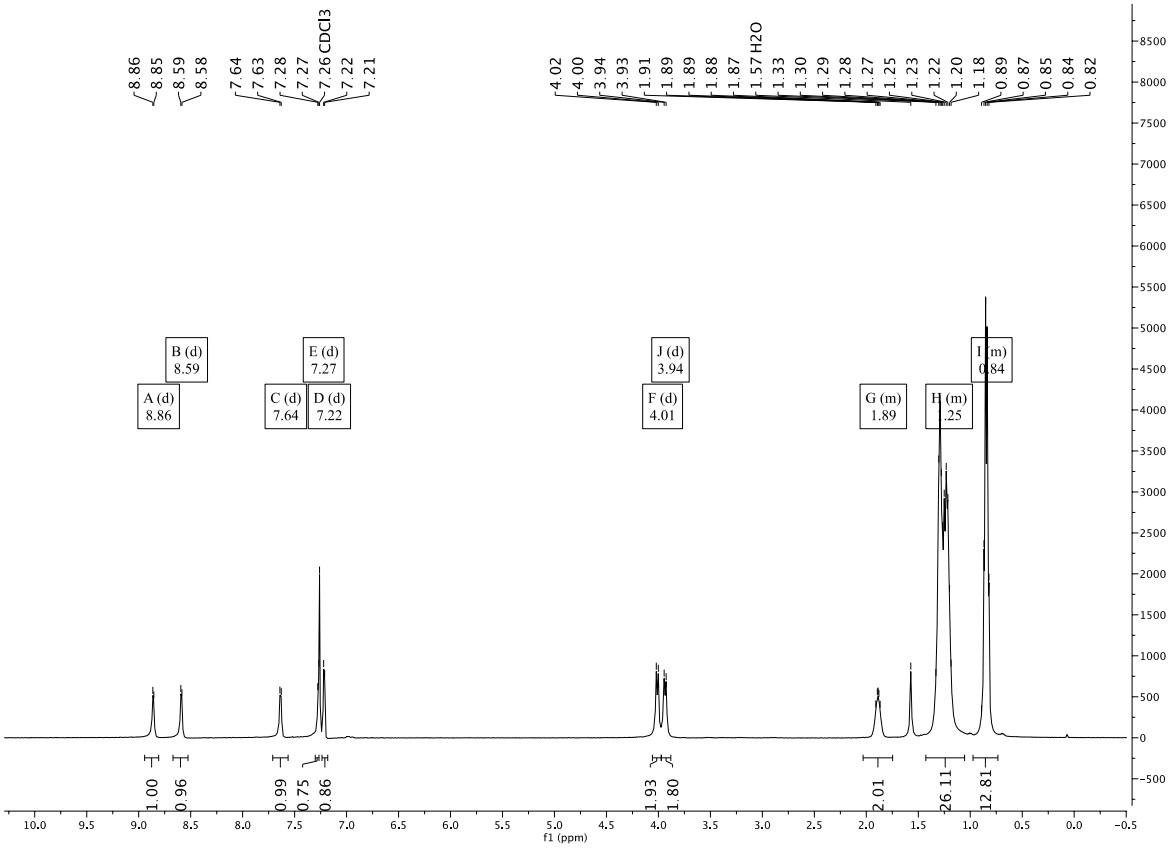


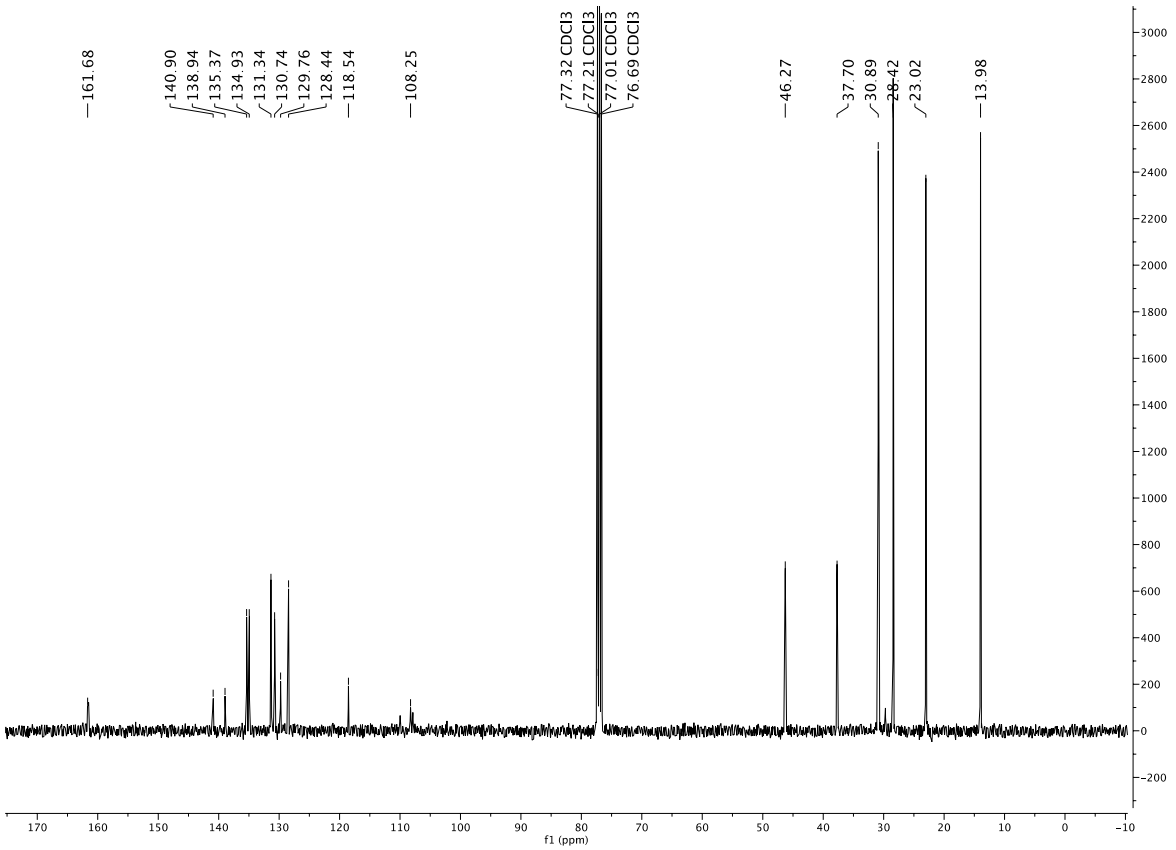

144.75
135.64
132.97
129.63
128.19
127.27
126.55
126.38
99.69
77.32 CDCl3
77.20 CDCl3
77.00 CDCl3
76.69 CDCl3
f1 (ppm)

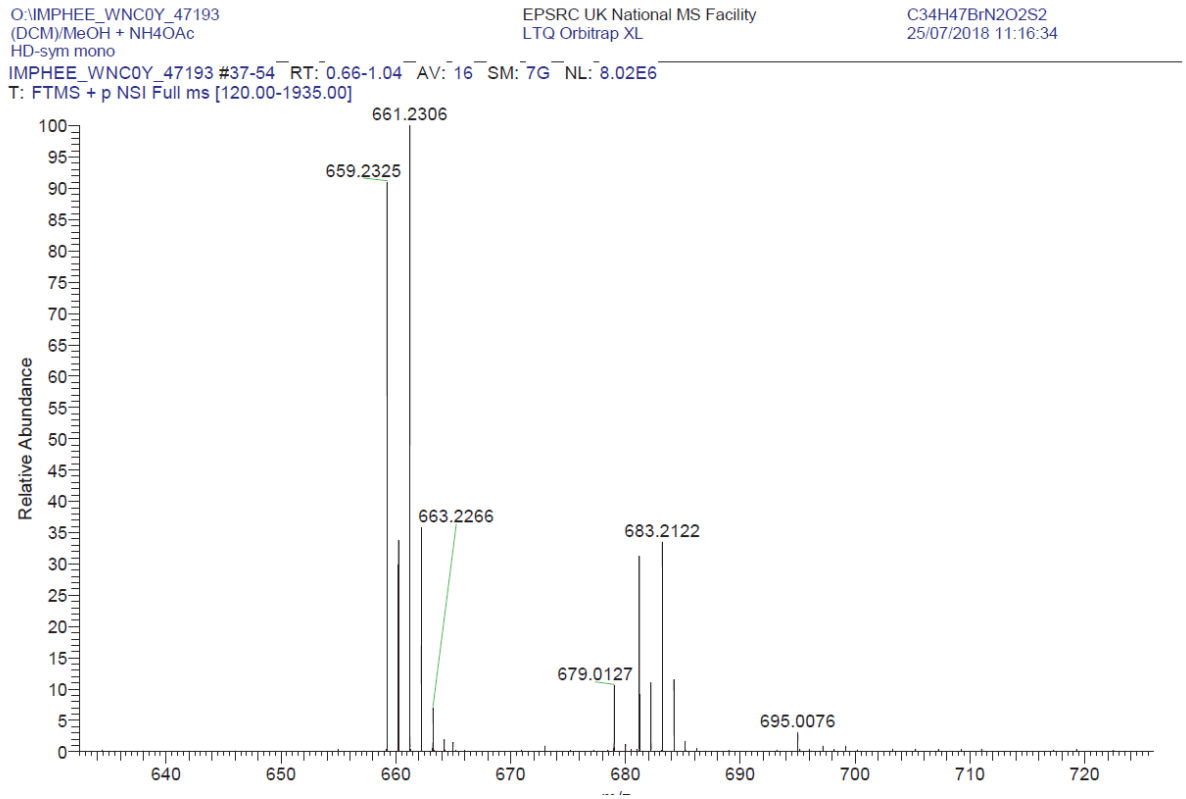

060919_HD #186 RT: 0.47 AV: 1 NL: 2.76E9
T: FTMS + p APCI corona Full ms [100.0000-750.0000]
380.0
213.2
195.1
381.0
518.9
253.1
214.2
505.9
519.9
172.1
190.1
252.1
254.1
296.3
332.0
334.0
379.0
382.0
424.0
462.1
472.9
548.9
m/z

3-(5-Bromothiophen-2-yl)-2,5-bis(2-butylhexyl)-6-(thiophen-2-yl)-2,5-dihydropyrrolo[3,4-*c*]pyrrole-1,4-dione

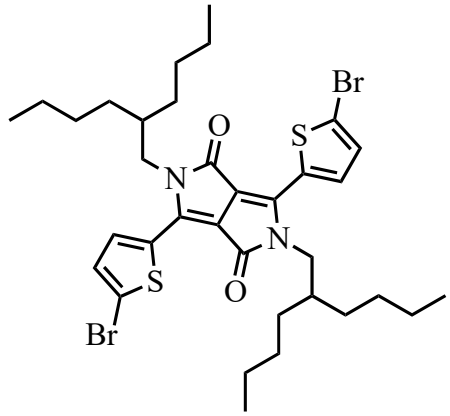


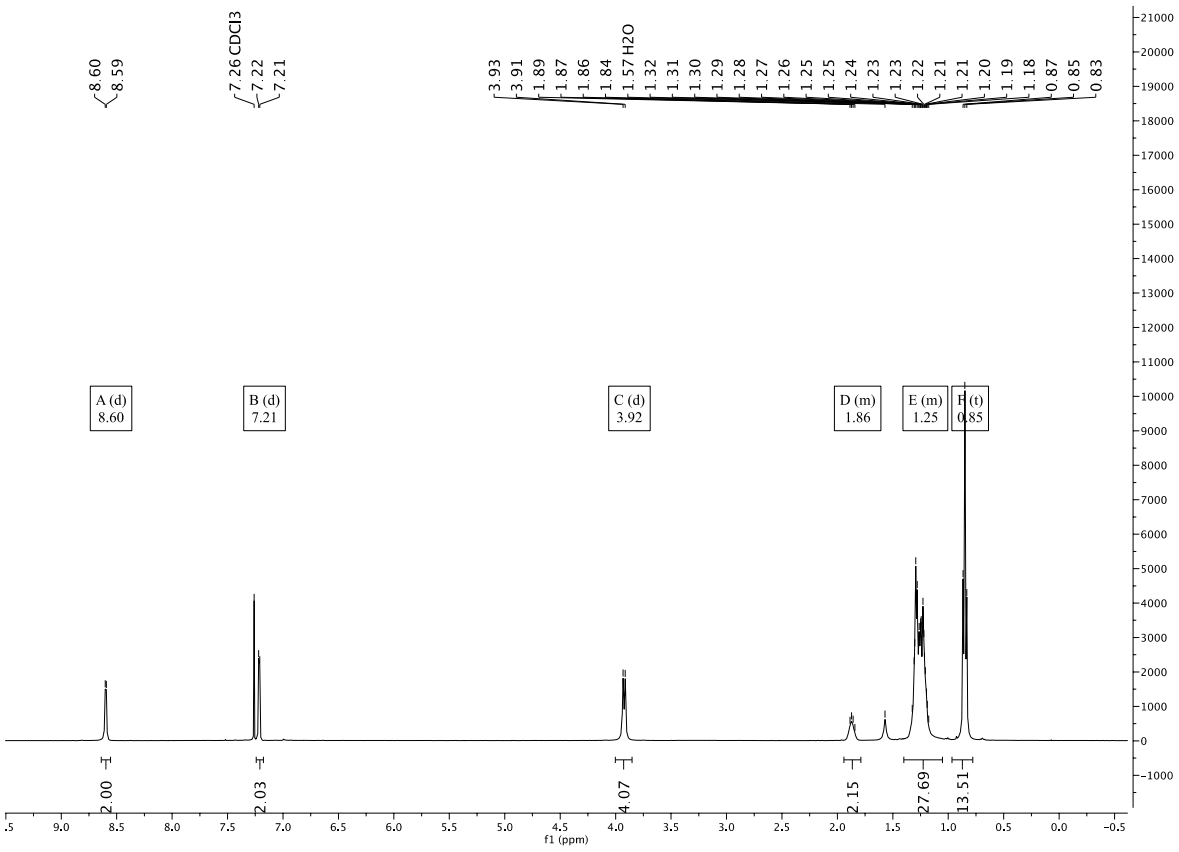


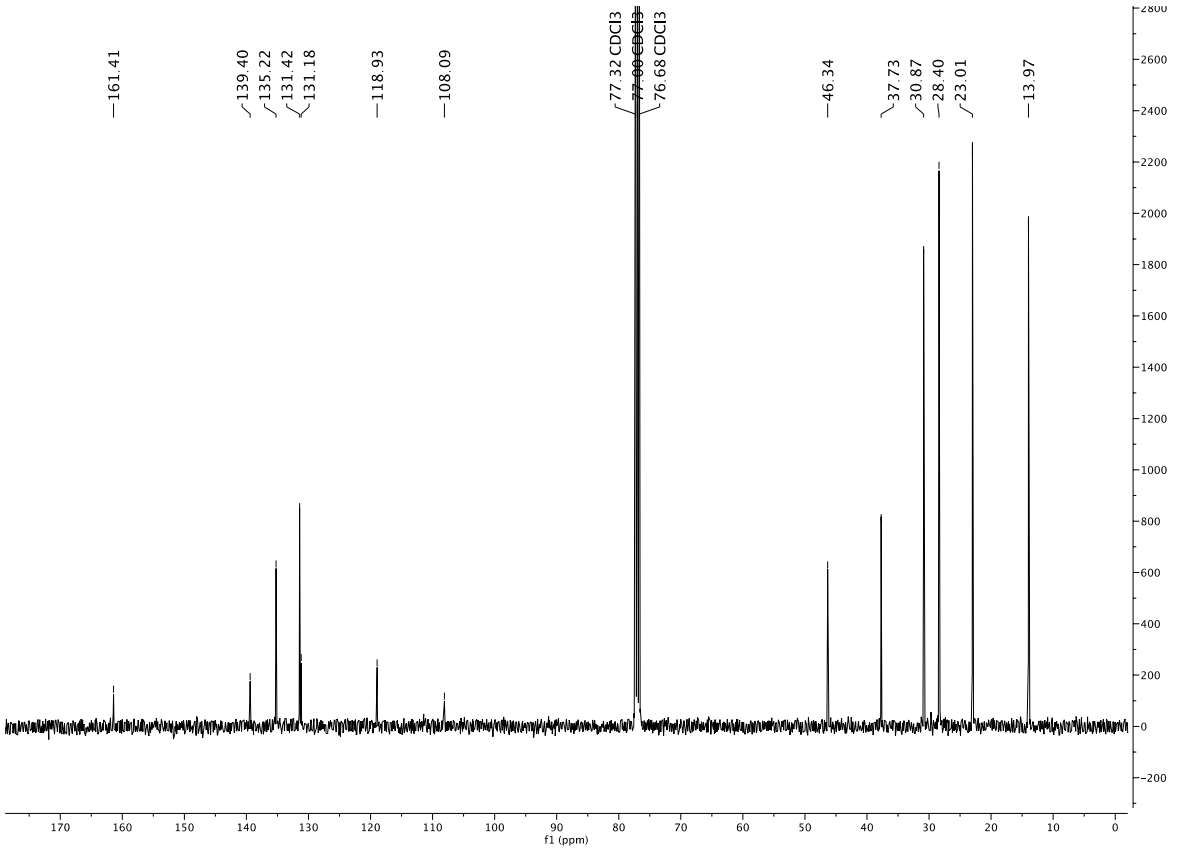

161.68
140.90
138.94
135.37
134.93
131.34
130.74
129.76
128.44
118.54
108.25
77.32 CDCl3
77.21 CDCl3
77.01 CDCl3
76.69 CDCl3
46.27
37.70
30.89
28.42
23.02
13.98
f1 (ppm)

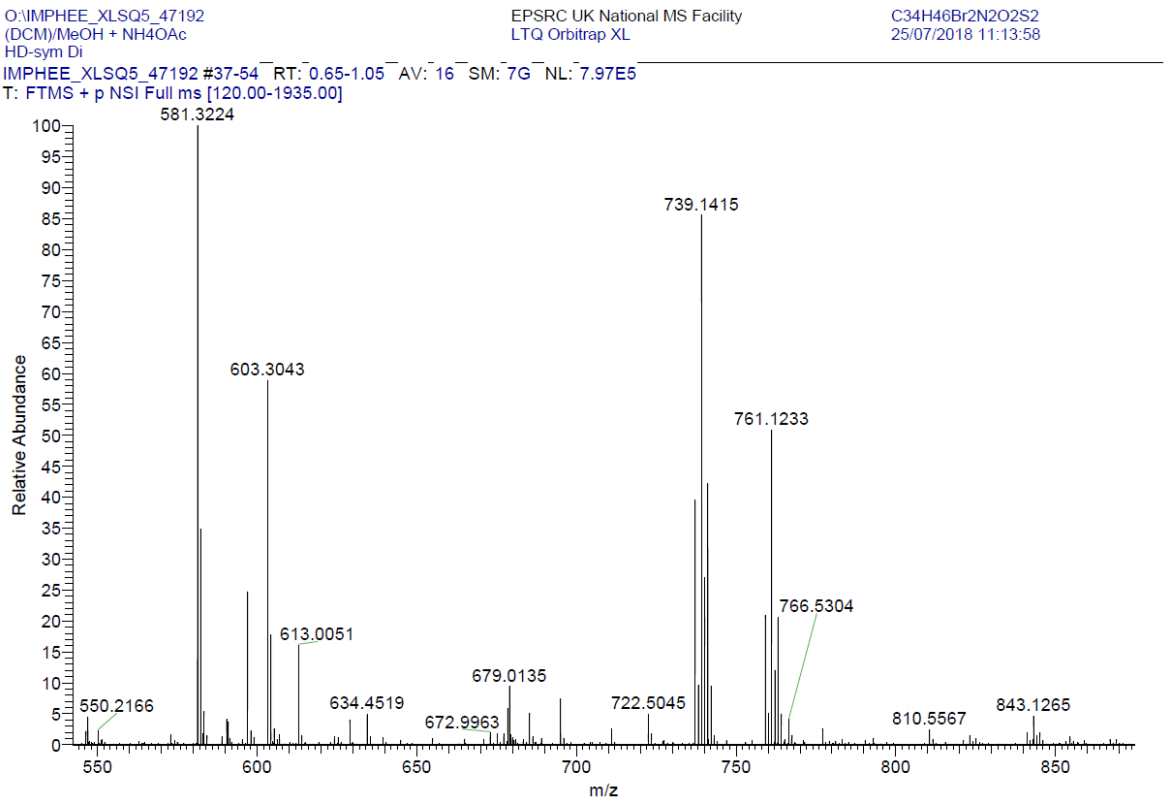

O:\IMPHEE_WNC0Y_47193
(DCM)/MeOH + NH4OAc
HD-sym mono
EPSRC UK National MS Facility
LTQ Orbitrap XL
C34H47BrN2O2S2
25/07/2018 11:16:34
IMPHEE_WNC0Y_47193 #37-54 RT: 0.66-1.04 AV: 16 SM: 7G NL: 8.02E6
T: FTMS + p NSI Full ms [120.00-1935.00]
661.2306
659.2325
663.2266
683.2122
679.0127
695.0076
Relative Abundance

3,6-Bis(5-bromothiophen-2-yl)-2,5-bis(2-butylhexyl)-2,5-dihydropyrrolo[3,4-*c*]pyrrole-1,4-dione

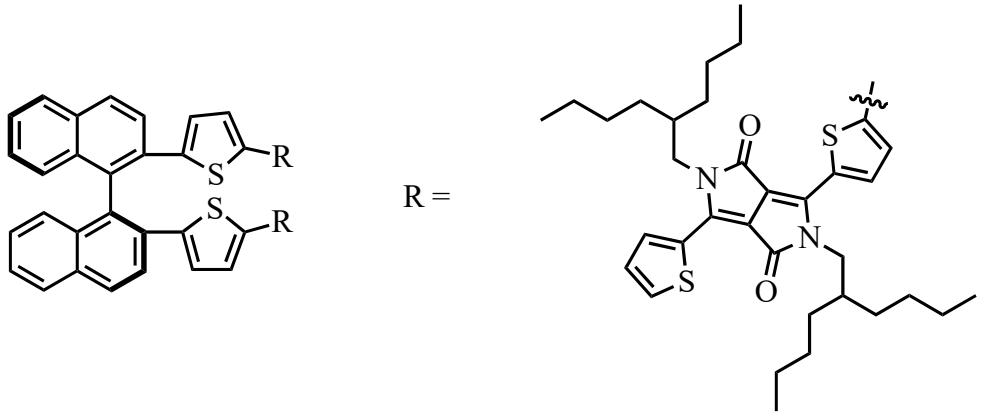


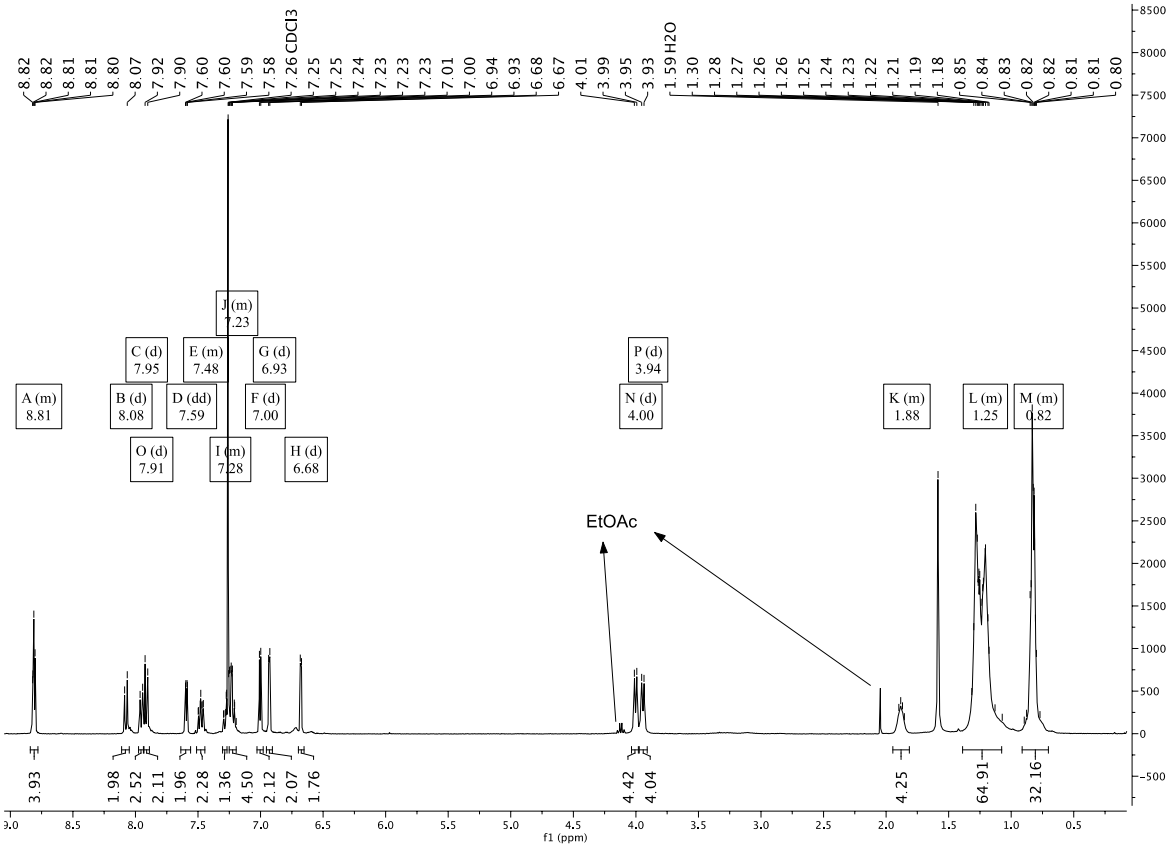


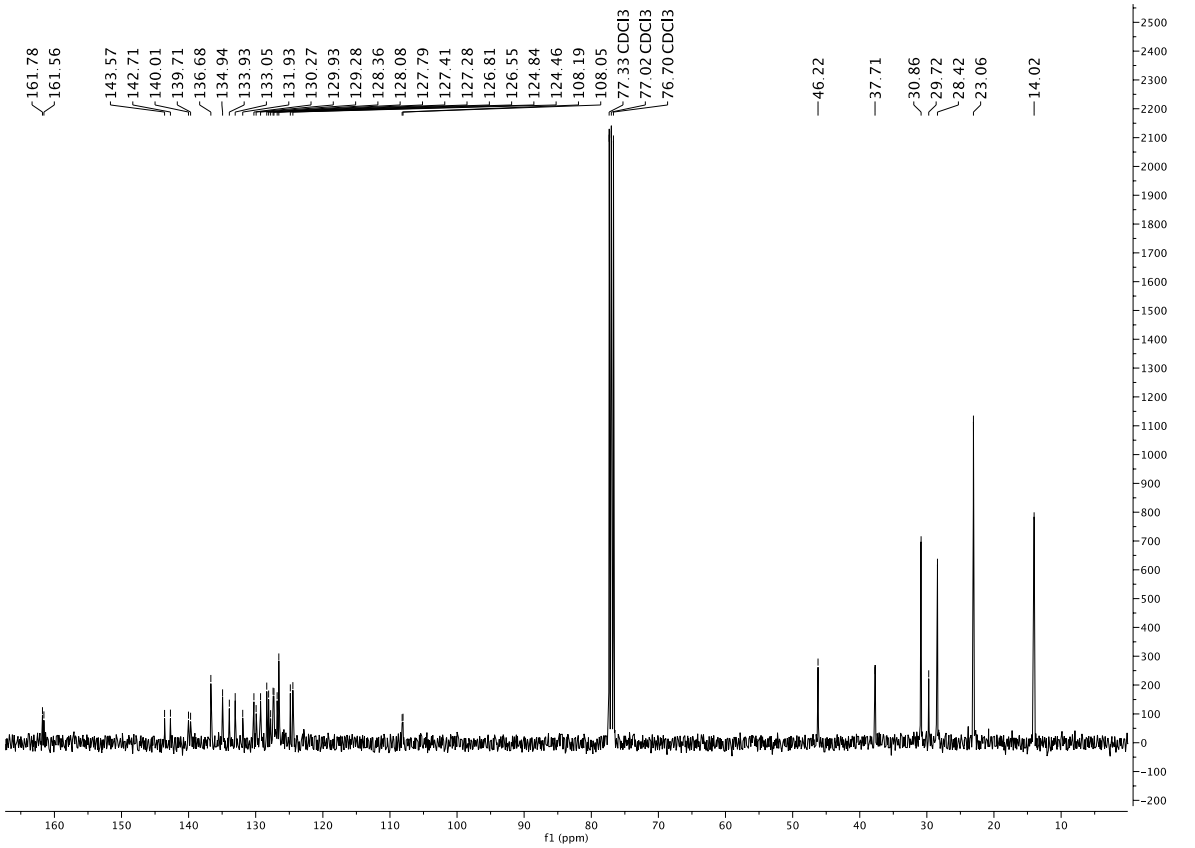

161.41
139.40
135.22
131.42
131.18
118.93
108.09
77.32 CDCl3
77.00 CDCl3
76.68 CDCl3
46.34
37.73
30.87
28.40
23.01
13.97
f1 (ppm)

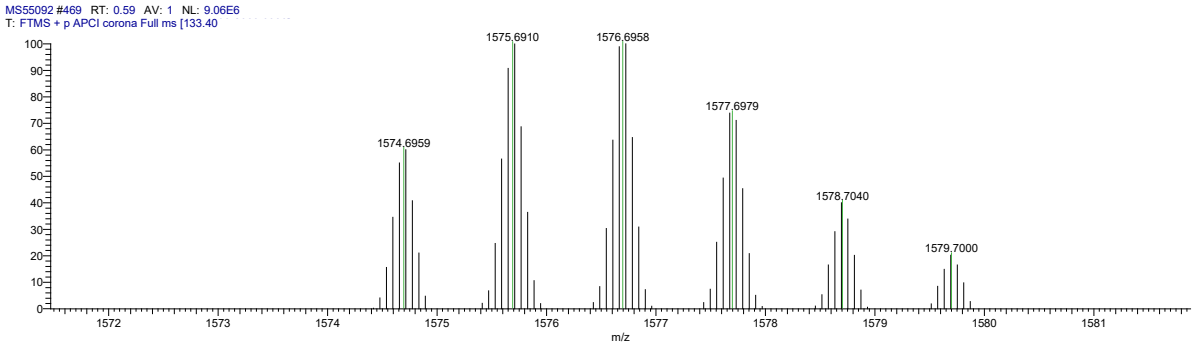

O:\IMPHEE_XLSQ5_47192
(DCM)/MeOH + NH4OAc
HD-sym Di
EPSRC UK National MS Facility
LTQ Orbitrap XL
C34H46Br2N2O2S2
25/07/2018 11:13:58
IMPHEE_XLSQ5_47192 #37-54 RT: 0.65-1.05 AV: 16 SM: 7G NL: 7.97E5
T: FTMS + p NSI Full ms [120.00-1935.00]
581.3224
739.1415
603.3043
761.1233
766.5304
613.0051
679.0135
550.2166
634.4519
672.9963
722.5045
810.5567
843.1265
Relative Abundance
m/z

S-6,6'-([1,1'-Binaphthalene]-2,2'-diylbis([2",2"'-bithiophene]-5',5"-diyl))bis(2,5-bis(2-butylhexyl)-3-(thiophen-2-yl)-2,5-dihydropyrrolo[3,4-*c*]pyrrole-1,4-dione)

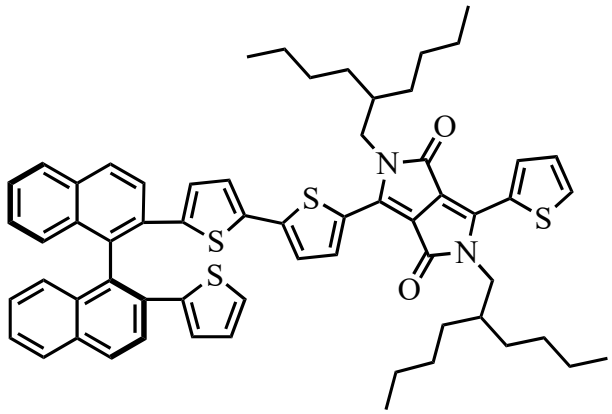


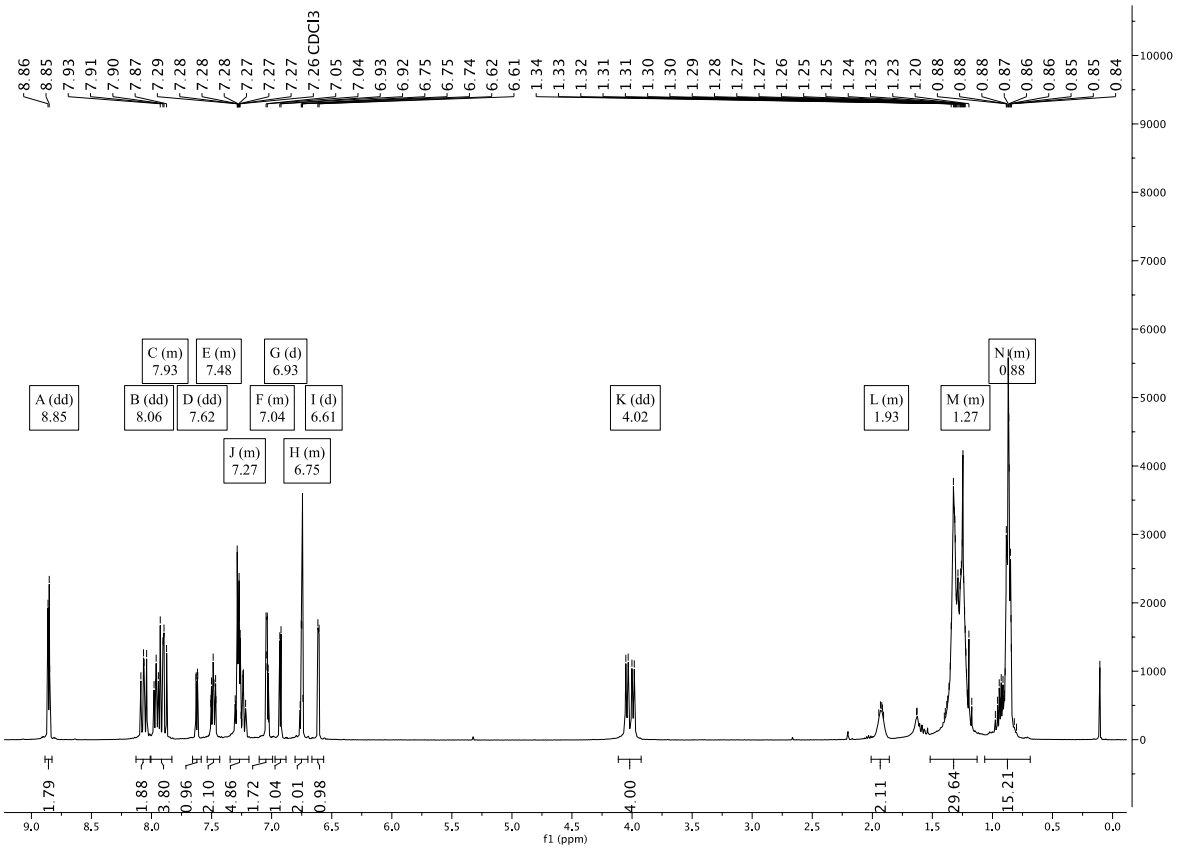


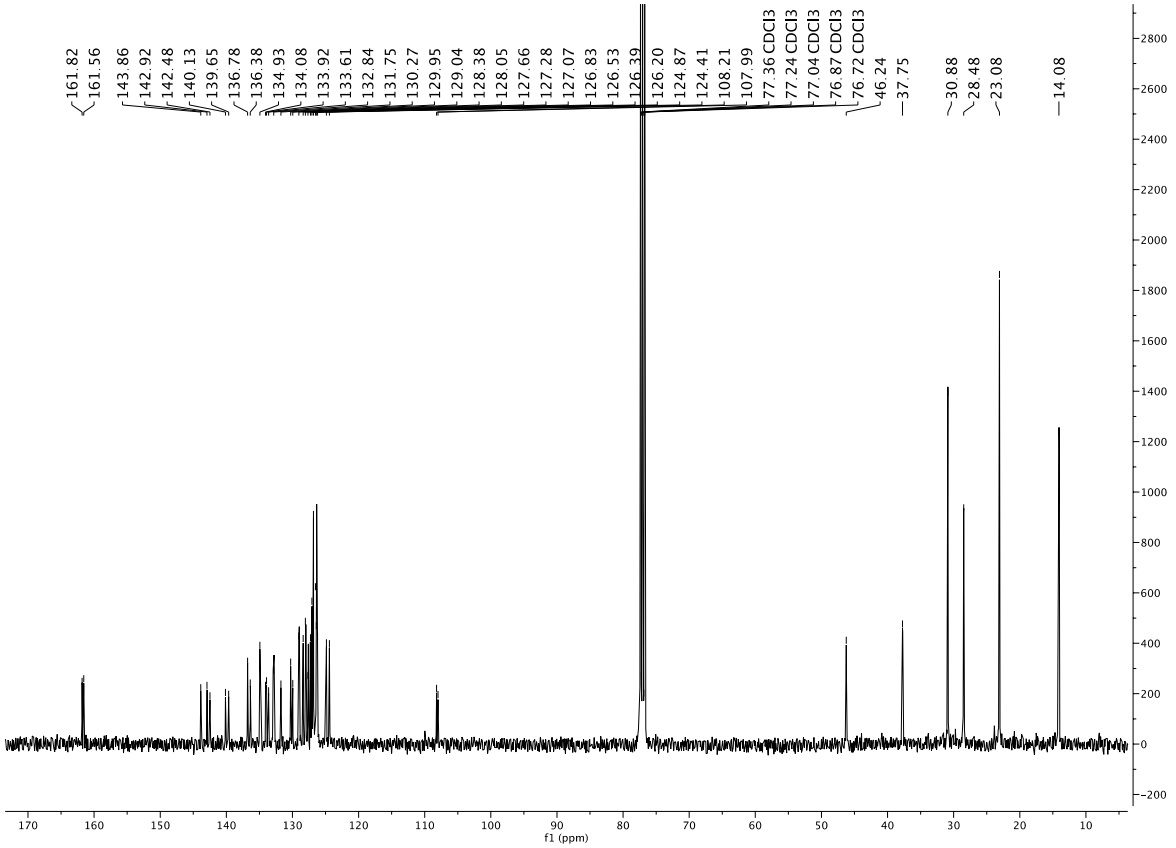

161.78
161.56
143.57
142.71
140.01
139.71
136.68
134.94
133.93
133.05
131.93
130.27
129.93
129.28
128.36
128.08
127.79
127.41
127.28
126.81
126.55
124.84
124.46
108.19
108.05
77.33 CDCl3
77.02 CDCl3
76.70 CDCl3
46.22
37.71
30.86
29.72
28.42
23.06
14.02
f1 (ppm)

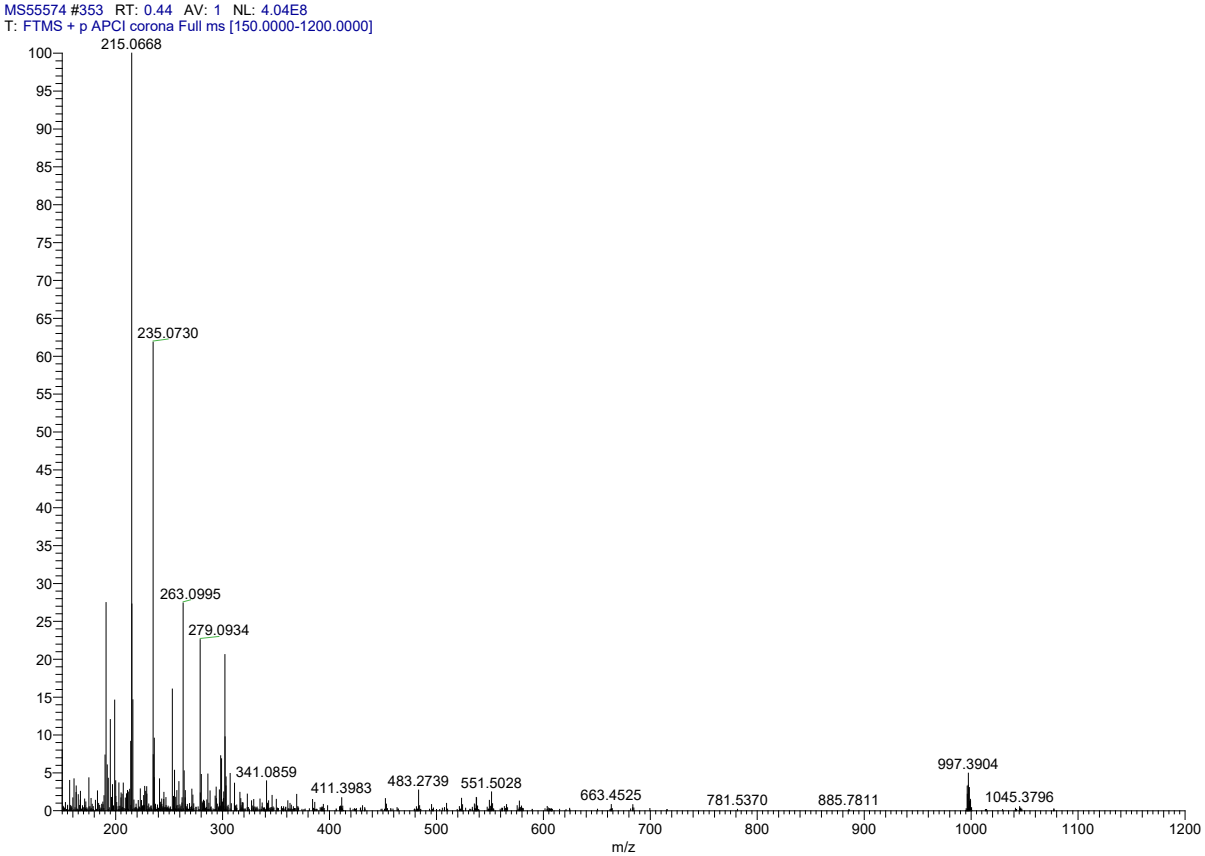

MS55092 #469 RT: 0.59 AV: 1 NL: 9.06E6
T: FTMS + p APCI corona Full ms [133.40
1575.6910
1576.6958
1577.6979
1574.6959
1578.7040
1579.7000
m/z

(*S*)-2,5-Bis(2-butylhexyl)-3-(thiophen-2-yl)-6-(5'-(2'-(thiophen-2-yl)-[1,1'-binaphthalen]-2-yl)-[2,2'-bithiophen]-5-yl)-2,5-dihydropyrrolo[3,4-*c*]pyrrole-1,4-dione



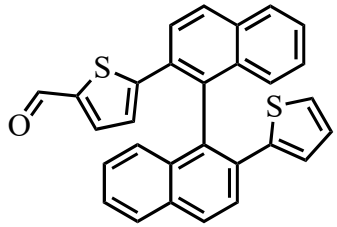


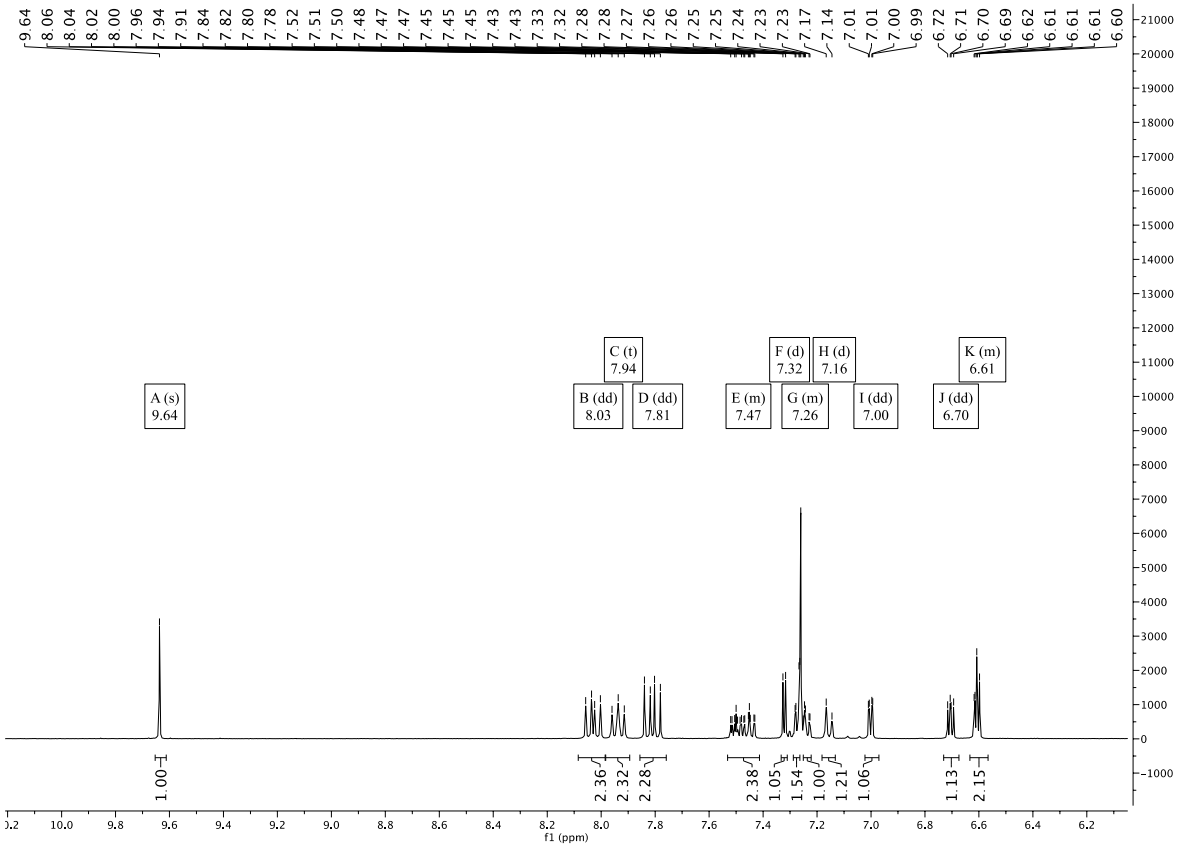

161.82
161.56
143.86
142.92
142.48
140.13
139.65
136.78
136.38
134.93
134.08
133.92
133.61
132.84
131.75
130.27
129.95
129.04
128.38
128.05
127.66
127.28
127.07
126.83
126.53
126.39
126.20
124.87
124.41
108.21
107.99
77.36 CDCl3
77.24 CDCl3
77.04 CDCl3
76.87 CDCl3
76.72 CDCl3
46.24
37.75
30.88
28.48
23.08
14.08
f1 (ppm)


MS55574 #353 RT: 0.44 AV: 1 NL: 4.04E8
T: FTMS + p APCI corona Full ms [150.0000-1200.0000]
215.0668
235.0730
263.0995
279.0934
341.0859
411.3983
483.2739
551.5028
663.4525
781.5370
885.7811
997.3904
1045.3796
m/z

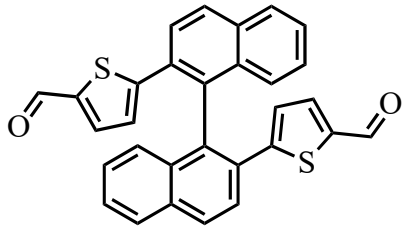
8.2 Chapter 3

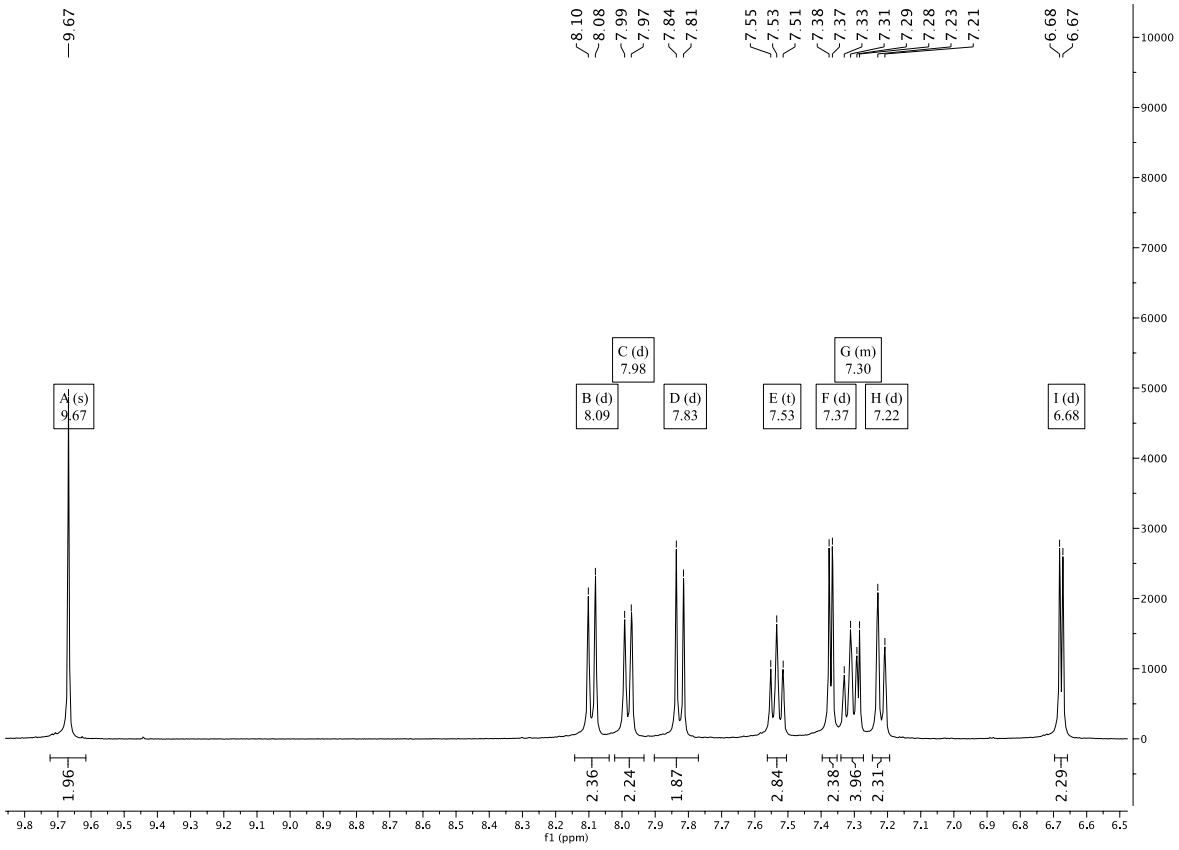
5-(2'-(Thiophen-2-yl)-[1,1'-binaphthalen]-2-yl)thiophene-2-carbaldehyde

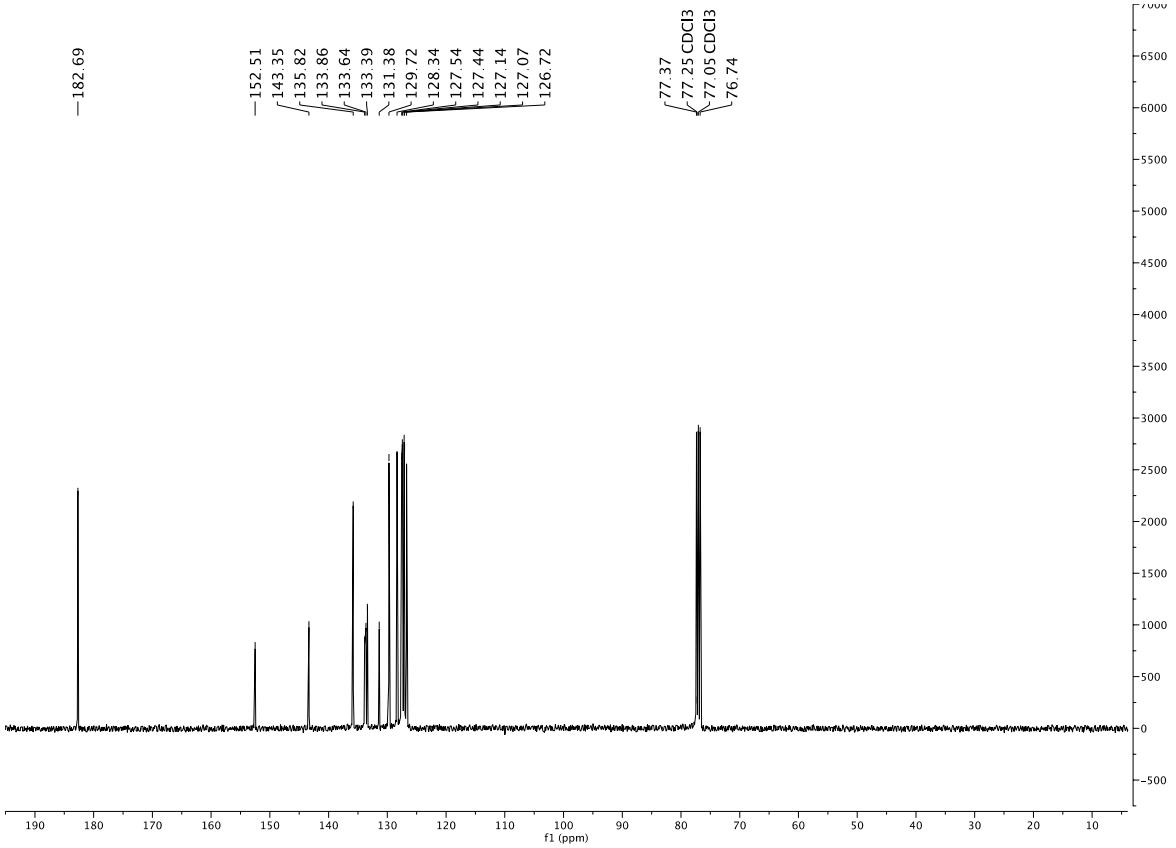


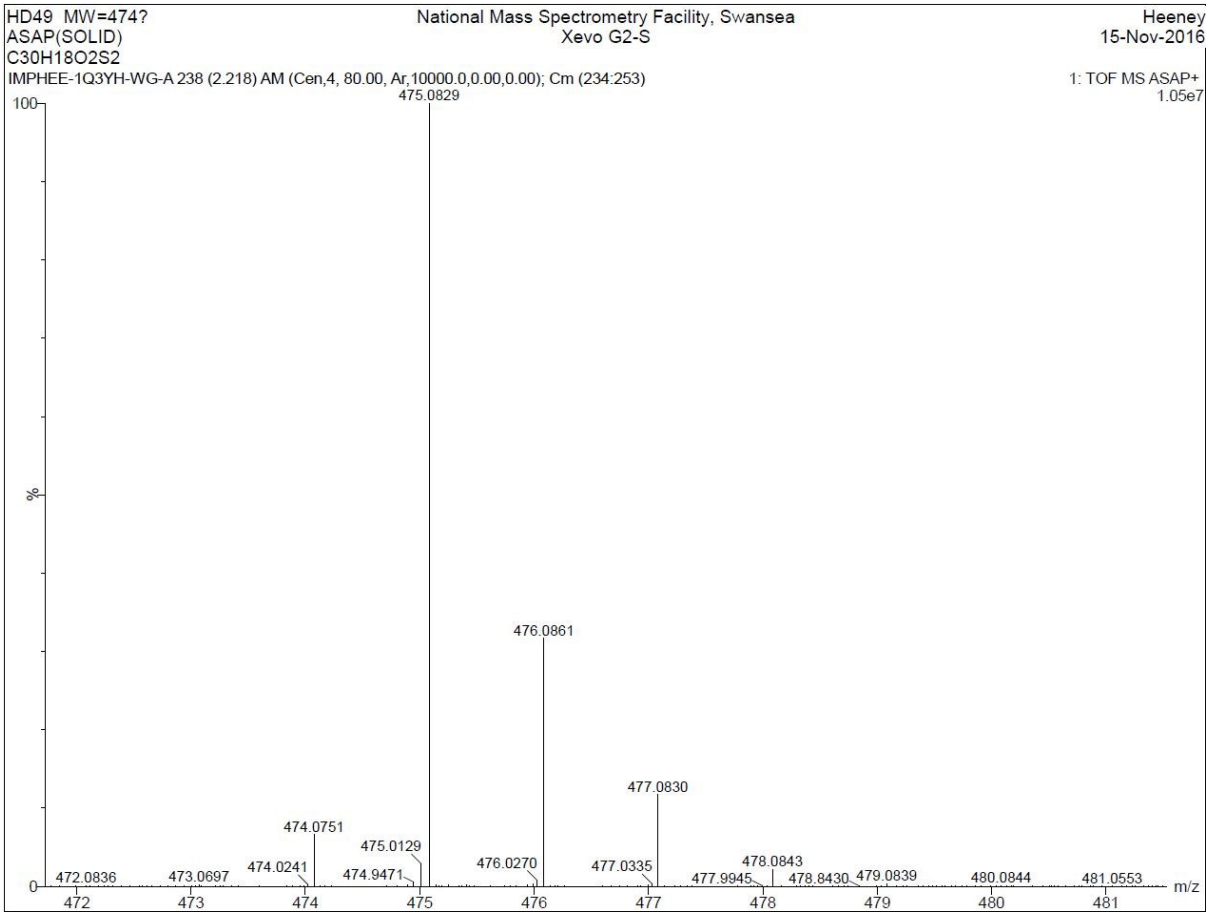


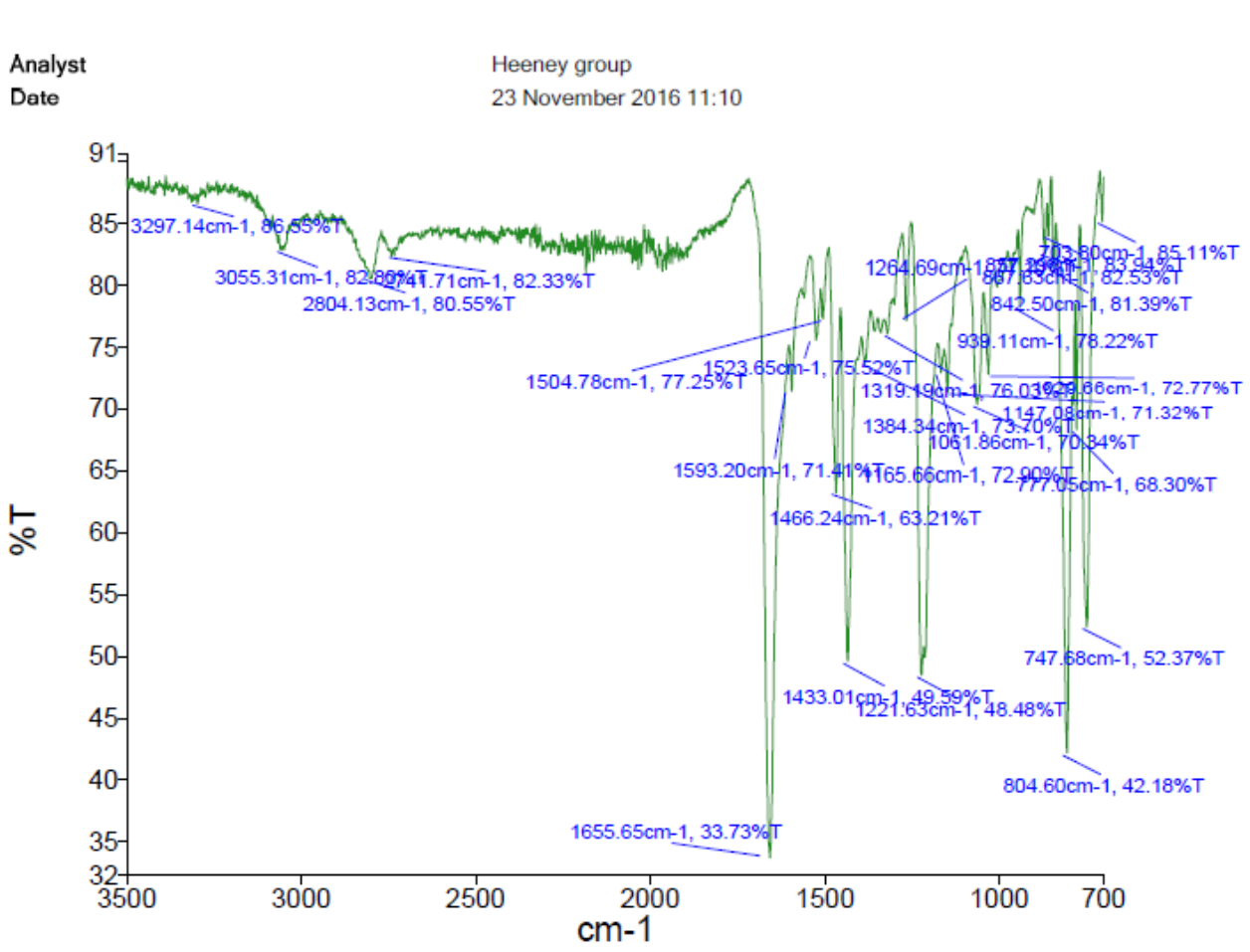
5,5'-([1,1'-Binaphthalene]-2,2'-diyl)bis(thiophene-2-carbaldehyde)



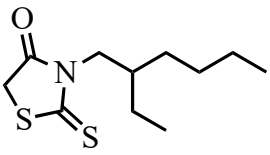


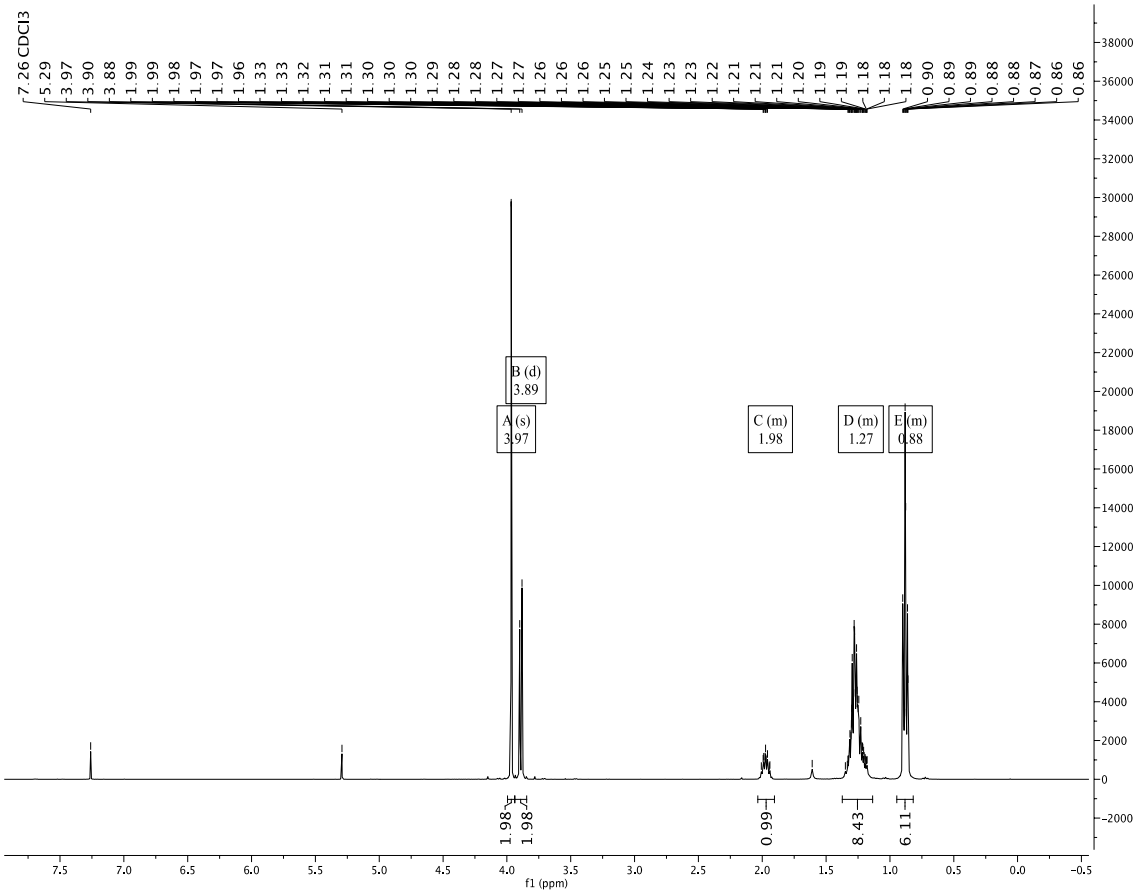

182.69
152.51
143.35
135.82
133.86
133.64
133.39
131.38
129.72
128.34
127.54
127.44
127.14
127.07
126.72
77.37
77.25 CDCl3
77.05 CDCl3
76.74
f1 (ppm)

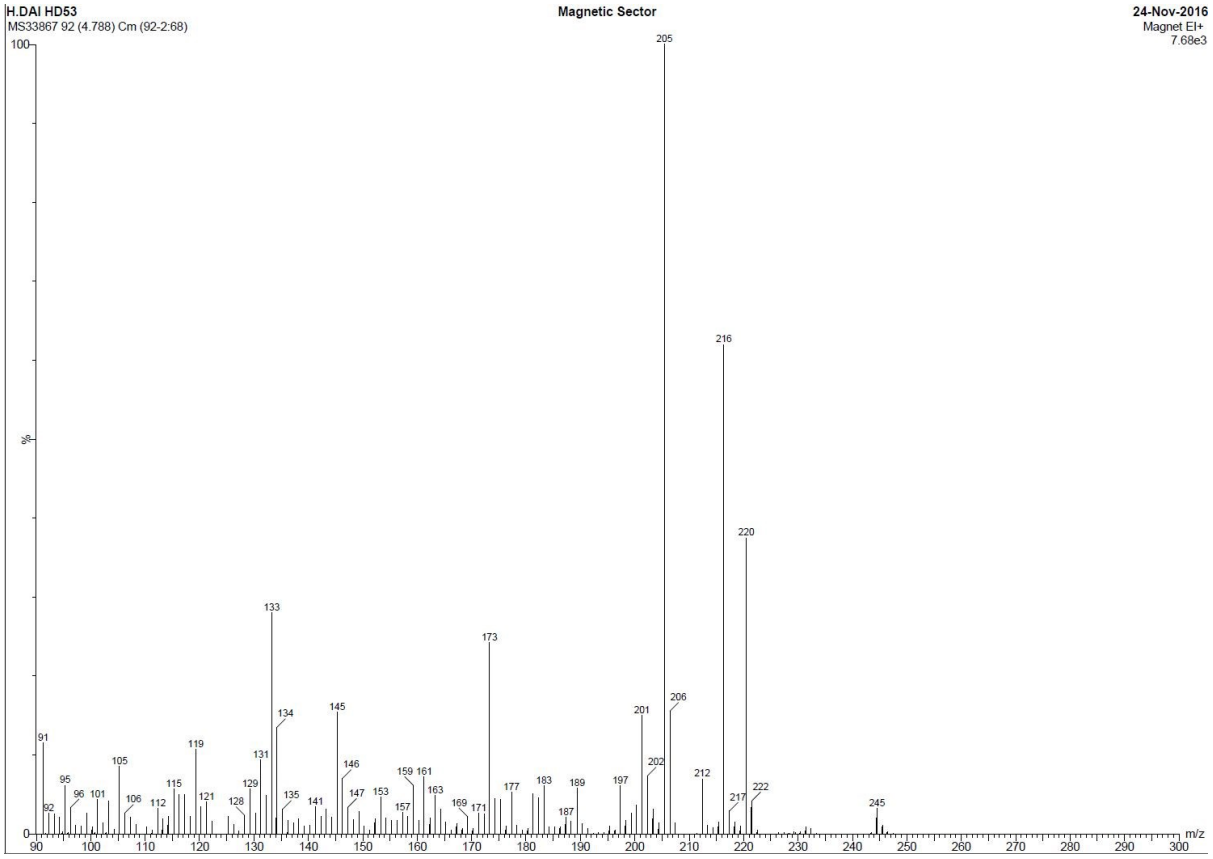

HD49 MW=474?
ASAP(SOLID)
C30H18O2S2
National Mass Spectrometry Facility, Swansea
Xevo G2-S
Heeney
15-Nov-2016
IMPHEE-1Q3YH-WG-A 238 (2.218) AM (Cen,4, 80.00, Ar,10000.0,0.00,0.00); Cm (234:253)
1: TOF MS ASAP+
1.05e7
475.0829
476.0861
477.0830
474.0751
475.0129
472.0836
473.0697
474.0241
474.9471
476.0270
477.0335
477.9945
478.0843
478.8430
479.0839
480.0844
481.0553
%
m/z


Analyst
Heeney group
Date
23 November 2016 11:10
%T
cm-1
3297.14cm-1, 86.65%T
3055.31cm-1, 82.88%T
2741.71cm-1, 82.33%T
2804.13cm-1, 80.55%T
1504.78cm-1, 77.25%T
1523.65cm-1, 75.52%T
1264.69cm-1, 83.94%T
867.83cm-1, 82.53%T
842.50cm-1, 81.39%T
939.11cm-1, 78.22%T
1319.19cm-1, 76.03%T
1147.08cm-1, 71.32%T
1384.34cm-1, 73.70%T
1061.86cm-1, 70.34%T
1593.20cm-1, 71.41%T
1165.66cm-1, 72.90%T
777.05cm-1, 68.30%T
1466.24cm-1, 63.21%T
747.68cm-1, 52.37%T
1433.01cm-1, 49.59%T
1221.63cm-1, 48.48%T
804.60cm-1, 42.18%T
1655.65cm-1, 33.73%T

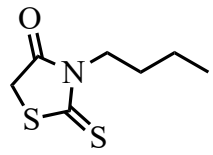
3-(2-Ethylhexyl)-2-thioxothiazolidin-4-one

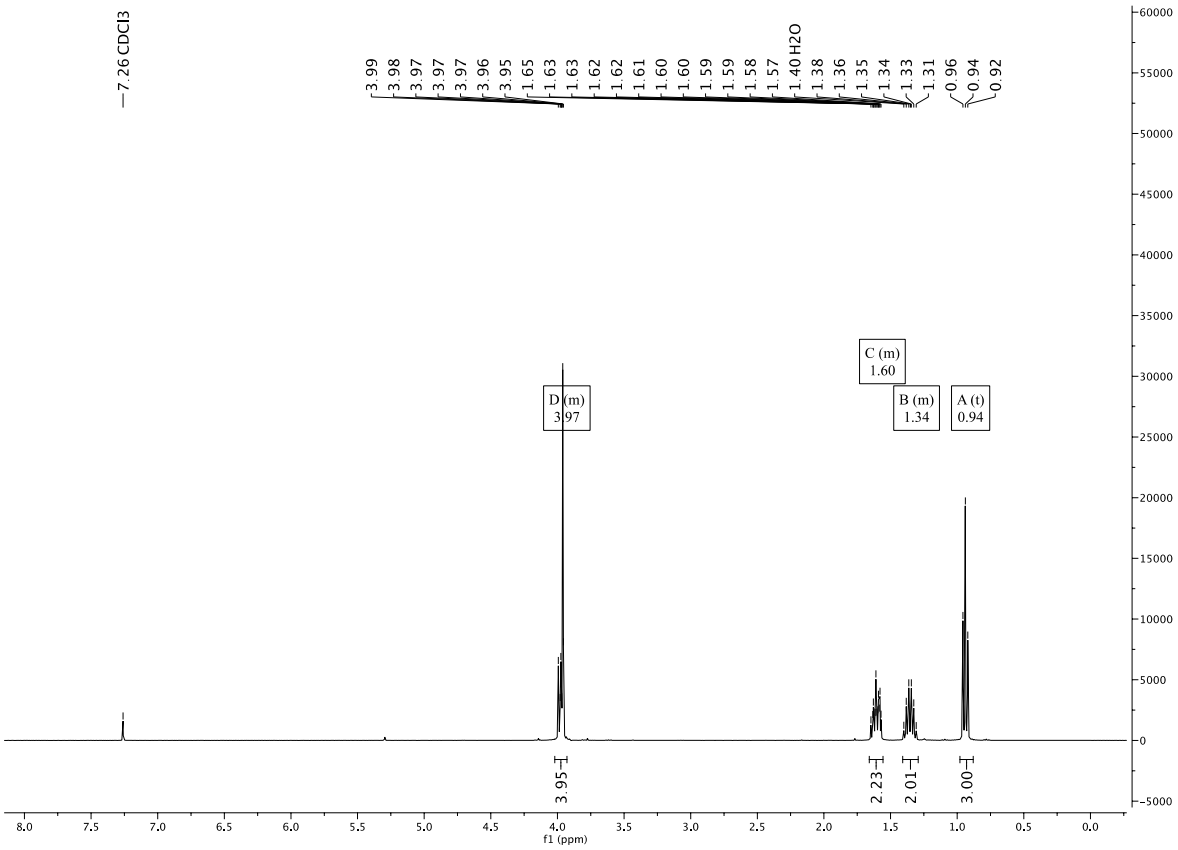


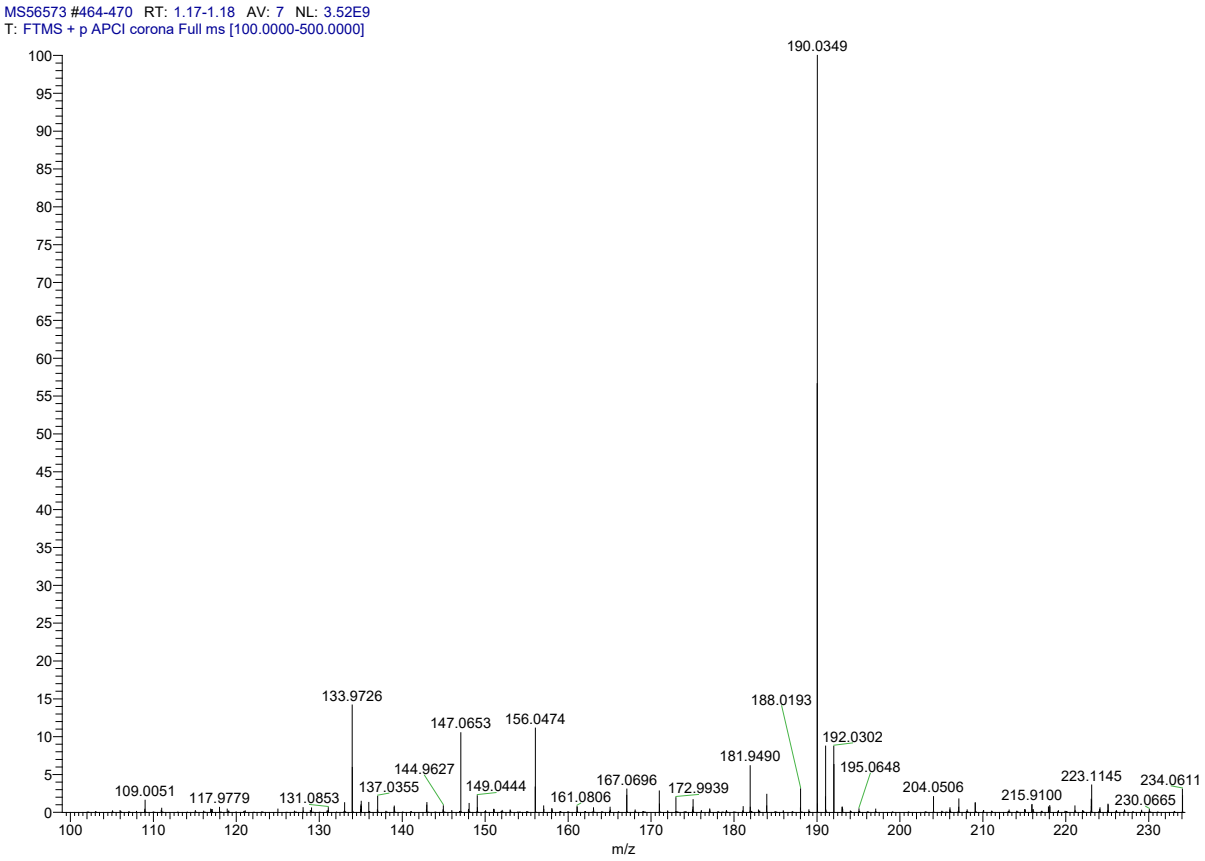



H.DAI HD53
MS33867 92 (4.788) Cm (92-2:68)
Magnetic Sector
24-Nov-2016
Magnet EI+
7.68e3
100
%
0
205
216
220
133
173
206
145
134
201
91
119
131
105
146
159
161
202
212
95
129
115
163
177
183
189
197
222
96
101
121
135
147
153
169
171
187
217
245
92
106
112
128
141
157
m/z
90
100
110
120
130
140
150
160
170
180
190
200
210
220
230
240
250
260
270
280
290
300

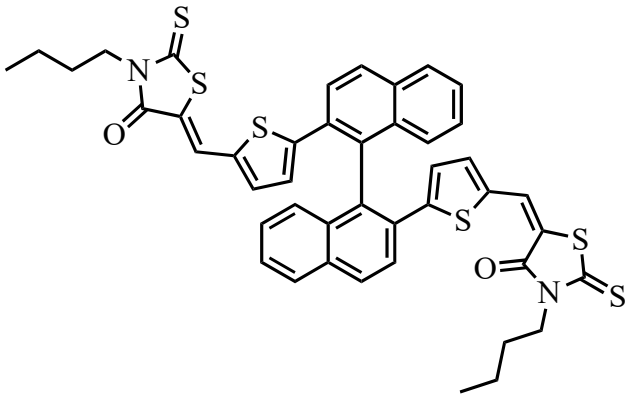
3-Butyl-2-thioxothiazolidin-4-one

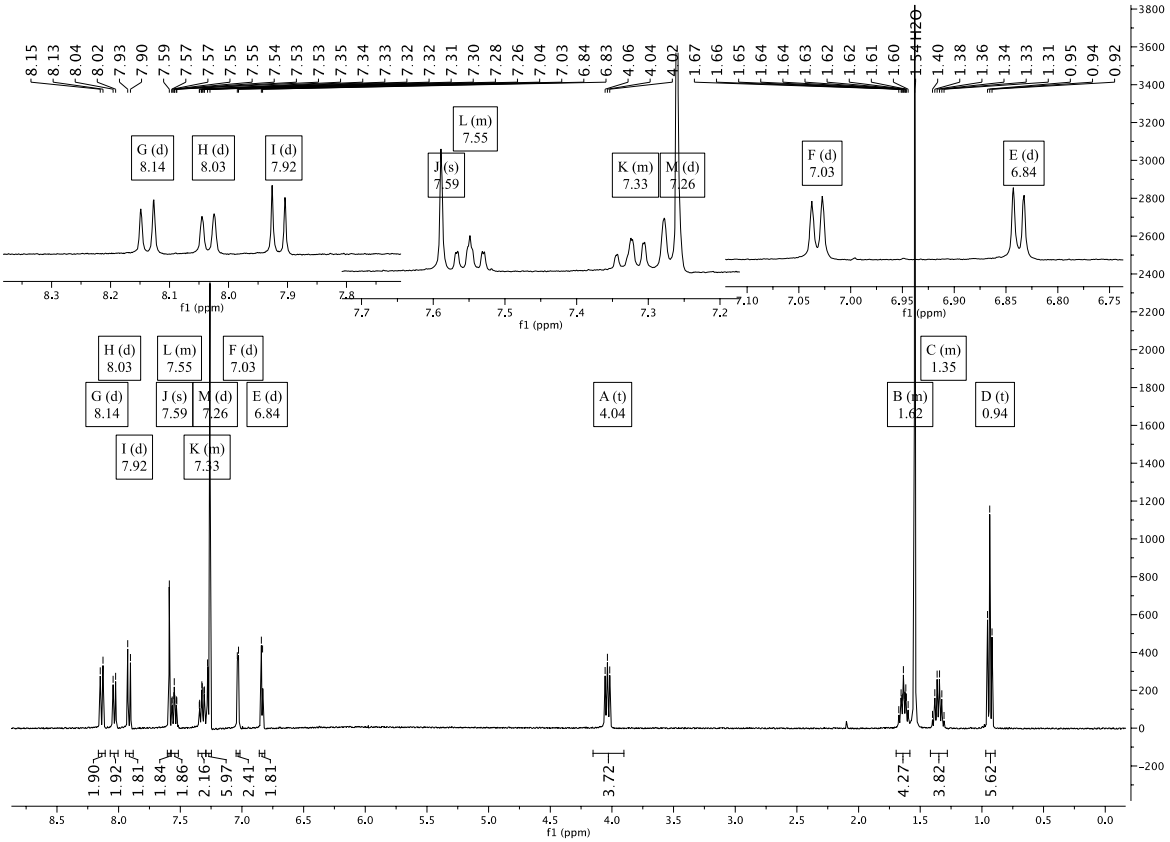


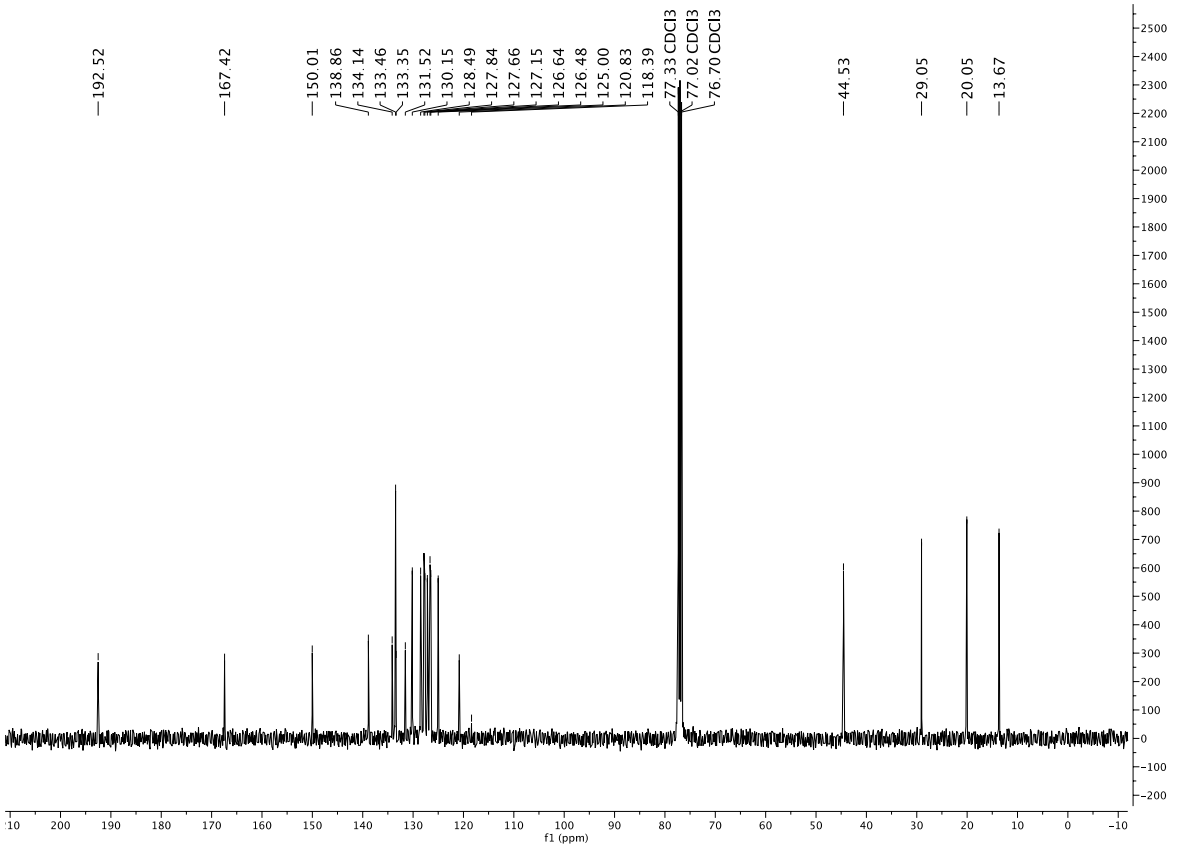


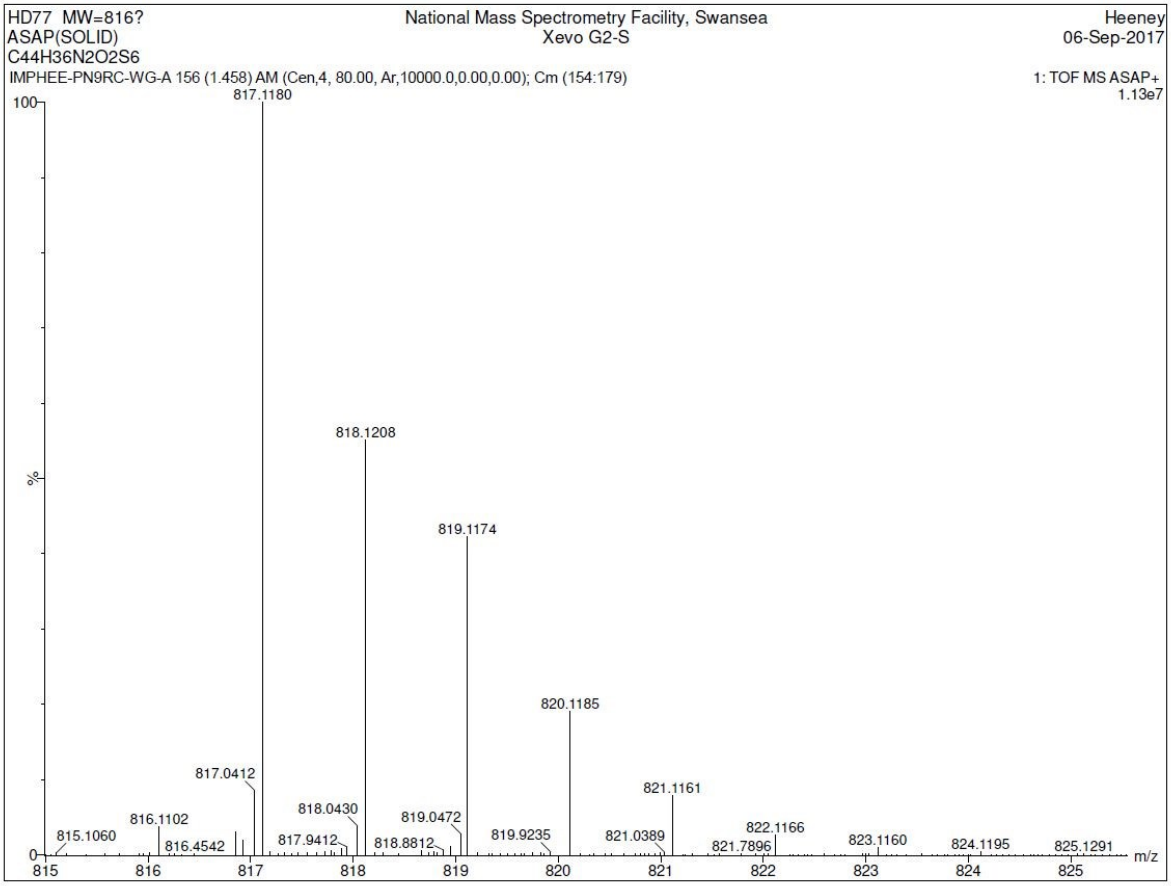

MS56573 #464-470 RT: 1.17-1.18 AV: 7 NL: 3.52E9
T: FTMS + p APCI corona Full ms [100.0000-500.0000]
190.0349
133.9726
147.0653
156.0474
188.0193
192.0302
181.9490
195.0648
144.9627
137.0355
149.0444
167.0696
172.9939
204.0506
223.1145
234.0611
109.0051
117.9779
131.0853
161.0806
215.9100
230.0665
m/z

(5*Z*,5'*E*)-5,5'-(([1,1'-binaphthalene]-2,2'-diylbis(thiophene-5,2-diyl))bis(methaneylylidene))bis(3-butyl-2-thioxothiazolidin-4-one)

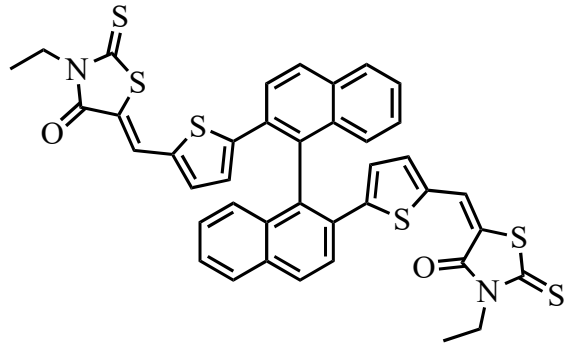


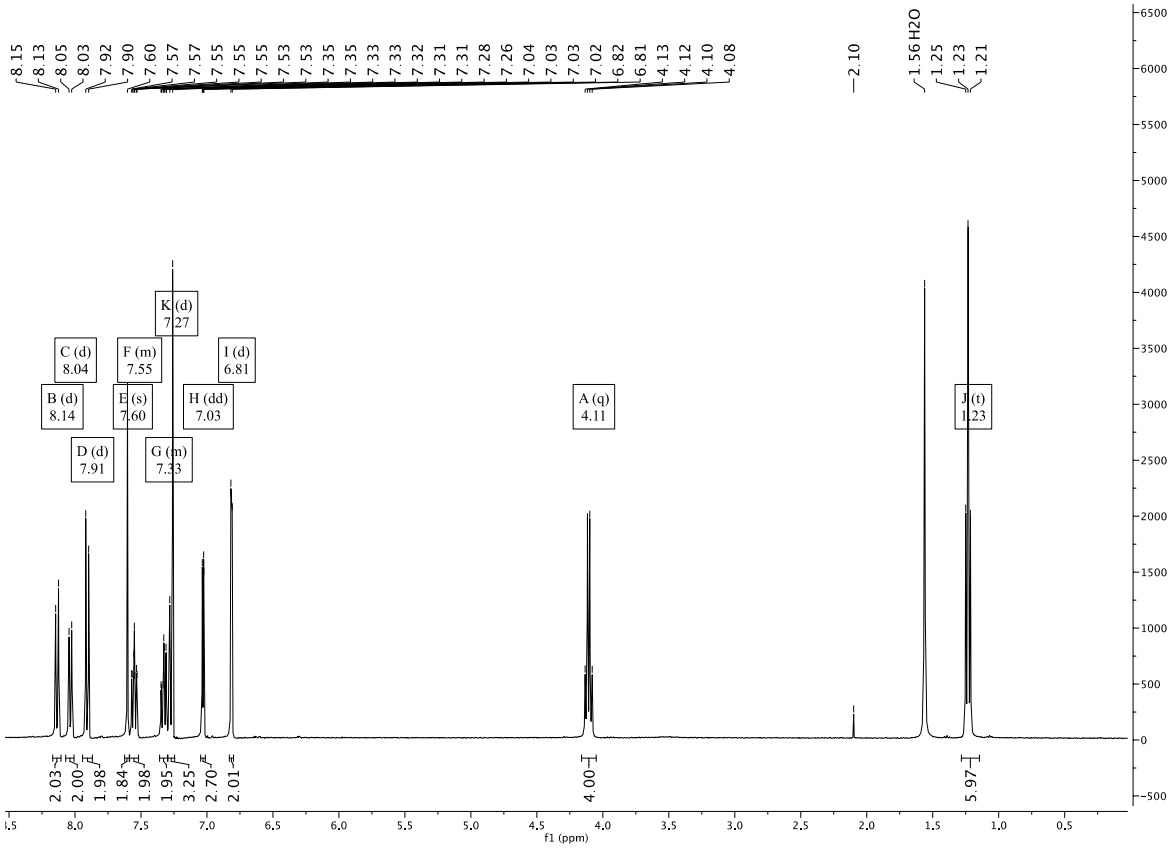


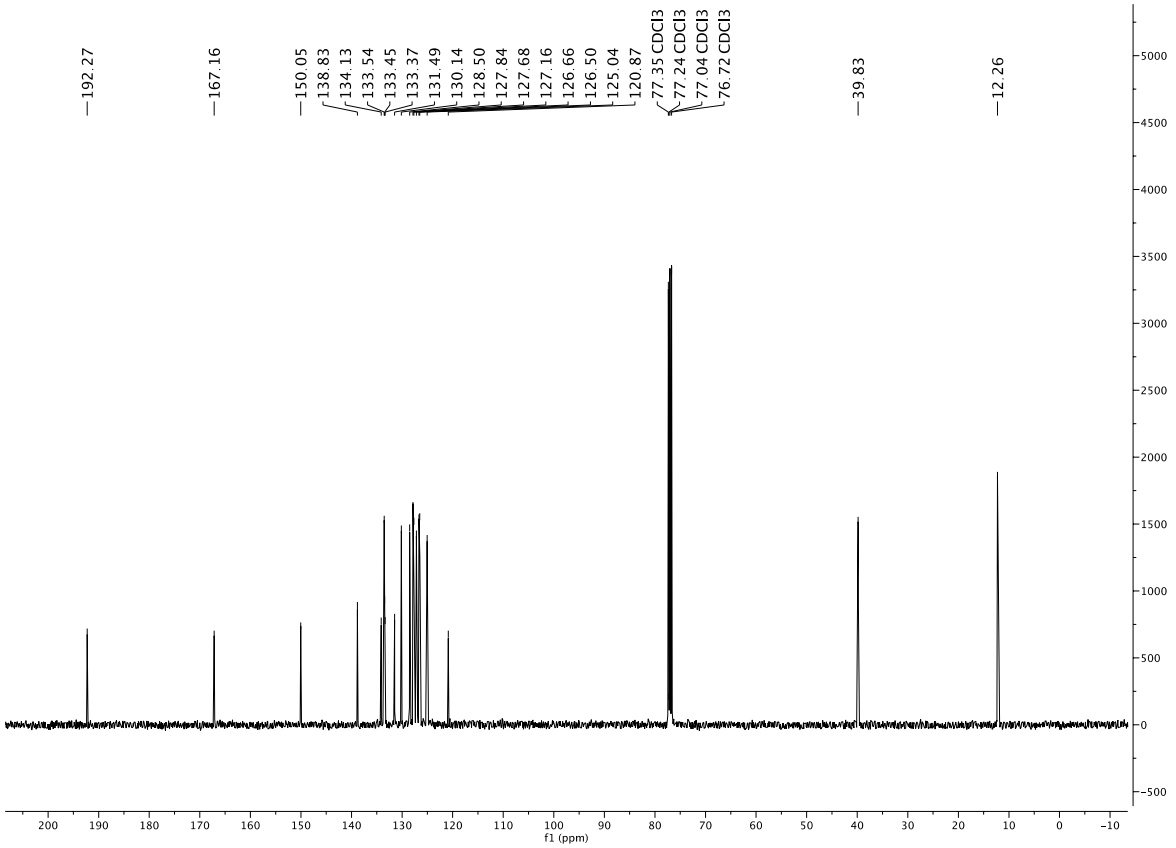

192.52
167.42
150.01
138.86
134.14
133.46
133.35
131.52
130.15
128.49
127.84
127.66
127.15
126.64
126.48
125.00
120.83
118.39
77.33 CDCl3
77.02 CDCl3
76.70 CDCl3
44.53
29.05
20.05
13.67
f1 (ppm)

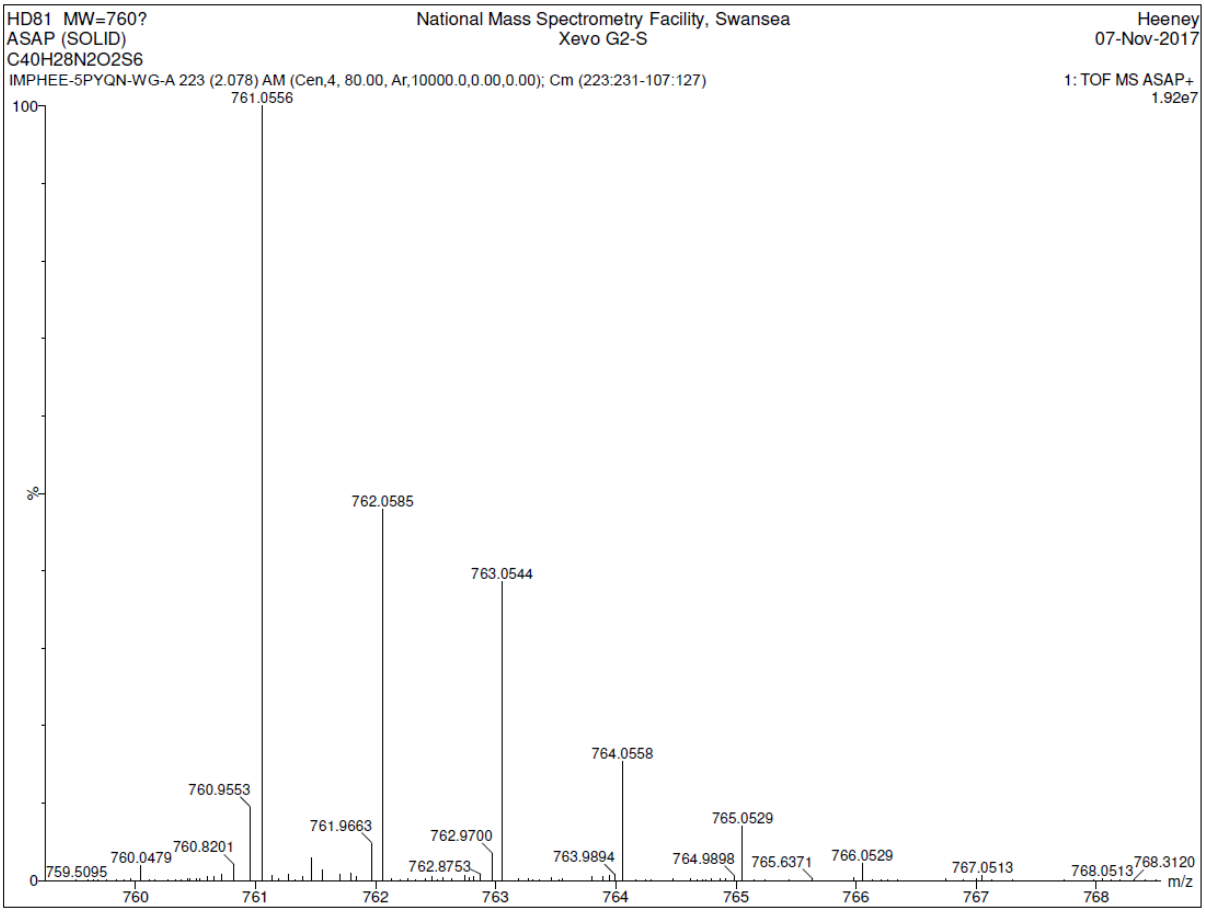

HD77 MW=816?
ASAP(SOLID)
C44H36N2O2S6
National Mass Spectrometry Facility, Swansea
Xevo G2-S
Heeney
06-Sep-2017
IMPHEE-PN9RC-WG-A 156 (1.458) AM (Cen,4, 80.00, Ar,10000.0,0.00,0.00); Cm (154:179)
1: TOF MS ASAP+
1.13e7
817.1180
818.1208
819.1174
820.1185
817.0412
821.1161
818.0430
816.1102
819.0472
822.1166
815.1060
816.4542
817.9412
818.8812
819.9235
821.0389
821.7896
823.1160
824.1195
825.1291
%
m/z

(5*Z*,5'*E*)-5,5'-(([1,1'-binaphthalene]-2,2'-diylbis(thiophene-5,2-diyl))bis(methaneylylidene))bis(3-ethyl-2-thioxothiazolidin-4-one)

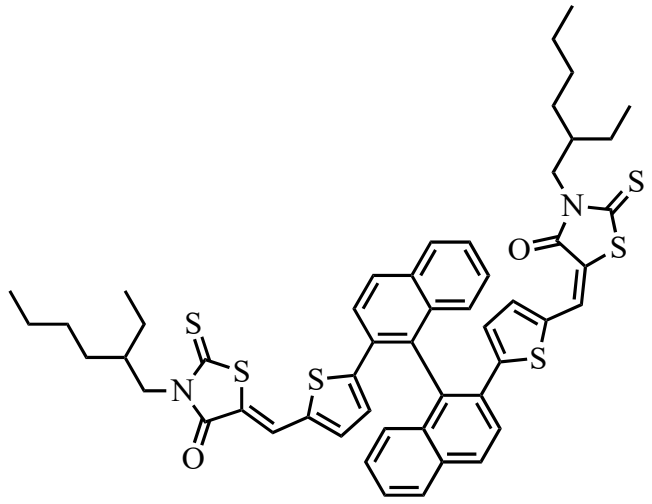


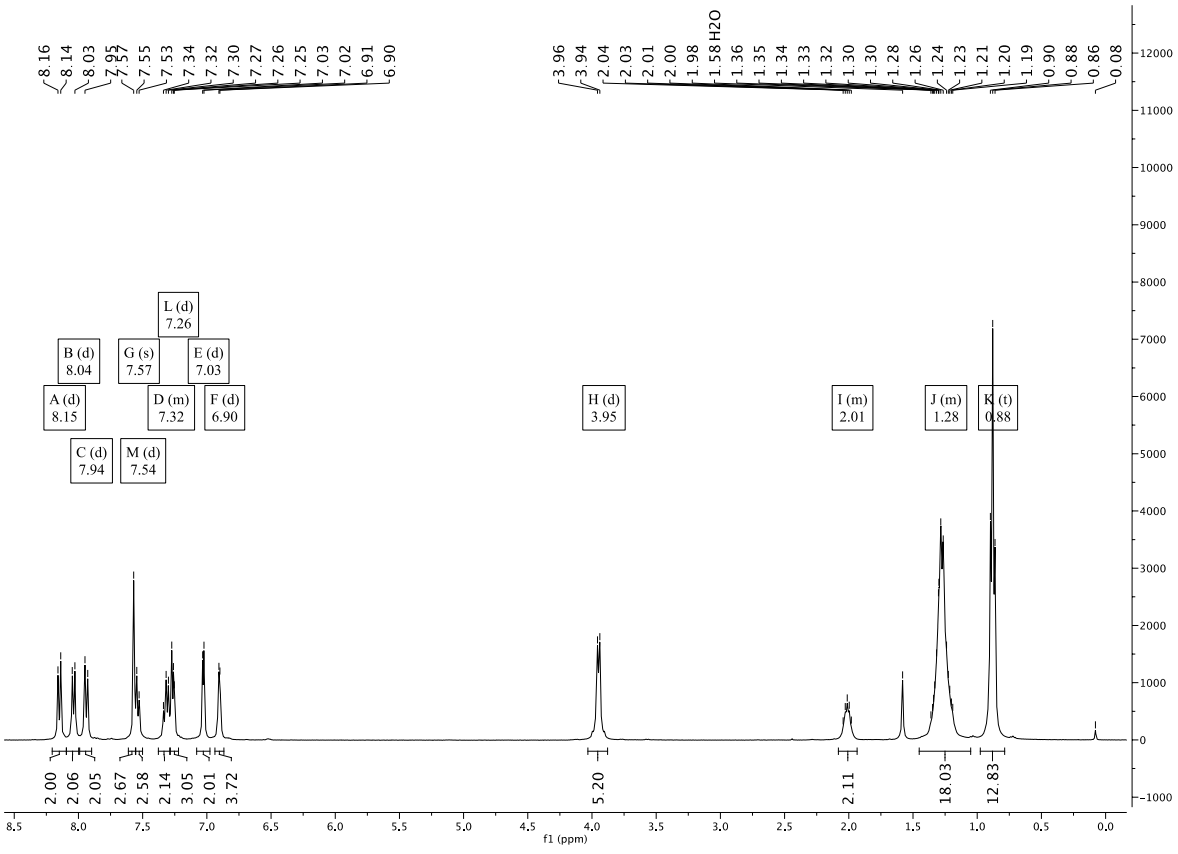


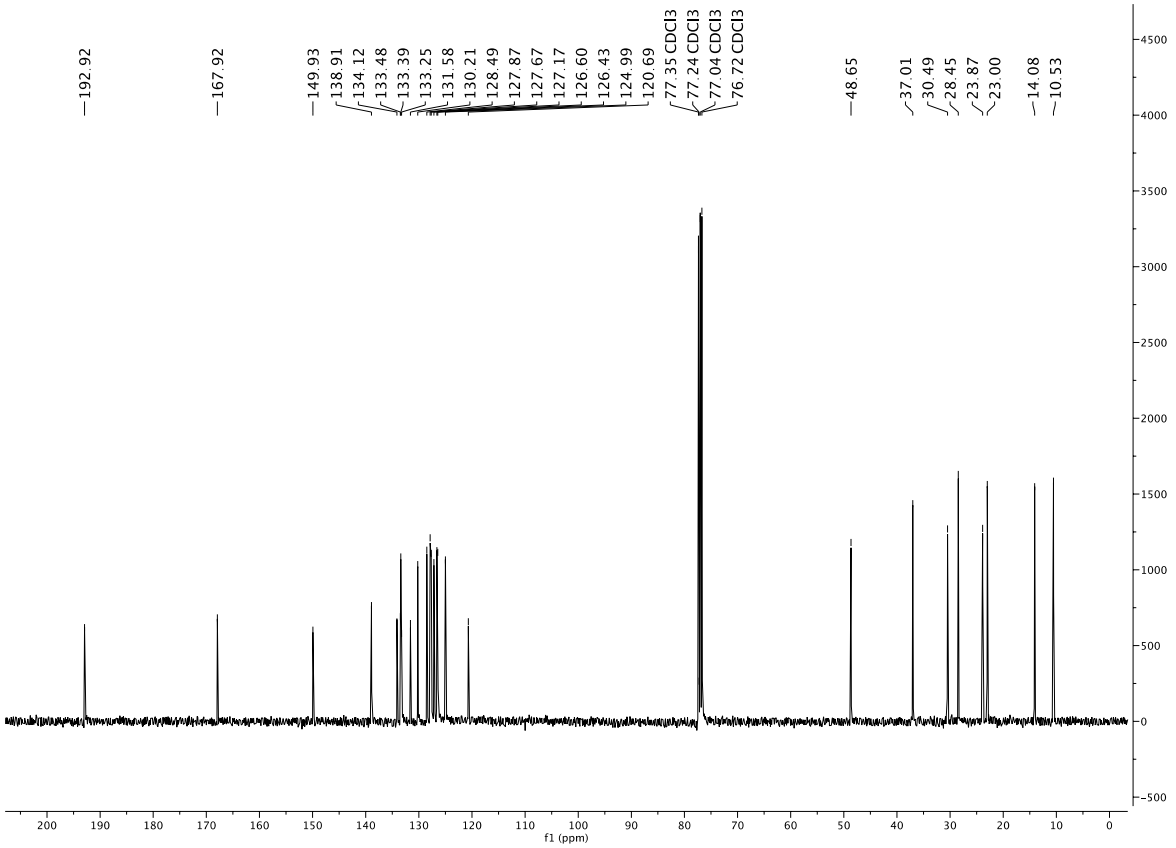

192.27
167.16
150.05
138.83
134.13
133.54
133.45
133.37
131.49
130.14
128.50
127.84
127.68
127.16
126.66
126.50
125.04
120.87
77.35 CDCl3
77.24 CDCl3
77.04 CDCl3
76.72 CDCl3
39.83
12.26
f1 (ppm)

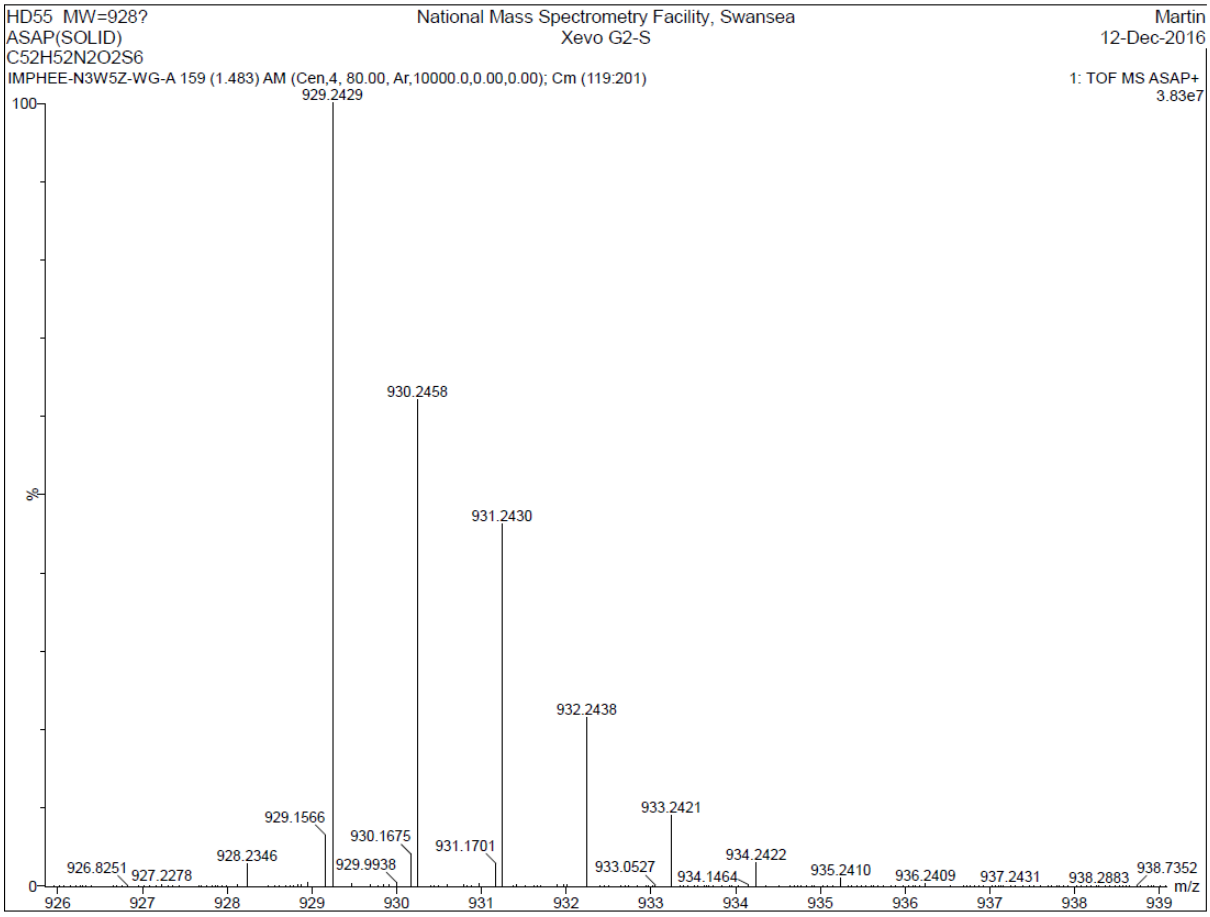

HD81 MW=760?
ASAP (SOLID)
C40H28N2O2S6
National Mass Spectrometry Facility, Swansea
Xevo G2-S
Heeney
07-Nov-2017
IMPHEE-5PYQN-WG-A 223 (2.078) AM (Cen,4, 80.00, Ar,10000.0,0.00,0.00); Cm (223:231-107:127)
1: TOF MS ASAP+
1.92e7
761.0556
762.0585
763.0544
764.0558
760.9553
761.9663
762.9700
765.0529
760.8201
760.0479
759.5095
762.8753
763.9894
764.9898
765.6371
766.0529
767.0513
768.0513
768.3120
%
m/z

(5*Z*,5'*E*)-5,5'-(([1,1'-binaphthalene]-2,2'-diylbis(thiophene-5,2-diyl))bis(methaneylylidene))bis(3-(2-ethylhexyl)-2-thioxothiazolidin-4-one)



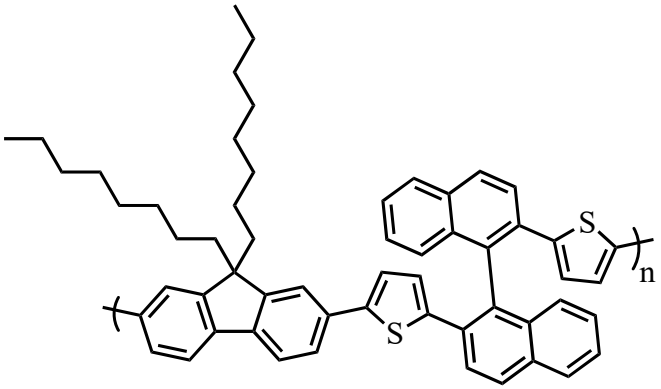


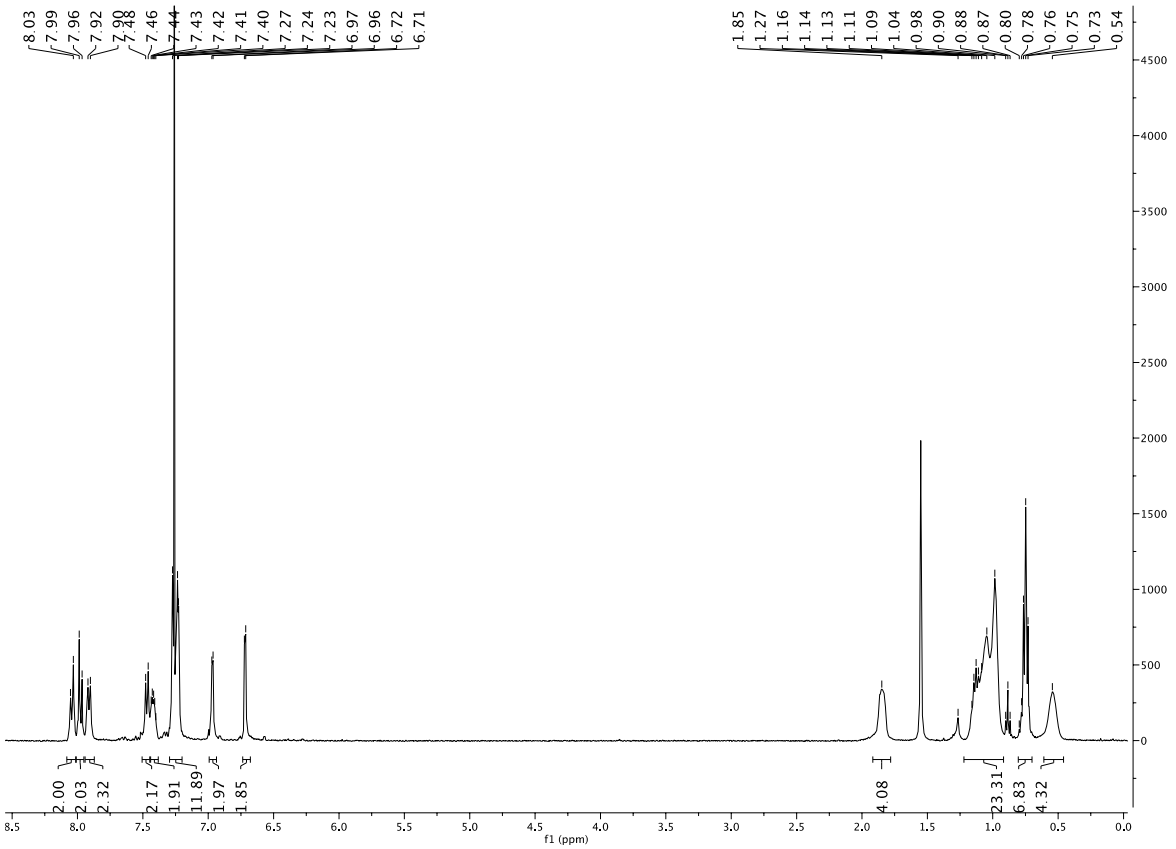

192.92
167.92
149.93
138.91
134.12
133.48
133.39
133.25
131.58
130.21
128.49
127.87
127.67
127.17
126.60
126.43
124.99
120.69
77.35 CDCl3
77.24 CDCl3
77.04 CDCl3
76.72 CDCl3
48.65
37.01
30.49
28.45
23.87
23.00
14.08
10.53
f1 (ppm)


HD55 MW=928?
ASAP(SOLID)
C52H52N2O2S6
National Mass Spectrometry Facility, Swansea
Xevo G2-S
Martin
12-Dec-2016
IMPHEE-N3W5Z-WG-A 159 (1.483) AM (Cen,4, 80.00, Ar,10000.0,0.00,0.00); Cm (119:201)
1: TOF MS ASAP+
3.83e7
929.2429
930.2458
931.2430
932.2438
933.2421
934.2422
929.1566
930.1675
931.1701
928.2346
929.9938
926.8251
927.2278
933.0527
934.1464
935.2410
936.2409
937.2431
938.2883
938.7352
%
m/z

8.3 Chapter 4

Poly{2-(9,9-dioctyl-9*H*-fluoren-2-yl)-5-(2'-(thiophen-2-yl)-[1,1'-binaphthalen]-2-yl)thiophene}





Poly{4,8-bis(5-(2-ethylhexyl)thiophen-2-yl)-2-(5-(2'-(thiophen-2-yl)-[1,1'-binaphthalen]-2-yl)thiophen-2-yl)benzo[1,2-*b*:4,5-*b'*]dithiophene}

